Draft Final Report

ENGINEERING EVALUATION OF POST-LIQUEFACTION STRENGTH

by

Joseph P. Weber, Raymond B. Seed, Juan M. Pestana, Robb E. S. Moss,
Chukwuebuka Nweke, Tonguc T. Deger and Khaled Chowdhury

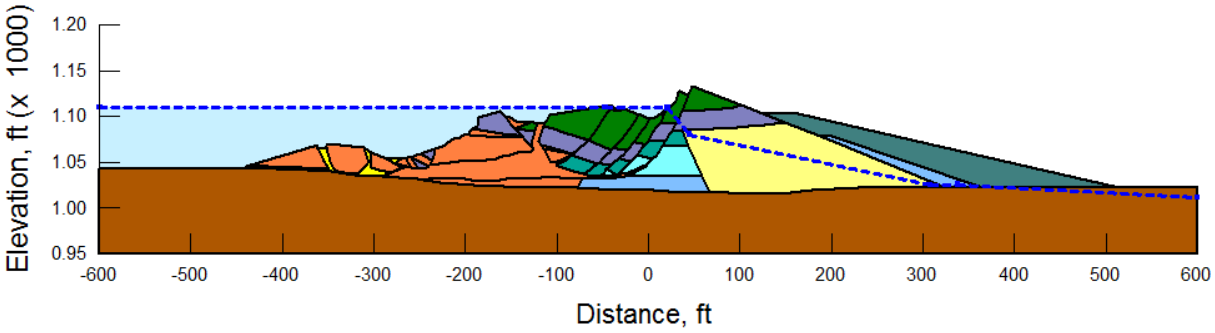

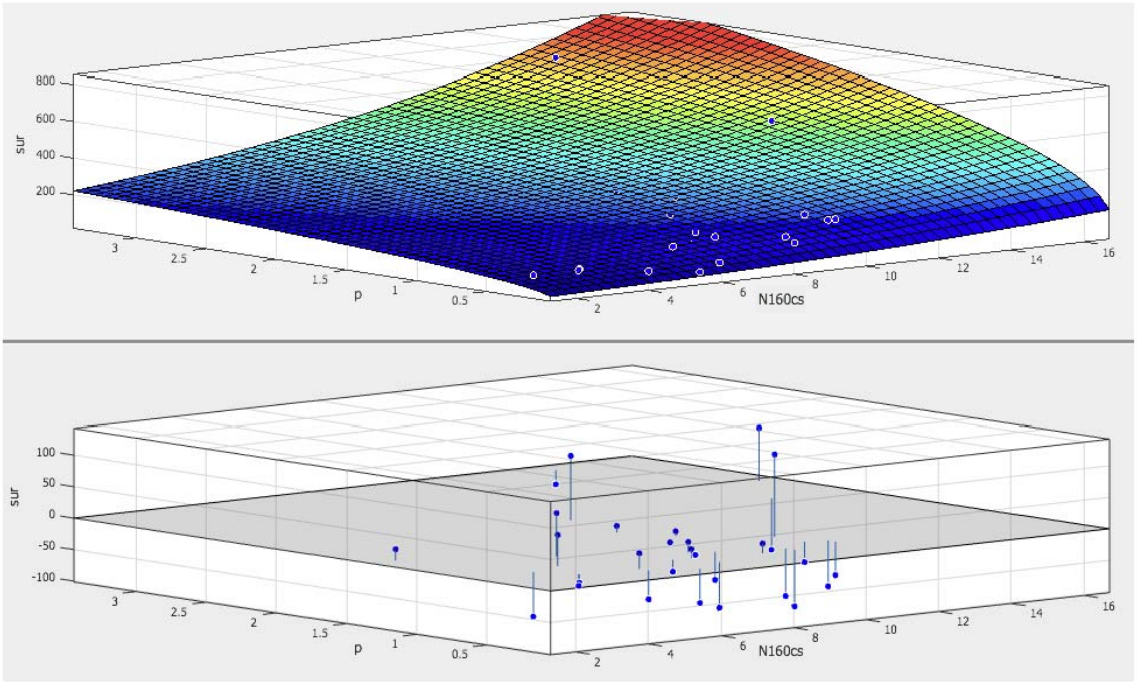

Department of Civil and Environmental Engineering
University of California at Berkeley

January 30, 2015

Prepared for: The U. S. Nuclear Regulatory Commission (NRC)

TABLE OF CONTENTS

Chapter One

Introduction and Overview

1.1 Introduction

Soil liquefaction came prominently to the attention of the geotechnical engineering profession in the mid-1960's, largely due to the widespread and severe liquefaction-induced damages wrought by the 1964 Great Alaskan Earthquake (M_W = 9.2) and by the 1964 Niigata Earthquake (M_W = 7.7). The phenomenon of soil liquefaction was, of course, already known but prior to these two events there were no well-established methods for dealing with soil liquefaction and its consequences.

In the wake of these two events, the first engineering investigation and analysis methods were developed for evaluation of the risk of triggering, or initiation, of soil liquefaction due to seismic loading (e.g.: Seed and Idriss, 1971; etc.). Methods for evaluation of seismic soil liquefaction potential, or likelihood of triggering, under both static and cyclic loading have continued to evolve, and today there are a wide variety of well-established methods that range from simplified empirically-based methods through laboratory-based methods and also increasingly advanced, fully nonlinear constitutive analysis models and methods implemented in either finite element or finite difference computer analysis frameworks.

The liquefaction-induced failure of the upstream side of the earthen embankment of the Lower San Fernando Dam during the 1971 San Fernando Earthquake (M_W = 6.6) nearly resulted in uncontrolled release of the Van Norman Reservoir, which would have had catastrophic consequences for the large urban population immediately downstream. This embankment failure was followed a year later (1972) by the non-seismically induced liquefaction failure of the Buffalo Creek mine tailings dam in West Virginia. The Buffalo Creek Dam failure resulted in uncontrolled release of the reservoir impoundment, and devastated the community immediately downstream. One hundred and twenty five lives were lost. These two events led to a surge of interest in liquefaction-related risks associated with dams, and helped to lead to the eventual creation of the U.S. National Dam Safety Program in 1986. This program has contributed considerably to the further development of improved methods for engineering treatment of soil liquefaction issues.

Additional impetus for advancement of liquefaction-related engineering analysis methods, and for corollary liquefaction risk mitigation measures, has come from interest and research associated with other critical infrastructure, and more recently the focus has continued to broaden to include more routine projects and structures.

Both in the U.S. and abroad, much of the focus of the rapidly evolving field of soil liquefaction engineering practice in the 1970's and 1980's was initially on dams and other critical facilities and infrastructure. Over the five decades that have now passed since the mid-1960's, attention has progressively extended to also consider and deal with liquefaction risk for an increasingly broad range of facilities and structures, including ports and harbors, transportation

facilities (bridges, roads, embankments, tunnels, airports, etc.), in-ground lifelines (power, gas water, telecommunications, etc,.), critical structures (power plants, industrial facilities, waste impoundments, etc.), more routine structures (e.g. homes and businesses), and more.

As the breadth of applications has increased, so has the development of increasingly accurate and reliable methods for evaluation not only of the risk of triggering or initiation of soil liquefaction, but also of the expected resulting performance consequences for a site or facility. Increasingly, engineers are being called upon to assess the expected consequences of potential liquefaction in terms of deformations, displacements, and damages to the structures or systems of concern.

Over the first 10 to 15 years after the two 1964 earthquakes in Alaska and Niigata, most liquefaction-related engineering was focused primarily on evaluation of the risk, or likelihood, of "triggering" or initiation of liquefaction. If liquefaction was considered likely to be triggered, either statically or cyclically, then negligible post-liquefaction strengths and stiffnesses were commonly assigned to the materials judged likely to liquefy as the next step in evaluation of expected consequences.

That was a very conservative approach, and it was clear early on that post-liquefaction strengths were not necessarily equal to zero; certainly not in all cases. The evolving understanding of the mechanics of soil liquefaction, and of critical state soil mechanics (e.g. Casagrande, 1940; Schofield and Wroth, 1968; etc.), and progressively advancing laboratory testing capabilities and also analytical capabilities, led to the continuing development of improved analytical tools for dealing not just with triggering of soil liquefaction, but also with the engineering assessment of resulting deformations and displacements of both the ground and the structures and systems affected.

This, in turn, has led to a need for better assessments of post-liquefaction strengths so that more accurate (and less over-conservative) engineering assessments of expected performance and consequences can be made.

It is here that these current studies are focused.

1.2 Overview of These Current Studies

Chapter 2 presents a brief history of the development of approaches for evaluation of post-liquefaction soil strengths, and a review of important methods, including an assessment of the advantages and drawbacks of the main approaches available for engineering evaluation of in situ post-liquefaction strengths. In most research investigations, this type of review is presented as a bit of a formality. For this current study, however, this close review and re-evaluation of previous efforts was a key element in the development of the findings eventually produced here. Armed with the advantage of hindsight, it turns out that multiple previous investigation efforts, and researchers, had developed important insights and/or elements of work that end up contributing to the overall solutions and findings of these current studies. In some interesting cases, the previous investigators did not (at the time) recognize the eventual importance of some of those pieces of the puzzle.

Chapter two discusses methods for evaluation of post-liquefaction strengths based on laboratory testing, as well as methods for assessment of post-liquefaction strengths using empirical relationships developed based on back-analyses of full-scale field failures. The main emphasis is on empirical methods, because a number of difficulties can arise with regard to the direct use of laboratory-based methods for project-specific applications, as is also discussed in Chapter 2. The development of improved empirical methods is then the principal focus of these current studies.

Chapter 3 presents an explanation of the review and selection of liquefaction field performance case histories for back-analyses in these current studies. A significant number of previous investigators have now worked on this problem, and a large number of potential case histories have been collected and analyzed by various investigators. The quality of cases histories available spans a considerable range, both with regard to the quality of data available for each case, and also the caliber of the documentation available regarding those data. In addition, some of the cases represent situations in which the nature of the field performance observed permits reasonably well-defined back-analysis for evaluation of post-liquefaction strengths. In other cases, the nature of the failure mechanism involved simply does not permit such an accurate assessment of post-liquefaction strengths. Selection of cases to be considered, and of cases to be back-analyzed and included in the development of the resulting probabilistic and deterministic relationships for evaluation of post-liquefaction strength, is thus an important issue.

Chapter 4 then presents an explanation of the back-analyses of field failure case histories performed for these current studies. The chapter begins with an overview of significant back-analysis approaches taken in these current studies, as well as in previous studies, with an assessment of strengths and drawbacks of each. This is important because the eventual predictive relationships developed will be cross-compared with existing relationships in Chapter 5, and it is thus important to understand the relative advantages and drawbacks of some of the back-analysis approaches taken in previous studies.

Chapter 4 then goes on to present and describe the development of a number of new back-analysis methods, and new empirical tools, and their application to the back-analyses of the case histories selected in Chapter 3. Many previous studies have not fully documented, or provided sufficient details, of back-analyses performed for purposes of assessing post-liquefaction strengths, and that has made it difficult to check and verify the general validity and reliability of the resulting recommended approaches for assessment of in situ post-liquefaction strengths for application to engineering analysis and design of real projects. One of the objectives of this current investigation is to break this trend, and to suitably document both the methods employed, and also the details of the analyses as these methods are applied to each individual case history. Methods and assumptions, cross-sections, modeling details and parameters, etc. involved in performing these back-analyses are presented and discussed. Even more detailed summaries of the back-analyses performed for each of the individual cases selected and analyzed are then presented in Appendices A and B.

Chapter 4 also presents a series of cross-checks of the values and parameters back-calculated from the liquefaction failure case histories. A series of empirical relationships developed in these current studies are used to check the internal consistency of the results of the 30 case histories back-analyzed based on a number of criteria. These cases are then further cross-

checked against the values back-calculated by previous investigators, with an understanding of the likely errors and systematic biases involved in some of those previous analyses.

Chapter 5 then presents and describes the use of the results of the back-analyses performed in Chapter 4 to develop recommended probabilistic and deterministic relationships for engineering evaluation of post-liquefaction strengths. The initial emphasis is on development of fully probabilistic empirical relationships for assessment of in situ post-liquefaction strengths based on engineering evaluations of in situ penetration resistance and of initial in situ vertical effective stresses. These methods are expected to be employed mainly for important projects that warrant a probabilistic or risk-based approach. The probabilistic methods are then used to develop recommended deterministic methods, with likely applications to more routine engineering analysis and design. Comparisons are then made between the probabilistic and deterministic tools and methods developed in these current studies, and a suite of other empirical approaches and relationships previously developed by other investigators. In the end, a coherent picture emerges and it now appears that the efforts of a significant number of previous investigations can be fit together, much like assembling a puzzle, and that a relatively coherent overall understanding of methods suitable for engineering evaluation of post-liquefaction strengths is achieved.

Chapter 6 presents an overall summary of the findings and recommendations from these studies.

Chapter Two

Previous Studies

2.1 Introduction

This chapter presents a review of existing methods for engineering evaluation of post-liquefaction strengths. This includes an overview of the historical progression of such methods, and an assessment of the strengths and shortcomings of each of these methods, and of the investigations performed to develop them.

2.1.1 Key Principles and Definitions

The term "soil liquefaction" has had many meanings ascribed to it by a large number of engineers and researchers. In these current studies, soil liquefaction will be taken as being: a significant reduction in strength and stiffness of a soil, primarily as a result of reduction in effective normal stresses due to pore pressure increase. This does not mean that pore pressure increase is the only cause of reduction in effective stress, or of reduction in strength and stiffness.

The term "flow failure" has also had multiple meanings. In these current studies, flow failure will refer to very large ground deformations and displacements that occur primarily because the static (gravity induced, non-seismic) "driving" shear stresses exceed the available shear strengths during some significant portion of the period over which displacements occur.

"Statically-induced liquefaction" will be taken as soil liquefaction that occurs in the absence of cyclic loading, either as a result of (1) monotonic increase in driving shear stresses, (2) decrease in effective stress due to non-cyclically induced increases in pore pressure, or (3) contractive behavior of the liquefying soil in the face of imposed deformations from moving boundary conditions (see the Fort Peck Dam failure).

"Seismically-induced liquefaction" will be taken as liquefaction triggered in some part by cyclic stresses, which may occur in combination with gravity-induced static driving shear stresses already in place. Seismically-induced liquefaction will generally include liquefaction resulting from seismic loading, and also vibrations from explosions, vibro-densification, passing trains, etc. In these current studies it will also include vibrations from large vibro-seis trucks (see the Lake Ackerman highway embankment failure).

"Post-liquefaction strength" has a very broad range of meanings and definitions to various engineers and researchers. In these current studies, the definition of this term will be a matter of context. When referring to post-liquefaction strength as deliberatively determined by others, their definition will generally be employed. When referring to post-liquefaction strength assessed in these current studies, the symbol used will be S_r and it will refer to the post-liquefaction shear strength that can be mobilized at non-insignificant strains to resist deformations and displacements.

Two additional terms warrant definition here as well. The first of these is "post-liquefaction initial yield stress" ($S_{r,yield}$). This is not an actual "strength", but rather the value of shear stress calculated to be needed within liquefied soils to provide an overall (theoretical) static Factor of Safety equal to 1.0 for conditions after (assumed) liquefaction and before significant resulting displacements begin to occur. This would, of course, over-estimate the actual value of available post-liquefaction strength (S_r) for cases in which significant displacements then do occur. If the value of S_r had actually been equal to $S_{r,yield}$, then displacements would not have resulted.

An additional term is "post-liquefaction residual strength based on residual geometry" ($S_{r,resid/geom}$), which is also not an actual "strength". Instead, it is the value of S_r back-calculated to provide a static Factor of Safety equal to 1.0 based on post-failure residual geometry. This is an over-conservative basis for estimation of actual post-liquefaction strength, as it neglects momentum effects as the moving slide mass has to be decelerated back to a stable residual condition. $S_{r,resid/geom}$ will therefore significantly underestimate the actual value of S_r during failure for most cases.

2.2 Laboratory Based Methods

2.2.1 Poulos, Castro and France (1985)

Poulos et al. (1985) proposed a laboratory based method for engineering assessment of in situ post-liquefaction strengths. This method was generally based upon principles of critical state soil mechanics (Casagrande, 1945; Schofield and Wroth, 1968; etc.), and it involved very carefully performed field sampling efforts as well as high quality laboratory testing.

The basic underlying principal of critical state soil mechanics is illustrated in Figure 2.1. This principle asserts that soils, when sheared, will seek to either dilate or contract depending on whether their current "state" (their current combination of void ratio and effective confining stress) is located above or below a locus of points known as the Critical State Line (CSL) in void ratio (e) vs. effective confining stress (σ_3') space. Soils above the CSL are "loose" and will exhibit contractive behavior when sheared, and soils below the CSL are "dense" and will exhibit dilatant behavior when sheared. Soils will dilate or contract until they reach a new state on the CSL, at which point further changes in void ratio and effective confining stress will cease to occur, and the soil will continue to shear at constant void ratio, constant effective confining stress, and constant shear strength. Soils that have reached the CSL, and that exhibit constant shear strength, void ratio, and effective stress are defined as having reached "critical state". Under drained shearing conditions, soils will change volume (and thus void ratio), moving vertically upwards or downwards in Figure 2.1, in order to proceed towards the CSL. Under undrained shearing conditions, soils instead exhibit either increases in pore pressure (contractive behavior) or decreases in pore pressure (dilatant behavior), resulting in equal and opposite changes in effective confining stress, and thus approach the CSL laterally as shown in Figure 2.1. Eventually all soils, if sheared sufficiently, will reach a (critical state) condition of constant shearing resistance at some point located on the CSL. The location and shape of the CSL is, of course, different for each individual soil.

Castro and Poulos (1977) and Poulos (1981) define a "steady state" wherein a soil sheared to large enough strains reaches a state of constant shearing resistance, constant effective stress, constant volume and constant strain rate. The main difference between this steady state and the previously defined critical state is the addition of the condition of constant strain rate, and it should be noted that the strain rate part of this definition is often ignored. Accordingly, the steady state and the critical state line are often analogous.

Figure 2.2 then illustrates the laboratory-based steady state method proposed by Poulos et al. (1985) for evaluation of post-liquefaction shear strengths of in situ soils based on sampling and laboratory testing. This illustrative figure shows the application of this approach to a high quality (nearly undisturbed) sample of silty sand hydraulic fill from the downstream shell of the Lower San Fernando Dam.

The first step is to obtain fully disturbed bulk samples of the in situ soils. Samples are then reconstituted in the laboratory, at different void ratios, and these are subjected to isotropically consolidated undrained (IC-U) triaxial compression tests to determine a steady state line (or critical state line) for these reconstituted samples. The resulting steady state line for the San Fernando hydraulic fill is shown by the solid line in Figure 2.2. Critical state lines, and steady state lines, are commonly plotted as void ratio vs. the logarithm of effective confining stress, and in this semi-log space steady state lines are generally approximately log-linear (or nearly so) over the range of principal engineering interest for liquefiable soils, and then they inflect downwards at higher effective stresses. The steady state line developed for these reconstituted samples is not taken directly as a basis for evaluation of in situ steady state strengths. Instead it is then used to "correct" the results of additional IC-U triaxial tests performed on a limited number of higher quality (more nearly undisturbed) samples. This "correction" addresses effects of sampling disturbance, and additional disturbance (and volume changes) that occur during sample transport, extrusion, mounting and reconsolidation prior to undrained shearing in the laboratory.

Higher quality samples are then also obtained, either by advancing sharp-edged and relatively thin-walled samplers, or by excavating a large diameter shaft and then lowering an engineer or technician into the base of the shaft to carefully hand carve a sample while slowly advancing a cylindrical sampling tube (mounted on a tripod) about the sample as it is carved. Advancing sharp-edged samplers is the more common method, and these must be pushed (not driven with hammers) to avoid vibratory densification of the soils being sampled. In either case, as samplers are advanced, the precise depth of penetration or sampler advance is closely measured. Sample recovery is carefully logged. Knowing the length of sampler advance, the radius of the cutting edge, the radius of the inside of the sampler tube, and the length of recovered sample within the tube, a calculation is then made to estimate volume (and thus void ratio) changes during sampling. When the sample is then returned to the laboratory, length is again measured, and any further volume (and void ratio) changes are calculated. When the sample is extruded and trimmed to length, and a confining membrane and top and base caps are applied, the new initial "mounted" sample height and diameter are measured and any further volume (and void ratio) changes are again recorded. Finally, additional volume (and void ratio) changes during reconsolidation are also measured. In this manner, the void ratio of the final, consolidated sample as actually subjected to undrained shearing is "known", and so is the original in situ void ratio prior to sampling.

The undrained shearing portion of the IC-U triaxial test is then performed to measure the undrained steady state strength ($S_{u,s}$) at the sample's final, laboratory consolidated void ratio. This is plotted in the lower right-hand corner of Figure 2.2 (the large, solid "square"), and it is plotted at the laboratory void ratio as tested. This laboratory value of $S_{u,s}$ is then "corrected" back to the initial in situ void ratio by assuming a correction path parallel to the steady state line developed based on testing of reconstituted samples, as shown in Figure 2.2, producing the solid "dot" in the upper left-hand corner of the figure. This assumed parallelism of the correction with the slope of the steady state line previously developed for reconstituted samples represents a major assumption, and there is no good explanation as to (1) why the steady state line for reconstituted samples is not the same as the steady state line for the higher quality samples, and (2) why the reconstituted and more nearly undisturbed steady state lines would be exactly parallel, justifying this assumption. Corrections in terms of $S_{u,s}$ tend to be very large, and any small change in the slope of the line followed in making this correction can significantly affect the final results.

The upstream slope of the Lower San Fernando Dam failed due to liquefaction that occurred during the 1971 San Fernando Earthquake, and this has been a much-studied case history. A multi-agency effort was formed in the mid-1980's to re-study this case history as one part of a two-part effort to investigate the viability and reliability of the laboratory-based steady state methodology proposed by Poulos et al. for evaluation of in situ post-liquefaction steady state strengths ($S_{u,s}$). The San Fernando Dam studies were overseen primarily by the U.S. Army Corps of Engineers. The other part of this effort was overseen primarily by the U.S. Bureau of Reclamation (USBR), and involved hiring Poulos et al. (GEI Consultants) to employ the steady state method to assess in situ $S_{u,s}$ for a number of soil zones and soil strata for five USBR dams and some of their foundation soils. This second part will be discussed further at the end of this current Section 2.1.1.

Four teams performed testing on reconstituted samples of the silty sand hydraulic fill materials from the lower portion of the downstream shell of the Lower San Fernando Dam, and one of the questions to be answered was the reliability with which different laboratories could develop similar steady state lines by this approach. Figure 2.3 shows the "consensus" steady state line developed for these studies. The four laboratories were all selected for good reputations with regard to high level testing, and these were (1) GEI Consultants, (2) the U.S. Army Corps of Engineers Waterways Experiment Station (WES), (3) Rensselaer Polytechnic University, and (4) Stanford University working jointly with U.C. Berkeley. As shown in this figure, this was difficult testing and two of the laboratories did not quite develop data that would have usefully defined in good detail the steady state line that was developed by consensus. But this element of the procedure was judged to be at least feasible (Seed, et al., 1988).

A series of IC-U triaxial tests were then performed by both the GEI and Stanford laboratories on higher quality (more nearly undisturbed) samples, and these were then corrected using the steady state procedure (assuming parallelism with the steady state line from Figure 2.3). Figure 2.4 shows the resulting corrected estimates of in situ $S_{u,s}$, and the laboratory $S_{u,s}$ values upon which they are based. This is the interpretation by Seed et al. (1988), and a slightly different interpretation was developed by Keller, et al. (1988), with one of the main differences being the amount of earthquake-induced void ratio change estimated to have occurred due to cyclic pore pressure generation and then subsequent reconsolidation after the 1971 earthquake.

Figure 2.4 illustrates several of the challenges involved in this method. The first is the very large correction from laboratory $S_{u,s}$ to the estimated field (in situ) $S_{u,s}$. Correction factors range from approximately 2.5 to more than 20, with 4 out of the 11 samples having corrections factors of greater that one full log-cycle (factors of 10 or greater). These are very large correction factors to be applying to shear strengths, especially given the unconfirmed assumption of parallelism between the steady state lines of (a) reconstituted samples, and (b) the higher quality (more nearly undisturbed) samples tested for Figure 2.4. A second problem is the wide scatter in the resulting corrected values of estimated in situ $S_{u,s}$ (the large dots in Figure 2.4), which range over more than a full log-cycle.

Back-calculated strengths for the upstream side slope failure that actually occurred due to the earthquake fall within the range of "corrected" values of in situ $S_{u,s}$ shown in Figure 2.4, but this is a large range.

A further evaluation of the potential usefulness and reliability of the steady state methodology was provided by the second part of these studies. Figure 2.5 shows the values of estimated in situ $S_{u,s}$ developed for 35 soil layers and strata at five U.S. USBR dams (Von Thun, 1986). These values of $S_{u,s}$ are plotted on the vertical axis, and the horizontal axis is the representative $N_{1,60}$ value ascribed to each of those sandy and silty soil units as a result of SPT investigations. Also shown in this figure is a shaded range proposed by Seed (1988) of $S_{u,s}$ values based on back-analyses of a number of full-scale field liquefaction failure case histories. As shown in Figure 2.5, a strong majority of the estimates of in situ $S_{u,s}$ developed by GEI using this procedure are higher than would be suggested by the empirical range suggested by Seed (1998) based on back-analyses of failure case histories.

Further laboratory investigations, and scale model tests, quickly followed and these would shed further light on some of the key issues affecting not only the original steady state methodology as proposed by Poulos et al. (1985), but also on the use of laboratory testing in broader and more general terms for evaluation of in situ post-liquefaction strength $S_{u,s}$ (or S_r).

2.2.2 Additional Laboratory Investigations and Approaches

The steady state methodology proposed by Poulos et al. (1985) led to significant further laboratory investigations, and some of these helped to clarify the likely causes of the apparently variable and often unconservative $S_{u,s}$ values developed based on the original steady state methodology. They also led to improved understanding of a number of mechanisms and factors affecting post-liquefaction strengths.

Vaid et al. (1990), Riemer and Seed (1997), and Yoshimini et al. (1998) all found that stress path (or method of shearing) affected measured $S_{u,s}$, or S_r, with triaxial compression (TXC) tests developing significantly higher $S_{u,s}$ values than either direct simple shear (DSS) tests or triaxial extension (TXE) tests. Triaxial compression is often a largely suitable mode of shearing for representing conditions at the back heel of a landslide, or the back heel of a bearing capacity failure surface. Triaxial extension generally better represents conditions at the toe of these types

of failure surfaces. And conditions across the base, or belly, of a failure surface are generally better represented by DSS. The use of TXC-based $S_{u,s}$ values can overestimate strengths and introduce systematic unconservatism. This can fixed, and the TXC tests of the original steady state procedure can be replaced with more representative tests providing a DSS-type of shearing, as is now often done.

Castro (1969) performed monotonic IC-U TXC tests on soils formed to a range of densities, and found three different types of resulting behavior based on initial density or relative density. Yoshimine and Ishihara (1998) further investigated this, and formalized a set of useful principles and nomenclature. Figure 2.6 (from Kramer, 2008) provides a simplified illustration of these findings. Sands and low plasticity silts with very low relative densities tend to follow "contractive" type undrained stress paths (and exhibit stress-strain behaviors) that lead to very low undrained residual strengths ($S_{u,s}$) at large strains. Dense soils, at the other extreme, follow "dilatant" type stress paths (and exhibit stress strain behaviors) that lead to high undrained strengths ($S_{u,s}$) at large strains. Soils of "intermediate" relative density can initially exhibit "contractive" type undrained stress paths and stress strain behaviors that consist of initial post-peak strength reduction (strain softening), but then they can experience a phase transformation to dilatant-type behavior and resulting strength increase at larger strains to a final (very large strain) undrained strength higher than the "low point" reached along the way.

The condition at which a locally minimum value of strength is observed at moderate strains (marked with a small "x" in Figure 2.6) in samples of intermediate density is increasingly referred to a "quasi-steady state" (after Alarcon-Guzman, 1988), and the values subsequently reached at very large strains can be referred to as ultimate steady state. Yoshimine and Ishihara (1993) investigated this, based on more extensive laboratory test data for a number of clean sands, and proposed four ranges of behavior based on initial relative densities from very low to high. Their resulting recommendations fit well within the behaviors shown in the simplified illustration of Figure 2.6. As shown in Figure 2.6, quasi-steady state strength can be lower than ultimate steady state strength for soils of intermediate relative density. Multiple additional investigators have now produced similar results (e.g. Yamamuri and Convert, 2001, etc.), and these behaviors are now well established. There is no full consensus as to whether ultimate steady state strength, or quasi-steady state strength, is the better engineering basis for post-liquefaction strength and modeling/analyses. Ishihara (1993) recommends in favor of quasi-steady state strength, and the authors here concur.

Another factor investigated by a number of researchers is the effect of the initial level of effective confining stress on post-liquefaction strengths observed. This issue is clouded to some extent by the question as to whether ultimate steady state strength or quasi-steady state strength should be taken as the basis. Based on the quasi-steady state basis, Riemer and Seed (1997) found that samples formed and consolidated to exactly the same post-consolidation void ratios, but at different initial effective confining stresses, and then subjected to undrained triaxial compression shearing produced higher $S_{u.s}$ values if the initial effective confining stresses were higher. This increase in $S_{u.s}$ is not linear with increase in initial confining stress, however, and the ratio of eventual steady state strength vs. initial vertical effective confining stress ($S_{u.s}$ /P) decreases with increasing initial effective confining stress.

Numerous additional laboratory investigations, and scale model experiments (both on shaking tables and on centrifuges), have now been performed and these continue to usefully illuminate many of the basic mechanics and fundamental mechanisms involved in the transition to post-liquefaction residual strengths from initial liquefaction-induced shear failures initiated either by monotonic or cyclic loading conditions.

This has not yet, however, resulted in the development of universally accepted laboratory-based approaches for evaluation of post-liquefaction strengths for in situ soils. There are two additional challenges or issues arise that continue to complicate this issue, and render the use of laboratory test data potentially unconservative with regard to determination of in situ post-liquefaction strengths for full-scale field applications. These are the phenomena of "void redistribution", and the sometimes related issue of "partial drainage".

Section 2.2.3: Void Redistribution and Partial Drainage

Void redistribution is the movement of both solid particles and also pore fluids within a soil zone of constant overall volume ("globally undrained") so that the localized void ratio (and relative density) changes occur in some portions of the overall volume of saturated material. This can produce localized changes in void ratio under monotonic and/or cyclic loading conditions thought to represent "globally" undrained shearing.

A good early discussion of this was presented by the National Research Council (1985), and Figure 2.7 shows a simplified illustration of this phenomenon from that report. In this figure, a layer of more pervious cohesionless soil is confined between less pervious overlying and underlying layers. As a result, this pervious stratum will initially behave in an "undrained" manner, with constant overall volume maintained, if loaded rapidly (e.g. by cyclic loading from an earthquake). Although this stratum is "globally" undrained, internally it will experience some rearrangements of both solids and pore fluids as cyclically generated pore pressures cause fluids to seek to escape towards the ground surface, increasing the void ratio near the top of the layer, while solids settle and void ratio decreases in the lower portions of the layer. This results in development of a looser top region up against the interface with the overlying less pervious stratum, and a slightly denser overall condition deeper within the liquefying stratum.

Minor changes in void ratio can produce significant changes in post-liquefaction steady state strength (e.g.: Figures 2.4 through 2.6). The result can therefore be significant reduction in strength at the top of the confined stratum as void ratio redistribution occurs. In extreme cases, a "blister" of water, or a water film, can develop at the top of a confined stratum, providing a potential shearing zone of essentially negligible post-liquefaction strength.

These phenomena have been observed and demonstrated in numerous laboratory model tests on both centrifuges and on shaking tables (e.g. Liu and Quio, 1984; Kokusho, 1999; Arulanandan et al., 1989; Fiegel and Kutter, 1994, etc.). The basic mechanics are generally well understood, and the observed effects in some of these model tests have been shown to be very significant. Failure surfaces have the opportunity to seek out the path of least resistance, and

when void redistribution results in a zone or sub-layer of weaker conditions the failure surface will attempt to exploit this.

This is very challenging with regard to the use of laboratory testing, and classical critical state theory (and steady state theory), to predict post-liquefaction behavior in the field. Post-liquefaction behavior will be controlled by the void ratio after void redistribution has occurred, not by the pre-event void ratio in situ. The mechanics of this void redistribution process are understood, and analytical modeling can be performed (e.g. Malvik et al., 2006), but it is not yet possible to reliably predict the amount and rate of void redistribution likely to occur in the field, and it is not yet feasible to reliably predict by analytical methods the resulting effects on post-liquefaction strengths at field scales.

It is also difficult to accurately pre-determine for most field situations the scale at which void redistribution will occur. This phenomenon occurs primarily within layered soils where some layers are less pervious and thus impede flow to dissipate excess pore pressures. Most liquefaction failures occur within alluvial sediments, hydraulic fills, poorly compacted fills placed in layers, and loess. All of these deposits are commonly layered (or sub-stratified) in a manner that lends itself to potentially adverse void redistribution effects. And these soils often have layering, and sub-layering, at variable scales.

Figure 2.8 shows a photograph of the side of one of the two investigation trenches excavated through the hydraulic fill near the base of the Lower San Fernando Dam after the dam experienced a liquefaction-induced slope failure in 1971. As shown in this photograph, the material is strongly striated (layered) with lighter colored sub-layers of sandier material and darker sub-layers of siltier soil with higher fines content. Closer inspection of any of the lighter sub-strata would reveal even smaller scale sub-layering within these sub-strata, with coarser and finer sublayers within the apparent lighter colored larger strata that are not visible at the scale of this photograph.

As explained by Seed (1987), the problem is not that laboratory testing, or critical state (and steady state) theory, do not serve to explain and characterize soil behavior. The problem is that void redistribution occurs in a manner that cannot yet be reliably well predicted, and that it produces changed conditions (that still conform to critical state and steady state theory) and it is these changed conditions that can control the overall behavior in the field. The inability to pre-determine the scale at which these void ratio distribution effects will occur, and the inability to predict the rate and severity with which these effects will occur, continues (so far) to often defeat laboratory-based efforts to deal with them for field design and performance assessments.

Void redistribution effects are naturally included in field performance case histories. These likely vary with the relative contrast in permeabilities between layers and strata, and with the scales and geometry at which this redistribution occurs, so no one individual case history can be expected to provide conclusive data regarding likely post-liquefaction strengths that can be mobilized for other sites. Accordingly, it is important to analyze observed full-scale field performance, and to back-analyze field failure case histories, for multiple field cases in order to inform efforts to evaluate likely post-liquefaction strengths for engineering analysis and design.

A second phenomenon that can be closely related is partial drainage. When pore pressure increases occur, either due to cyclic loading or due to contractive behavior under undrained monotonic loading, the resulting pore pressures begin to dissipate by means of flow away from the area of elevated pore pressure. Intuitively, this dissipation of pore pressures is a positive thing as it serves to re-establish higher effective stresses and thus higher shear strengths. But as the fluids travel, they can be temporarily impeded at less pervious boundaries, and this can result in a localized build-up in pore pressure, resulting in a second type of void redistribution that can occur over a larger time scale than the more localized type of void redistribution illustrated in Figure 2.7. Partial dissipation of pore pressures, or ongoing dissipation in progress, can thus also potentially serve to locally exacerbate void redistribution effects.

2.3 Empirical and Semi-Empirical Methods

2.3.1 Seed (1987) and Seed and Harder (1990)

The late Prof. H. Bolton Seed developed a several evolving proposed correlations between S_r values back-calculated from liquefaction failure case histories and SPT penetration resistance during the mid-1980's, and these culminated in the relationship proposed in Seed (1987). This relationship is presented in Figure 2.9.

This 1987 paper presented an excellent overview of many of the challenges in evaluating post-liquefaction strength S_r, and it also presented this proposed empirical relationship which Prof. Seed describe as a "tentative" relationship. Immediately after the paper had been published, it was pointed out that one of the twelve case histories back-analyzed had been plotted with S_r values based on pre-failure geometries, which would have provided an unconservative assessment of the likely actual S_r value. Based on an assumption that momentum effects were minor, the Lower San Fernando Dam case is plotted too high in Figure 2.9; with $S_r \approx 750$ lbs/ft^2 and $N_{1,60,CS} = 15$ blows/ft. Prof. Seed subsequently determined this to be an error, but was too ill with the cancer that would shortly take his life to repair it. So his son, and a recent former doctoral student, jointly undertook to posthumously correct this error. The resulting modified relationship was published by Seed and Harder (1990), and it was published in an unusual venue; appearing in the Proceedings of the late Prof. Seed's Memorial Symposium rather than in the ASCE geotechnical journal. Both Seed and Harder had previously been involved in earlier stages of development of some of the case histories involved. They re-evaluated the 12 cases originally presented in Seed (1987), and they added five additional cases to bring the total number of cases to seventeen.

Figure 2.10 shows the resulting revised correlation between post-liquefaction strength S_r and corrected $N_{1,60,CS}$ values of Seed and Harder (1990), with a reduced value of S_r for the Lower San Fernando Dam failure case history, and with additional case histories added.

Back-analysis methods were not yet well-established at this time, so a variety of approaches and assumptions were applied to various cases within this limited suite of available case histories. Many of the "smaller" cases involving embankments and slopes of modest height, and with low values of $N_{1,60,CS}$, were analyzed with relatively approximate methods. The Upper San Fernando Dam case history was a non-failure case history, and assessment of the likely value

of S_r for this case was based on the value having been higher than that for which a major flow-type failure would have occurred, with some additional judgment as to likely cyclic inertial effects. Three of the largest failures were the Calaveras dam, the Upper San Fernando Dam and the Fort Peck Dam, and Seed and Harder approximately incorporated "inertial" effects (momentum effects) in the back-analyses of these two cases by selecting S_r values between the values that would have been calculated as $S_{r,yield}$ for pre-failure geometry, and $S_{r,resid/geom}$ for post-failure residual geometry. Davis et al. (1988) were also performing back-analyses during this same period, and their method for more explicitly incorporating inertial effects produced values between $S_{r,yield}$ and $S_{r,resid/geom}$. Seed and Harder were aware that their estimates would be reasonable approximations of S_r with inertial effects included.

The S_r values of Seed (1988) and Seed and Harder (1990) were plotted as a function of procedurally corrected, overburden corrected, and fines adjusted $N_{1,60,CS}$ values. The fines adjustment proposed by Seed (1987) differed slightly from that of contemporary SPT-based liquefaction triggering correlations, and was as follows:

$$(N_1)_{60\text{-}CS} = (N_1)_{60} + \Delta(N_1)_{60} \qquad \text{[Eq. 2-1]}$$

where $\Delta(N_1)_{60}$ was the fines adjustment, which was a function of fines content as

Fines Content (%)	SPT Correction, $\Delta(N_1)_{60}$ in blows/ft
0	0
10	1
25	2
50	4
75	5

Seed and Harder (1990) employed the same fines adjustment.

Figure 2.11 repeats the base figure of Figure 2.10, but this time adds the result of a least squares regression performed as part of these current studies. The resulting R^2 value of $R^2 = 0.64$ indicates a moderately good fit.

Idriss (1998) would go on to employ the same suite of 17 failure case histories to develop an additional proposed relationship. He "re-interpreted" the case history database of Seed and Harder (1990), but in fact employed the same S_r values as proposed by Seed and Harder for all 17 cases. He did modify selection of "representative" $(N_1)_{60}$ values to formally employ median values, but the values plotted did not visibly change as Seed and Harder had previously done largely the same. He then presented a single central curve fitting the data, as shown in Figure 2.12, rather than the upper and lower bounds as proposed by Seed and Harder (1990), and extended this curve beyond the upper bound of the available data with a dashed line that presumably indicates extrapolation beyond the range of the available data. This curve fits neatly between the upper and lower bounding curves proposed by Seed and Harder (1990) as presented in Figure 2.10, and is largely parallel to these upper and lower bounding curves but at a location slightly below the mid-

point between the bounding curves of Seed and Harder. It is also similar to the least squares fit line of Figure 2.11, but is slightly lower at $(N_1)_{60\text{-}CS}$ values of about 7 to 12 blows/ft.

2.3.2 Stark and Mesri (1992)

Stark and Mesri examined the available data, and concluded that post-liquefaction strength S_r was likely linearly dependent upon initial vertical effective stress ($\sigma_{v,i}'$). They took the S_r values back-calculated by Seed and Harder (1990), and added three additional case histories. They calculated average initial effective vertical stress along the eventual failure surface for each case, and developed ratios of S_r/P where P = initial effective vertical effective stress within liquefiable materials on the failure plane. Their resulting relationship was the first to express post-liquefaction strength in terms of liquefied "strength ratio" (S_r/P). This relationship is shown in Figure 2.13.

This relationship proposed by Stark and Mesri (1992) established a second "school of thought", and set up a contrast between empirical relationships based (1) on classical critical state theory wherein post-liquefaction strength (S_r) would be expected to be constant for any given relative density, as with the Seed and Harder (1990) relationship, and (2) relationships based on assumed constant strength ratio (S_r/P) in a manner somewhat analogous to the framework of SHANSEP for clays.

This led to some debate within the profession, but it was never a serious issue. It was clear early on that the best answer likely lay between these two points of view. In the end, in these current studies, that turns out to be the case.

A series of nonlinear least squares regressions were performed on the data from Stark and Mesri (1992). A second order polynomial curve was fit to the data, but the inflection was a slight downward curvature with increasing penetration resistance. The resulting R^2 value was $R^2 \approx 0.22$. Because the curvature of the initial regression was slightly downwards, and the associated regressed quadratic coefficient was very close to zero, a linear fit was next investigated. This also resulting in a value of $R^2 \approx 0.22$, as shown in Figure 2.14. Second order polynomial curves with a positive quadratic coefficient were then also imposed on the data, but resulting R^2 values were very low. A curve that approximately represented the median line recommended by Stark and Mesri was then imposed, and manual calculations showed that this resulted in a value of $R^2 = 0.12$. These results suggest that the data is poorly behaved (randomly scattered) and that the regression is not well able to provide a good predictive "fit", especially when compared to the correlation bounds proposed in Stark and Mesri (1992).

This does not mean, however, that there is no merit to their suggestion of a strong relationship between S_r and initial effective stress, and the results of these current studies will in fact result in findings that suggest that initial in situ vertical effective stresses do indeed significantly affect S_r (see Chapter 5). It simply suggests that the data as plotted in Figures 2.13 and 2.14 do not support well-defined relationship between penetration resistance and post-liquefaction strength as plotted.

2.3.3 Ishihara (1993)

Prof. Ishihara developed a multi-step procedure based on extensive laboratory test data for estimation of post-liquefaction strength S_r as a function of SPT penetration resistance. The data were developed for a number of Japanese sands, and were of high quality. As discussed previously in Section 2.2.2, Prof. Ishihara preferred to use quasi-steady state strength rather than ultimate steady state strength, and so targeted this approach accordingly. Prof. Ishihara noted a clear dependence of $S_{u,s}$ on initial effective confining stress. He suggested that while there is a clear dependence here, it is a different relationship for different sands. His approach was based on an assumed log-linear relationship between void ratio (e) and logarithm of effective vertical stress (σ_v') for steady state lines, and he characterized the slopes of the quasi-steady state lines in e vs. log σ' space based on indices derived from the laboratory data for each of several well-characterized clean sands. SPT $(N_1)_{60}$ values were also inferred for each sand as a function of density (void ratio) and effective overburden stress.

He then compared the resulting relationships between quasi-steady state strength against the values of strength ratio calculated by Stark and Mesri (1992), with an adjustment of $(N_1)_{60}$ values to conform with Japanese standards of practice with regard to SPT equipment and procedures. Figure 2.15 shows the proposed relationships for several test sands, and a comparison with the values of strength ratio calculated by Stark and Mesri. As shown in this figure, the relationships developed appear to provide unreasonably steep curves of strength ratio vs. $(N_1)_{60}$, when compared to the relationships developed based on back-analyses of field case histories by most other investigators, including Seed and Harder (1990), Stark and Mesri (1992), Idriss (1998), Olsen and Stark (2002), Kramer (2008) and these current studies.

The reasons for this are not fully clear, but it is noted that this procedure assumes a log-linear relationship for the slope of the quasi-steady state line, which may not be valid at the low densities (high void ratios) of principal interest here, and that the high quality laboratory data sets employed did not include potential full scale "field" effects such as void redistribution, partial drainage, and inter-layer mixing as shearing occurs along interfaces between soil layers. It is also interesting to note, however, that Wride et al. (1999) subsequently developed a proposed relationship between $(N_1)_{60\text{-}CS}$ and S_r based on back-analyses of liquefaction failure case histories, but employing "reasonable lower bound" values of $(N_1)_{60}$ as being "representative" based on the assumption that the weakest strata would control the failures. Their resulting relationship between post-liquefaction strength ratio (S_r/P) and $(N_1)_{60}$ has a form much like that of Ishihara, with steeply rising values of S_r/P at relatively low $(N_1)_{60}$ values (see Section 2.3.5).

2.3.4 Konrad and Watts (1995)

Konrad and Watts proposed a method for estimation of post-liquefaction strength S_r as a function of SPT penetration resistance that was based on a theoretical framework based on critical state soil mechanics. This framework was then calibrated based on a limited number of back-analyzed failure case histories. As with Ishihara (1993), this methodology assumed a series of log-linear relationships, including a log-linear slope of the steady state line, but an additional calibration factor χ was then developed based on back-analyses of five large displacement

liquefaction failure case histories. Figure 2.16 shows the estimated relationship between this calibration factor χ and the slope of the steady state line (λ) based on the five field case histories. Three of the five case histories are represented with two points each in this figure, reflecting the ranges of values employed.

This was a "hybrid" method, involving both an empirically-based calibration factor based on S_r values back-calculated from previous field failure case histories, and also laboratory tests for the specific soil of interest for a given project. A four step procedure was employed. Step 1 was site characterization by means of SPT. The fines adjustment of Seed (1987) was employed here. Step 2 was the performance of laboratory tests to ascertain the maximum void ratio (e_{max}) and the slope (λ) of the steady state line. Step 3 was the estimation of χ based on the relationship shown in Figure 2.12. Step 4 was then the estimation of mobilized shear strength (S_r) based on (1) the laboratory determined value of shear strength at e_{max}, (2) the slope (λ) of the laboratory determined steady state line, and (3) the calibration factor χ.

Konrad and Watts reportedly employed this procedure to successfully predict cases of failure and non-failure of artificial sand fills (islands) constructed in the Beaufort Sea for petroleum exploration. This procedure was apparently effective in estimating values of S_r for newly created loose sand fills, but there are a number of important assumptions involved (e.g. a log-linear slope of the steady state line). Additional potential drawbacks of this procedure include the need to accurately determine the slope of the steady state line, the assumption that laboratory-based tests will correctly determine the steady state line for field placement conditions, and the neglect of potential void redistribution effects, etc. in the field.

2.3.5 Wride, McRoberts and Robertson (1999)

Wride et al. (1999) performed a thoughtful review of 20 liquefaction failure case histories that were available and being back-analyzed and used for development of one or more empirical relationships between penetration resistance and either post-liquefaction strength or post-liquefaction strength ratio. This was a paper that warranted more attention than it received.

Wride et al. studied all 20 cases, and eliminated the Lake Merced bank case from their data set. The remaining 19 cases were then examined in a number of ways and were characterized as to mode of failure, method of initiation of failure, and failure mass runout characteristics (various measures of eventual displacement or runout distances, some of them normalized vs. slope height). A number of useful insights were developed as a result of this exercise. Having learned some important lessons from this, indices regarding failure and displacement modes, and runout characteristics, are also developed and employed in these current studies.

Wride et al. then re-evaluated the "representative" $(N_1)_{60}$ values being used to characterize the 19 failure case histories of interest. They took an approach that had been discussed, but not employed, before. It was their view (widely shared) that failure surfaces would tend to seek out and follow weak spots and weak sub-strata, and that it might be more reasonable to use a much lower than mean or median value of penetration resistance to characterize the failure zones controlling displacements and deformations. This was analogous to the "weakest-link-in-the

chain" argument of Fear and McRoberts (1995) with regard to triggering or initiation of these types of failures. Based on the work of Popescu et al. (1997) regarding effects of spatial variability on soil liquefaction, Yoshimine et al. (1999) had recommended the use of a 20^{th} percentile value (20% of the measured penetration resistances are lower) for CPT tip resistance data for liquefaction studies. Wride et al. took a similar view, and targeted a "reasonable lower bound" which, in practice, was either the lowest value measured for cases where penetration data were sparse, or the near lower bound when more data were available.

There is less explanation and discussion presented regarding selection of representative post-liquefaction strengths for each of the 19 case histories considered. Values of S_r developed by previous investigators were collected and tabulated, and the values then selected as best estimates for each case history are tabulated and presented as well. The most useful comment in the text of the paper regarding the basis for selection of representative S_r values for each case is to note that "When possible, the value of S_u was selected as one which incorporated energy effects (Poulos, 1988; Davis et al. 1988) as this was felt to be closer to the "true" value of S_u". On balance, the values of S_u (or S_r) selected appear reasonable.

Figures 2.17 and 2.18 present the resulting data points for the 19 case histories re-evaluated, and also a number of relationships developed by previous investigators for comparison. It should be noted that most previous investigators did not take a near lower bound approach to estimation of $(N_1)_{60\text{-}CS}$.

Figure 2.17 shows data points plotted as post-liquefaction strength (S_u) vs. "reasonable minimum" $(N_1)_{60\text{-}CS}$ as developed by Wride et al. (1999). The range proposed by Seed and Harder (1990) is shown, and so is the additional (more steeply rising) range proposed by Konrad and Watts (1995) for Kogyuk and Erksak sands. Also shown are (1) the lower bound relationship proposed by Ishihara (1993), (2) the relationship proposed by Yoshimine et al. (1999) for triggering of flow slides, and (3) an additional material-specific relationship developed by Wride et al. (1995) for Ottawa sand based on laboratory testing and CPT data.

Figure 2.18 shows data points plotted as post-liquefaction strength ratio (S_u/P) vs. minimum $(N_1)_{60\text{-}CS}$ as developed by Wride et al. The range proposed by Stark and Mesri (1992) is shown, and so is the additional (more steeply rising) range proposed by Konrad and Watts (1995) for Kogyuk and Erksak sands. Also shown are (1) the lower bound relationship proposed by Ishihara (1993), (2) the relationship proposed by Yoshimine et al. (1999) for triggering of flow slides, and (3) an additional material-specific relationship developed by Wride et al. (1995) for Ottawa sand based on laboratory testing and CPT data.

In both of these figures, data points for cases where there is especially high uncertainty (or variance) with regard to SPT N-values are highlighted by open symbols around the solid symbols.

In examining these figures, it appears that the available data, as interpreted by Wride et al. (1999), could be construed as supporting, or at least partially supporting, any of the previous relationships shown, especially given that some of the relationships did not employ near lower bound assessments of penetration resistance. This served to illustrate the importance of being clear on the basis for development of empirical relationships for estimation of in situ S_r, and it also

suggests the potential validity of near lower bound strengths (and associated penetration resistances) asserting some measure of control over field failure outcomes.

2.3.6 Olsen (2001) and Olsen and Stark (2002)

Olsen and Stark performed studies to develop their own evaluations of post-liquefaction strengths for an expanded suite of 33 field failure case histories. Olsen employed an adapted version of the methodology of Davis et al. (1988) to account for the "kinetics" of flow failures (i.e. momentum effects), and applied this to 10 of the field failure case histories for which it was judged that sufficient information and data were available, in order to develop new estimates of S_r that explicitly included consideration of momentum effects. For the remaining 23 cases, new estimates of S_r were developed based either on simplified analyses, or on back-analyses of the post-failure residual geometry with an assumed Factor of Safety equal to 1.0. The simplified analyses appear to have been somewhat conservative, as would be appropriate for simplified analyses, and the back-analyzed residual geometry analyses resulted in calculated values that represent $S_{r,resid/geom}$, and they therefore significantly underestimated the actual values of S_r for these cases.

The analytical approach employed to incorporate "kinetic" effects (momentum and inertia) in analyses of 10 of the best-documented case histories was adapted, with some modifications, from the approach proposed by Davis et al. (1988) as illustrated schematically in Figure 2.19. Davis et al, proposed that a displacing failure mass would initially accelerate downslope, accumulating increasing velocity and momentum, and then it would decelerate, with reducing velocity and momentum until it finally came to rest. With simplifying assumptions, it is then possible to track the progressive development and dissipation of acceleration, velocity, displacement, and momentum of the center of gravity.

Davis et al. (1988) also postulated that at some point between start and finish there would be a transition from acceleration to deceleration, and that there would be no net shear force transfer of inertial force to the base of the moving slide mass (which would be at peak displacement velocity) at that moment. That, in turn, means that at this intermediate displacement condition (at the moment of transition from acceleration to deceleration) when there is zero inertial force, a static stability analysis can be performed to calculate S_r directly, and the resulting value would correctly incorporate inertial effects. There is, however, significant difficulty and subjective judgment involved in ascertaining the likely geometry of the failing slope at this moment of transition. As a result, Seed and Harder (1990) preferred to calculate the "apparent" $S_{r,yield}$ for the pre-failure geometry, and the "apparent" $S_{r,resid/geom}$ for the final, residual (post-failure) geometry, and then adopt a value of S_r between these two as the best estimate of S_r with consideration of inertial forces (momentum). Wang (2003) and Kramer (2008) chose, instead, to attempt to infer the geometry (displaced cross-section) of this intermediate transitional condition with zero inertial force (ZIF), giving rise to their "ZIF method" for back-analyses incorporating inertial effects as will be discussed in Section 2.3.7. And in these current studies, a new method is presented that incrementally tracks the evolving displaced geometry and uses this as the basis for a progressive analysis that incorporates inertial effects (momentum) in back-calculation of S_r from failure case histories.

Olsen elected to perform a full progressive inertial analysis tracking the evolution of acceleration, velocity and displacement of the center of gravity of the failure mass. Olsen's analysis procedure is illustrated schematically (for the Wachusett dam case history) in Figure 2.20.

The first step was to determine the initial and final locations of the center of gravity for the full failure mass, as shown at the top of Figure 2.20.

A third order polynomial function was then fitted to approximate the progressive locus of points through which the center of gravity would then be assumed to travel from inception of failure to post-failure residual geometry. It was important that this polynomial function produced a "curve" parallel to the average curvature of the overall sliding surface, or at least with a localized slope parallel to the average slope of the overall sliding surface associated with each successive position of the overall (field) sliding surface, as best this could be estimated.

Driving forces in the downslope direction (tangent to the polynomial curve) at any displaced location of the center of gravity were taken as the weight of the overall failure mass multiplied by $\sin\Theta$, where Θ is the slope at any point on the polynomial curve. As a result, it was actually important that this slope of the polynomial curve result in a good approximation of the total downslope driving shear stresses in the field at any displaced location of the center of gravity. The current investigation team have performed a number of these analyses for selected cases to assess this approach, and the difficulty involved here in achieving this is a significant challenge.

A single strength S_r was reportedly assigned along the failure surface in the full scale cross-section, and the shear strength along the failure plane multiplied by the length of the failure plane was then calculated and used as the resisting (upslope) force acting on the center of gravity in a direction tangent to the sliding surface of the polynomial curve. Comparing upslope vs. downslope forces at each point in time, any force imbalance was then applied to create acceleration (a) based on Newton's second law ($F = M \bullet a$). The system was then solved incrementally using a time-step algorithm to calculate progressive changes in accruing and dissipating acceleration, velocity and displacement of the center of gravity.

The value of S_r employed was iteratively adjusted until the calculated final displacement of the center of gravity of the failure mass equaled the observed displacement of this center of gravity in the field failure. At that point, the post-liquefaction strength along the actual lengths of the failure surface controlled by liquefiable materials was reportedly adjusted to account for strengths of non-liquefied materials based on Equation 2-2 as

$$S_u(LIQ) = \frac{S_u - \left(\frac{L_d}{100} \cdot S_d\right)}{\left(1 - \frac{L_d}{100}\right)} \qquad \text{[Eq. 2-2]}$$

in which the overall average shear strength along the failure plane is sub-partitioned into (a) S_r for the lengths of the failure plane controlled by post-liquefaction strengths, and (b) S_d for the portions of the failure plane controlled by non-liquefied materials.

This conforms to the description and explanation presented in Olsen (2001), but it appears that Olsen actually did a better and more clever job than this with these analyses. Failure plane lengths and geometries, and the sub-sections of the failure plane controlled by liquefied and non-liquefied materials, change progressively as failure displacements accrue. Olsen also modeled reduced shear strength at the base of portions of the toe of the failure mass that entered into water to account for potential hydroplaning effects. And Olsen also accounted for progressive buoyancy increase as failure masses entered into bodies of water. Each of these effects would likely have been progressively adjusted as failure movements progressed, and that would have involved a far more detailed, tedious, and time consuming analytical effort than is suggested by Equation 2-2.

Examining a number of the calculated plots of shear strength mobilized along the failure plane (e.g. the one near the top of Figure 2.16) in Olsen's dissertation, it is clear that overall shear strength along the failure plane progressively changes as the failure displacements proceed. This suggests that an even more correct analysis was performed which included progressively implementing some level of changes in conditions and geometry as displacements progressed.

Olsen assigned reduced shear strengths (50% reduction) for soils that travelled beyond the initial toe of a slope and entered into a reservoir to account for potential hydroplaning effects, and then allowed this to vary from 0% to 100% for subsequent parameter sensitivity studies. He did not explicitly discuss potential sliding along the top of weak reservoir sediments, or weak offshore slope sediments, beneath the advancing toe of the failure, but his approximation of 50% strength reduction is reasonable for both situations. Wang (2003), and these current studies, each take different approaches on these issues (hydroplaning and potentially weak reservoir sediments), but it should be noted that Olsen's modeling approach was also reasonable here.

Figure 2.20 shows an example calculation for the Wachusett Dam failure case history. The top of the figure shows the shape of the selected polynomial curve along which the center of gravity of the overall failure mass is assumed to slide. The next four figures below show the evolution (vs. time) of: (1) total shear resistance along the field failure surface, (2) acceleration (and then deceleration) of the center of gravity, (3) velocity of the center of gravity (which eventually drops back to zero), and (4) accumulated displacements of the center of gravity.

Figure 2.21 shows another illustration of this analytical procedure, this time for the upstream slope failure of the Lower San Fernando Dam. The top figure shows the pre-failure and post failure geometries, and also the pre-failure and post-failure positions of the center of gravity of the overall failure mass, and the shape of the curved (polynomial) curve along which the sliding of the center of gravity was calculated. The four figures below show (1) total shear strength vs. time along the failure surface, (2) acceleration vs. time of the center of gravity of the overall failure mass, (3) velocity vs. time of the center of gravity, and (4) displacement vs. time of the center of gravity.

There are a number of challenges and drawbacks to this analytical approach by Olsen's kinetics method.

One of these is potential sensitivity of the calculations to the selected shape of the polynomial curve along which the center of gravity slides, and the concurrent difficulty of suitably

modelling a slope that approximates the overall "driving" shear stresses along the actual (full scale) field failure plane at each successive stage of calculated displacement of the center of gravity. Simply aiming at being largely "parallel" to the overall failure surface is not sufficient here; it is the sum total of driving shear stresses in the field (associated with field conditions and geometry) that should match well with the driving shear stresses resulting from the modeling of the slope of the curved path along which the center of gravity slides, and at each successive step of development of displacements.

Another challenge is the fact that non-liquefied soils routinely had to be modeled with fully drained frictional shear strengths, so that S_d was a function of effective normal stresses on those portions of the field failure plane. This is difficult to implement in the framework as described by Olsen (2001) because effective normal stresses (and geometry) would have been changing as movements occurred.

A similar challenge would have been the modeling of shear strengths along portions of the field failure surface where two different soil materials progressively come into contact as the failure movements progress. Ideally, the weaker of the two materials should control shear strength over portions of the failure surface where two different materials progressively come into contact.

Finally, it appears that several of the failure case histories may have been incrementally progressive failures, with initial failures (or failure "slices") initially occurring close to the front of the eventual overall failure mass, followed by retrogressive development of additional slices farther from the front face, with each successive slice sequentially beginning to initiate its own displacements as it becomes partially unbraced due to movements of the preceding slice(s), until the failure surface eventually reaches the back heel of the final, overall failure. This would be tremendously difficult to model with the simplified kinetics approach.

In the face of all of these challenges, it should also be noted that the overall value of S_r calculated is well "bounded" for these analyses. As observed by Davis et al. (1988), assessment of the initial yield stress ($S_{r,yield}$) required within liquefiable materials to provide a calculated Factor of Safety equal to 1.0 will necessarily overestimate the actual value of S_r, because otherwise large displacements would not have occurred. Similarly, assessment of the "apparent" value of $S_{r,resid/geom}$ required within liquefied soils to provide a calculated Factor of Safety equal to 1.0 for the eventual post-failure residual geometry will significantly underestimate the actual value of S_r as it fails to account for momentum effects as the moving slide mass must be brought to rest. So a finite range of possible values of S_r would be between $S_{r,yield}$ and $S_{r,resid/geom}$. If the initial slope of the polynomial curve along which the center of gravity of the failure mass will slide is "set" so as to provide the correct initial (pre-failure) overall driving shear stresses, and the final slope of the polynomial curve is "set" so as to provide the correct final (post-failure, residual) overall driving shear stresses, then values of S_r calculated by this type of kinetics approach would naturally fall within this finite range. With better modeling, and judgment, significantly better answers could be expected.

And Olsen appears to have executed excellent kinetics analyses, and with good judgment. His calculated values of S_r for nine of the ten case histories to which this kinetics analysis method was applied produced values of S_r in generally good agreement with the values subsequently

calculated employing other methods by (1) Wang and Kramer (2003, 2008) and (2) these current studies. For the other case (Shibecha Cho embankment) Olsen's back-calculated value of S_r was significantly lower than those subsequently calculated by Wang & Kramer, and by these current studies. Based on the cross-sections and explanations of Olsen's analysis for this case, the Shibeca-Cho failure was modeled as a progressively incremental failure, but only the movements of the first failure slice (near the front face of the failure) were tracked by the kinetics analysis performed. This points up the difficulty of applying the simplified "kinetics" analysis approach to analysis of these types of incrementally progressive failures.

Overall, Olsen's back-calculated values of S_r for the ten cases that he analyzed using the kinetics method to account for momentum effects appear to have produced generally good answers.

There were then 23 additional ("lesser") case histories for which Olsen judged that there were insufficient information and data available as to justify the full incrementally progressive kinetics analysis approach. For 11 of these cases, "simplified" analyses, or estimates, were employed to assess values of S_r. These were approximate approaches, and so they were (appropriately) conservatively implemented and tended to produce conservative estimates of S_r. For the other 12 cases, the apparent post liquefaction strength ($S_{r,resid/geom}$) required to provide a calculated static Factor of Safety equal to 1.0 for residual post-failure geometry and conditions was calculated, and this was then taken as the value of S_r. As discussed previously, and as demonstrated later in Chapter 4, this use of $S_{r,resid/geom}$ was very conservative and would have significantly underestimated the actual values of S_r because it neglected to account for the effects of momentum as the moving failure masses had to be decelerated back to zero velocity at the end of slide movements.

As a result of these conservative approaches taken to the back-analyses of these 23 less-well defined and less-well characterized case histories, there was then a disparity between the S_r values calculated for the 23 lesser cases and the remaining 10 cases to which the higher order kinetics analysis approach had been applied. The 23 lesser cases had overly conservative (low) values of S_r, and the 10 kinetics cases had what tended to be more accurate (higher) values. The two sets of cases were essentially analyzed on very different bases, and the disparity in bias (or level of conservatism) of estimated S_r values served to obscure trends when the data were subsequently plotted jointly as a function of penetration resistance.

Olsen then calculated average values of effective initial vertical effective stress along portions of the eventual plane occupied by liquefiable materials, and the S_r values determined for the full 33 case histories were divided by the effective vertical stresses to produce back-calculated values of post-liquefaction strength ratio (S_r/P) for each case.

Representative values of $(N_1)_{60}$ were also developed for each case. It was the position of Olsen, and of Olsen and Stark, that the fines adjustment proposed by Seed (1987) was not well founded, and they elected to apply no fines adjustment and so the values employed were $(N_1)_{60}$ values rather than $(N_1)_{60,CS}$ values. That was unfortunate, because a large number of the 33 case histories analyzed had liquefiable soils that were comprised mainly of silty sands and sandy silts, and those materials likely warranted significant fines adjustments. So the lack of a fines

adjustment may have biased the representations of some of the penetration resistances for this particular data set.

Figure 2.22 shows the overall relationship recommended by Olsen and Stark (2002) for estimation of post-liquefaction strength ratio as a function of $(N_1)_{60}$, along with the data pints from the 33 back-analyzed case histories. The two solid lines show the recommended range, and the heavy dashed line between these is the center of this range.

The recommended range and best estimate relationship proposed represents some degree of engineering judgment, because it does not well match the slope of the overall trend of the data presented. A least squares regression was performed as part of these current studies, and the results are presented as Figure 2.23. As shown in this figure, the actual slope of the regressed relationship is somewhat flatter than the recommended relationship, and the calculated R^2 value ($R^2 = 0.23$) indicates that the data is poorly behaved (randomly scattered) and that the regression is not well able to provide a good predictive "fit".

The recommended relationship is likely conservatively biased overall, due in large part to the conservative underestimation of S_r for the 23 back-analyzed case histories that were evaluated on an overly conservative basis as discussed previously. The lack of a clearly discernable strong trend between Sr and $(N_1)_{60}$ in Figures 2.22 and 2.23 appears to have three main causes. The first of these is the disparity in average level of conservatism between the S_r values calculated for 10 case histories based on the kinetics back-analysis approach, and the far more conservatively biased S_r values calculated for the remaining 23 cases, as discussed previously. A second contributing cause may have been the lack of an applied fines adjustment for the SPT penetration resistances. A third cause was the assumption that ratios of S_r/P would not vary as a function of effective overburden stress.

It is interesting to note that Olsen had also calculated the initial post-liquefaction yield stress ($S_{r,yield}$) for each of his 33 case histories, and had also calculated the "apparent" post-liquefaction residual strength based on residual post-failure geometry ($S_{r,resid/geom}$) for all 33 cases. As demonstrated in Chapter 5, averaging these two values (simply adding then together and then dividing by two) might have been expected to produce significantly better estimates of the actual S_r values for the 23 case histories not back-analyzed by the higher-order kinetics method.

Finally, it should be noted that Olsen's work was a significant milestone achievement in its day. Those were turbulent times, rife with discussion and debate. Olsen made two important contributions that were likely not fully appreciated at the time. The first of these was the level of detail and transparency with which he documented his analyses (the assumptions, procedures, cross-sections, properties, failure surfaces analyzed, etc.) This had no similar precedent, and no subsequent study has been as well documented either. One of the objectives of these current studies is to set a similarly high standard for documentation and transparency as well.

A second important contribution was that he calculated $S_{r,yield}$ and also $S_{r,resid/geom}$ for all 33 of his case histories. Because the analyses were so well documented, the details of these calculations are well understood. Now, 14 years later, these values turn out to be an important piece of the overall puzzle, and good use is now made of them in these current studies.

2.3.7 Wang (2003) and Kramer (2008)

Wang (2003) examined the case histories that had been used by previous investigators, and developed his own estimates of the key indices (S_r, $N_{1,60,CS}$ and $\sigma'_{v,i}$) that would eventually be employed to develop new probabilistic relationships for SPT-based assessment of in situ post-liquefaction strengths (Kramer, 2008).

As a first step, he examined and vetted case histories of small to moderate displacement (e.g. most of the lateral spreading case histories) and compared observed displacements against the values that would be predicted by the empirical relationship for lateral spreads developed by Youd et al. (2002). Cases where the observed displacements were not significantly greater than predicted by the relationship of Youd et al. were deleted from further study, because it was assumed that cyclic inertial forces were a significant contributor to observed displacements, and current analytical methods do not yet permit very accurate assessment of S_r based on back-analyses of such cases.

The remaining 31 cases were then examined more closely, and were back-analyzed to develop estimates of the three indices (S_r, $N_{1,60,CS}$ and $\sigma'_{v,i}$), and also assessments of uncertainty or variance associated with these estimates.

The nine highest quality case histories were back-analyzed using a new methodology that Wang developed that will be referred to here as the zero inertial factor (or ZIF) method. This was based on the observation by Davis et al. (1988), as described previously and illustrated in Figure 2.19, that a slide mass moving downslope initially accelerates, and then decelerates and comes to rest. Davis et al. further postulated that at some point between start and finish there would be a transition from acceleration to deceleration, and that there would be no net shear transfer of inertial force to the base of the moving slide mass (which would be at peak displacement velocity) at that moment. That, in turn, means that at this intermediate displacement condition (at the moment of transition from acceleration to deceleration) when there is zero inertial force transfer, a static stability analysis can be performed to calculate S_r directly, and the resulting value would correctly incorporate inertial effects.

Wang elected to attempt to estimate or infer the displaced position and geometry (displaced cross-section) corresponding to this transitional moment of zero inertial force. The fraction of eventual overall (final) displacement required to reach this transitional displaced cross-section geometry was termed the zero inertial factor (or ZIF). Once this ZIF had been estimated, the pre-failure geometry was then judgmentally transitioned part-way towards the final displaced (post-failure) geometry in proportion to this ZIF. Static limit equilibrium stability analyses were then performed using this ZIF cross-section to back-solve for the post-liquefaction strength needed to provide a static Factor of Safety equal to 1.0 at this ZIF displacement geometry.

The estimation or inference of the likely displaced (and deformed) cross-section geometry at this ZIF moment for any given geometry is very challenging. One cannot simply assume a displaced condition exactly mid-way between the initial geometry and location and the final residual geometry and location, in part because the ZIF transition from overall acceleration to overall deceleration appears to occur before half of the overall displacements have occurred due

to progressive diminishment of driving static shear stresses as the failure progresses and the slope "flattens". This is clearly illustrated in the "kinetics" analyses performed by Olsen (2001), and also in the incremental inertial analyses performed for these current studies as described in Chapters 3 and 4, and as presented in Appendix A.

The difficulties involved in estimating this displaced geometry at the transitional moment were recognized by Wang (and Kramer) who explained that the approach taken was to begin by examining the pre-failure and post-failure geometries (cross-sections) for selected, well-characterized case histories. Then the kinetics displacement analyses performed by Olsen (2001) for these cases were examined to determine what fraction of overall (final) displacement, or ZIF, that appeared to correspond to the point of transition from acceleration to deceleration of the overall failure mass. A number of "points" on the pre-failure cross-section were then selected, and these were partially displaced towards the final (post-failure cross-section) geometry in approximately the estimated proportion required. This was used to create an approximate cross-section, and this was then iteratively refined to develop a cross-section that was reasonable based on considerations of soil mechanics, the materials and geometries involved, the inferred failure mechanism and mechanics, and the observed pre-failure and post-failure cross-sections. This was an iterative process, requiring both art and judgment.

Wang (2001) provided a single illustration of this process, for the Wachusett Dam failure case history. Figure 2.24(a) shows points selected on the pre-failure cross-section (solid line) and connected locations of the same points on the post-failure cross-section (dashed cross-section). For this case, Olsen estimated that the ZIF was 43.3%, so 43.3% of the displacements from initial to final locations of the points selected, and the resulting initial estimates of the locations of these points on the zero inertial geometry in Figure 2.24(a) were then the initial best estimates of the locations of those points for the ZIF cross-section. This was then artfully modified, allowing for curved paths between initial and ZIF locations of selected points, in a manner judged to be consistent with soil mechanics and the inferred failure mechanism. The resulting eventual ZIF displaced cross-section for the Wachusett Dam that was analyzed by means of static limit equilibrium methods is then shown in Figure 2.24(b).

As Kramer (2008) notes: "The procedure was laborious and is recognized as being approximate, a fact that was accounted for in the Monte Carlo analyses described subsequently."

There are a number of challenges and potential drawbacks to this approach. One is the question as to whether the ZIF calculated by Olsen was fully accurate, so that the correct fractional displacement was modeled for the ZIF cross-section in Wang's subsequent studies. Another is the reliability with which the ZIF ross-section details can be inferred by this approach. Another is the question as to whether the projected ZIF cross-section could then be suitably further advanced to eventually produce the post-failure cross-section actually observed. [In the incremental inertial analyses performed for these current studies, incremental displaced/deformed cross-sections are developed progressively from initial to final observed field cross-section geometries; much like an "animation" or progressive simulation of the progressing failure. This turned out to be very useful, providing insights as to progression paths of successive incremental geometries that could successfully finish with the actual observed post-failure cross-section. In some case this helped to shed light on likely failure mechanics details.]

Despite these challenges, it is the opinion of the current investigation team that for well-characterized failure case histories, with well-defined pre-failure and post-failure cross-section geometries, this ZIF approach can (if wielded with suitable engineering judgment) be expected to provide useful back-calculated values of S_r with levels of accuracy and reliability at least compatible with those developed by the kinetics method employed by Olsen (2001), and likely even a bit better. Cross-comparisons between S_r values back-calculated (1) by this ZIF method, (2) by the kinetics method of Olsen (2001), and (3) by the incremental inertial analysis method employed in these current studies (see Chapters 4 and 5) bear this out.

Wang developed a simplified approach to estimate the amount of hydroplaning that would occur as the toes of failure masses entered into bodies of water, based on a review of available research. The likelihood and lateral extent of hydroplaning at the toe was taken as a function of displacement velocity of the displacing mass, and was limited to not more than 10 times the thickness of the toe mass entering the reservoir. This was a rational approach, but the procedure should be considered somewhat speculative, however, as it was constructed based on research that was far from definitive.

Wang systematically varied a number of parameters and variables for each of the 9 case histories back-analyzed by this ZIF approach. Cross-section details, failure surface locations, phreatic surface locations, unit weights, and soil material strength parameters for soils that did not liquefy were then all systematically varied within estimated reasonable ranges, and 50,000 Monte Carlo simulations representing randomized combination within these ranges were analyzed for each individual case. This was done to provide an assessment of variability in S_r values back-calculated, and also to provide a basis for more formal assessment of both means and variability of means expressed in terms of standard deviation of the means for the three key indices (S_r, $N_{1,60,CS}$ and $\sigma'_{v,i}$).

Unfortunately, the ZIF cross-sections used and other key analysis details (including failure surfaces considered, phreatic surfaces, and soil properties, etc.) were not presented for any of the nine cases analyzed, so it is not possible to check these analyses, nor to know exactly what was done for each individual case. The example illustrative ZIF cross-section for the Wachusett Dam case history shown in Figure 2.24 was the only ZIF cross-section presented.

Another lapse was the lack of documentation or explanation of the basis and approaches used to develop procedurally corrected and overburden corrected values of $N_{1,60}$, and the fines correction applied to develop $N_{1,60,CS}$ values. It must be assumed, based on the date of the work, that these would have been largely compatible with the SPT procedural corrections and overburden stress corrections of either Seed et al. (1984), Youd et al. (2001) or Cetin et al. (2000), and that the fines correction would have been compatible either with one of these procedures or with the fines correction recommended by Seed (1987) specifically for purpose of evaluation of S_r. Differences between the resulting $N_{1,60,CS}$ values based on variations between these approaches to development of $N_{1,60,CS}$ values would have been relatively small, but it would have been useful to know exactly what was done here.

This lack of documentation and transparency is unfortunate, and it appears to have prevented the overall work (including development of recommended correlations for assessment of in situ S_r) from garnering the attention that it appears to have deserved.

It should be noted that these ZIF analyses were performed before the incremental inertial analyses developed and performed for these current studies, and that Wang and Kramer thus did not know what the answers developed by these current studies would be. There is generally good to very good agreement between the results from these nine ZIF analyses, and the corresponding results of the incremental inertial analyses from these current studies for these same nine cases (see Chapter 4). And so it must be concluded that the judgments required for implementation of the ZIF approach were generally well executed.

The 22 remaining case histories were judged to not have sufficient data and information as to warrant or support ZIF-type analyses, and Wang referred to these as the "secondary" cases. Wang was then in the same position as Olsen (2001) of having to decide how to develop suitable estimates for these lesser cases. The mean value of S_r for each of these 22 cases was taken as the average of values selected from among available values back-calculated by previous investigators. Only values considered to be applicable were employed here, and the basis for judgment as to applicability was not documented. This was, statistically, likely a better approach than the conservatively biased approaches used by Olsen to estimate Sr for his 23 "lesser" cases (see Section 2.3.6), but it was not an ideal approach.

Coefficients of variation (COV) for each of the 22 secondary cases were estimated based on the COV's calculated for the nine cases previously back-analyzed using the ZIF-based approach, with increases in estimated COV or dispersion in S_r to account for the more simplified analysis methods represented by the available estimated of S_r developed by other investigators, and the less well documented data and other information for these cases. Monte Carlo analyses were performed for each case based on these estimates of variability to assess variability in the three key indices. This was largely circular logic, as the Monte Carlo analyses largely evidenced the levels of dispersion or uncertainty assumed.

Representative penetration resistances for all cases, both the 9 ZIF cases and the 22 secondary cases, were based on estimated mean values of $\overline{N_{1,60,CS}}$. Rigidly prescribed approaches were employed to evaluate variance (standard deviation) of the mean value of $N_{1,60,CS}$ (expressed as σ_N) based primarily on the number and variance of available individual N-values. The current investigation team did not feel that these relatively rigidly constrained procedures resulted in consistently good estimates of variance or uncertainty of mean $N_{1,60,CS}$ for all of the cases, as key contributors to uncertainty for some cases (e.g. in estimating N-values based on alternate measures of penetration resistance, or simply on the basis of observed soil conditions and placement history, etc.) were not well-captured by these approaches. Nonetheless, generally good estimates of $\overline{N_{1,60,CS}}$, and generally reasonable estimates of σ_N, appear to have been developed. And the approaches taken here had the benefits of being well-defined and repeatable.

The eventual regressed predictive relationship developed by Kramer (and Wang) predicted S_r based on both $N_{1,60,CS}$ and also initial effective vertical stress ($\sigma_{v,i}'$). Surprisingly, values of mean $\sigma_{v,i}'$, and of the standard deviations of these means, for the 31 cases analyzed were also

never explicitly stated; neither in the thesis work of Wang (2003) nor in the subsequent WashDOT report of Kramer (2008) which presented the regressions performed and the resulting development of probabilistic and deterministic correlations for evaluation of S_r. Table 2.1 is from Kramer (2008), and it presents the mean values, and standard deviations in mean values, of both S_r and $N_{1,60,CS}$ for each of the 31 cases, along with weighting factors developed by Kramer for use in performing the regressions which followed. Not listed are the mean values, and standard deviations in mean values, of initial effective vertical stress; despite the fact that effective vertical stress turns out to be of essentially co-equal importance along with $N_{1,60,CS}$ for prediction of S_r in the predictive correlations subsequently developed. This was another significant lapse in terms of suitable transparency of documentation.

The weighting factors shown in Table 2.1 are potentially important. These weighting factors were developed by Kramer in order to account for the variable quality of information and documentation of data available for the individual case histories. Poorer documentation would be expected to lead to higher levels of uncertainty. Unfortunately, full details involved in development of these weighting factors are not presented. They appear to have been a matter of engineering judgment. That said, they do appear to be generally reasonable in the view of the current investigation team, although any two different investigation teams would likely have differences of opinion as to the details or the relative weighting factor assigned for any specific case history. (In these current studies, it was preferred to incorporate uncertainties associated with poor documentation of information and data, as well as with the variable quality of data, directly in the variances ascribed to the key regression parameters; so no additional weighting factors were applied in these current studies.) Weighting factors in Table 2.1 range from w = 1.0 for well documented cases, to very low values for poorly documented cases. The two cases with the lowest assigned weighting factors are Asele Road (w = 0.20) and Soviet Tajik – May 1 Slide (w = 0.22). With these very low weighting factors, these two cases are virtually eliminated.

Kramer performed a large number of nonlinear least squares regressions to ascertain the forms of useful predictive relationships (general equation forms) that would be well suited to the data set and provide generally good model fit across the domain of the data set. He then performed fully probabilistic Bayesian regressions using the maximum likelihood method to develop a better probabilistically based relationship incorporating all uncertainties. This relationship was what Kramer described as a "hybrid" model, with predicted values of S_r being dependent upon both SPT penetration resistance and initial effective vertical stress.

In examining the resulting predictive correlation, Kramer observed that values of S_r predicted at very low initial effective stresses appeared to be unreasonably low. He reasoned that if such values actually occurred, then larger numbers of very shallow flow slides would be observed. He examined the suite of field case history data for lateral spreading cases (not flow slides) developed by Youd et al. (2002), and reasoned that the value of S_r within the liquefied materials for each of these lateral spreading cases must have been at least as large as the static driving shear stress; otherwise these would have been flow failure case histories rather than lateral spreads. He made simplified estimates of the static driving stresses at shallow depth for these cases, based on an infinite slope assumption, and in this manner estimated the minimum (lower bound) potential value of S_r for each lateral spreading case at initial vertical effective stresses of less than 0.6 atmospheres. These were plotted vs. effective vertical effective, and the resulting

plot is shown in Figure 2.25. Based on this, but without explanation of details, Kramer concluded that one of his model fitting parameters (Θ_4) would be modified to slightly increase the values of S_r predicted at very low confining stresses. This was a "judgmental" manipulation, but it appears to have had little effect on predicted values of S_r at higher effective stresses more typically of engineering interest.

His regressed model, with the parameters developed by the maximum likelihood method, and with Θ_4 thus slightly constrained, was then reformulated into a more tractable form for use by engineers. The final proposed relationship was then

$$\overline{\ln S_r} = -8.444 + 0.109N + 5.379S^{0.1} \qquad \text{[Eq. 2-3]}$$

where

$$\sigma_{\ln S_r} = \sqrt{\sigma_m^2 + 0.00073\overline{N}^2\ COV_N^2 + 4.935S^{-0.2}\ COV_S^2} \qquad \text{[Eq. 2-3a]}$$

and

$$\sigma_m^2 = 1.627 + 0.00073N^2 + 0.0194N - 0.27NS^{0.1} - 3.099S^{0.1} + 1.621S^{0.2} \qquad \text{[Eq. 2-3b]}$$

Figure 2.26 shows the median (50th percentile) values of S_r based on this relationship. A series of curves are shown relating S_r to $\overline{N_{1,60,CS}}$, with each curve labeled with the value of $\overline{\sigma'_{vo}}$ for which that curve would apply. The overall relationship is fully probabilistically based, and similar curves can be developed and plotted for other percentiles or likelihoods of exceedance.

Kramer than goes on to further consider appropriate levels of conservatism for deterministic values of S_r for engineering applications, and determines that 40th percentile values would be appropriate here. These values, recommended for routine geotechnical design, are shown in Figure 2.27.

2.3.8 Idriss and Boulanger (2008)

Idriss and Boulanger (2008) considered a subset of 17 of the 33 large-displacement liquefaction failure case histories in the data set complied by Olsen and Stark (2002). The basis for selection of each of these was not explicitly explained, but it is understood that they selected the cases that were best characterized and best documented, and deleted the rest. They then categorized each of these 17 case histories into one of three groups; Groups 1, 2, and 3. Group 1 were the cases considered to be those that were best characterized and documented, and Group 3 those that were least well characterized.

They did not perform any of their own independent back-analyses of these 17 case histories. Instead, they next adopted the values developed from back-analyses by (1) Seed (1987), (2) Seed and Harder (1990), and (3) Olsen and Stark (2002) for cases which each of these previous

teams had analyzed. Ten of the cases had been back-analyzed by Seed (1987), 13 by Seed and Harder (1990) and all 18 by Olsen and Stark (2002). Values of S_r back-calculated by Seed (1987) and by Seed and Harder (1990) were normalized by dividing by estimated representative values of effective vertical stress to develop post-liquefaction strength ratios for each case.

The resulting values of strength ratio were then plotted vs. $N_{1,60,CS}$ values developed by each of the three previous investigation teams. The results are shown in Figure 2.28. In this figure, the shapes of the symbols identify the investigation team responsible for the values of S_r and $N_{1,60,CS}$ plotted, and the sizes of the symbols indicate whether the case was considered by Idriss and Boulanger to be a Group 1 (high quality) or Group 2 and 3 (lower quality) case.

A line was drawn through these plotted data (the solid line in the lower left-hand portion of the figure), based on judgment, and this line was then extended as a dashed line to express additional judgment as to the likely extrapolation to higher $N_{1,60,CS}$ values. An equation was then fitted to this proposed relationship for ease of implementation in spreadsheet calculations and similar.

A second dashed line was then added, inflecting steeply upwards, to represent recommended values of S_r as a function of $N_{1,60,CS}$ for situations in which void redistribution effects are expected to be negligible. This upper line is not well explained, but it is independent of the back-analyzed field case history data plotted and it is reportedly based primarily on laboratory test data.

There are a number of problems and drawbacks in this proposed relationship, and with the figure presented. The first of these is the fact that the large, solid "dot" plotted at $N_{1,60,CS} = 15$ blows/ft and $S_r/P \approx 0.21$ (Point "A" in Figure 2.29) represents the value initially proposed by Seed (1987) for the Lower San Fernando Dam case history. As described previously in Section 2.3.1, Prof. Seed later reconsidered this and concluded that this was an error and that the strength that he had originally proposed was too high. Seed and Harder (1990) and Stark and Olsen (2002) both back-analyzed this case, and had developed lower S_r values. The values of Seed and Harder (1990) and Olsen and Stark (2002) are in such close agreement that they plot largely over each other in Figure 2.29 (Points B & C in this figure). For clarity, Figure 2.29 repeats Figure 2.28, but this time the erroneous data point for Lower San Fernando Dam is circled with a dashed line (and partly dimmed), and the locations of the (arguably more correct) plots of the data points developed by Seed and Harder, and by Stark and Olsen for the Lower San Fernando Dam are clearly indicated.

This changes the figure significantly, especially on a visceral (graphical) basis. It removes the large "dot" that otherwise appears to "anchor" the upper dashed curve. This dot was never actually part of the upper curve, because all of the back-analyzed field case histories were actually ascribed to situations wherein void redistribution was assumed to have potentially occurred. But many engineers do not read text, and simply view the figure and assume that the upper curve is somehow associated with this (very prominent) erroneous data point.

With the erroneous data point thus relocated, Figure 2.29 then shows clearly the degree of judgment involved in recommending the upwards bending curve to extrapolate the lower solid

line's recommended relationship to values of $N_{1,60,CS}$ greater than about 15 blows/ft. There is nothing obvious in the data, as presented, that supports this interpretation.

It should also be noted that six data points plot high in the upper left-hand corners of Figures 2.28 and 2.29. These high "floating" points are unexplained by this relationship, as presented and described by Idriss and Boulanger, but it turns out that they are actually well-explained by the predictive relationships developed by Wang and Kramer (see Section 2.3.7) and by these current studies (see Chapter 5).

Finally, it should be noted that the "upper" dashed line is intended to be applied only to field cases in which void redistribution will not be significant. It has proven difficult to define such cases in the field. Many engineers are well used to having an upper bound and lower bound relationship proposed (as with Seed and Harder, 1990, Stark and Mesri, 1992, and Olsen and Stark, 2002) and so they are used to interpolating between the upper and lower bounds as presented to select values of post-liquefaction strength for actual projects. This is not the apparent intent of Idriss and Boulanger who intend the lower line to represent not a "lower bound" but rather the "recommended" values for field cases wherein void redistribution effects can occur (most field situations), and who intend the upper dashed line (which was based on laboratory test data) to represent not an "upper bound" but rather a second relationship for situations in which void redistribution effects will not be significant.

Idriss and Boulanger also present their selected data points, and recommended relationships, in the form of S_r (not S_r/P), and these are shown in Figure 2.30. The same issues discussed above apply here as well. This includes the large solid "dot" representing the values initially proposed by Seed (1987) for the Lower San Fernando case history. Relocation of this data point (to the positions determined by Seed and Harder, 1990, and by Olsen and Stark, 2002) is illustrated in Figure 2.31.

2.3.9 Olsen and Johnson (2008)

Olsen and Johnson (2008) recognized the paucity of liquefaction-induced failure case histories for back-analyses of post liquefaction strengths at full field scale. To address this, they collected a large number of available lateral spreading case histories (39 cases).

Lateral spreading case histories differ from liquefaction flow failure case histories in that they experience more limited displacements, and a large fraction of their displacements are usually driven primarily by cyclic inertial lurching during strong earthquake shaking. Lateral spreads tend to be of finite thickness and/or slope (though they can sometimes be very large), and thus the initial (pre-earthquake) gravity-induced static shear stresses tend in most cases to be equaled or overshadowed by the cyclic "lurching" induced stresses during strong shaking.

Accordingly, Olsen and Johnson applied various Newmark-type analyses to back-analyze the displacements observed in the field for these cases in order to estimate the post-liquefaction strengths involved. Newmark-type analyses are not a very precise analysis methodology (e.g. Bray and Rathje, 1998) and this was further exacerbated by the sensitivity of calculated displacements to the intensity and details of actual earthquake shaking at each site, and the lack of

site-specific ground motion records for each case. As a result, there was significant scatter (or variance/uncertainty) in the resulting estimates of S_r for each case.

A tentative recommended relationship between strength ratio ($S_r/P_)$ and penetration resistance was developed, but the large variance or uncertainty made this of little apparent value relative to relationships already available. In the end, the most important lesson from this study was the difficulty of assessing S_r based on performing back-analyses of cases with only limited displacements wherein cyclic lurching generates a significant fraction of the overall displacements that accrue.

2.3.10 Gillette (2010)

Faced with the apparently conflicting views that post-liquefaction strengths might best be evaluated based on a "classical" critical state basis using post-liquefaction strength S_r assumed to be independent of effective overburden stress, or on the basis of post-liquefaction strength ratio (S_r/P) with an assumed linear dependence between S_r and initial effective vertical stress, a number of engineers have recommended a middle position.

Seed (2003) suggested that the best answer likely lay somewhere in between these two extreme views, and that there was likely a significant influence of initial effective stress on S_r, but that it was not likely that S_r was fully linearly correlated with initial effective vertical stress. He recommended evaluating S_r based on each approach, and then averaging the two results (with weighting factors varying a bit as a function of fines content) to produce values of S_r with some partial dependence on initial effective vertical stress until this could be better resolved. This was an interim suggestion, until better "hybrid" approaches could be developed.

As described in Section 2.3.7, Kramer (and Wang) developed "hybrid" predictive correlations for post-liquefaction strength based on both SPT penetration resistance and effective vertical effective stress, with the influence of vertical effective stress modeled as not being linearly related to S_r.

Gillette (2010) used a selected subset of the back-analyzed data bases of Seed and Harder (1990) and Olson and Stark (2002), and performed least squares regressions implementing a number of relatively simple potential equational forms that allowed for varying levels of partial (or nonlinear) dependence of S_r on initial effective vertical overburden stress. His resulting best fit relationships were

$$S_{ur} = 0.022\ (N_1)_{60-cs}{}^{1.0} \times \sigma'_{vo}{}^{0.80} + 1 \pm 5\ kPa \quad \text{with } R^2 \approx 0.87 \qquad \text{[Eq. 2-4]}$$

and

$$S_{ur} = 0.014\ (N_1)_{60}{}^{0.95} \times \sigma'_{vo}{}^{0.95} + 1 \pm 4\ kPa \quad \text{with } R^2 \approx 0.94 \qquad \text{[Eq. 2-5]}$$

When the full data set of Seed and Harder (1990) was regressed, the best fit relationship produced an R^2 value of $R^2 \approx 0.78$.

These R^2 values are significantly higher than the R^2 values previously calculated for the relationships proposed by Seed and Harder (1990), by Stark and Mesri (1992) and by Olsen and Stark (2002) in Sections 2.3.1, 2.3.2 and 2.3.6 respectively, further supporting the merit of a middle position wherein S_r would be taken as being nonlinearly dependent upon initial effective vertical effective stress.

Table 2.1: Component values and final weighting factors for all case histories as employed in the regressions performed (from Kramer, 2008)

Case History	$\overline{N}$	σ_N	$\overline{S_r}$	σ_{S_r}	w_{total}
Asele Road	11.0	10.7	163.6	54.6	0.20
Calaveras Dam	10.5	9.7	636.9	223.1	0.55
Chonan Middle School	6.4	6.9	178.7	32.0	0.74
El Cobre Tailings Dam	6.8	0.9	195.2	64.8	0.60
Fort Peck Dam	15.8	0.9	671.6	130.2	0.85
Hachiro-Gata Roadway	5.7	2.8	65.0	24.7	0.55
Helsinki Harbor	5.9	8.0	53.2	19.0	0.39
Hokkaido Tailings	5.1	1.4	250.6	71.9	0.31
Kawagishi-cho Building	4.3	1.2	123.5	56.7	0.50
Koda Numa Embankment	3.6	4.1	48.0	15.9	0.44
Lake Ackerman Roadway	4.8	1.2	98.0	20.4	1.00
La Marquesa Downstream	9.9	3.0	343.5	113.8	0.72
La Marquesa Upstream	6.5	2.8	185.1	82.1	0.76
La Palma Dam	4.2	1.8	193.3	86.3	0.80
Lake Merced Bank	5.9	8.0	139.5	41.4	0.39
Lower San Fernando Dam	14.5	1.1	484.7	111.0	1.00
Metoki Road	2.0	1.5	116.8	53.7	0.39
Mochi Koshi Tailings Dam 1	8.9	0.6	158.9	47.7	0.34
Mochi Koshi Tainilgs Dam 2	10.0	1.3	233.6	78.0	0.67
Nalband Railway	6.3	5.6	139.9	40.2	0.51
Nerlerk Berm	11.4	7.7	179.1	32.1	0.41
Route 272 Roadway	8.5	2.6	130.5	33.5	0.70
Sheffield Dam	8.2	6.8	100.0	29.8	0.37
Shibecha-Cho Embankment	5.6	2.2	208.9	38.6	0.70
Snow River Bridge Fill	8.5	9.0	50.1	16.6	0.50
Solfatara Canal Dike	4.9	6.9	77.1	25.6	0.42
Soviet Tajik – May 1 Slide	8.9	5.7	334.3	110.9	0.22
Tar Island Dike	8.9	9.7	364.2	115.6	0.32
Uetsu-Line Railway	2.9	4.2	43.7	24.8	0.55
Wachusett Dam	7.3	1.9	348.0	74.8	1.00
Zeeland	8.5	5.5	226.0	75.0	0.39

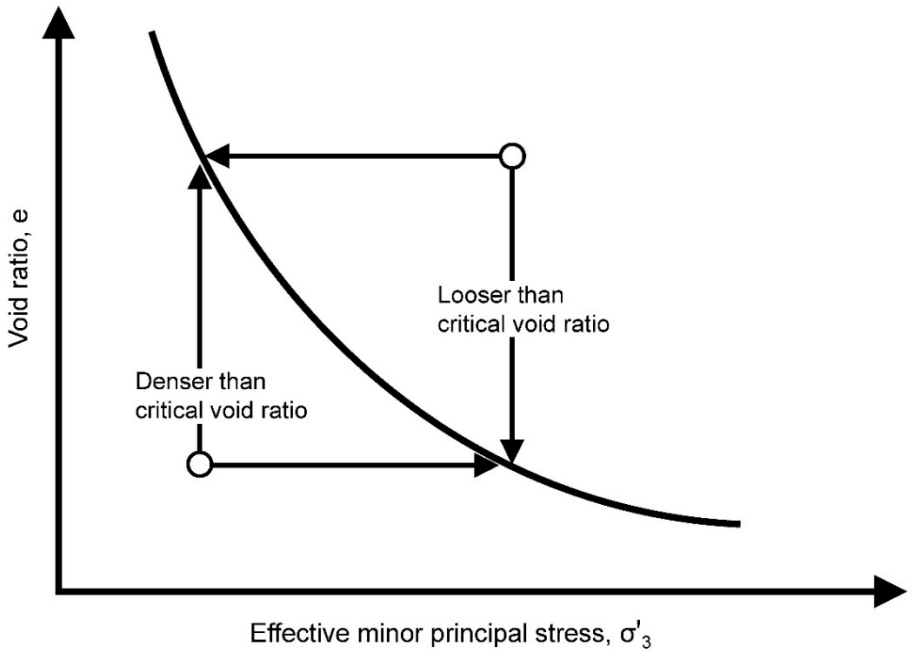

Figure 2.1: Simplified representation of the critical state line.

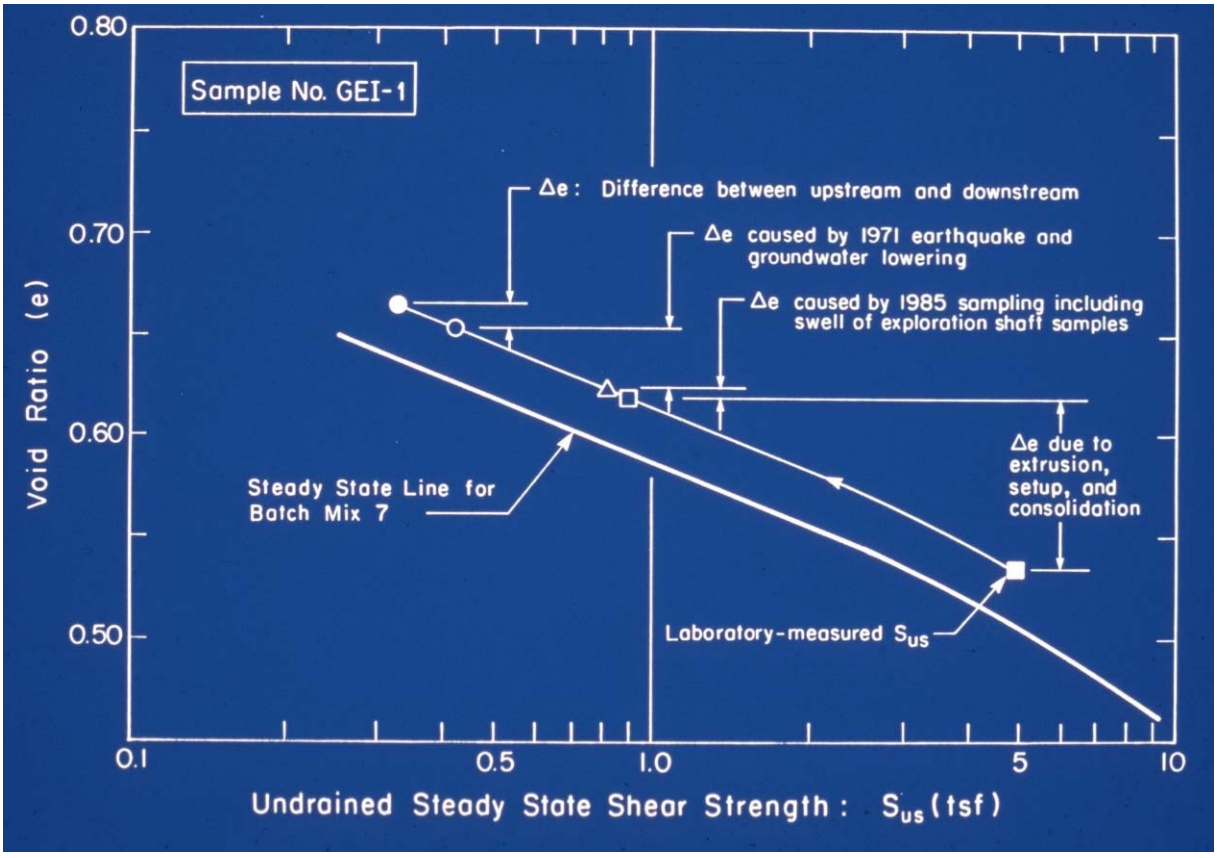

Figure 2.2: Illustration of the Steady State method of Poulos, et al. (1985) for assessing post-liquefaction strength for a sample of silty sand hydraulic fill from the Lower San Fernando Dam (Castro et al., 1992)

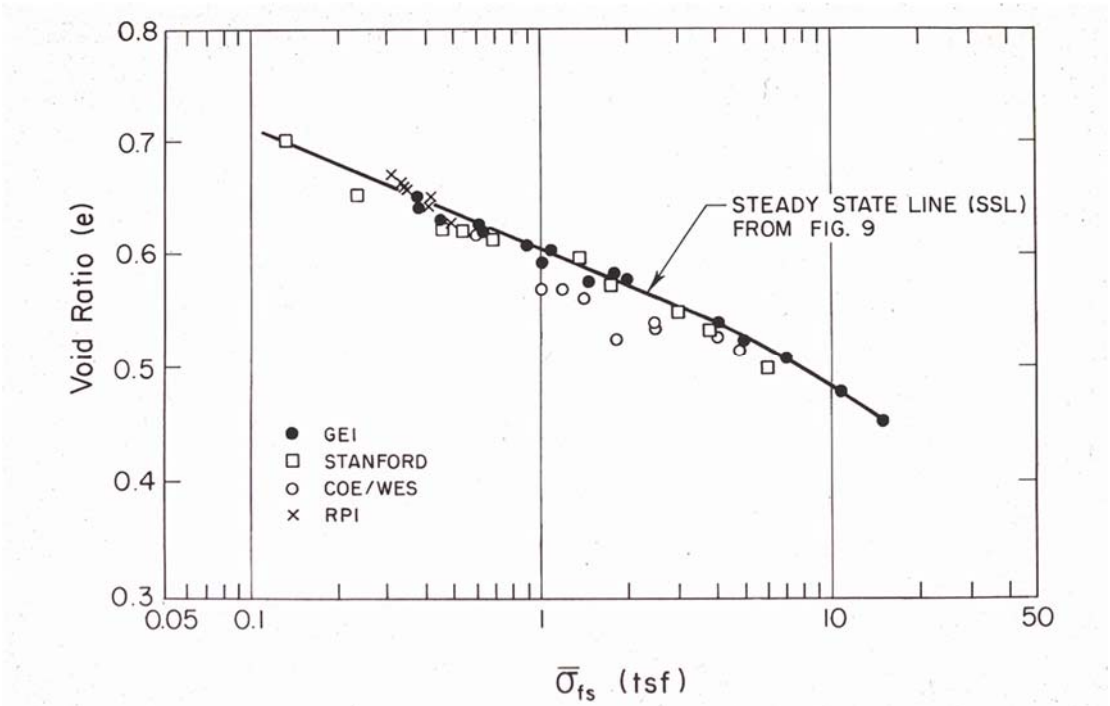

Figure 2.3: Steady state line based on IC-U triaxial tests performed by four laboratories on re-constituted samples of silty sand hydraulic fill from the lower portions of the down-stream shell of the Lower San Fernando Dam. (Figure from Castro, et al., 1992)

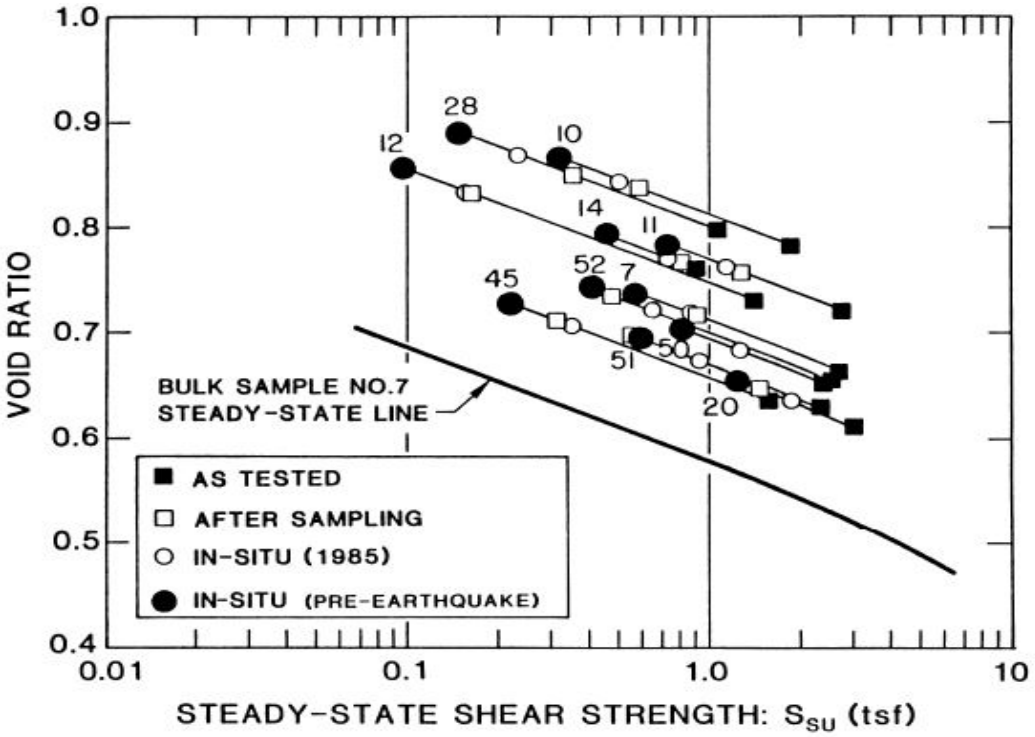

Figure 2.4: Corrections of IC-U triaxial tests of silty sand hydraulic fill from the Lower San Fernando Dam by the steady state method in order to develop estimates of in situ undrained steady state strengths. (Figure from Seed et al., 1988)

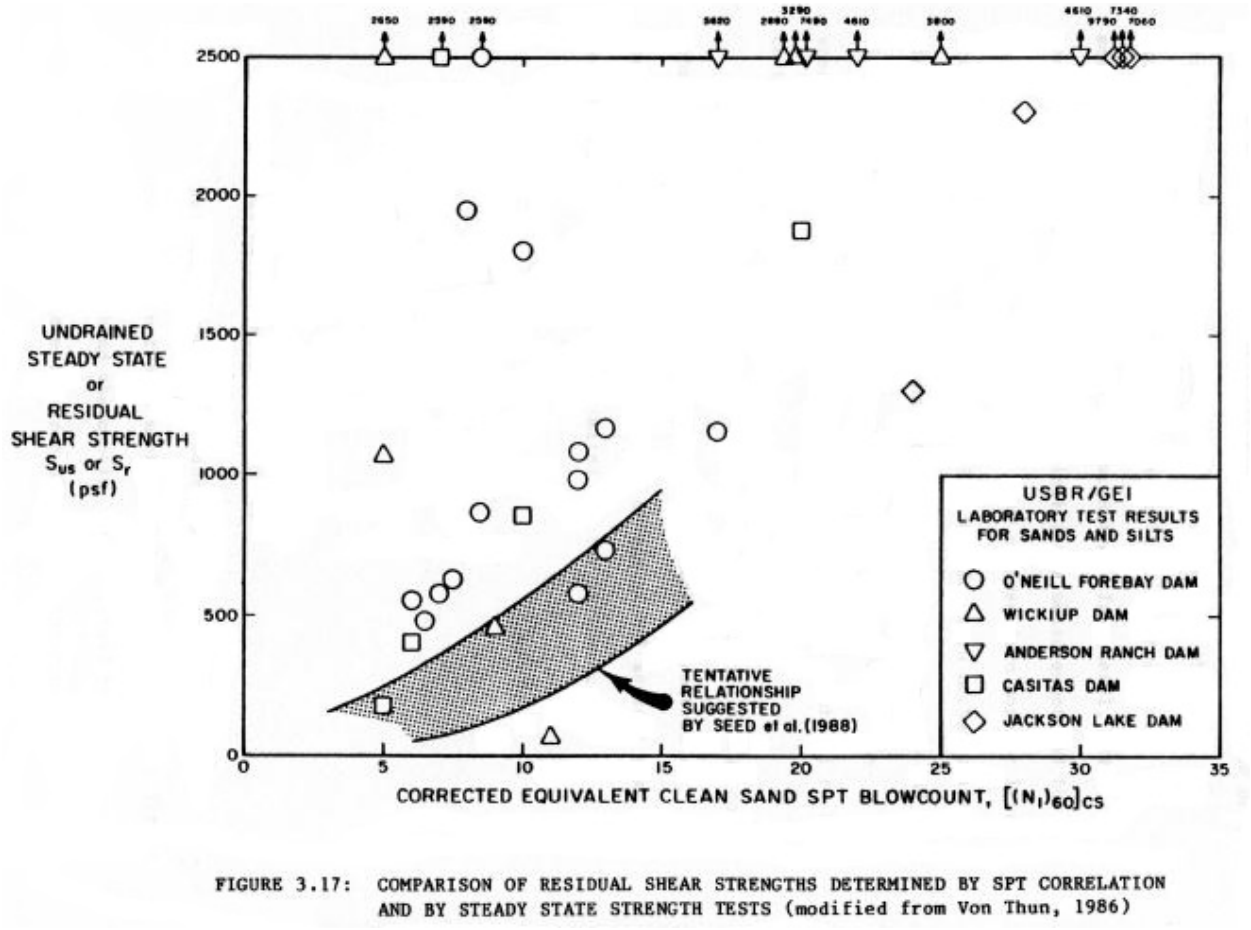

Figure 2.5: Values of estimated in situ steady state strength (S_r) developed by GEI, Inc. based on the laboratory-based steady state method of Poulos et al. (1985) for five U.S. Bureau of Reclamation dams. (Figure from Harder, 1988; modified after Von Thun, 1986)

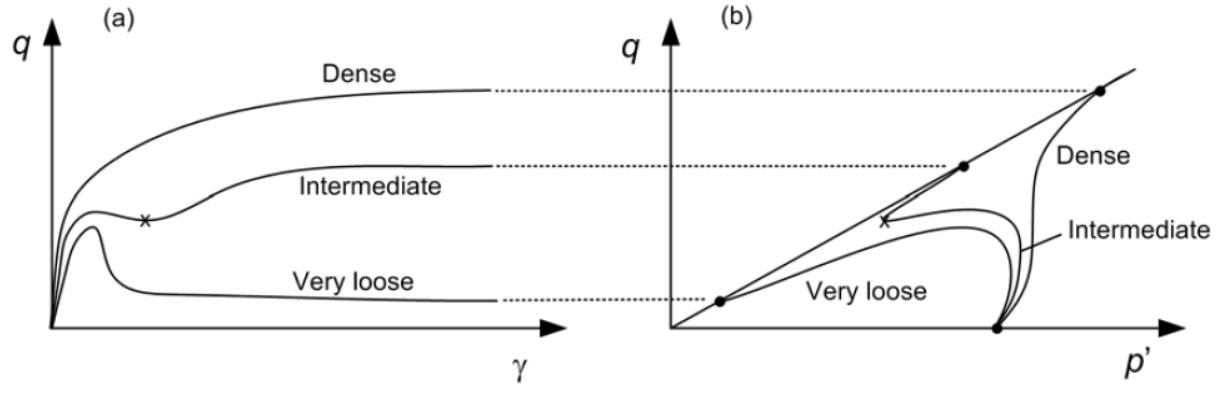

Figure 2.6: Simplified schematic illustration of stress-strain and stress path behaviors of sands of different relative densities under monotonic loading. (Figure from Kramer, 2008)

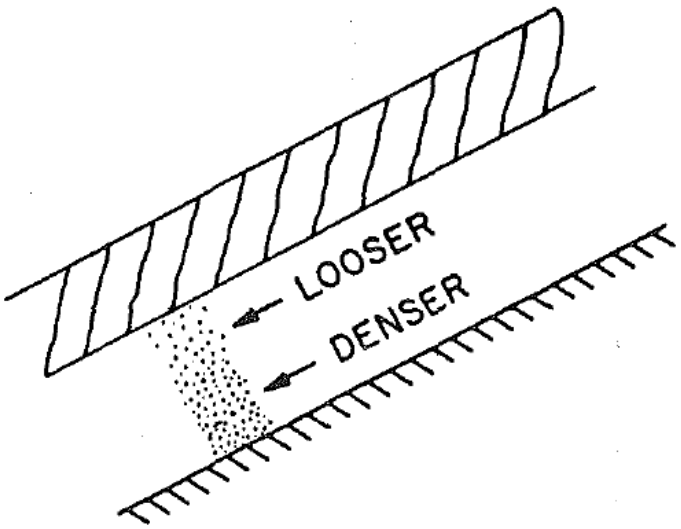

Figure 2.7: Simplified illustration of void redistribution within a confined soil stratum (National Research Council, 1985).

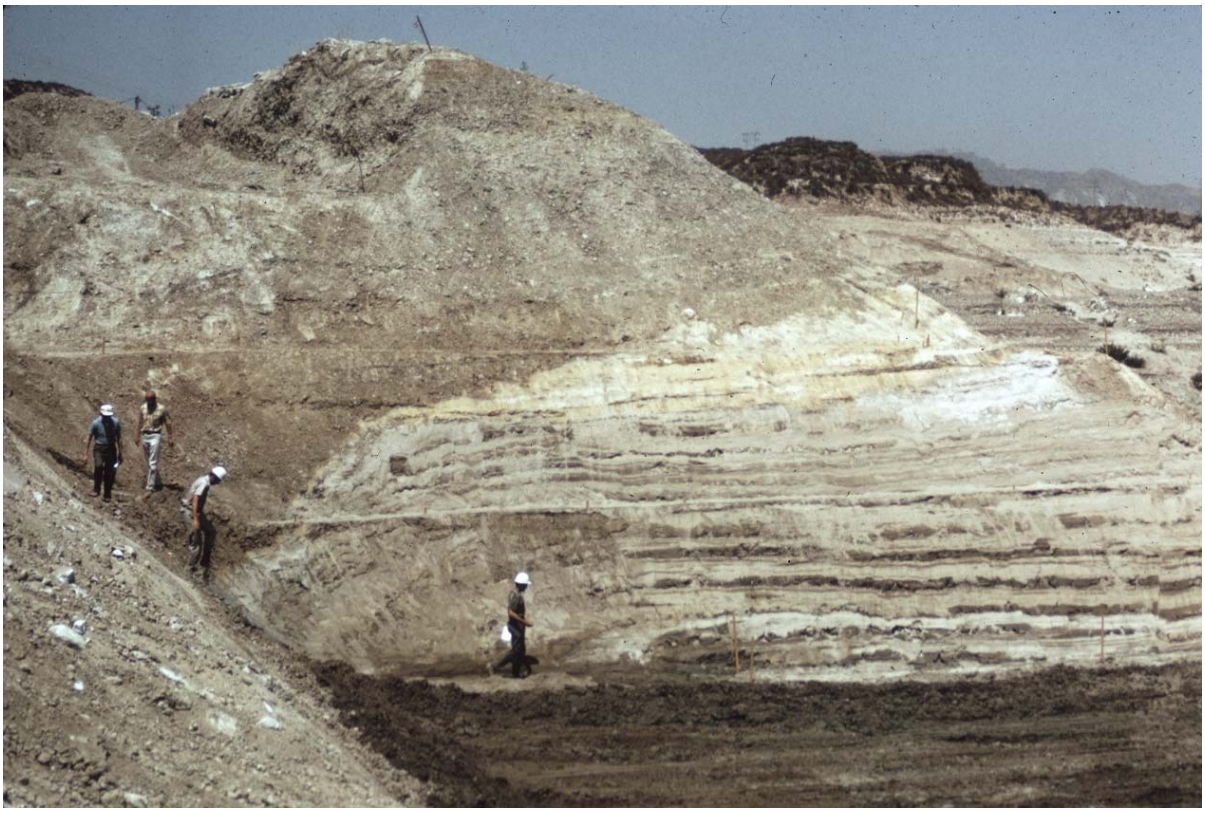

Figure 2.8: Photograph showing layering in the hydraulic fill of the Lower San Fernando Dam (photo by the California Department of Water Resources).

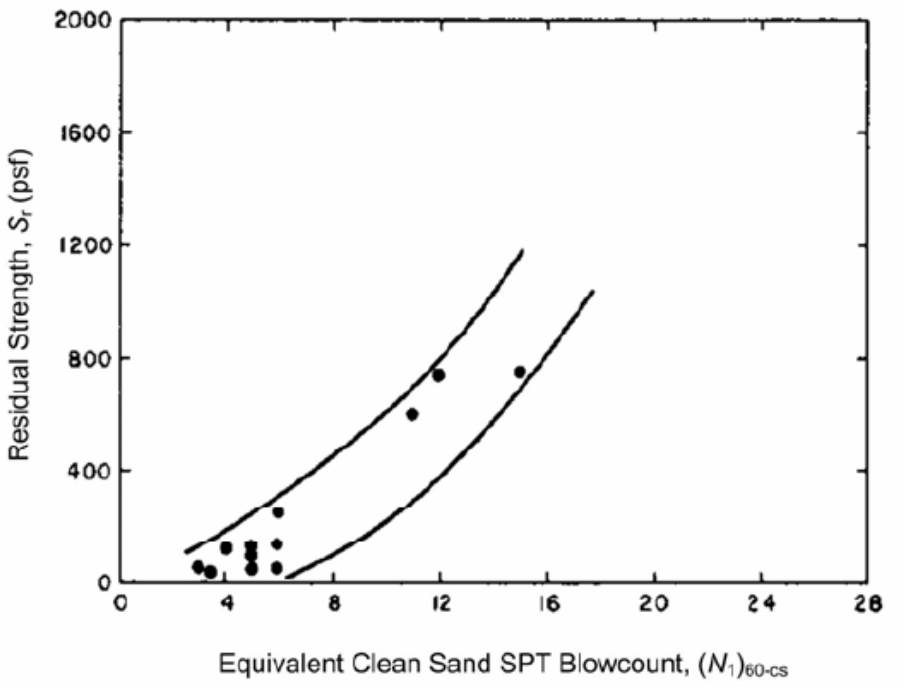

Figure 2.9: Variation of post-liquefaction residual strength Sr as a function of fines adjusted SPT penetration resistance $(N_1)_{60\text{-}CS}$ (Seed, 1987).

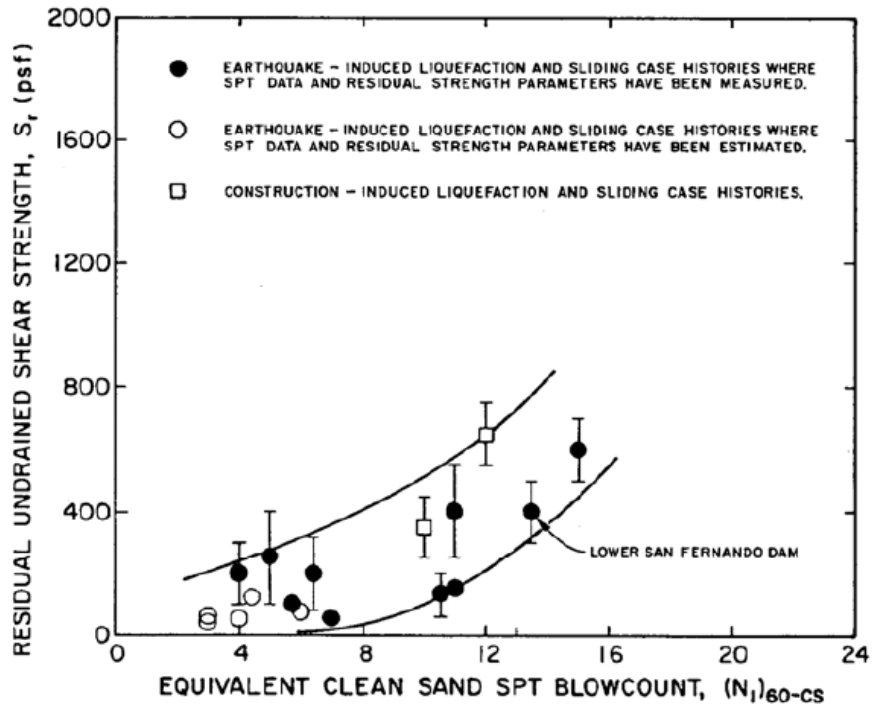

Figure 2.10: Variation of post-liquefaction residual strength S_r as a function of fines adjusted SPT penetration resistance $(N_1)_{60\text{-}CS}$ (Seed and Harder, 1990).

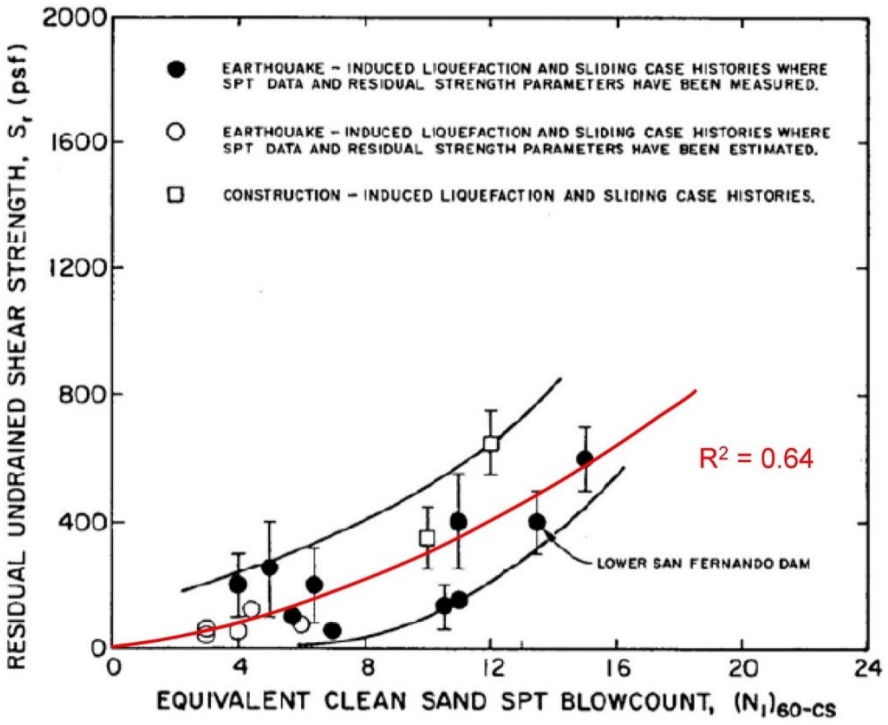

Figure 2.11: Figure 2.10 repeated, this time showing a least squares regression of the data.

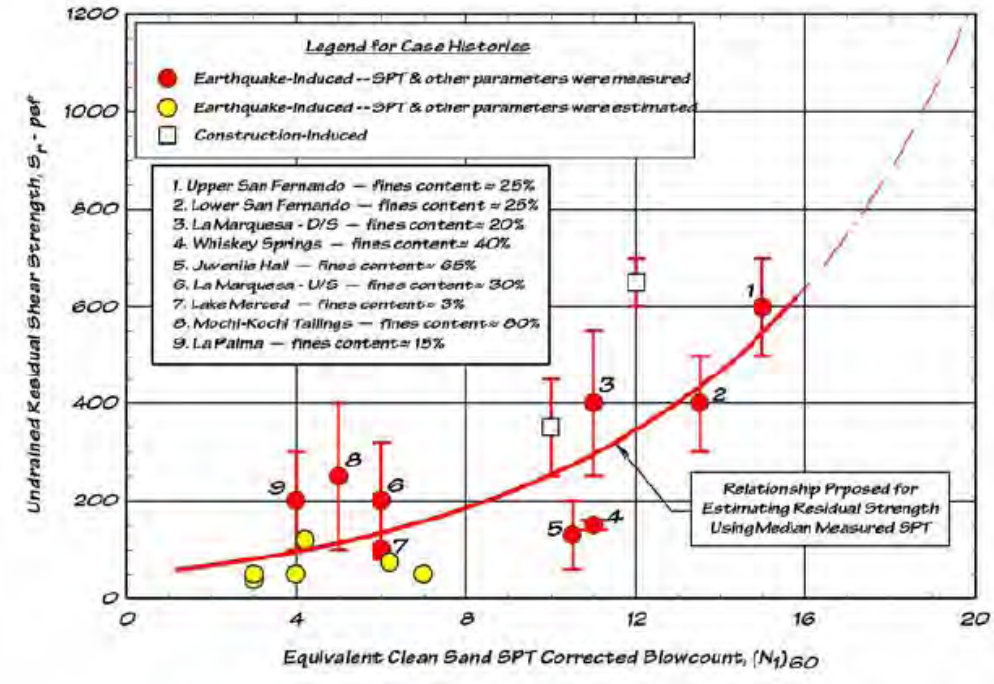

Figure 2.12: Variation of post-liquefaction residual strength S_r as a function of fines adjusted SPT penetration resistance $(N_1)_{60\text{-}CS}$. (Idriss, 1998)

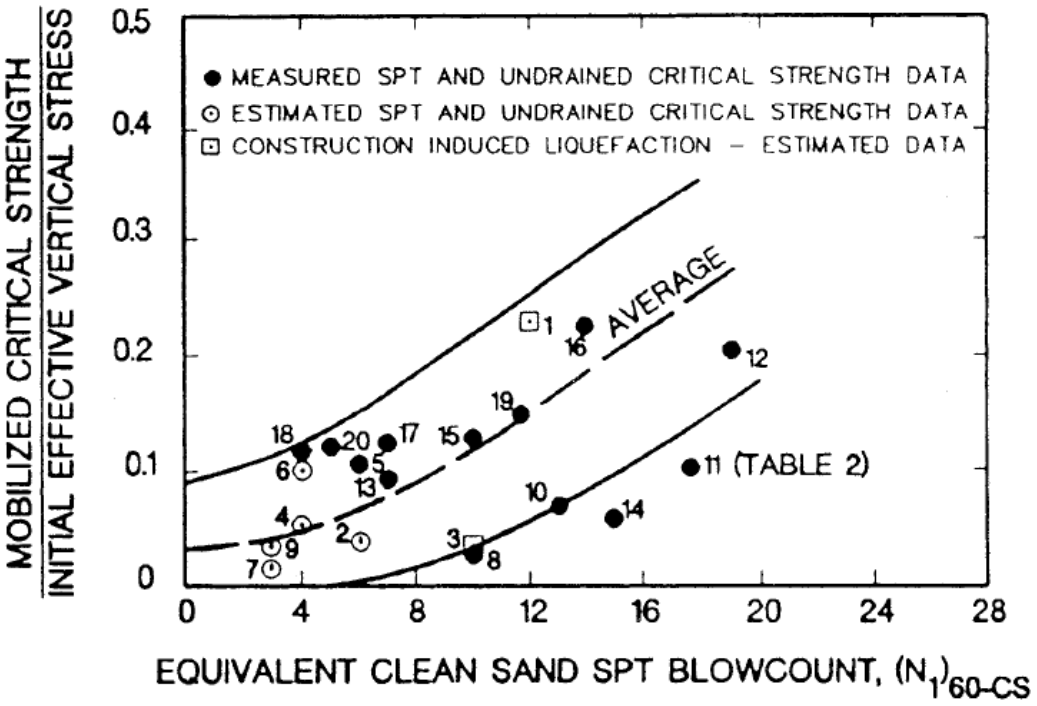

Figure 2.13: Variation of post-liquefaction residual strength ratio (S_r/P) as a function of fines djusted SPT penetration resistance $(N_1)_{60\text{-}CS}$ (Stark and Mesri, 1992).

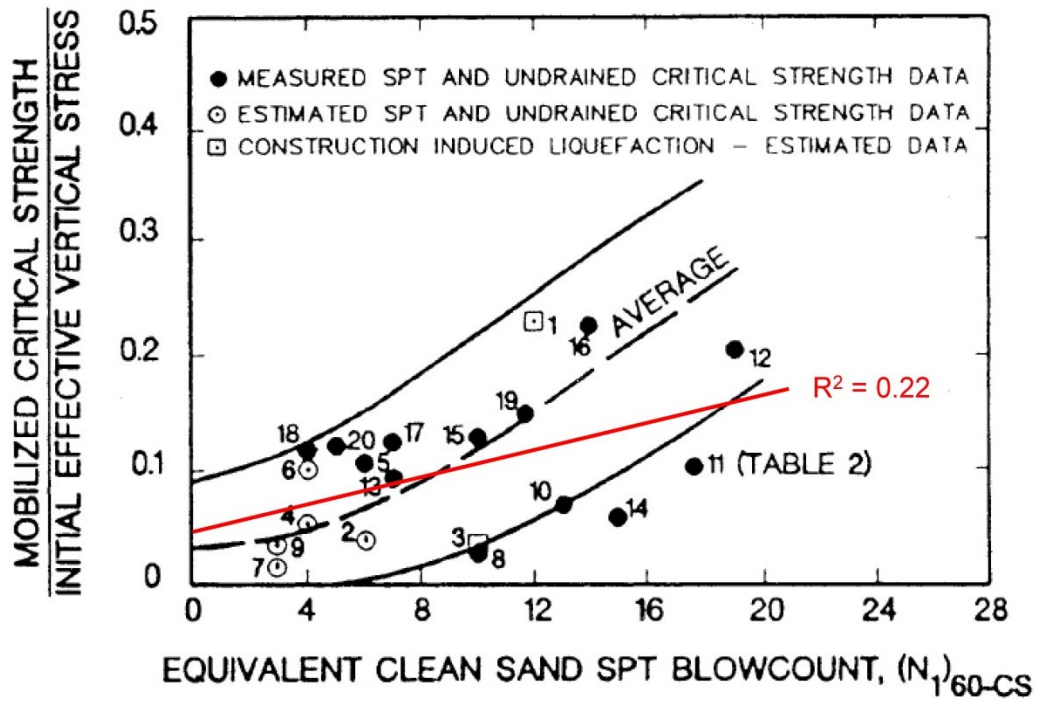

Figure 2.14: Figure 2.13 repeated, this time showing the results of a least squares regression.

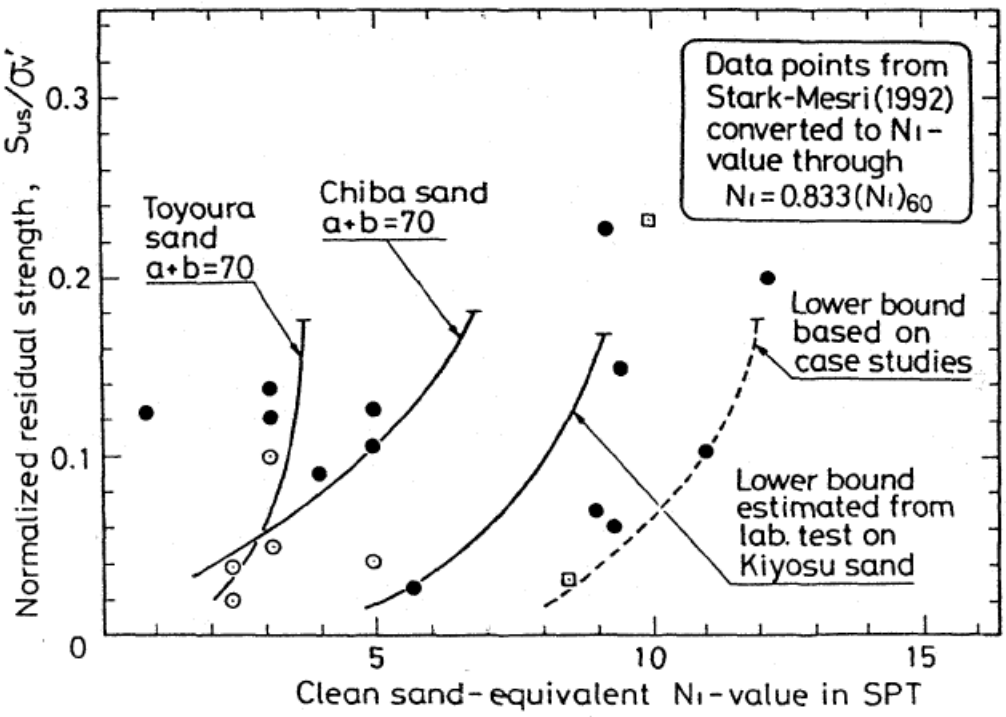

Figure 2.15: Ishihara (1993) relationship between quasi-steady state strength ratio $S_{u,s}/P$ and $(N_1)_{60}$, and comparison with values calculated by Stark and Olsen (1992).

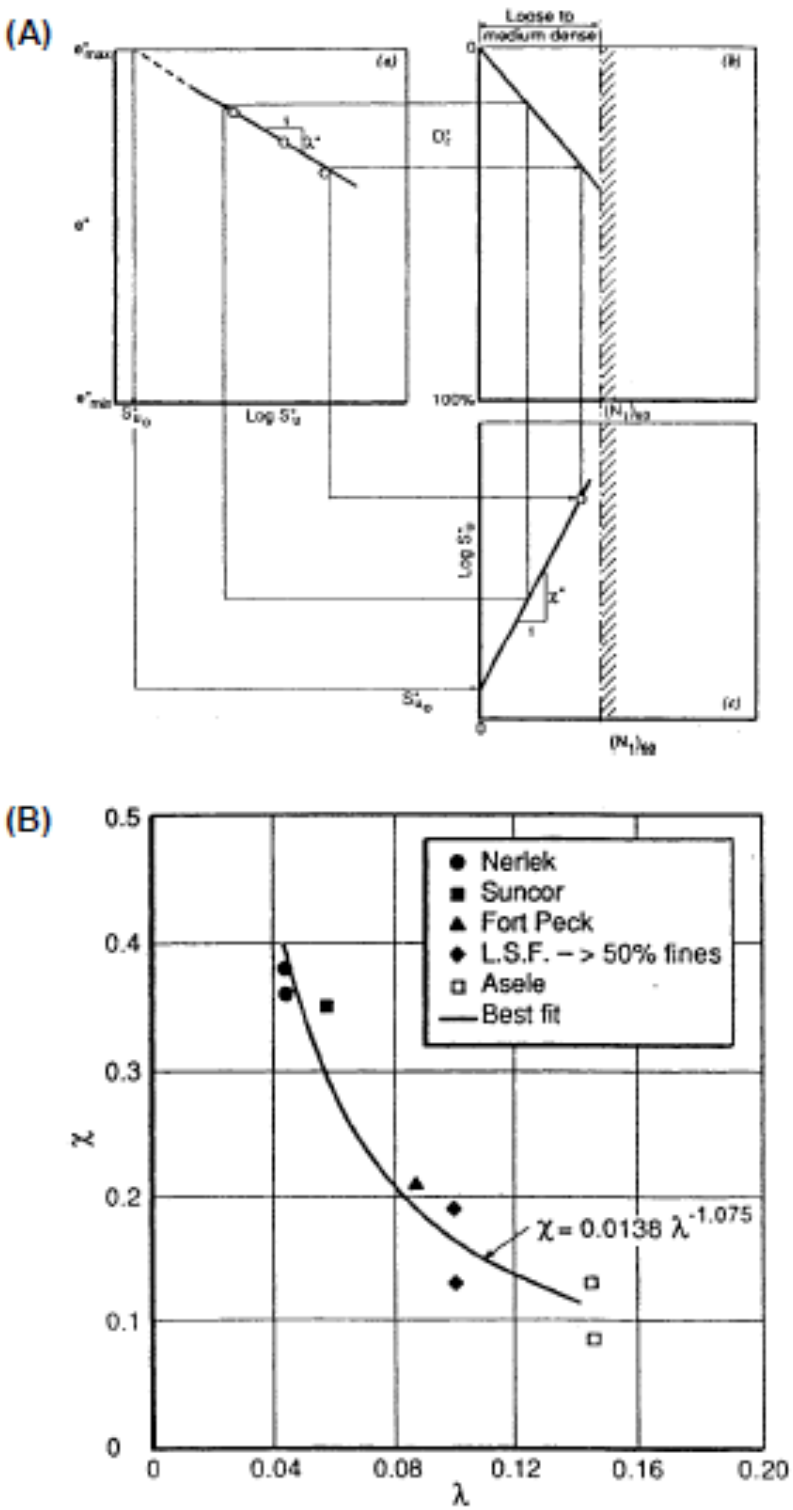

Figure 2.16: Derivation of the calibration factor χ as a function of λ, based on five back-analyzed field failure case histories (Konrad and Watts, 1995).

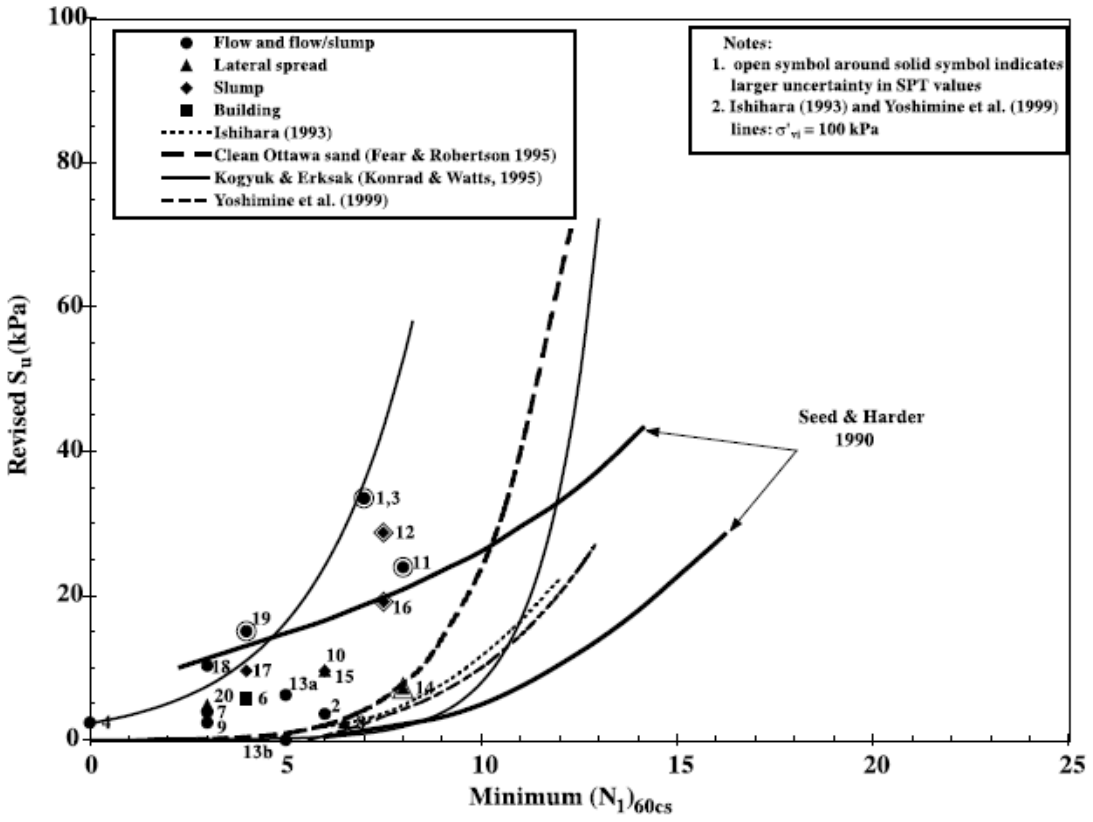

Figure 2.17: Re-evaluated data points (S_u and $N_{1,60,CS}$) for 19 failure case histories, and selected relationships proposed by previous investigators. (Wride et al., 1999)

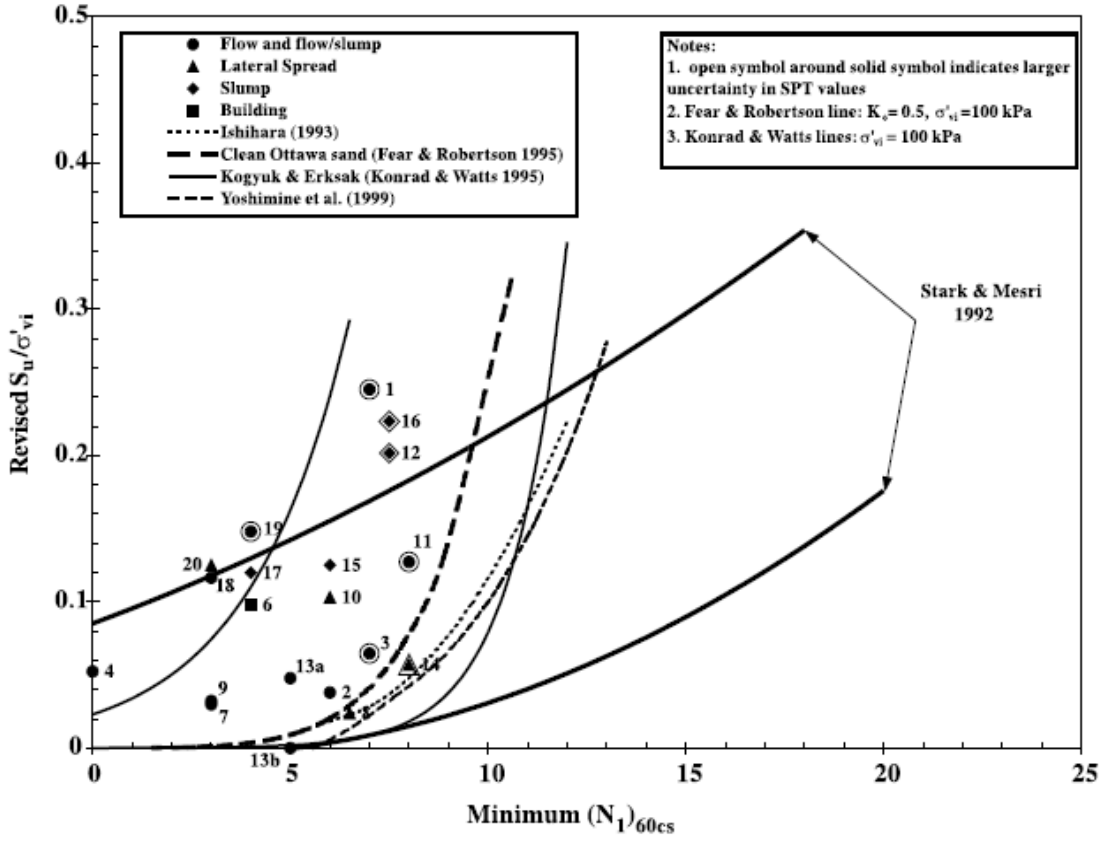

Figure 2.18: Re-evaluated data points (S_u/P and $N_{1,60,CS}$) for 19 failure case histories, and selected relationships proposed by previous investigators (Wride et al., 1999).

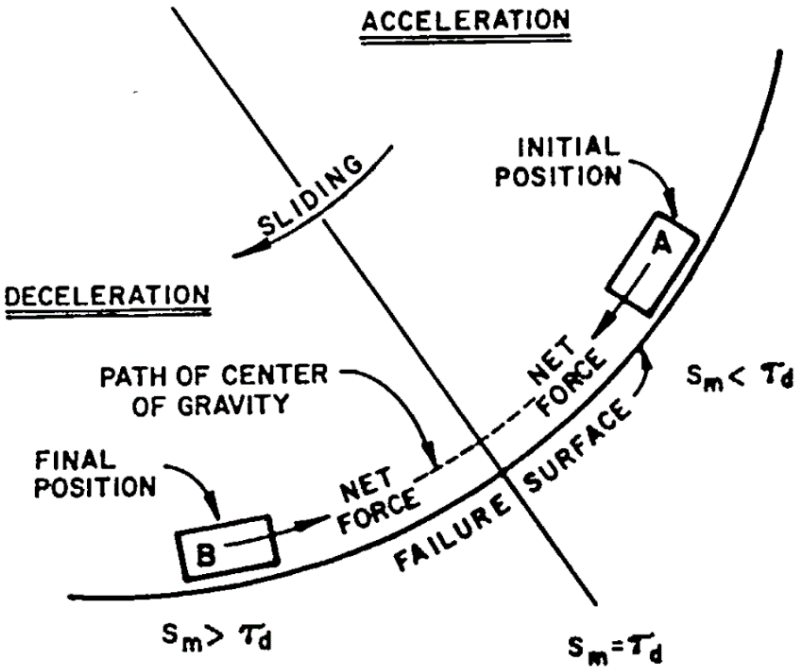

Figure 2.19: Schematic illustration of failure dynamics showing the progression of a mass moving downslope and the net forces on the base shear surface as the mass initially accelerates downslope, and then decelerates and comes to rest (Davis et al. 1998).

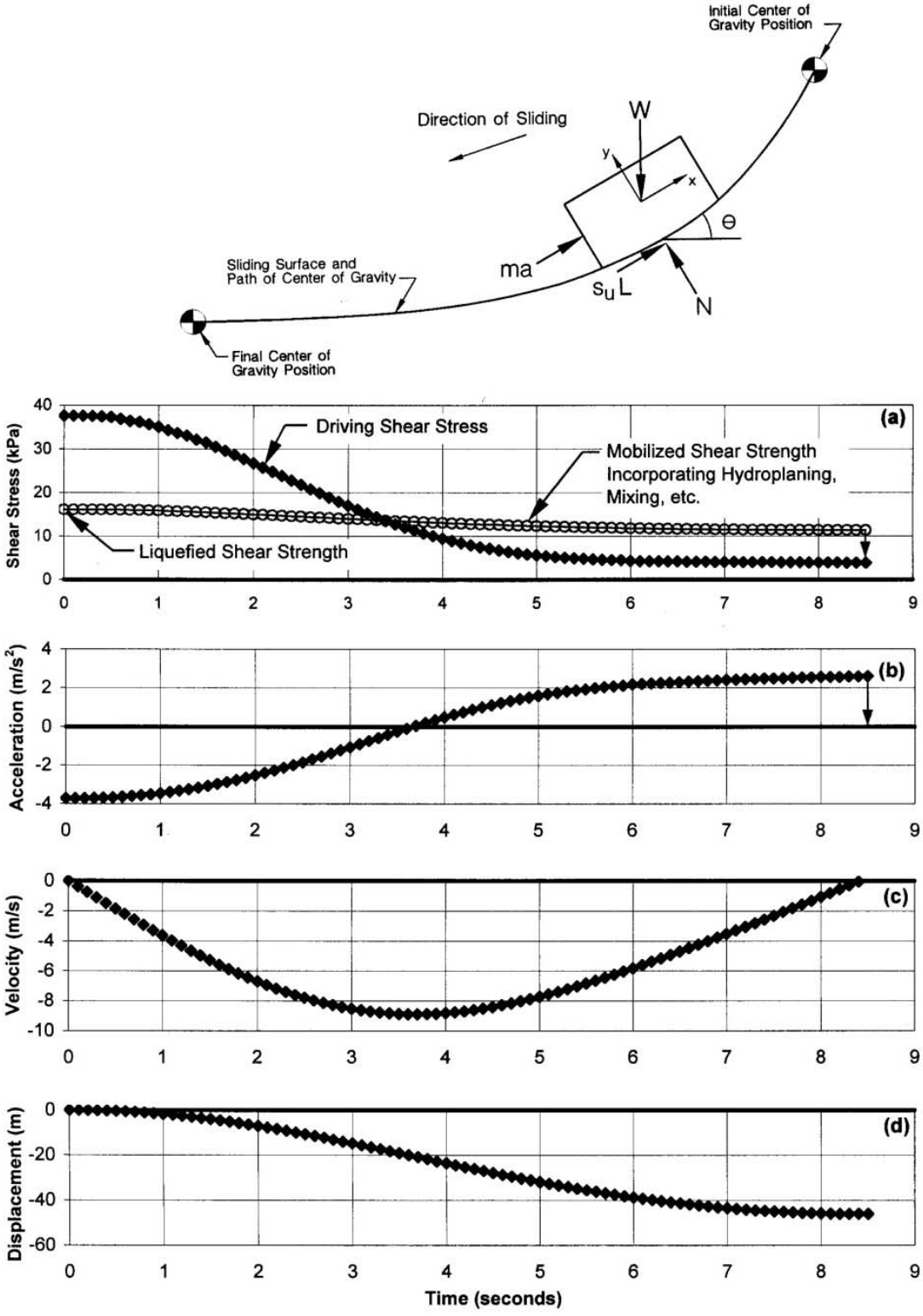

Figure 2.20: Schematic illustration of Olsen's "kinetics" analysis of the failure of the upstream slope of Wachusett Dam (Olsen, 2001).

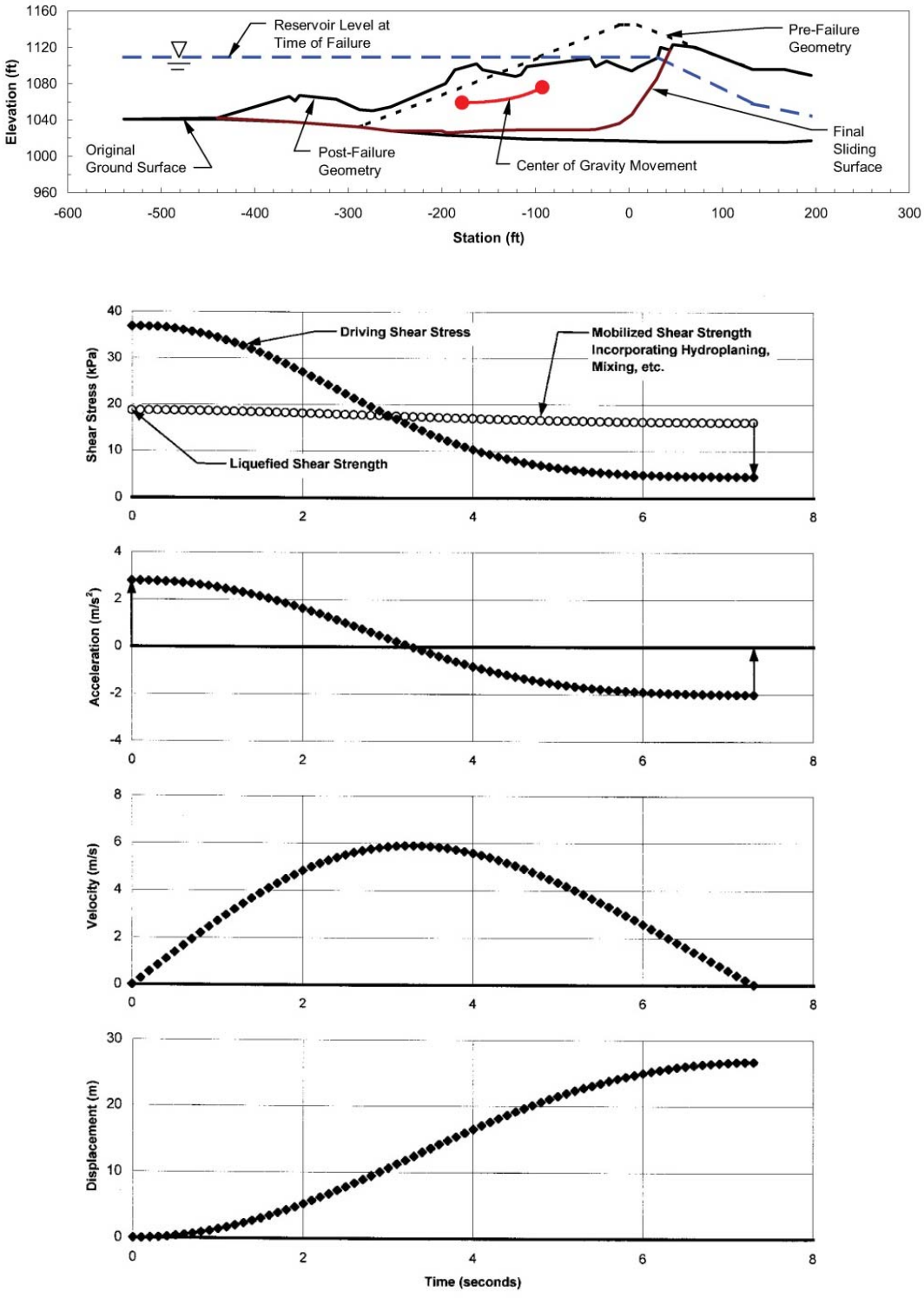

Figure 2.21: Illustration of "kinetics" analysis of the failure of the upstream slope of the Lower San Fernando Dam (Olsen, 2001).

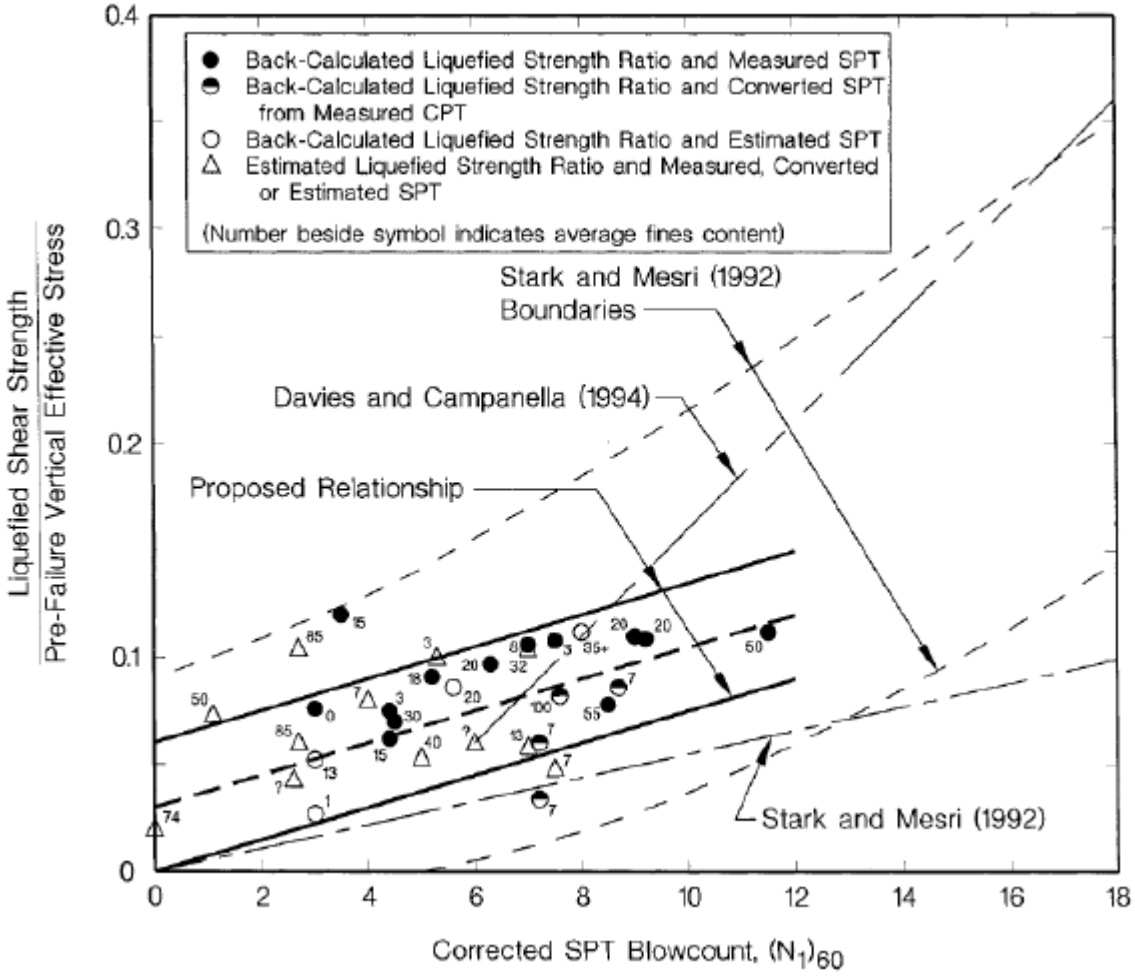

Figure 2.22: Recommended relationship for estimation of normalized residual strength ratio as a function of SPT penetration resistance (Olsen and Stark, 2002)

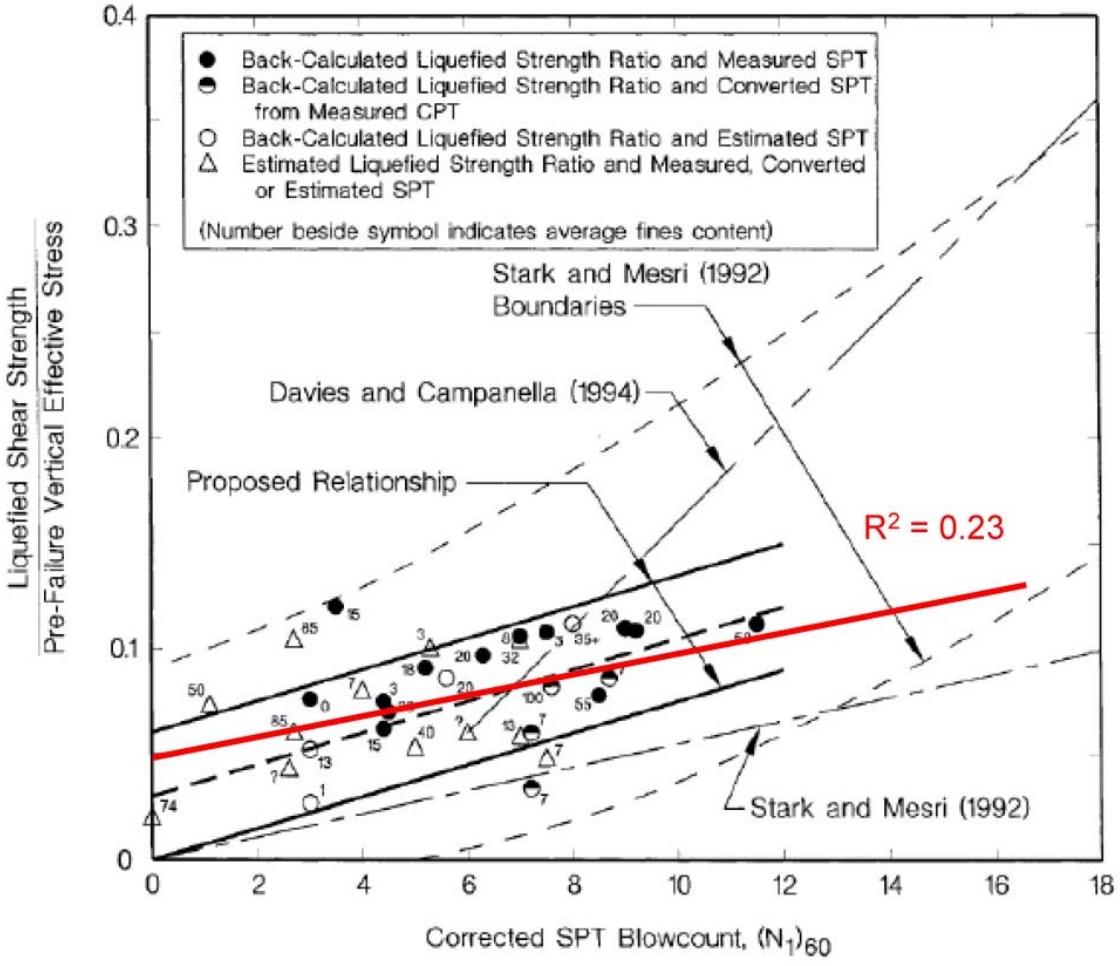

Figure 2.23: Least squares regression of the data set developed by Olsen and Stark from Figure 2.22.

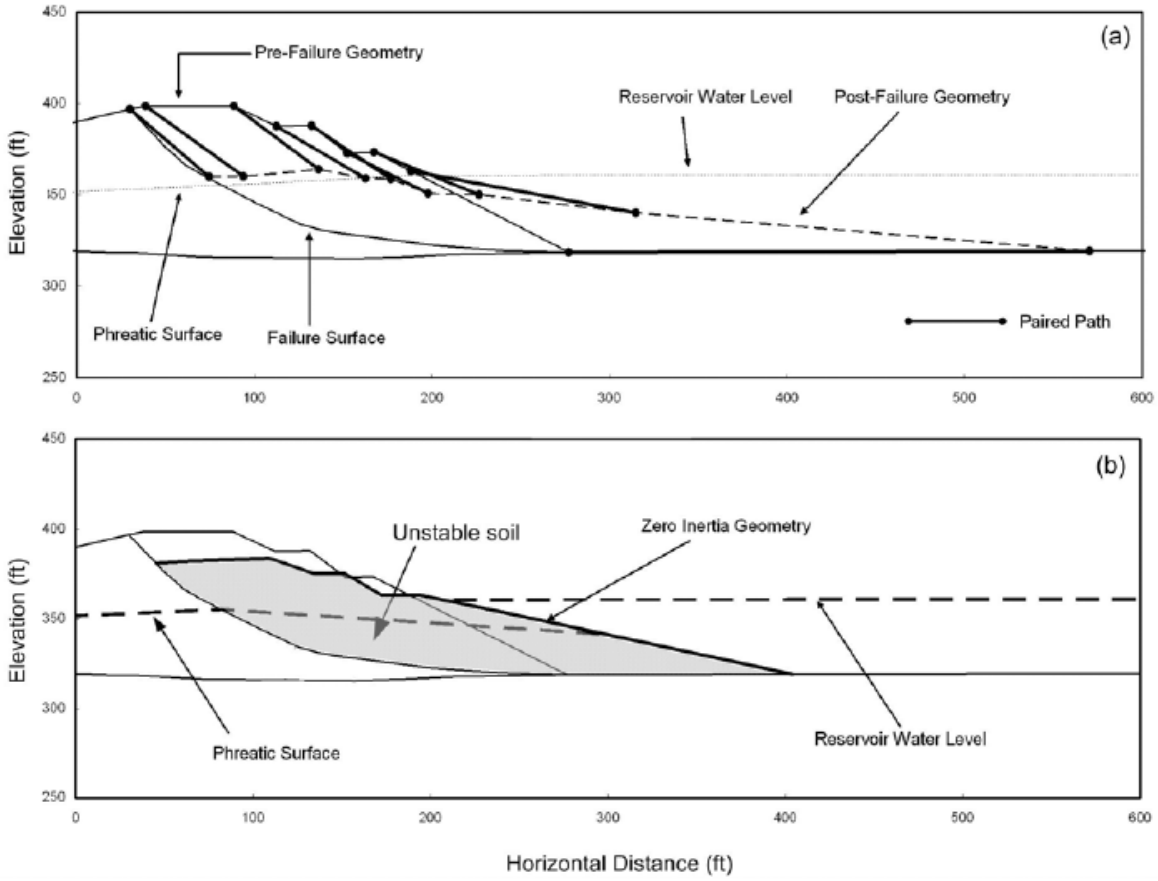

Figure 2.24: Illustration of the procedure employed by Wang (2001) for estimating zero inertial geometry (Figure from Kramer, 2008, after Wang, 2003)

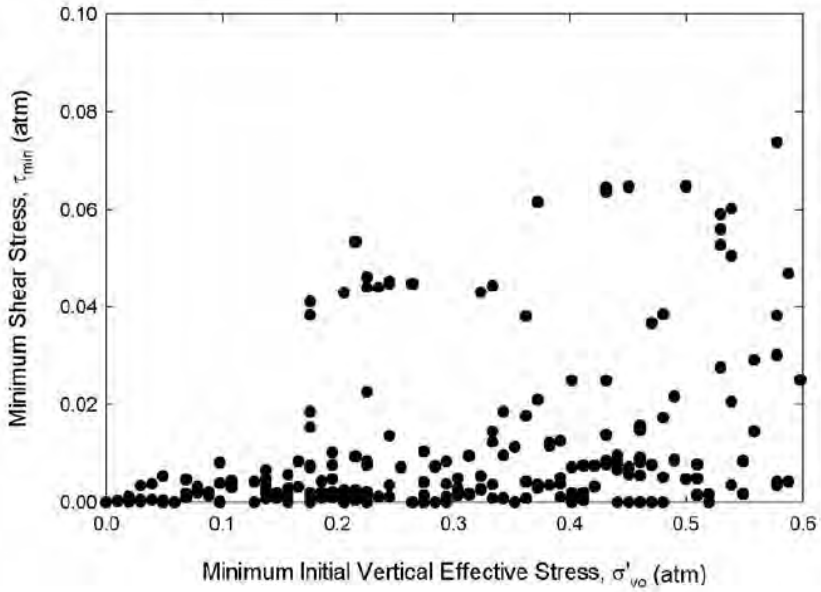

Figure 2.25: Combinations of minimum shear stress and minimum initial vertical effective stress from database of shallow lateral spreading case histories (Kramer, 2008).

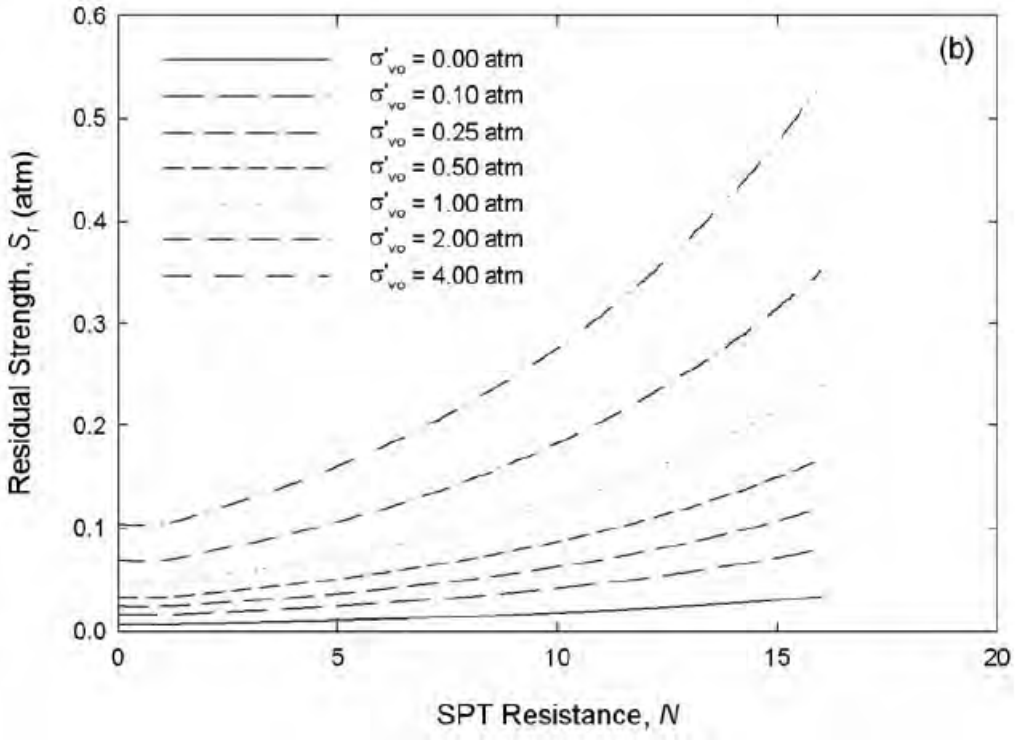

Figure 2.26: Median residual strength curves based on SPT resistance and initial effective vertical stress (Kramer, 2008).

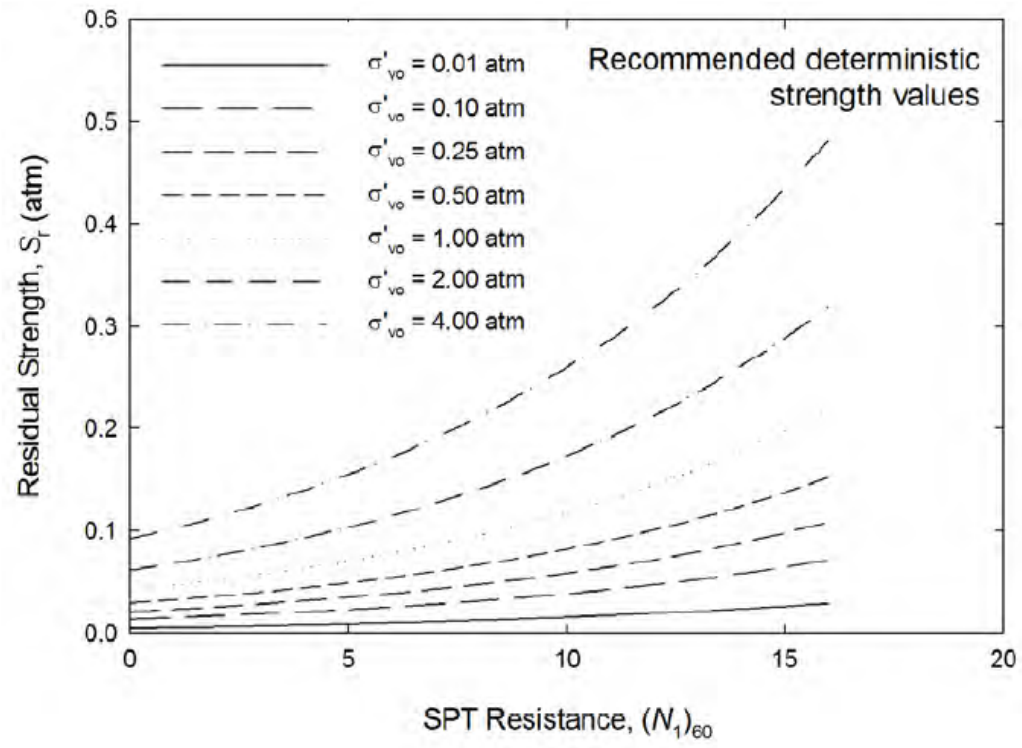

Figure 2.27: Recommended deterministic residual strength curves based on SPT resistance and initial effective vertical stress (Kramer, 2008).

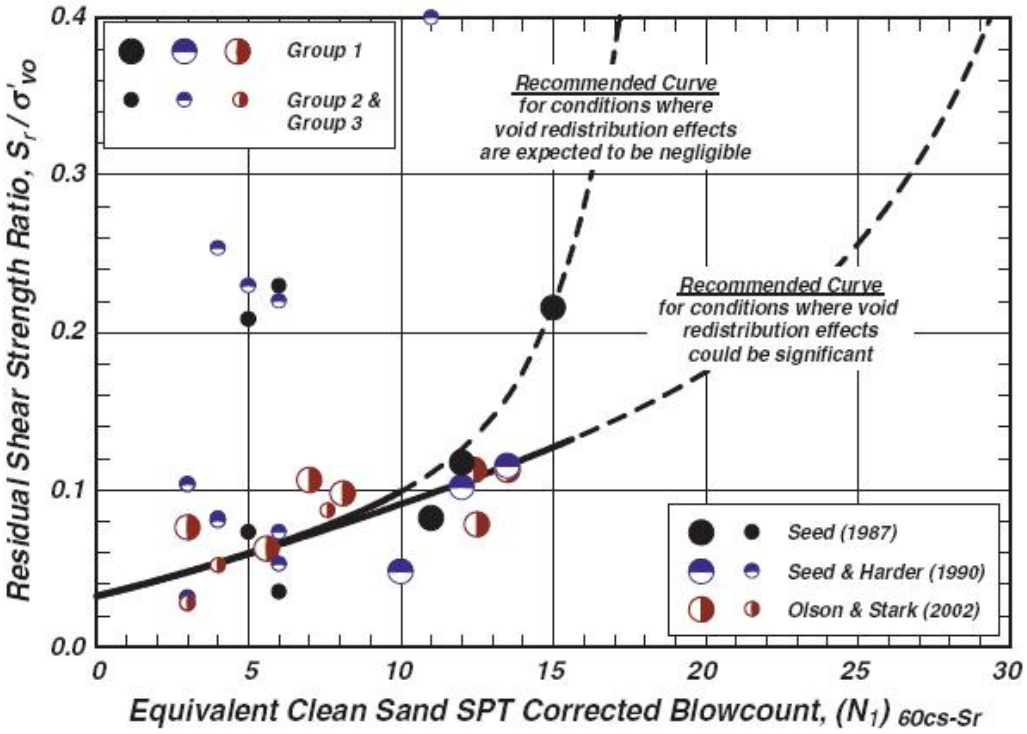

Figure 2.28: Recommended relationship for estimation of normalized residual strength ratio as a function of SPT resistance (Idriss and Boulanger, 2008)

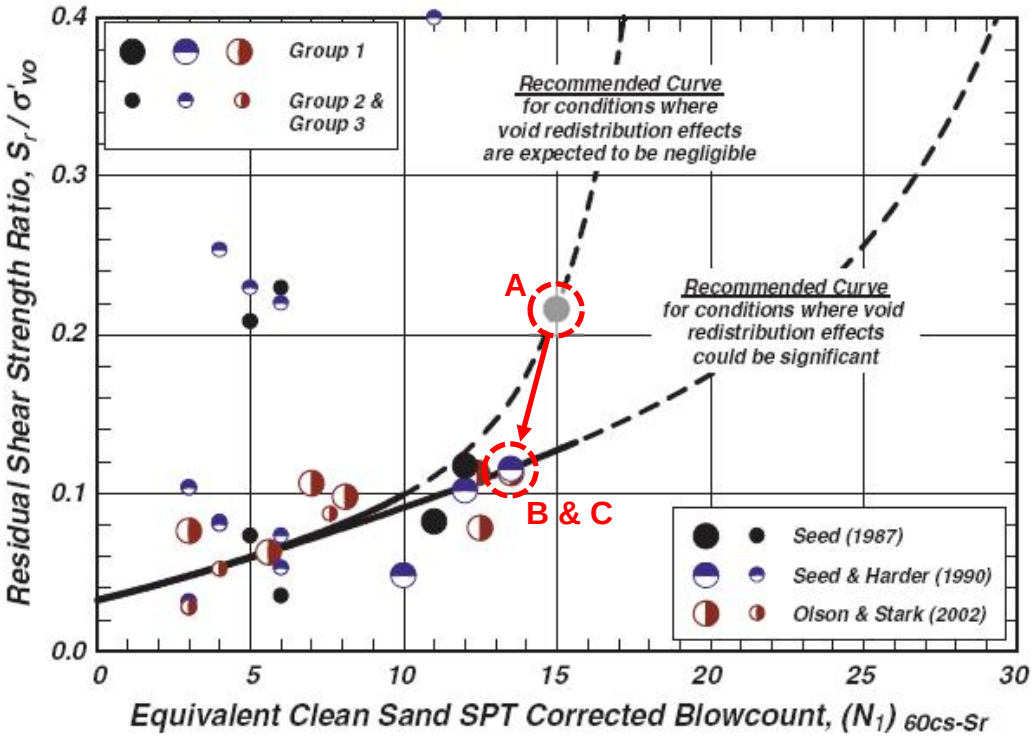

Figure 2.29: Figure 2.28 repeated, showing relocation of the data point for the Lower San Fernando Dam.

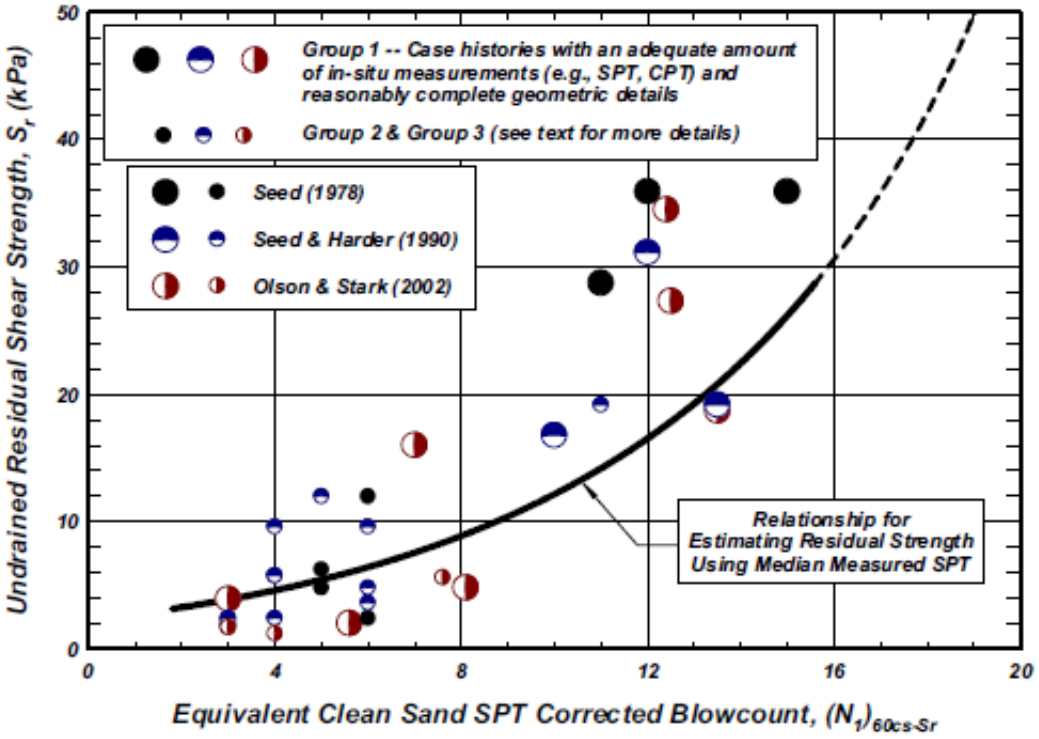

Figure 2.30: Recommended relationship for estimation of residual strength as a function of SPT resistance (Idriss and Boulanger, 2008)

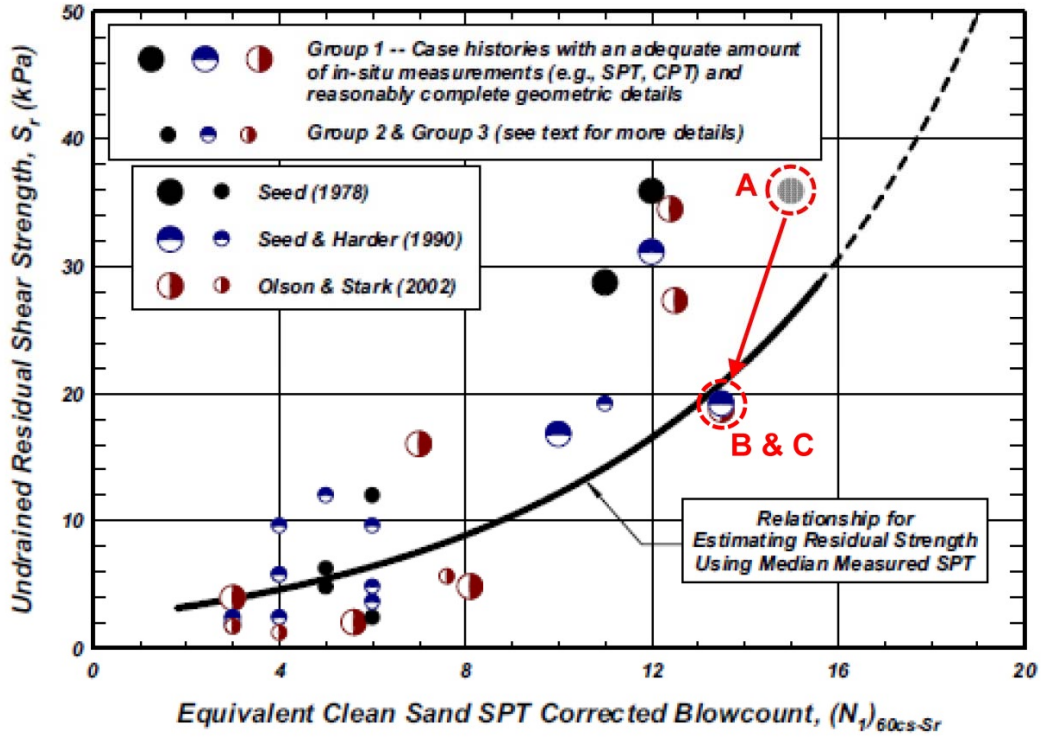

Figure 2.31: Figure 2.30 repeated, showing relocation of the data point for the Lower San Fernando Dam.

Chapter Three

Review and Selection of Liquefaction Case Histories for Back-Analyses

3.1 Introduction

The selection of full-scale liquefaction case histories to be back-analyzed for purposes of development of empirical methods for evaluation of in situ post-liquefaction strengths represents an important set of judgments and decisions.

A large number of previous investigations, and experts, have (a) back-analyzed sub-sets of the available case histories, or (b) employed the results of back-analyses performed by other investigation efforts, in their own development of empirical approaches for evaluation of post-liquefaction strengths. Different decisions, and different selections, were made by various investigators. In some cases (early efforts) there were only a limited number of potential field case histories available, so selections were often made on the basis of attempting to optimize use of these limited opportunities.

In more recent investigations (after about the mid-1990's), selection or de-selection of cases for back-analyses or for inclusion in development of empirical relationships were more often made on the basis of one or more of the following considerations:

1. Perceived availability, quality and documentation of information regarding pre-failure and post-failure geometry and conditions. In addition to basic geometry and stratigraphy, this also includes information constraining the location of the phreatic surface at the time the failure occurred.
2. Perceived quality and/or availability of information or data available for characterization of the soil units suspected of having liquefied. Highest quality data here were generally considered to be well-documented SPT or CPT data. Lesser quality data were sparse penetration data, non-standard penetration data, and cases in which penetration resistance had to be inferred more qualitatively from apparent relative density, soil placement history, etc.
3. Additional data and information, including witness accounts, information and data regarding soil properties (unit weights, strength parameters, etc.) for both liquefied and non-liquefied soils, etc.
4. Tractability of the observed (or suspected) failure mechanism with regard to relatively accurate and reliable back-analysis for the specific purpose of assessment of post-liquefaction strength S_r.
5. Personal preferences. For example some previous efforts preferred to consider only cases in which CPT data were available.

Not all previous studies presented clear explanations as to the reasons for selection and de-selection of case histories considered and/or back-analyzed.

Some level of general consensus can be inferred by the common choices made by a significant number of previous investigators with regard to a number of the available case histories. But as new information has developed, some of these choices now appear less attractive (e.g. the Calaveras Dam case history).

In these current studies, the full suite of case histories considered to date were fully re-considered, with (1) understanding of the decisions and selections made by previous investigation teams, (2) the benefits of examination and review of previous back-analysis efforts and of previously developed approaches for assessment of in situ post-liquefaction strength (see Chapter 2), and (3) new information that appears to have been developed recently and not made available to a number of investigation teams (e.g. the Calaveras Dam case history).

Table 3.1 presents a listing of the field liquefaction case histories back-analyzed, or included in empirical correlations, by a select sub-set of six previous in investigation efforts. These six previous efforts were selected for presentation in this table because (1) they were notably comprehensive efforts with regard to inclusion of case histories at their time, and (2) between them they comprise a list of essentially all potentially useful cases (currently known) for purposes of back-analyses to evaluate in situ S_r.

3.2 Lateral Spreading Case Histories

Having noted the relative paucity of available case histories of large-displacements liquefaction failures, Olsen and Johnson (2008) back-analyzed a significant number of lateral spreading case histories, many of them from the lateral spreading case history database assembled by Youd et al. (2002), as discussed previously in Section 2.3.9. Youd et al. had compiled this database for purposes of developing empirical methods for prediction of lateral spreading displacements. Olsen and Johnson employed Newmark-type methods to attempt to back-analyze the lateral spreading case histories to extract estimates of post-liquefaction strength. One of the principal findings was the difficulty of extracting reliable estimates of back-calculated S_r for cases (lateral spreads) wherein the overall movements included a strong contribution from transient cyclic lurching forces.

Lateral spreads are differentiated from the other (and generally larger displacement) cases in these current studies as being cases in which relatively moderate levels of gravity-induced static "driving" shear stresses do not, by themselves, generate a large majority of the observed movements and displacements. Instead, transient cyclic seismic loading, and resulting cyclic lurching forces, are also an important contributor. These cyclic forces are difficult to accurately back-analyze for several reasons. One reason is that simplified Newmark-type analysis methods do not provide a high degree of precision here. Another difficulty is the importance of details of the transient seismic loads (e.g. acceleration time histories) that actually occurred at the site in question. A potentially high degree of sensitivity of calculated displacements to these details contributes to further to the uncertainties involved in back-analyses of these case for purposes of back-estimation of S_r.

Accordingly, it was determined in these current studies that cases wherein transient cyclic lurching forces appear to be of sufficient importance as to potentially obscure, or prevent reliable assessment of, post-liquefaction strengths would not be included in the data set.

In addition to the lateral spreading cases added by Olsen and Johnson (2008), a number of additional lateral spreading cases collected and processed by Faris (2004) specifically for the purpose of developing relationships for prediction of lateral spreading displacements were also examined.

The semi-empirical method for prediction of lateral spreading displacements developed by Faris (2004) was employed to assess the potential usefulness of these lateral spreading cases for purposes of back-evaluation of S_r. Figure 3.1 illustrates this procedure for a typical case the Shonan-Cho lateral spread which occurred during the 1983 Nihonkai-Chubu earthquake. As shown in the top left figure, a liquefaction triggering evaluation was made for each SPT $N_{1,60,CS}$ value measured within materials considered potentially liquefiable. Those judged likely to liquefy were then re-plotted in the upper right-hand figure on a plot showing shear strain potential as a function of (1) $N_{1,60,CS}$ and (2) equivalent uniform cyclic stress ratio (CSR_{eq}) for a causative event of $M_W = 7.5$. These shear strain potentials are based on laboratory cyclic triaxial testing, and do not (yet) include effects of initial "driving" shear stresses. The resulting estimates of strain potential are then ascribed to the interval in each boring represented by the individuals $N_{1,60,CS}$ values, and accumulated displacement potential from bottom to top of the boring (up to the ground surface) is then calculated as shown in the plot of the right-hand middle figure. In this figure, depth ranges over which liquefaction strain potential are summed vary due to changes in overall thickness of the potentially liquefiable materials at different locations within the overall lateral spreading feature. This results in an estimated displacement potential "index" (DPI) at the location of each SPT boring.

These estimated DPI values are not direct estimates of expected displacements; they are only indices of stiffness or deformability. Faris compiled these indices for a large number of field case histories, and then performed regressions to develop empirical correlations for prediction of expected lateral spreading displacements as a function of (1) DPI, (2) initial driving shear stresses (estimated in a simplified manner based on slope and/or free face height at the toe of a lateral spreading feature, and (3) earthquake magnitude (serving as an approximation of duration or number of cycles). Each value of DPI, for each boring, is then transformed using the regressed relationship, to develop values of predicted actual displacements at each boring location. This is shown in the bottom left-hand corner of the figure. The resulting calculated "predictions" of expected displacement are then averaged together to develop an average calculated displacement (or predicted displacement). The displacements actually observed in the field (ideally at the boring locations) are then also averaged to produce the average observed displacement. These averaged calculated and observed displacements are plotted in the figure in the bottom left-hand corner. The ratio of predicted vs. observed displacements is calculated.

For this screening level exercise, it was determined that cases in which either (1) observed displacements were less than 3 feet, or (2) the ratio of observed vs. predicted displacements was less than a factor of 2, would be assumed to have had sufficiently significant cyclic lurching effects that it would not be appropriate to attempt to back-analyze them for purposes of trying to discern

post-liquefaction strength S_r. Cases only marginally exceeding these two limits would be more closely examined on an individual basis.

This screening level analysis was applied to all of the cases compiled by Olsen and Johnson (2008), and to the cases compiled by Faris (2004) for purposes of development of empirical relationships for prediction of lateral spreading displacements. A number of cases had observed displacements that differed from predicted displacements by factors of greater than 2, but some of these had displacements where the observed values were smaller (by a factor of 2 or more) than those observed. Of the few cases where the ratio of displacements observed vs. those predicted were greater than 2, some had overall (average) displacements of less than 3 feet.

The one case that came closest to being carried forward for further back-analysis was the Shitayama School lateral spread from the 1964 Niigata earthquake. This case had an observed average displacement of 12.2 feet, and an average calculated (predicted) displacement of 5.4 feet based on Faris' semi-empirical method. The resulting ratio was then 12.7 ft. / 5.4 ft. ≈ 2.4. This case was then examined further, and the engineering team determined that we would not be confident that cyclic inertial effects did not contribute significantly to observed displacements at this site due to (1) the relatively moderate pre-earthquake static driving shear stresses, and (2) the estimated intensity and duration of shaking at this site.

In the end, none of the "lateral spreading" case histories from either the Youd et al. (2002) database examined by Olsen and Johnson (2008) or from the additional cases developed by Faris (2004) were carried forward for these current studies of post-liquefaction S_r.

3.3 Remaining Potential Candidate Liquefaction Case Histories

3.3.1 Separation of Case Histories into Groups Based on Assessed Quality and Reliability

With most of the lateral spreading case histories thus eliminated, 36 potential candidate cases remained. These are listed in Table 3.2. When available, the results of back-analyzed values of post-liquefaction strength, or post-liquefaction strength ratio, as well as representative vertical effective stress and SPT penetration resistance are presented, as developed by (1) Seed and Harder (1990), (2) Olsen and Stark (2002), and Wang and Kramer (2003 and 2008).

After studying these cases, they were sub-divided into four groups: Groups A, B, C and D, as shown in Figure 3.2.

Group A case histories were judged to be generally of the highest quality with regard to well-documented data and information regarding (1) pre-failure and post-failure geometry, (2) penetration resistance within the critical liquefiable materials, and (3) other details including phreatic surface at the time of failure, shear strengths of non-liquefied soils, etc. These 13 case histories were judged to warrant the application of the incremental momentum back-analysis methods described in Chapter 4, Section 4.2 to develop best possible estimates of post-liquefaction strengths.

The single Group C case history (Calaveras dam) was also judged to have high quality data and information regarding geometries, etc., needed for high-level back-analyses to evaluate post-liquefaction strength, and so it was also back-analyzed using the incremental momentum methodology. But this case was not then subsequently used to help to develop empirical relationships for evaluation of in situ post-liquefaction strength, as will be explained further in Section 3.3.2.

The 16 case histories of Group B were judged to have lesser quality data, or less well-documented data, than the Group A cases, leading to greater uncertainties. These cases were judged not to warrant the performance of full incremental momentum analyses, but it was judged that useful estimates of post-liquefaction strength could be made, and useful estimates of representative penetration resistance and of representative vertical effective stress as well. Uncertainties associated with these values would generally be expected to be higher than for Group A cases.

The six cases of Group D had all been used in one or more previous studies, but upon detailed review and assessment these were deleted from further consideration as explained in Section 3.3.3.

Section 3.3.2: The Calaveras Dam Case History

This case had been a prominent case in the work of multiple previous investigation teams. But information developed in the late 1990's as part of seismic investigations of the repaired dam showed clearly that many of the embankment's hydraulic fill materials had a significant clay content. The main (pre-failure) dam was being constructed by the hydraulic fill method, with hydraulic deposition of fill materials simultaneously from the upstream and downstream sides. These fill materials were sourced form weathered colluvium on the local hillsides, and form weathered alluvium deposits also derived largely from the weathered colluvium. As shown in Figure 3.3 (and additional Figures in Appendix A, Section A.14), and Table 3.3, the resulting hydraulic fill zones were complex in terms of the nature and distribution of materials (Olivia Chen Consultants, 2002). The massive failure of 1918 occurred on the downstream side, and so the materials shown in Figure 3.3 on the downstream side of the dam represent the "post-repair" section, and not the original materials that controlled the failure.

In the current cross-section, the materials of Zones V and VI best represent (by approximate symmetry) the materials that would have controlled the 1918 failure. Materials in these zones are highly variable, and consist of broadly well-graded mixes of gravels, sands and clayey fines. Gravel contents vary greatly, are often high enough as to warrant the use of Becker Penetrometer testing (BPT) as well as short-interval SPT, as part of the 1990's investigations. But variability was high enough that some portions of these same hydraulic fill zones were judged to be clearly "cohesive fines dominated". Fines contents also varied greatly, form very low to as high as 70% or more in some zones. The fines were mainly low to moderate plasticity clays (CL), with PI generally between approximately 15% to 25%.

The dam failed in 1918 as initial construction was nearing completion. As a result, these materials, and especially those comprised of sufficient clay as to be subject to significant

consolidation, were still consolidating under the rising fill loads. These soils were likely variably underconsolidated, and conditions at the time of failure are not likely to be well-represented by the modern SPT or BPT penetration resistances obtained many decades later. As a result, it was the reluctant conclusion of this engineering team, and with the unanimous concurrence of the informal advisory group of experts, that it is not reasonable to attempt to correlate back-calculated strengths from this failure with available penetration resistance data.

This does not mean that this is a poor case for back-analyses. On the contrary, this is an excellent case of liquefaction-induced failure, and it was back-analyzed with the best available methods (including the incremental momentum method). The results of these back-analyses were then used, along with the results of back-analyses of cases from group A, to develop empirical correlations for estimation of post-liquefactions strengths as a function of runout characteristics, etc. These, in turn, were then used (1) to internally cross-check the back-analysis results of the case histories in Group A, and (2) to assist in development of assessments of post-liquefaction strengths from the case histories of Group B, and for cross-checking some of the back-analysis results for group B cases.

But the SPT and BPT penetration resistance values cannot be directly correlated with the back-analyzed estimates of post-liquefaction strength for this otherwise important case history.

It should be noted that most previous efforts to develop relationships for estimation of post-liquefaction strengths did employ the Calaveras dam case history, and that it was one of a limited number of cases providing high S_r values at relatively high penetration resistances. The information regarding materials character developed by the studies of Olivia Chen and Associates (2002) was not available to these previous investigators. The deletion of this case history from relationships and correlations based on the new information and data from the 1990's seismic studies would be expected to result in potential changes in these previous relationships.

3.3.3 Group D Cases

3.3.3.1 Kawagishi-Cho Building

The Kawagishi-Cho apartment building suffered a liquefaction-induced bearing capacity failure and toppled over during the 1964 Niigata earthquake (M_W = 7.5). This was a well-documented case history, but it is a difficult one to back-analyze. The bearing capacity failure does not appear to have been symmetric and the building toppled as it failed. Cyclic inertial forces are unknown, and difficult to estimate, and the cyclic overturning moments exerted on the structure, and the resulting non-uniform bearing pressures at the base of the structure that contributed to the failure, cannot be reliably estimated. This case was eliminated from further analysis or use in these current studies.

3.3.3.2 Snow River Bridge Fill

The Snow River bridge fill suffered a liquefaction-induced failure during the 1964 Alaskan earthquake (M_W = 9.3). This liquefaction-induced failure has also been employed in previous

studies. This case was eliminated from further consideration in these current studies because (1) of uncertainties with regard to pre-failure geometries, (2) uncertainties with regard to actual failure mode (e.g. depth of failure), and (3) uncertainties associated with soil-structure interaction effects associated with the piles supporting the bridge.

3.3.3.3 Koda Numa Railway Embankment

The Koda Numa railway embankment suffered a liquefaction-induced stability failure with large displacements during the 1968 Tokachi-Oki earthquake (M_W = 7.9). This case had also been used in multiple previous studies. This case was eliminated for further back-analyses in these current studies because of lack of confidence in the information and documentation available regarding the post-failure geometry and runout characteristics. The mass of the post-failure "displaced" material appears to be more than twice the mass that this same material occupied in the pre-failure geometry, and this discrepancy could not be resolved.

3.3.3.4 San Fernando Valley Juvenile Hall

The large hill slope adjacent to the San Fernando Valley Juvenile Hall facility suffered a liquefaction-induced downslope movement during the 1971 San Fernando earthquake (Mw = 6.6). This case had been employed in the previous studies, and relationships, of Seed (1987), Seed and Harder (1990) and Idriss (1998). This was a lateral spreading case history, and it was judged by the current engineering team that cyclic lurching forces likely contributed significantly to the observed displacements, and that the difficulties of dealing analytically with these cyclic forces would render accurate assessment of post-liquefaction S_r challenging. This case was deleted from further consideration.

3.3.3.5 Whisky Springs Fan

The Whiskey Springs Fan was essentially another lateral spreading case, and it occurred during the 1983 Borah Peak earthquake (M_W = 7.3). This case had also been employed in the previous studies, and relationships, of Seed (1987), Seed and Harder (1990) and Idriss (1998). It was judged by the current engineering team that cyclic lurching forces likely contributed significantly to the observed displacements, and that the difficulty of having to analytically deal with these cyclic lurching forces would render accurate assessment of post-liquefaction strength challenging at best. This case was deleted from further consideration.

3.3.3.6 Fraser River Delta

The Fraser River Delta case history involved a static liquefaction flow failure in the Fraser River Delta that occurred in 1985. It was employed in relationships developed by Olsen and Stark (2002) and by Robertson (2010). This case was eliminated from further consideration in these current studies (1) because of lack of reliable pre-failure and post-failure geometries, and (2) because the post-liquefaction strength ratio had therefore been estimated only on the basis of laboratory tests performed on reconstituted samples of Fraser River Delta sands.

Table 3.1: Candidate Liquefaction Case Histories Considered

Case History	Apparent Cause of Sliding	Seed and Harder (1990)	Stark and Mesri (1992)	Olson and Stark (2002)	Robertson (2010)	Faris (2004)	Olson and Johnson (2008)
Zeeland - Vlietepolder	1889 High Tide	--	--	X	X	--	--
Coyote Creek	1906 San Francisco, California	--	--	--	--	X	--
Salinas River	1906 San Francisco, California	--	--	--	--	X	--
Sullivan Marsh	1906 San Francisco, California	--	--	--	--	X	--
Mission Creek	1906 San Francisco, California	--	--	--	--	X	--
Calaveras Dam	1918 Construciton	X	X	X	X	--	--
Wachusett Dam - North Dike	1918 Reservior Filling	--	--	X	X	--	--
Sheffield Dam	1925 Santa Barbara Eq. (M_L = 6.3)	X	X	X	X	--	--
Helsinki Harbor	1936 Construction	--	--	X	X	--	--
Fort Preck Dam	1938 Construction	X	X	X	X	--	--
Solfatara Canal Dike	1940 El Centro Eq. (M = 7.2)	X	X	X	X	--	--
Lake Merced Bank	1957 San Francisco Eq. (M = 5.7)	X	X	X	X	--	--
Snow River Bridge	1964 Alaska Eq. (M = 8.5)	X	X	--	--	--	--
Kawagishi-Cho Building	1964 Niigata Eq (M = 7.5)	X	X	X	X	X	--
Uetsu Railway Embankment	1964 Niigata Eq (M = 7.5)	X	X	X	X	--	--
North of Bandai Bridge	1964 Niigata, Japan					X	
Echigo Railway	1964 Niigata, Japan	--	--	--	--	X	--
Hokuriku Building	1964 Niigata, Japan	--	--	--	--	X	--
Hotel Niigata	1964 Niigata, Japan	--	--	--	--	X	--
NHK Building	1964 Niigata, Japan	--	--	--	--	X	--
South of Niigata Station	1964 Niigata, Japan	--	--	--	--	X	--
North of Niigata Station	1964 Niigata, Japan	--	--	--	--	X	--
North of Route 345	1964 Niigata, Japan	--	--	--	--	X	--
Shitayama Shool	1964 Niigata, Japan	--	--	--	--	X	--
Showa Bridge	1964 Niigata, Japan	--	--	--	--	X	--
Portage Creek	1964 Prince William Sound, Alaska	--	--	--	--	X	--
Twentymile River	1964 Prince William Sound, Alaska	--	--	--	--	X	--
El Cobre Tailings Dam	1965 Chilean Eq. (M_L = 7 to 7.25)	--	--	X	X	--	--
Koda Numa Railway Embankment	1968 Tokachi-Oki Eq. (M = 7.9)	X	X	X	X	--	--
Metoki Road Embankment	1968 Tokachi-Oki Eq. (M = 7.9)	--	--	X	X	--	--
Hokkaido Tailings Dam	1968 Tokachi-Oki Eq. (M = 7.9)	--	--	X	X	--	--
San Fernando Valley Juvenile Hall	1971 San Fernando Eq. (M_W = 6.6)	X	X	--	--	X	X
Lower San Fernando Dam U/S	1971 San Fernando Eq. (M_W = 6.6)	X	X	X	X	--	--
Lower San Fernando Dam D/S	1971 San Fernando Eq. (M_W = 6.6)	--	--	--	--	--	--
Upper San Fernando Dam	1971 San Fernando Eq. (M_W = 6.6)	X	X	--	--	--	--
Jensen Filtration Plant	1971 San Fernando, California	--	--	--	--	X	--
Tar Island Dyke	1974 Construction	--	--	X	X	--	--
Mochi-Koshi Tailings Dams	1978 Izu-Oshima Eq. (M = 7.0)	X	X	--	--	--	--
- Dike 1	1978 Izu-Oshima Eq. (M = 7.0)	--	--	X	X	--	--
- Dike 2	1978 Izu-Oshima Eq. (M = 7.0)	--	--	X	X	--	--
Heber Road	1979 Imperial Valley Eq. (M_W = 6.5)	--	X	--	--	X	X
Whiskey Springs Fan	1983 Borah Peak Eq. (M = 7.3)	X	X	--	--	X	X
Pence Ranch	1983 Borah Peak, Idaho	--	--	--	--	X	--
Hachiro-Gata Road Embankment	1983 Nihon-Kai-Chubu Eq. (M = 7.7)	--	--	X	X	--	--
East Slope of Maeyama	1983 Nihonkai-Chubu, Japan	--	--	--	--	X	--
South Slope of Maeyama	1983 Nihonkai-Chubu, Japan	--	--	--	--	X	--
Adjacent to Road No. 7	1983 Nihonkai-Chubu, Japan	--	--	--	--	X	--
Shonan-Cho	1983 Nihonkai-Chubu, Japan	--	--	--	--	X	--
Yoneshiro River	1983 Nihonkai-Chubu, Japan	--	--	--	--	X	--
Asele Raod Embankment	1983 Pavement Repairs	--	--	X	X	--	--
La Marquesa Dam - U/S Slope	1985 Chilean Eq. (M_S = 7.8)	X	X	X	X	--	--
La Marquesa Dam - D/S Slope	1985 Chilean Eq. (M_S = 7.8)	X	X	X	X	--	--
La Palma Dam	1985 Chilean Eq. (M_S = 7.8)	X	X	X	X	--	--
Fraser River Delta	1985 Gas Desaturation and Low Tide	--	--	X	X	--	--

Table 3.1: Candidate Liquefaction Case Histories Considered (Continued)

Case History	Apparent Cause of Sliding	Seed and Harder (1990)	Stark and Mesri (1992)	Olson and Stark (2002)	Robertson (2010)	Faris (2004)	Olson and Johnson (2008)
Chonan Middle School	1987 Chiba-Toho-Oki Eq. (M = 6.7)	--	--	X	X	--	--
Landing Road Bridge	1987 Edgecumbe, New Zealand (M_W = 6.5)	--	--	--	--	--	X
James Street Loop	1987 Edgecumbe, New Zealand (M_W = 6.5)	--	--	--	--	--	X
Whakatane Pony Club	1987 Edgecumbe, New Zealand (M_W = 6.5)	--	--	--	--	--	X
Lake Ackerman	1987 Seismic Survey	--	X	X	X	--	--
Wildlife Site	1987 Superposition Hills (M_W = 6.5)	--	--	--	--	--	X
Nalband Railway Embankment	1988 Armenian Eq. (M_S = 6.8)	--	--	X	X	--	--
Moss Landing MBARI Bldg 4	1989 Loma Prieta (M_W = 7.0)	--	--	--	--	--	X
Moss Landing MBARI Bldg 3	1989 Loma Prieta (M_W = 7.0)	--	--	--	--	--	X
Moss Landing MLML Bldg Eastward Spread	1989 Loma Prieta (M_W = 7.0)	--	--	--	--	--	X
Moss Landing MLML Bldg Westward Spread	1989 Loma Prieta (M_W = 7.0)	--	--	--	--	--	X
Miller Farm	1989 Loma Prieta (M_W = 7.0)	--	--	--	--	X	X
Farris Farm	1989 Loma Prieta (M_W = 7.0)	--	--	--	--	X	X
Leonardini Farm	1989 Loma Prieta (M_W = 7.0)	--	--	--	--	--	X
Sea Mist Farm	1989 Loma Prieta (M_W = 7.0)	--	--	--	--	--	X
Marina District, St. Francis Yacht Club	1989 Loma Prieta (M_W = 7.0)	--	--	--	--	--	X
Treasure Island	1989 Loma Prieta (M_W = 7.0)	--	--	--	--	--	X
MBARI	1989 Loma Prieta, California	--	--	--	--	X	--
MLML	1989 Loma Prieta, California	--	--	--	--	X	--
Leonardini Farm	1989 Loma Prieta, California	--	--	--	--	X	--
Soviet Tajik - May 1 Slide	1989 Tajik, Sovit Union Eq. (M_L = 5.5)	--	--	X	X	--	--
Nerlerk Embankment	1990 Construction	--	X	--	X	--	--
Eastbank	1990 Luzon, Phillippines	--	--	--	--	X	--
Southbank	1990 Luzon, Phillippines	--	--	--	--	X	--
Perez Blvd	1990 Luzon, Phillippines	--	--	--	--	X	--
Magsaysay Bridge, E. bank, d/s	1990 Luzon, Phillippines (M_W = 7.6)	--	--	--	--	--	X
Nable Street West	1990 Luzon, Phillippines (M_W = 7.6)	--	--	--	--	--	X
Nable Street East	1990 Luzon, Phillippines (M_W = 7.6)	--	--	--	--	--	X
Magsaysay Bridge, E. bank, u/s	1990 Luzon, Phillippines (M_W = 7.6)	--	--	--	--	--	X
Magsaysay Bridge, W. bank, u/s	1990 Luzon, Phillippines (M_W = 7.6)	--	--	--	--	--	X
Pogo Chico W. bank	1990 Luzon, Phillippines (M_W = 7.6)	--	--	--	--	--	X
Rudbaneh Town Canal	1990 Manjil, Iran (M_W = 7.4)	--	--	--	--	--	X
Sullivan Tailings	1991 Dyke Rising, British Columbia	--	--	--	X	--	--
Shibecha-Cho Embankement	1993 Kushiro-Oki Eq.(M_L = 7.8)	--	--	X	X	--	--
Route 272 at Higashiarekinai	1993 Kushiro-Oki Eq.(M_L = 7.8)	--	--	X	X	--	--
Aichi East	1993 Nansei-oki, Japan	--	--	--	--	X	--
Aichi West	1993 Nansei-oki, Japan	--	--	--	--	X	--
Jamuna Bridge	1994 Construction, Bangladesh	--	--	--	X	--	--
Balboa Blvd.	1994 Northridge (M_W = 6.7)	--	--	--	--	X	X
Wynne Ave.	1994 Northridge (M_W = 6.7)	--	--	--	--	--	X
Potrero Canyon	1994 Northridge (M_W = 6.7)	--	--	--	--	--	X
Wufeng Site C (A-A')	1999 Chi-Chi, Taiwan (M_W = 7.6)	--	--	--	--	--	X
Wufeng Site C (B-B')	1999 Chi-Chi, Taiwan (M_W = 7.6)	--	--	--	--	--	X
Wufeng Site C1	1999 Chi-Chi, Taiwan (M_W = 7.6)	--	--	--	--	--	X
Wufeng Site B	1999 Chi-Chi, Taiwan (M_W = 7.6)	--	--	--	--	X	X
Wufeng Site M	1999 Chi-Chi, Taiwan (M_W = 7.6)	--	--	--	--	--	X
Nantou Site N	1999 Chi-Chi, Taiwan (M_W = 7.6)	--	--	--	--	--	X
Hotel Sapanca	1999 Kocaeli, Turkey (M_W = 7.4)	--	--	--	--	X	X
Police Station	1999 Kocaeli, Turkey (M_W = 7.4)	--	--	--	--	--	X
Soccer Field	1999 Kocaeli, Turkey (M_W = 7.4)	--	--	--	--	X	X
Yalova Harbor	1999 Kocaeli, Turkey (M_W = 7.4)	--	--	--	--	--	X
Norswing Drive	2003 San Simeon (M_W = 6.5)	--	--	--	--	--	X
Juanita Ave.	2003 San Simeon (M_W = 6.5)	--	--	--	--	--	X
Canadian Mine	(See Robertson (2010))	--	--	--	X	--	--

Table 3.2: Case Histories More Closely Considered for Potential Back-Analyses for Evaluation of Post-Liquefaction Strength (S_r)

Group	Case	Failure Date	Seed and Harder (1990)		Olson and Stark (2002)				Wang (2003) + Kramer (2008)			This Study
			S_r	$N_{1,60,CS}$	S_u(Liq)	S_u(Liq)/σ'_{vo}	σ'_{vo}	$N_{1,60}$ [1]	$\overline{S}_r$ [2]	S_r/σ_{vo}'	$\overline{N}_{1,60,CS}$	
A	Wachusett Dam - North Dike	1918 Reservior Filling			334	0.106	3158	7	348	0.136	7.3[3]	Analyzed
	Fort Peck Dam	1938 Construction	350	10	570	0.078	7341	8.5	671.5	0.091	15.8	Analyzed
	Uetsu Railway Embankment	1964 Niigata Eq (M = 7.5)	40	3	36	0.027	1280	3	43.5	0.048	2.9	Analyzed
	Lower San Fernando Dam - U/S Slope	1971 San Fernando Eq. (M_W = 6.6)	400	13.5	390	0.120	3482	11.5	484.7	0.133	14.5	Analyzed
	Hachiro-Gata Road Embankment	1983 Nihon-Kai-Chubu Eq. (M = 7.7)			42	0.062	670	4.4	65	0.164	5.7	Analyzed
	La Marquesa Dam - U/S Slope	1985 Chilean Eq. (M_S = 7.8)	200	6	65	0.07	911	4.5	(185.2)	0.110	6.5[3]	Analyzed
	La Marquesa Dam - D/S Slope	1985 Chilean Eq. (M_S = 7.8)	400	11	111	0.11	1000	9	(343.5)	0.186	9.9[3]	Analyzed
	La Palma Dam	1985 Chilean Eq. (M_S = 7.8)	200	4	100	0.12	789	3.5	(193.3)	0.123	4.2	Analyzed
	Lake Ackerman Highway Embankment	1987 Seismic Survey			82	0.076	1076	3	98	0.114	4.8	Analyzed
	Chonan Middle School	1987 Chiba-Toho-Oki Eq. (M = 6.7)			100	0.09	1119	5.2	(178.7)	0.091	6.4[3]	Analyzed
	Soviet Tajik - May 1 Slide	1989 Tajik, Sovit Union Eq. (M_L = 5.5)			175	0.08	2170	7.6	(334)	0.082	8.9[3]	Analyzed
	Shibecha-Cho Embankement	1993 Kushiro-Oki Eq.(M_L = 7.8)			117	0.086	1351	5.6	208.9	0.200	5.6	Analyzed
	Route 272 at Higashiarekinai	1993 Kushiro-Oki Eq.(M_L = 7.8)			100	0.097	1030	6.3	130.5	0.125	8.5	Analyzed
B	Zeeland - Vlietepolder	1889 High Tide			115	0.05	2396	7.5	(226.1)	0.048	8.5[3]	Analyzed
	Sheffield Dam	1925 Santa Barbara Eq. (M_L = 6.3)	75	6	75	0.05	1429	5	(99.8)	0.043	8.2[3]	Analyzed
	Helsinki Harbor	1936 Construction			32	0.06	522	6	(52.4)	0.067	5.9[3]	Analyzed
	Solfatara Canal Dike	1940 El Centro Eq. (M = 7.2)	50	4	50	0.08	624	4	(77.1)	0.063	4.9[3]	Analyzed
	Lake Merced Bank	1957 San Francisco Eq. (M = 5.7)	100	6	144	0.11	1372	7.5	(139.5)	0.106	5.9[3]	Analyzed
	El Cobre Tailings Dam	1965 Chilean Eq. (M_L = 7 to 7.25)			40	0.020	1946	0	(195.2)	0.020	6.8	Analyzed
	Metoki Road Embankment	1968 Tokachi-Oki Eq. (M = 7.9)			38	0.04	875	2.6	(116.8)	0.044	2.0	Analyzed
	Hokkaido Tailings Dam	1968 Tokachi-Oki Eq. (M = 7.9)			100	0.07	1376	1.1	(250.6)	0.074	5.1	Analyzed
	Upper San Fernando Dam - D/S Slope	1971 San Fernando Eq. (M_W = 6.6)	600	15								Analyzed
	Tar Island Dyke	1974 Construction			251	0.06	4300	7	(364.2)	0.058	8.9[3]	Analyzed
	Mochi-Koshi Tailings Dam, Dikes 1 and 2	1978 Izu-Oshima Eq. (M = 7.0)	250	5	75	0.06	1251	2.7	(158.9)	0.091	8.9	Analyzed
					113	0.10	1090	2.7	(233.6)	0.081	10.0	
	Nerlerk Embankment, Slides 1 ,2 and 3	1983 Construction			52	0.09	616	8.7	(178.5)	0.124	11.4[3]	Analyzed
					36	0.06	650	7.2				
					31	0.03	925	7.2				
	Asele Road Embankment	1983 Pavement Repairs			132	0.10	1251	7	(163.7)	0.104	11.0[3]	Analyzed
	Nalband Railway Embankment	1988 Armenian Eq. (M_S = 6.8)			119	0.11	1101	9.2	(139.9)	0.109	6.3[3]	Analyzed
	Sullivan Tailings	1991 Dyke Rising, British Columbia										Analyzed
	Jamuna Bridge	1994 Construction, Bangladesh										Analyzed
C	Calaveras Dam	1918 Construction	650	12	721	0.112	6422	8	632.7	0.099	10.5[3]	Analyzed
D	Kawagishi-Cho Building	1964 Niigata, Japan (M = 7.5)	120	4	111	0.08	1474	4.4	(123.5)	0.089	4.3	Not Analyzed
	Snow River Bridge Fill	1964 Alaskan Eq. (M = 8.5)	50	7					(50)	0.025	8.5[3]	Not Analyzed
	Koda Numa Railway Embankment	1968 Tokachi-Oki Eq. (M = 7.9)	50	3	25	0.05	485	3	(48)	0.045	3.6	Not Analyzed
	San Fernando Valley Juvenile Hall	1971 San Fernando Eq. (M_W = 6.6)	130	10.5								Not Analyzed
	Whiskey Springs Fan	1983 Borah Peak Eq. (M = 7.3)	150	11								Not Analyzed
	Frasier River Delta	1985 Low Tide			N/A	0.100	N/A	5.3				Not Analyzed

Notes : (1) No fines content correction utilized in Olson and Stark (2002).
(2) Where noted in parentheses, $S_{u,r}$ values shown are for secondary cases in Wang (2003) and were not fully reanalyzed.
(3) $N_{1,60,CS}$ values were changed in Kramer (2008) from the values reported in Wang (2003). The updated values are shown.

Table 3.2: Case Histories Back-Analyzed for Evaluation of Post-Liquefaction Strength (S_r)

Group	Case Number	Case	Failure Date
A	1	Wachusett Dam - North Dike	1907 Reservior Filling
	2	Fort Peck Dam	1938 Construction
	3	Uetsu Railway Embankment	1964 Niigata Eq (M = 7.5)
	4	Lower San Fernando Dam - U/S Slope	1971 San Fernando Eq. (M_W = 6.6)
	5	Hachiro-Gata Road Embankment	1983 Nihon-Kai-Chubu Eq. (M = 7.7)
	6	La Marquesa Dam - U/S Slope	1985 Chilean Eq. (M_S = 7.8)
	7	La Marquesa Dam - D/S Slope	1985 Chilean Eq. (M_S = 7.8)
	8	La Palma Dam	1985 Chilean Eq. (M_S = 7.8)
	9	Lake Ackerman Highway Embankment	1987 Seismic Survey
	10	Chonan Middle School	1987 Chiba-Toho-Oki Eq. (M = 6.7)
	11	Soviet Tajik - May 1 Slide	1989 Tajik, Sovit Union Eq. (M_L = 5.5)
	12	Shibecha-Cho Embankement	1993 Kushiro-Oki Eq.(M_L = 7.8)
	13	Route 272 at Higashiarekinai	1993 Kushiro-Oki Eq.(M_L = 7.8)
B	15	Zeeland - Vlietepolder	1889 High Tide
	16	Sheffield Dam	1925 Santa Barbara Eq. (M_L = 6.3)
	17	Helsinki Harbor	1936 Construction
	18	Solfatara Canal Dike	1940 El Centro Eq. (M = 7.2)
	19	Lake Merced Bank	1957 San Francisco Eq. (M = 5.7)
	20	El Cobre Tailings Dam	1965 Chilean Eq. (M_L = 7 to 7.25)
	21	Metoki Road Embankment	1968 Tokachi-Oki Eq. (M = 7.9)
	22	Hokkaido Tailings Dam	1968 Tokachi-Oki Eq. (M = 7.9)
	23	Upper San Fernando Dam - D/S Slope	1971 San Fernando Eq. (M_W = 6.6)
	24	Tar Island Dyke	1974 Construction
	25	Mochi-Koshi Tailings Dam, Dikes 1 and 2	1978 Izu-Oshima Eq. (M = 7.0)
	26	Nerlerk Embankment, Slides 1 ,2 and 3	1983 Construction
	27	Asele Road Embankment	1983 Pavement Repairs
	28	Nalband Railway Embankment	1988 Armenian Eq. (M_S = 6.8)
	29	Sullivan Tailings	1991 Dyke Rising, British Columbia
	30	Jamuna Bridge	1994 Construction, Bangladesh
C	14	Calaveras Dam	1918 Construction

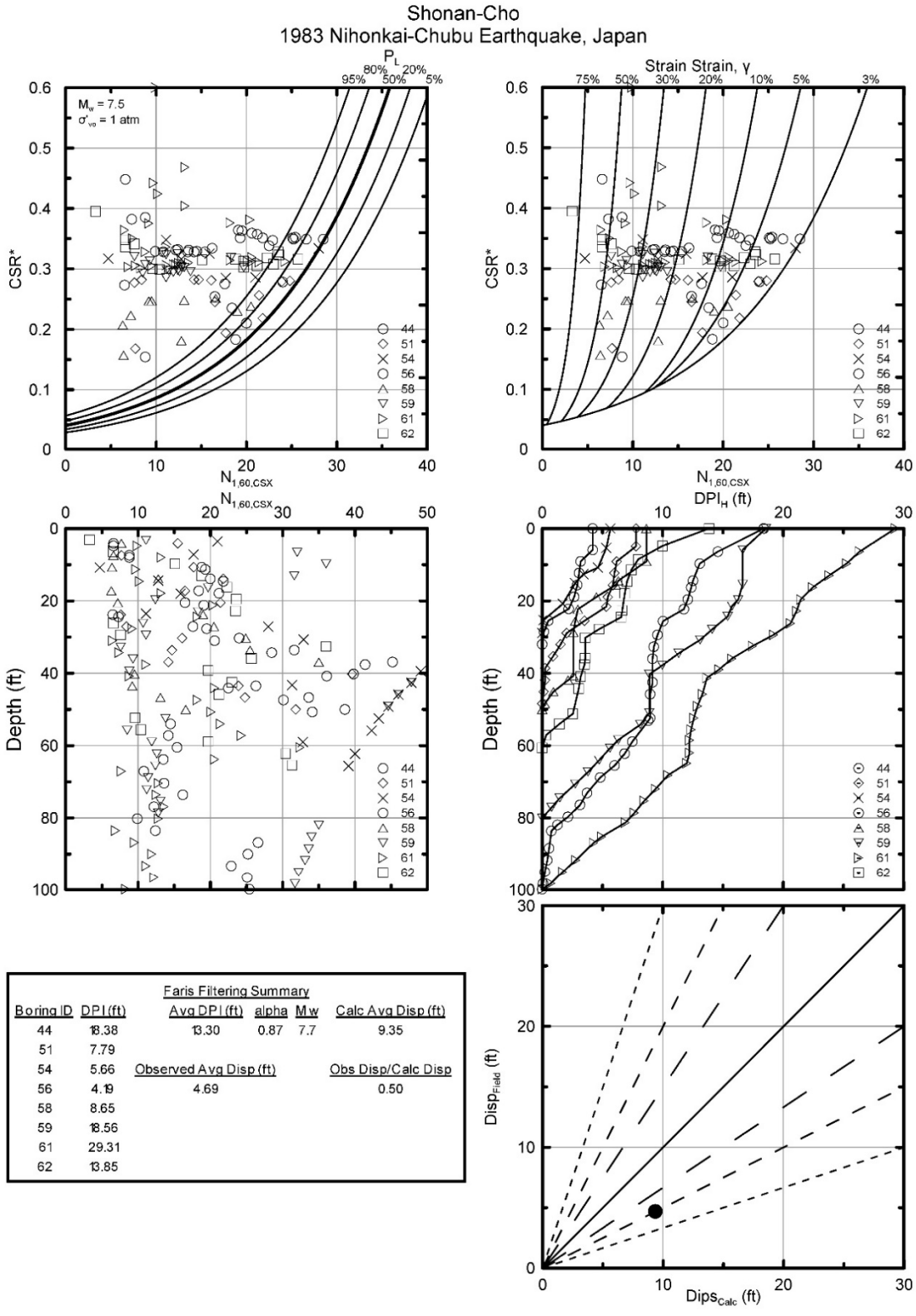

Figure 3.1: Illustration of the methodology developed by Faris (2004) for prediction of lateral spreading displacements; example analysis applied to the Shonan-Cho case history.

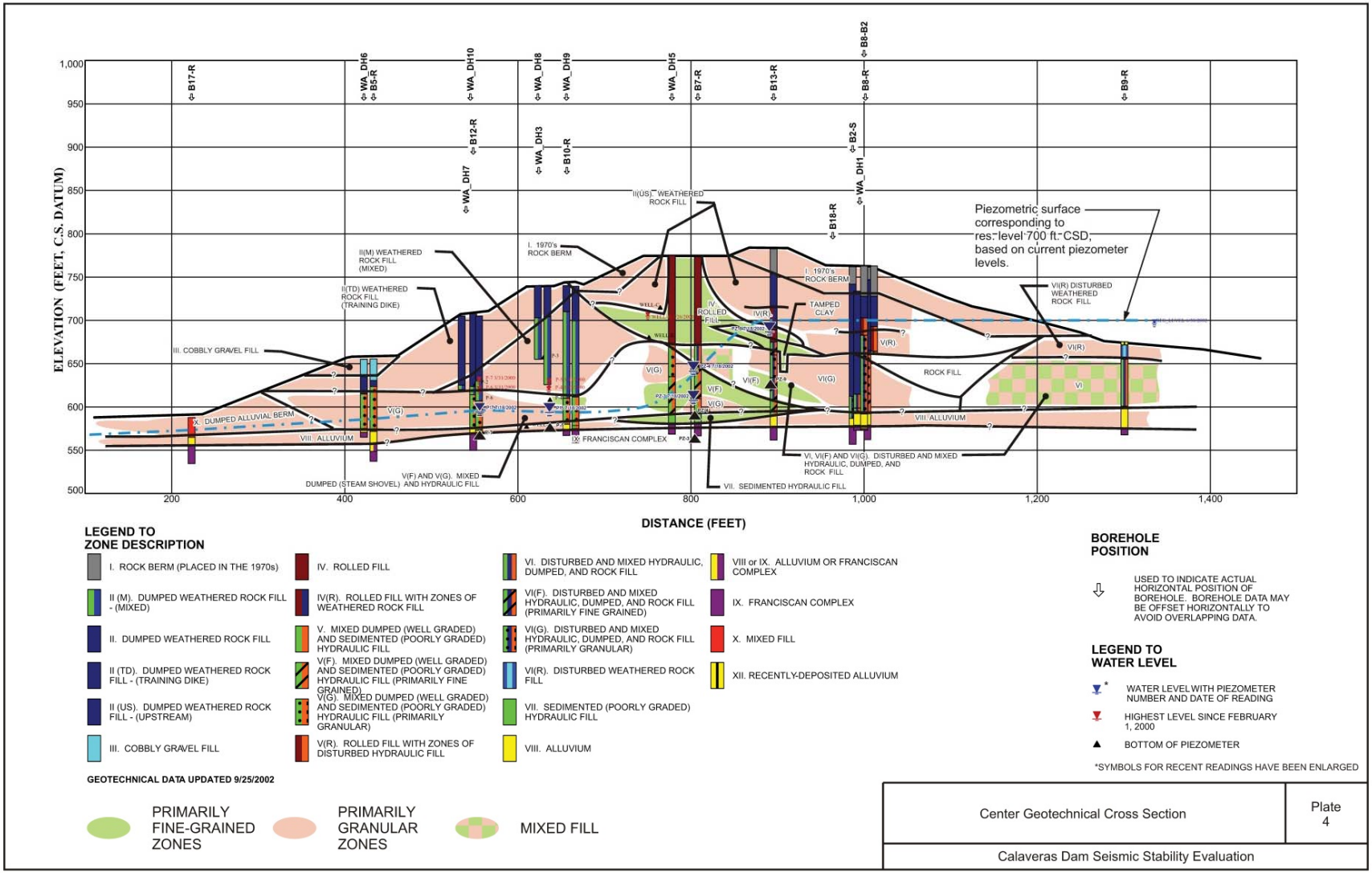

Figure 3.2: Cross-section of the reconstructed Calaveras dam showing general soil material zones as developed based on recent Seismic investigations (Olivia Chen and Associates, 2002).

Chapter Four

Back-Analyses of Liquefaction Failure Case Histories

4.1 Introduction

The 30 liquefaction failure case histories selected for inclusion in Table 3.3 were subjected to back-analyses and back-assessments by a variety of methods, depending upon the amounts and quality of data available for each of these cases. Cross-comparisons were made with other case histories back-analyzed in these current studies, and cross-comparisons were also made with the results and findings from previous investigations.

A number of new methods were developed in these current studies for improved back-analyses and assessments of post-liquefaction strengths, and these will be presented and explained as this chapter proceeds. It is also important to understand the approaches and procedures used by a number of previous investigators for similar back-analyses or back-assessments of post-liquefaction strengths in order to understand the juxtaposition of the results of those previous studies with the new results presented herein. Accordingly, this chapter will also discuss a number of previous methods, and their strengths and drawbacks.

Table 4.1 presents a list of the principal methods of interest for these current studies. These include methods employed by previous investigators, and also new methods developed for these current studies. This list provides a useful template for some of the discussions that will follow. Methods listed towards the top of the list tend to provide the highest levels of accuracy and reliability with regard to back-analyzed values of post-liquefaction strengths for cases to which they can be applied. But they tend to require good quality and information, and cannot be applied to all case histories. Methods listed lower on the table tend to provide intermediate to lower levels of accuracy and reliability, but can more readily be applied to cases with lesser levels of information and data available.

4.2 The Incremental Momentum Method

4.2.1 General Overview

A new method was developed to provide a more accurate and reliable means of incorporating momentum effects in back-analyses of large displacement liquefaction failures performed for purposes of assessment of post-liquefaction strength (S_r). This new method will be referred to as the incremental momentum analysis method.

This method is illustrated in Figures 4.1 through 4.3, for the case of the liquefaction-induced slope failure that occurred on the upstream side of the Lower San Fernando Dam as a result of the 1971 San Fernando earthquake. A full explanation of this failure, and a more complete exposition of all back-analyses performed, is presented in Appendix A, Section A.5.

As shown in Figure 4.1, the upstream slope failure was the result of liquefaction of the lower portion of the hydraulic fill materials comprising the upstream shell of the dam during the 1971 San Fernando earthquake. This was an unusually well-investigated failure, and two large trenches were excavated fully through the failed section so that a detailed mapping of the displaced locations of recognizable portions of the embankment could be documented. Largely intact portions (or "blocks") of the displaced upstream side of the dam were then mapped back to their initial positions, and it could be seen that the failure involved liquefaction of the lower portion of the hydraulic fill on the upstream side, with the overlying embankment sections translating outwards in the upstream direction borne along atop the liquefied materials.

The incremental momentum method involves developing a series of estimated (feasible) cross-sections incrementally tracking the progression of displaced geometries from inception of movements to the final, residual post-failure geometry. This is more challenging than the approach taken in estimation of the "ZIF" interim cross-section geometry by Wang (2003), because it requires that all intermediate geometries must provide a reasonable path forward all the way to the observed final residual geometry. It is therefore a very tedious and time-consuming process, involving numerous iterations between analyses and estimation and drawing of cross-sections, and one that requires both engineering judgment and some artistic capability.

Important benefits of this approach, relative to the previous "kinetics" approaches taken by Olsen (2001), and the previous "ZIF" method of Wang (2003), include the following:

1. This process is constrained by the eventual need to converge on the observed final geometry, requiring a more reasonable and reliable path forward at each incremental cross-section.

2. The process lends itself to creating a step-wise "animation" which can be clicked forward and in reverse on a computer screen, much like a step-wise video, and these animations have proven to be useful with regards to engineering insight and understanding.

3. The series of incremental cross-sections permit updated evaluations of (a) driving shear stresses, (b) failure plane details (e.g. lengths of the failure plane currently controlled by liquefied or non-liquefied materials, overall failure plane lengths, sections of the failure plane where stronger of weak soils have over-ridden weaker or stronger soils as shearing progressed (weaker soils then control), and (c) evolving geometries and properties as displacing and deforming embankment toes enter bodies of water and potentially either hydroplane or ride out atop weaker reservoir or offshore sediments, etc. These are potentially very important benefits, but the ability to "update" the evolving analyses in all of these regards also poses an additional responsibility, and also takes further time and effort.

4. The analysis is performed with basic physics (Newton's Second Law) and basic soil mechanics governing the progressive evolution of accelerations, velocities, momentum, and displacements during the slide movements. The analysis proceeds continuously from inception of movements to completion. There is therefore no need to "estimate" the partial displacement stage that corresponds to the "ZIF" displacement.

5. Driving shear stresses are correctly calculated at each increment, so there is no difficulty or uncertainty with regard to the level of accuracy with which the curvilinear polynomial surface of the kinetics method of Olsen (2001) suitably approximates the driving shear forces at each stage of partial displacement.

The resulting analysis is thus more accurate, more reliable, and better able to account for evolving details as the failure progresses. The corollary price to be paid is then the additional level of effort, and time, involved in performing these very challenging analyses.

Figure 4.2 shows the incremental progression of cross-sections judged to represent this current engineering team's "best estimate" of the likely progressive evolution of failure for the Lower San Fernando Dam upstream failure. The benefits of this progressive approach, in terms of approximate "animation" and visualization, were of special value here, as it has long been debated whether this failure occurred either (1) as an initially monolithic failure, with subsequent "break-up" of individual slices and blocks occurring as the failure progressed, or (2) as an incrementally progressive failure, with the slices nearest the front face of the slide mass moving first, followed by successive slices, in sequence, as each successive slice was "unbraced" by the displacement of the slice that preceded it, until the failure eventually retrogressed in incremental fashion back to the eventual back heel. By creating multiple potential realizations of the failure sequence, it became clear that this particular failure likely initiated relatively monolithically, and then broke up as it traveled, because it was otherwise not feasible to re-produce the observed final positions of some of the more rear-ward slices. This could not be reliably ascertained a priori, and it should be noted that some of the other case histories back-analyzed in these current studies clearly did proceed in an incrementally progressive (retrogressive) manner, and that others did not.

Figure 4.3 then illustrates the calculated evolution of acceleration, velocity and displacement of the center of gravity of the eventual overall failure mass. At each step in time, the best estimate of (a) driving (downslope) shear forces and (b) resisting (upslope) shear resistance are compared, and any overall force imbalance is then applied to the overall failure mass by Newton's Second Law ($F = m \bullet a$). The resulting acceleration (or deceleration) is then calculated, and so is the corollary resulting increase or decrease in velocity, and the associated incremental accumulation of displacements as well. As shown in Figure 4.3 velocity initially increases as the mass begins to move downslope, and then decreases as the mass eventually comes to rest.

Shear strengths for non-liquefied soils are modeled at each stage based on the best available information and data, and basic principles of soil mechanics. Liquefied zones are assigned a post-liquefaction strength of S_r, and the value of S_r is then iterated until the calculated progression (e.g. Figure 4.3) shows the final displacements to match those observed in the field. This requires another series of iterative adjustments, and analyses, further adding to the effort required. The seven "dots" for small circles on the plots of Figure 4.3 show the situation at time-steps corresponding to the first seven updated (incremental) cross-sections of Figure 4.2. The eighth and final cross-section of Figure 4.2 differs from the seventh only in that the reservoir has eventually seeped through and infilled the "dip" near the top back-heel of the slide mass of the preceding (seventh) incremental cross-section.

Once a best-estimated case had been established and analyzed, parameter (and assumption) sensitivity studies were next performed. Only a few additional fully incremental momentum analyses were usually performed here. Instead a case-specific relationship between pre-failure and post-failure geometries, strengths, and representative S_r was established for each case (see Section 4.4), and then simpler analyses of pre-failure and post-failure geometries were performed to more efficiently evaluate the effects of changes in conditions and parameters over the ranges considered plausible and/or feasible. In some cases, additional full incremental analyses had to be performed to examine modeling of challenging situations such as (1) ranges of potential conditions with regard to monolithic vs. incrementally retrogressive initiations of failures, and (2) ranges of modeling choices for toes of slide masses entering into bodies of water, etc.

In this manner, the effects of variations in properties, assumptions, and modeling details on back-calculated values of S_r were evaluated to inform estimates of uncertainty or variance. Variations that were commonly modeled and analyzed here often included: (1) shape and location of the failure surface, (2) whether or not the failure was incrementally progressive (retrogressive) or monolithic, (3) location of the phreatic surface at the time of the failure, (4) shear strengths of soils judged not to have liquefied, (5) variations in unit weights, and (6) variations in assumptions and modeling of conditions at the bases of toes of failures that enter into bodies of water.

4.2.2 Modeling of Strengths at the Toes of Slide Masses Entering Bodies of Water

A number of the failure case histories involved liquefaction flow slides that either entered into reservoirs, or that progressed underwater in offshore waters. In these cases, the question arises as to whether hydroplaning occurred, and if so to what extent and what effect would it have had on shear strengths at the bases of the toes of these masses.

This had been addressed very approximately on a case by case basis by Seed (1987) and by Seed and Harder (1990). Most other previous investigators did not address this issue, or did not discuss it if they did. Olsen discussed this for some specific cases, and appears to have assigned a 50% reduced post-liquefaction strength ($0.5 \times S_r$) at the bases of toes of a number of slides as they entered into bodies of water, and then examined variations of between 0% reduction to 100% reduction in assessing potential parameter sensitivity effects. Wang (2003) [and Kramer] examined the available literature regarding hydroplaning, and developed a simplified but repeatable, quantitative (and semi-probabilistic) procedure for analysis of the likelihood that hydroplaning would occur, and for the likely resulting effects on strengths at the bases of toes of slide masses entering into water. They allowed a maximum lateral penetration of hydroplaning effects of up to 10 times the thickness of the soils entering into water, and the amount of this maximum distance that was specifically assumed (modeled) to be affected by hydroplaning for any given case was then primarily a function of velocity of movements.

In these current studies, yet another approach was taken.

Examining the available research, it was our conclusion that the available knowledge does not yet support rigorous analytical treatments of potential hydroplaning. Likelihood of hydroplaning is clearly affected by velocities of the traveling soil masses, but this does not yet give rise to fully reliable calculation methods. (Wang (2003) addressed this with probabilistic

estimates of likelihood and extent of hydroplaning, and with subsequent Monte Carlo simulations of the effects of these variations on back-calculated S_r values.) Similarly, available research suggests that hydroplaning would occur only to some limited depth of penetration beneath advancing toes of slopes, but attempting to extrapolate table-top scale models to field situations is challenging, and it is further complicated by the tapered shapes of the toes of advancing slide masses making it difficult to select a "representative" thickness of the slope materials entering the water.

A second issue potentially also affecting a number of the liquefaction failure case histories is the presence of weak reservoir sediments, or the presence of weak offshore slope sediments, or weak sediments in agricultural fields adjacent to roadway or railway embankments. Advancing toes of slide masses traveling out onto such weaker sediments can be partially "lubricated" if the advancing slide mass rides atop the weaker sediments, in which case the strengths of the weaker sediments can control here. Previous investigations have usually not been clear as to whether, or how, they addressed the effects of potential sliding atop weaker sediments of the toes of failure masses.

In these current studies, it was decided to address these two issues (potential hydroplaning, and potential sliding atop weak sediments) on a case by case basis.

In considering hydroplaning, velocities of the advancing toes would be considered but would only provide some guidance. And some limitations on depths of potential penetration of hydroplaning laterally beneath the toes of advancing slide masses would be imposed, but this would vary over a broader range than just a maximum of 0 to 10 times the thickness of the advancing soils, in part because selection of a representative thickness was not well-defined. When possible, details of the actual observed eventual runout of the failure flow slide mass were examined for clues as to likely hydroplaning. As an example, for the failure of the Fort Peck Dam (see Appendix A, Section A.2) it appears that a portion of the extreme toe of the failure mass separated itself to some extent from the more intact rest of the failure mass, and extended itself more thinly out into the reservoir. In other cases, failure masses traveled very large distances and did not really "come to rest" in the classical sense; also suggesting hydroplaning. In many cases, however, this was simply a source of uncertainty, and the full range of possible hydroplaning conditions were included within the parameter sensitivity analyses performed. Similarly, strengths where hydroplaning was modeled were varied from 20% to 80% of the overlying soil (or liquefied soil) strengths.

Weak sediments were handled in a similar manner. Strengths at the bases of slide masses traveling outwards onto likely weak sediments were assigned strengths equal to values that varied from 25% to 100% of the overlying soil (or liquefied soil) strengths as part of the parameter sensitivity studies performed.

More detailed explanations of modeling and treatment of hydroplaning, and of weak sediments, are presented for individual case histories in Appendices A and B.

4.2.3 Incrementally Progressive (Retrogressive) Failures

A number of the liquefaction failure case histories were suspected of having possibly proceeded in an incrementally progressive manner, initiating with movements of a smaller "slice" or wedge near the front face, and then retrogressing back towards the eventual rear heel of the overall slide in a sequence of subsequent initiations of movements of additional slices or wedges as each becomes unbraced by partial loss of support from the slices that preceded it.

This type of incrementally progressive (retrogressive) failure propagation was not tractable to accurate analyses by previous methods, and so the potential impacts of this (as opposed to assumed monolithic initiation of the entire failure as a single coherent mass right from the start) was unknown.

The incremental momentum method developed and employed in these current studies can successfully address this.

This is illustrated in Figures 4.4 and 4.5 for the Shibecha-Cho embankment case history. A more complete exposition of this case history is presented in Appendix A, Section A.2.

The Shibecha-Cho embankment was a very large side-hill fill that supported a development, and which failed during the 1983 Kushiro-Oki earthquake. The failure was known to have been an incrementally progressive (retrogressive) failure, and so it was analyzed as such in these current studies.

Stability analyses performed for the un-displaced (pre-failure) cross-section, assuming that liquefaction has occurred, show that a slice near the front face is the most critical (has the lowest factor of safety). This failure was modeled (best estimate case) as beginning with the inception of movements of this first slice, and then progressing with successive inceptions of movements of two additional successive "slices", as shown in Figure 4.4. After the first slice had progressed some distance, a second slice began to move, and then eventually a third.

The analyses tracking the incremental development of acceleration, velocity and displacements for this case were performed for two parallel sets of centers of gravity, and the results are shown in Figure 4.5. The incremental values for the center of gravity of the initial slice (the slice closest to the front face) are initially tracked by the dashed lines in Figure 4.5. Simultaneously, the values for the eventual overall failure mass are also calculated (by weighted mass averaging of the moving slice, and of the portions of the eventual failure mass not yet in motion), and these are shown by the solid lines in Figure 4.5. The initial failure slice is thus the "active" element in the opening stages. When the second slice begins to move, the dashed lines then track the evolving values for the center of gravity of the combined first and second slice masses (by weighted mass averaging), while the solid lines continue to track the evolving movements of the overall eventual slide mass (also by weighted mass averaging). The same is then done when the third and final slide mass begins to move, at which point the overall slide mass center of gravity is tracked by the remainders of the solid lines.

Modeling initiation of successive slices reduced overall peak velocities, and also corollary reduced overall momentum, and thus produced a lower back-calculated value of S_r than would

have been produced by a monolithic inception of failure. The value of S_r back-calculated with modeling of incrementally progressive failure for the Shibecha-Cho embankment case history (as illustrated in Figures 4.4 and 4.5) was $S_r \approx 224$ lbs/ft^2. When this case was modeled instead as a monolithically initiated failure, the somewhat higher momentum effects produced a higher value of $S_r \approx 263$ lbs/ft^2.

4.2.4 Evaluation of Representative Penetration Resistance

Appendix C presents an expanded discussion of the basis for evaluations of representative SPT $N_{1,60,CS}$ values for each of the case histories back-analyzed. An abridged discussion will be presented here.

For cases where modern, and properly well-documented SPT data were available, correction of SPT N-values to generate equipment and procedurally corrected N_{60}-values were made using largely the corrections proposed by Cetin et al. (2004), except that a slightly reduced adjustment was made for short rod effects at shallow depths as per Deger (2014). This slightly reduced short rod correction had essentially negligible effect in these current studies, as few SPT data were used from the shallow depths at which this might have produced a noticeable difference. The procedural and equipment corrections made herein were thus largely similar to those of Seed et al. (1984), and of Idriss and Boulanger (2007), and would produce largely compatible results.

Normalization of N_{60}-values for effective overburden stress effects was performed using the relationships recommended by Deger (2014), which provide normalization curves somewhat intermediate between those of Cetin et al. (2004) and of Idriss and Boulanger (2007).

Fines corrections for this study were made using the fines corrections recommended by Cetin et al. (2004). This is an area where some minor differences occur between various investigation teams working on studies of post-liquefaction S_r. The fines adjustment of Cetin et al. is somewhat intermediate between the fines adjustments of Seed et al. (1984) and the fines adjustment that Seed (1987) suggested specifically for S_r purposes. In the end, the fines corrections of these studies, and those employed by Seed (1987) and recommended by Idriss and Boulanger (2007) do not produce major differences, but they do vary slightly relative to each other. Olsen and Stark (2001, 2002) elected not to employ any fines corrections, so that they used $N_{1,60}$-values rather than $N_{1,60,CS}$-values, and that causes a number of their characterizations of SPT penetration resistance to vary somewhat from the other studies for soils with higher fines contents.

Different investigation teams took different approaches to determining what "representative" penetration resistances were. It is widely understood that lower than median values of penetration resistance will likely control actual field failures because nature will choose to exploit zones of weakness within a zone of heterogeneity of strengths. Wride et al. (1999) specifically developed predictive correlations for estimation of post-liquefaction strength (S_r) based on near lower bound values of penetration resistance, as discussed in Section 2.3.5. A drawback of that approach is volatility of the near lower bound value, especially for cases with sparse data.

In these current studies, it was decided instead to use "scalped" median values of penetration resistance to characterize the liquefiable soils of interest. Median values have the advantage of providing a more stable characterization when data are sparse, and they can be approximately correlated with lower-percentile enveloping of corrected N-values (values representing lower probabilities of non-exceedance).

"Scalped" in these current studies means deletion of potentially spurious high penetration resistance values, and also examination of penetration resistance values for SPT performed in mixed soils with the fines representing potentially cohesive clayey soils. High individual SPT N-values that separate themselves from the main body of data for a soil zone or stratum are examined, and if this separation is large then as many as a few percent of these high values are deleted as likely spurious. These may be the result of potential gravel effects, or their cause may be unknown. When sufficient data are available, SPT performed in soils classified as SC are also deleted. Currently available fines adjustments do not well handle these materials, and their corrected SPT N-values often tend to be lower than many of the rest of the SPT performed on less cohesive materials, even after fines adjustments, in mixed soil zones of varying fines content and consistency.

The resulting scalped, or slightly filtered, $N_{1,60,CS}$ values tend to have distributions that vary in a range that is intermediate between normal distributions and more log-normal distributions. D ( ) examined a number of N-value data sets for different soils, and concluded that . Based on cases examined in these current studies with sufficient numbers of SPT data as to provide insight, this appears to be about right.

"Representative" $N_{1,60,CS}$ values were selected in these current studies by examining the median and mean values from the scalped or slightly filtered data sets, and then selecting a value usually close to the average between these two. In small data sets, median values were generally used here. $N_{1,60,CS}$ values were assumed to be normally distributed in performing regressions to develop empirical relationships between penetration resistance and post-liquefaction strength. Median and mean values were thus assumed to be essentially the same, and standard deviations of the mean of $N_{1,60,CS}$ were modeled as a measure of estimated variance. These variances were in many cases controlled more by uncertainties involved with conversion of non-SPT penetration resistance data to estimates of equivalent SPT $N_{1,60,CS}$ values, than by variance among the individual penetration resistance values measured for a given soil stratum. When either CPT data, or non-standard penetration data, or lesser quality information regarding placement conditions and history, were used to develop estimates of equivalent SPT $N_{1,60,CS}$ values, the details are presented on a case by case basis in Appendices A and B.

For two of the case histories (Wachusset Dam and Fort Peck Dam) additional corrections were required for ageing effects, as multiple decades elapsed between the occurrences of the failures and the eventual performance of modern SPT investigations. The details for of the corrections made for ageing effects in these two case are presented in Appendix A, Sections A.1 and A.2.

4.2.5 Evaluation of Representative Initial Effective Vertical Effective Stress

Values of "representative" initial effective vertical stress on liquefied materials for each case history were evaluated by averaging the pre-failure effective vertical stresses along the portion of the failure plane that would be controlled by liquefied materials. Approximate calculations were made by summing vertical stresses at the bases of slices in liquefied materials in slope stability calculations for the pre-failure geometries, and averaging these along the liquefied slide plane lengths. These provided adequately close approximations of initial vertical effective stresses, and they also appear to provide good agreement with estimates of initial vertical stresses made by (1) Wang (2003) and Kramer (2008), and (2) Olsen and Stark (2001, 2002) for most cases, especially if Olsen's values are adjusted slightly (reduced a bit) to account for the fact that he generally assumed slightly shallower failure surfaces for most of his cases.

4.3 Back-Analyses of the 14 Case Histories of Groups A and C

4.3.1 Back-Analyses and Results

The 14 "high quality" case histories of groups A and C were back-analyzed, and the details of these analyses are presented in Appendix A. The main analyses were performed by the incremental momentum method, and additional analyses were also made using simple static limit equilibrium to develop back-calculated values of (1) the "apparent" pre-failure stress ($S_{r,yield}$) along liquefied portions of the eventual slide surfaces required to provide a calculated static Factor of Safety equal to 1.0 for pre-failure geometry, and (2) the "apparent" residual stress ($S_{r,resid/geom}$) required to provide a post-failure calculated static Factor of Safety equal to 1.0 for the final, residual post-failure geometry. These values of $S_{r,yield}$ and $S_{r,resid/geom}$ would prove useful (1) in evaluating the results of the incremental momentum analyses, and (2) in developing empirical methods for checking these types of back-analyses and for making back-assessments for some of the case histories in the set of Class B cases, as will be described in Section 4.4.

Table 4.2 shows the results of the back-analyses performed for the 14 Class A and C case histories (in the columns to the far right). Also shown are values developed by the previous investigations of Seed and Harder (1990), Olsen and Stark (2002), and Wang and Kramer (2003, 2008). Values shown are "representative" values developed by each investigation team. For these current studies these are "best estimate mean values". The values for the other three investigation teams appear to be largely compatible with this basis.

The values of effective vertical overburden stress listed for Wang and Kramer (2003, 2008) in Table 4.1 are inferred from their stated values of S_r and S_r/σ'_{vo}, because they did not state their actual values of effective overburden stress.

4.3.2 Comparison with Results from Previous Studies

Table 4.2 shows a modified presentation of the same cases shown in table 4.1.

Ten of the S_u(Liq) values listed by Olsen and Stark (2002) were calculated using their "kinetics" method, which appears to have largely correctly incorporated momentum effects. These values are listed in Table 4.2 without parentheses. The other 23 cases were back-analyzed largely on the basis of "apparent" post-liquefaction strengths based on the value of S_u(Liq) required to provide a calculated static Factor of Safety equal to 1.0, and those values thus represent values of $S_{r,resid/geom}$. These $S_{r,resid/geom}$ values would significantly underestimate the actual S_r values, and so are not directly comparable with the values calculated in these current studies for the Class A and C cases. Olsen (2001) calculated values of both $S_{r,yield}$ and $S_{r,resid/geom}$ for each of the 33 cases he back-analyzed. As a result, it is possible to use his values of these two indices to develop better estimates of S_r that would then be more directly comparable with the S_r values back-calculated for the Class A and C cases in these current studies. As will be developed in detail in Section 4.4, reasonably good estimates of the actual S_r values for most cases can be estimated as

$$S_r \approx \xi \bullet (S_{r,yield} + S_{r,resid/geom}) / 2 \qquad \text{[Eq. 4-1]}$$

where ξ can be taken as approximately 0.8.

This produces values of S_r that approximately incorporate momentum effects. Given the availability of values of $S_{r,yield}$ and $S_{r,resid/geom}$ back-calculated by Olsen (2002), the values not calculated by the "kinetics" methods can be replaced with values estimated by Equation 4-1, employing a value of $\xi = 0.8$, and these are shown in Table 4.3 [within square brackets].

The values of S_r back-calculated by Wang (2003), using the "ZIF" method which largely correctly incorporated momentum effects, are listed in Table 4.2 with no parentheses. Values of S_r listed with parentheses in Table 4.2 are those for cases where Wang did not perform the full ZIF analysis, and instead adopted values based on judgmental averaging of values developed by other previous investigators. These are probably not systematically biased, but they will be less likely accurate and reliable.

The modified values shown in Table 4.3 then represent the best available basis for cross-comparison of back-calculated values of S_r that incorporate momentum effects for the cases of Classes A and C.

The value of S_r from Seed and Harder (1990) shown for the Fort Peck dam case history is notably low compared to the other three investigation teams. That is because the runout distance was very large for this case, and Seed and Harder underestimated the multiplier (ξ) in Equation 4-1 that would provide a good estimate of S_r with approximate inclusion of momentum effects. (Better values of ξ as a function of runout indices are developed next in these current studies, as presented and described in Section 4.4.)

The value of Olsen and Stark (2002) for the Shibecha-Cho embankment case history is notably low compared to the results of the other investigation teams. This is because the Shibecha-Cho failure was a strongly incrementally progressive failure, retrogressing backwards in slices towards the eventual back heel, as described previously in Section 4.2.2 (and Appendix A, Section A.12). Olsen correctly recognized this, and attempted to account for this retrogressive progression by performing his "kinetics" analysis by tracking only the initial (front-most) failure slice. This was not successful, and it resulted in underestimation of S_r for this case.

Olsen and Wang (2003, 2008) appear to have selected high averaged values of Sr for the two La Marquesa Dam failures (upstream side and downstream side failures). Because these were developed by averaging the values developed by multiple previous investigators, it is difficult to track the origins of these differences.

Wang and Kramer calculated a somewhat lower S_r value, based on their ZIF analysis method, for the Calaveras Dam case history than the values back-calculated by Olsen and Stark (2002) and by these current studies. Olsen and Stark employed their kinetics method, and these current studies employed the incremental momentum approach. All three of these analysis methods explicitly incorporate momentum effects, and it must be suspected that the differences here are the result of modeling and parameter details in the three different sets of analyses.

For the remainder of the 14 Class A and C cases, values of S_r are judged to be in generally good agreement, especially given the differences between analytical approaches taken by the different investigation teams. There are approximations and judgments required in each of these analyses, and overall agreement among the 14 cases comprising Classes A and C is judged to be good.

There is, of course, a preference here for the values developed by the more difficult, and more flexible, incremental momentum method which better addresses some of the details of some of these cases and appears likely to provide higher levels of reliability of back-calculated S_r values as well. The cross-comparisons of Table 4.3 are interpreted herein as reflecting a good level of support for the values back-calculated by this method.

4.4 Development of New Empirical Relationships for Back-Analyses of Case Histories for Assessment of S_r

The values back-calculated and presented in Section 4.3 were next used to develop two sets of empirical relationships for (a) cross-checking the results of back-analyses of liquefaction flow failures for consistency, and (b) making back-estimates of S_r from other liquefaction failure case histories where lesser quality data and information are available. In the end, these new relationships also provide a basis for approximate checking of engineering analyses of expected liquefaction-induced displacements and deformations for large displacements case, with likely useful applications for evaluations of interim reservoir restrictions for dams that require eventual seismic hazard mitigation.

4.4.1 Pre-Failure and Post-Failure Analyses Calibrated Based on Runout Characteristics

As noted in a number of previous sections, simple static limit equilibrium analyses can be performed to evaluate (1) the back-calculated value of the "apparent" pre-failure stress ($S_{r,yield}$) along liquefied portions of the eventual slide surface required to provide a calculated static Factor of Safety equal to 1.0 for pre-failure geometry, and (2) the "apparent" residual stress ($S_{r,resid/geom}$) required to provide a post-failure calculated static Factor of Safety equal to 1.0 for the final, residual post-failure geometry. These values of $S_{r,yield}$ and $S_{r,resid/geom}$ would "bracket" the actual value of Sr for any given case history.

Further discussion of this is now warranted.

For cases in which "flow" displacements are small, there would be relatively little difference between $S_{r,yield}$ and $S_{r,resid/geom}$, and momentum effects would also be small. In such cases, simply adding $S_{r,yield}$ plus $S_{r,resid/geom}$, and then dividing by two would provide a good estimate of S_r. This could be expressed as

$$S_r \approx \xi \bullet (S_{r,yield} + S_{r,resid/geom}) / 2 \qquad \text{[Eq. 4-2]}$$

where ξ can be taken as nearly 1.0.

At the other extreme, for cases in which runout distances were infinitely large, post-liquefaction strength would be essentially equal to zero, in which case S_r could be estimated as

$$S_r \approx \xi \bullet (S_{r,yield} + S_{r,resid/geom}) / 2 \qquad \text{[Eq. 4-3]}$$

where ξ can be taken as nearly equal to zero.

This reasoning then gives rise to the observation that the general form of Equations 4-1 through 4-3 can be improved by making the value of ξ a function of observed runout distance.

Figure 4.6 shows best estimate values of post-liquefaction strength (S_r) back-calculated by the incremental momentum analyses for the 14 case histories of Classes A and C, plotted on the vertical axis, and on the horizontal axis it shows the averaged "before and after" values of ($S_{r,yield}$ + $S_{r,resid/geom}$) / 2 as calculated by Equation 4-1 with ξ assumed equal to 1.0. This "before and after" average is thus simply the average of $S_{r,yield}$ and $S_{r,resid/geom}$.

As shown in this figure, better fitting of the back-calculated data is achieved if the value of ξ is set a bit lower than 1.0, with most of the back-analyses being well-represented by values of ξ of between 0.6 to 1.0.

Three of the cases plotted in Figure 4.6 are cases in which incrementally progressive (retrogressive) failure initiation is thought to have affected back-calculated values of Sr, and it was necessary to develop a slightly modified version of Equation 4-1 for these types of cases. The initial value of SS for these cases was calculated for (1) the initial (smaller) initial failure mass nearer the front face of the failure, and (2) for the overall failure mass. These two values were then averaged to develop the "representative" value of SS. This was then employed, along with SS from the eventual post-failure residual geometry (for the entire failure mass) in Equation 1 to develop the "before and after" averaged value for the case. These analyses were also performed for each of these three cases, but this time employing only the SS value for the initial (smaller) initial failure slice and then the SS value for the overall residual post-failure condition of the overall failure mass.

The three cases to which this slightly modified calculation was applied were Case 2 (Fort Peck Dam), Case 3 (Uetsu Railway Embankment) and Case 12 (Shibecha-Cho Embankment). For each of these cases, that values calculated based on only the SS avalues calculated for the initial

(smaller) initial failure slices are shown with dashed circles, and the values calculated using the averages SS values for the initial (smaller) initial slices and the larger (overall) failure mass are shown with solid circles. These latter values are judged to be the better and more representative values.

The Fort Peck Dam failure case history was modeled as being only slightly progressive/retrogressive (see Appendix A, Section A.2) and the differences here between the two approaches, supporting both the interpretations here, and the modeling of the case as only slightly progressive. For the Uetsu and Shibecha Cho embankment failure case histories, the differences were more significant, as would have been expected (see Appendix A, Sections A.3 and A.12).

The next step was then to plot values of ξ for each of the 14 back-analyzed case histories against different measures of runout distance. The best relationship was found to be achieved by cross-correlation of ξ with "scaled runout distance", defined as the total distance travelled by the center of gravity of the overall failure mass divided by the initial slope height from the toe to the top of the back-heel of the failure.

This is plotted for each of the 14 Class A and C case histories back-analyzed by the incremental momentum method in Figure 4.7. As shown in this figure, a relatively strong relationship between ξ and scaled runout resistance can be observed. It can also be seen that the value of ξ would approach 1.0 for zero runout distance, as would be expected if cyclic inertial effects were either zero or were neglected.

This Figure 4.7 serves to demonstrate again the relatively good internal consistency between the back-calculated values of S_r for these 14 well-defined field case histories. It also represents a basis for evaluation of ξ as a function of runout distance, which in turn makes Equation 4-1 significantly more useful for empirical estimation of S_r.

A second set of empirical relationship were then developed by plotting "Initial Factor of Safety" vs. "Final Factor of Safety" for these 14 Class A and C cases, as shown in Figure 4.8. Initial factor of safety here is defined as the apparent static Factor of Safety calculated for pre-failure geometry with the strength of the of the liquefiable soils set equal to the best estimate value of S_r back-calculated using the incremental momentum method. Similarly, the final factor of safety is the static value of FS calculated using this best-estimate value of S_r from the incremental momentum back-analyses and assigning it to the liquefied soils in the post-failure (final) residual geometry.

As shown in Figure 4.8, the values back-calculated for the 14 cases all occur within a reasonably well-defined range. Closer inspection of the individual cases (identified by number in the figure, and by name in the "key" in the upper right-hand corner of the figure) shows that cases with larger "scaled runout distance" have lower Initial FS values, and higher Final FS values. Figure 4.9 then repeats Figure 4.8, but this time each case history's "dot" is annotated (in parentheses) with the ratio representing scaled runout height (distance traveled by the center of gravity of the overall failure mass divided by the initial slope height from the toe to the top of the back heel of the failure). It is clear that the cases tend to move from the bottom right hand portion

of the observed range, towards the top left portion of the figure, with increasing scaled runout distance.

The two relationships of Figures 4.6/4.7 and Figures 4.8/4.9 provide a systematic basis for understanding some of the interactions between the runout mechanics of liquefaction failures, and the post-liquefaction strengths and various calculated stability measures associated with these failures.

These relationships can then be used for several purposes:

1. They can be used as an internal check for consistency and reasonableness for back-analyses of S_r performed within a study such as this current one. There had not previously been any useful tools for that.

2. They can also be used to cross-check engineering analyses of expected deformations, and resulting displaced geometries, for forward analyses of engineering projects. As an example, it is not uncommon once a major dam has been studied and found likely to pose an unacceptable risk with regard to potential for liquefaction-induced failure, for the reservoir to be "restricted" until repairs/mitigation can eventually be implemented. Reservoir restrictions imposed are usually the result of assessments of likely worst-case deformations, in order to ensure that these will not result in uncontrolled release of the reservoir as long as it is as or below the restricted level. High-order finite element and finite difference analyses can be brought to bear here. These analyses involve a number of choices and decisions with regard to modeling and parameters, and there are potential additional difficulties associated with mesh deformations as calculated deformations become large. The accuracy, and the acceptable conservatism, of such analyses can be difficult to verify. There are currently no widely accepted way to reliably "check" the results of such analyses. Both of the relationships developed here (Figures 4.7/4.7 and Figure 4.9) can be employed for that purpose.

3. Finally, these two sets of relationships can also be employed to help to extract reasonable back-analyzed or back-estimated values of Sr for liquefaction failure case histories of lesser overall quality, reliability, or documentation that the 14 cases of Classes A and C. These relationships are thus useful in back-analyses of the 16 additional liquefaction failure case histories of Class B, as described in Appendix B and in Section 4.5 which follows.

4.5 Back-Analyses of the 16 Case Histories of Group B

4.5.1 Back-Analyses and Results

The 16 lesser quality liquefaction case histories of Group B were next back-analyzed. Details of individual analyses and assessments for each of these case histories are presented in Appendix B. The quality, quantity, reliability and level of documentation of data and information regarding various aspects of these Class B cases varied considerably. As a result, these cases were judged not to warrant the incremental momentum analyses applied to the Class A and C cases.

But it was not sufficient here to simply take the values back-calculated, or estimated, by previous investigators. One of the objectives of these current studies was to make the best achievable assessments of both the best estimated values of $\overline{S_r}$, $\overline{N_{1,60,CS}}$ and representative $\overline{\sigma'_{vo}}$ for each case history, and also the best possible estimates of uncertainty or variance for each of these three indices. Considerable effort was therefore also expended on back-analyses and back-assessments of these "lesser" cases.

This served to differentiate these current studies from all previous efforts. A number of previous studies had done a relatively good job, or at least applied a good deal of effort, to back-analyses of the Class A and C cases. But none of those studies had then continued on to devote significant effort to the Class B back-assessments as well.

It is not possible to simply and concisely describe the ranges of approaches, judgments, etc. that were employed in back-assessments of the 16 additional cases. Engineers who are interested should be encouraged to examine the case-by-case explanations and expositions presented in Appendix B, as the details of the judgments made in processing some of these cases can be important.

The values that resulted from these back-analyses and assessments generally carried larger values of uncertainty (and of standard deviations) that was common for the Class A and C cases. This often reflected significant uncertainties associated with lack of data, poor quality of data, poor documentation of data, etc. The values of standard deviations reported for each parameter are, for each case, the best estimates of this investigation team taking all uncertainties into account.

Table 4.4 presents the back-analysis results for the Class B cases, in the form of best estimate values of representative $\overline{S_r}$, $\overline{N_{1,60,CS}}$ and $\overline{\sigma'_{vo}}$ for each case. In this table, the values shown are the values recommended by each of the investigation teams.

Table 4.5 then repeats the presentation of the back-analysis results for the Class B back-analyses, but the values shown in square parentheses for Olsen and Stark again are modified values representing values calculated using Equation 4-1, with $\xi = 0.8$, and the case-specific values of $S_{r,yield}$ and $S_{r,resid/geom}$ reported by Olsen (2001).

Similarly, the values shown in parentheses for Wang and Kramer (2003/2008) are values that were selected based on averaging of selected values from other previous investigators.

Generally good agreements among the several sets of values shown for the 16 Class B cases for most cases appears to provide good support for the values developed in these current studies.

The value of S_r reported by Olsen (2001) for the El Cobre Tailings Dam case history could not be modified to the value produced by Equation 4-1 because the necessary initial yield and post-failure residual geometry values of $S_{r,yield}$ and $S_{r,resid/geom}$ were not presented. The value shown is that recommended by Olsen and Stark, but as discussed in Appendix B, Section B it appears to be estimated based on a very conservative back-calculation of $S_{r,resid/geom}$ and thus appears to be too low.

Wang and Kramer (2003, 2008) appear to have inexplicably high values of S_r for two cases: the Hokaido Tailings Dam failure and the Nerlerk Embankment Slides. Details of the basis for the values that they reported for these two cases are not presented, so the sources of these differences cannot be examined.

In these current studies, values of S_r back-calculated for the two Moshi-Koshi Tailings Dam failures (Dikes 1 and 2) were averaged, because these were two very similar failures and it was judged that using them as two separate cases would over-emphasize their contribution to the regressions that will follow. Similarly, the three Nerlerk Embankment slides were also averaged in these current studies.

No cross-comparisons can be made for the values calculated in these current studies for two cases: the Sullivan Tailings case history and the Jamuna Bridge case history. This is because the other investigation teams listed in Tables 4.4 and 4.5 did not include those more recent cases in their studies.

A second comparison of the results developed for the Class B cases can be made by plotting the results onto what was previously presented as Figure 4.9. This is presented as Figure 4.10, with the solid "dots" now representing the 16 new Class B cases. This appears to indicate reasonable overall results for the Class B cases, with consideration of the relatively high levels of uncertainty (and standard deviation) ascribed to some of the Class B case parameters due to poor quality and/or poor documentation of data for some of these cases.

4.6 Summary of Back-Analysis Results

The results of the back-analyses of all 30 cases (Classes A, B and C) are presented in Table 4.6. This table presents both the best-estimate mean values, and also the best estimate standard deviations, for each of the three indices that will next be used to develop predictive relationships for in situ S_r.

Only one other study has been carried forward far enough as to provide useful values for cross-comparison here, and that the work of Wang (2003) and Kramer (2008).

Table 4.6 presents a comparison between the indices developed in these current studies and those employed by Kramer (2008) in his regressions to develop predictive relationships for S_r. Wang (2003) and Kramer (2008) did not report values of representative initial vertical effective stress, so the values shown in this table are inferred from their reported values of S_r and S_r/σ_{vo}'. Wang (2003) and Kramer (2008) also did not report their values of variance or standard deviation for mean effective stress, so no cross-comparison can be made for that parameter here.

As discussed previously in Section 2.3.7, the means and basis by which Wang (2003) and Kramer (2008) developed both their mean estimates and their estimates of standard deviation or variance of these means differed greatly from the approaches taken in these current studies. Their approaches did not fully incorporate the influence of uncertainties related to poor documentation of case history data and information, and so they subsequently applied judgmental weighting

factors to don-weight the contributions of the less well-documented cases. That was prudent with regard to development of predictive relationships with good median fit (50% relationships), but it may not have fully characterized overall model uncertainty. The weighting factors (WF) employed by Kramer (2008) in performing regressions to develop predictive relationships are also listed in Table 4.6. These range from 1.0 for cases that are well-characterized and well-documented to 0.22 for cases with poor data and information quality.

In these current studies, the investigation team has preferred instead to put forth the best estimates of overall uncertainty of each parameter ($\overline{S_r}$, $\overline{N_{1,60,CS}}$ and $\overline{\sigma'_{vo}}$), including <u>all</u> factors (including paucity of data, poor quality data, poor information on pre-failure or post-failure geometries, uncertainty with regard to phreatic surface, poor documentation, etc.) As a result, the standard deviations shown for these current studies in Table 4.6 incorporate all uncertainties as best that can be accomplished, and this results in natural "self-weighting" of each case in the probabilistic regressions that will follow in Chapter 5 as cases with higher uncertainties provide less "pull" on the regressed relationships. This approach is preferred here, because (1) it does not require the engineering team to impose its judgment in the form of weighting factors, and (2) it permits the subsequent regressions to incorporate the best available characterizations of individual case history uncertainties in developing assessments of overall predictive model uncertainties. Because the cases are "self-weighting" with their total uncertainty estimates, the additional weighting factors (WF) applied for for the cases in these current studies are taken as WF = 1.0.

The single exception is the Calaveras dam case history, which was reluctantly deleted from use in the regressions that will follow due to new information developed in the late 1990's that led the current investigation team to conclude that it was not possible to cross-relate the Sr values from the failure that occurred in 1918 with SPT data from more recent studies, given the variability of fines contents in the main hydraulic fill zones, and the variably cohesive nature of those fines, and the fact that portions of the dam's embankment fill were likely underconsolidated under the still rising fill loads (see Appendix A, Section A.14). Because the Calaveras Dam case history is deleted from use in the regressions that will follow, the weighting factor assigned is WF = 0.

Both the approaches taken in these current studies, and those taken by Wang and Kramer, with regard to treatment of uncertainties should be considered valid alternatives. And so this just represents another set of differences in choices between the current engineering team and the efforts of Wang and Kramer (2003/2008). In the end, the multiple, and potentially significant, differences in approaches taken by these two studies are a positive thing, as they permit two independent looks at a problem that is only moderately well constrained by data and thus subject to engineering judgment at multiple steps along the way.

Table 4.1: Selected Methods for Back-Analyses of Liquefaction Failure case Histories for Purposes of Assessing Post-Liquefaction Residual Strength

Group A: Methods that explicitly address momentum effects:
A-1. Incremental momentum analysis method (Current studies). A-2. Kinetics analysis method (Olsen and Stark; 2001, 2002). A-3. Zero inertial factor (ZIF) method (Wang, 2003; Kramer, 2008).
Group B: Methods that implicitly address momentum effects:
B-1. Displacement-calibrated pre-failure/post-failure analyses (Current studies). B-2. Pre-failure/post-failure analyses (Seed & Harder, 1990).
Group C: Methods that may or may not suitably incorporate momentum effects.
C-1. Adoption of the results of back-analyses from previous investigators.
Group D: Methods that do not incorporate momentum effects.
D-1. Back-analyses of pre-failure geometries with an assumed static factor of safety equal to 1.0. D-2. Back-analyses of post-failure geometries with an assumed static factor of safety equal to 1.0.

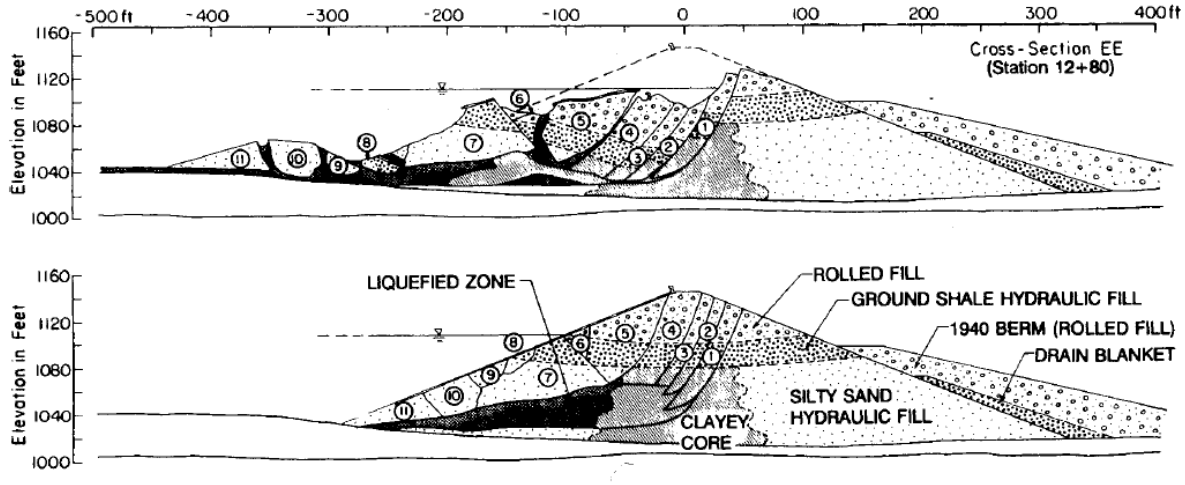

Figure 4.1: Pre-failure and post-failure cross-section of the Lower San Fernando Dam (Castro et al., 1992)

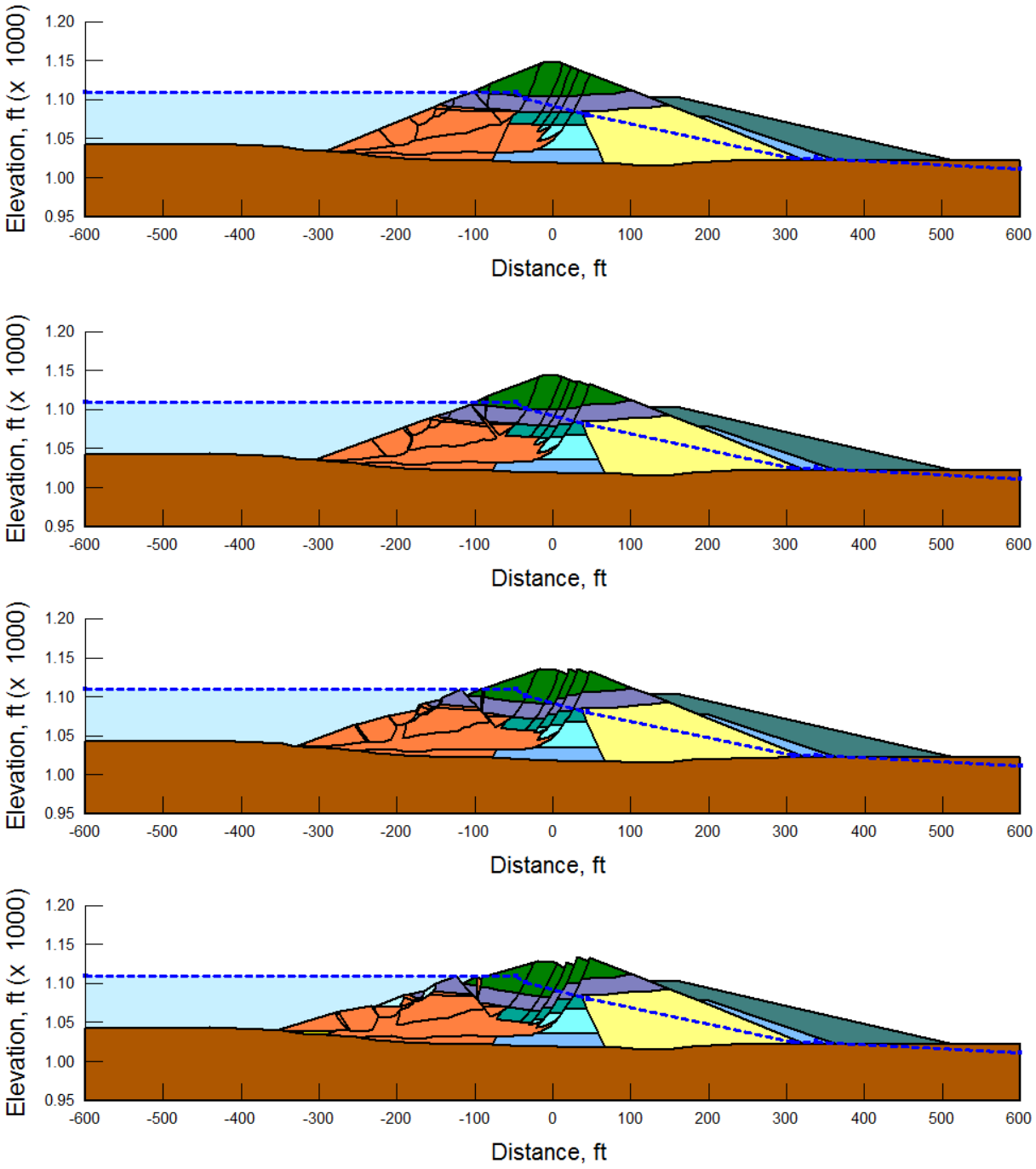

Figure 4.2: Incremental cross-sections used to model and back-analyze the liquefaction-induced upstream slide of the Lower San Fernando Dam (showing the first four cross-sections).

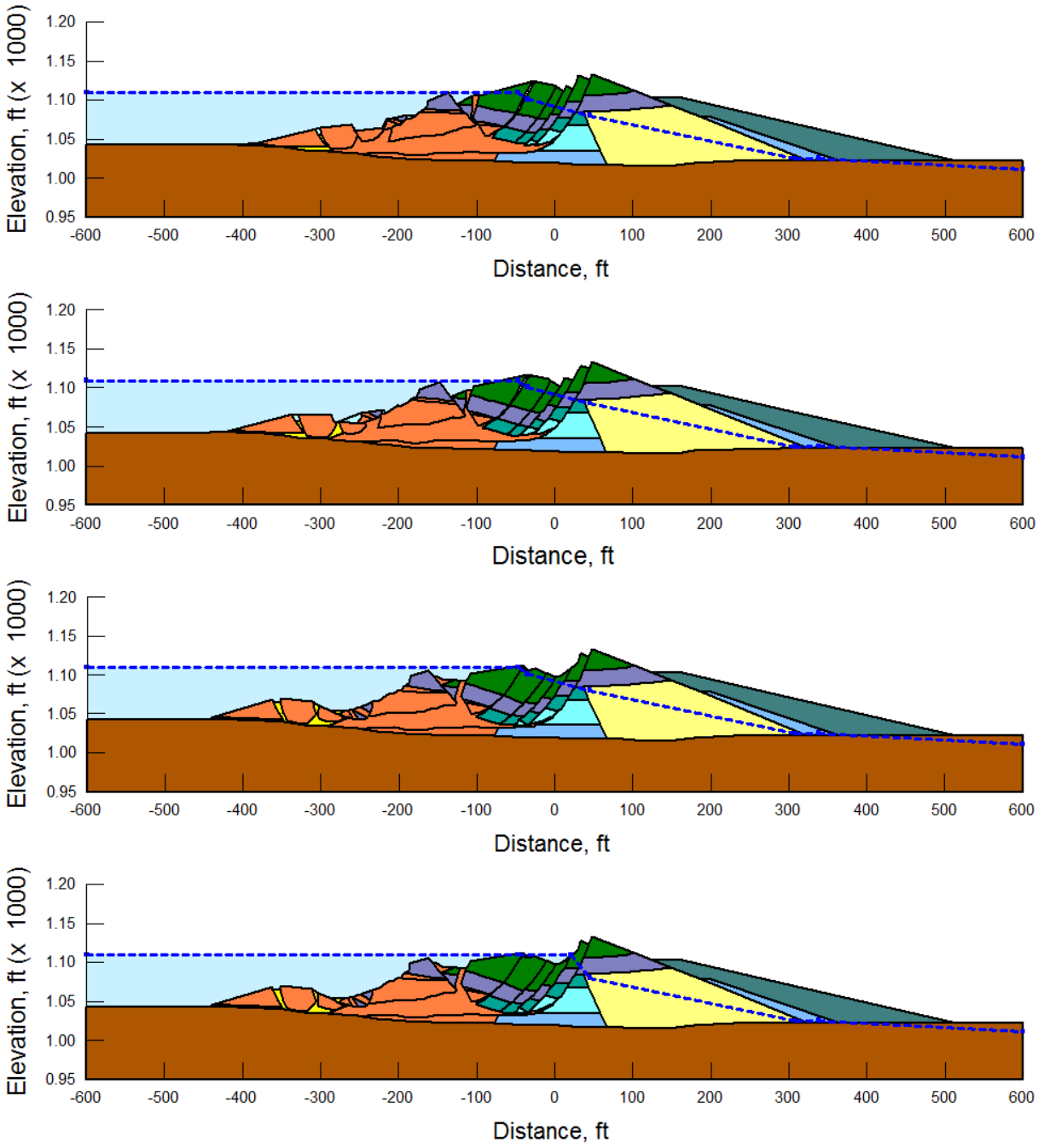

Figure 4.2 (Continued): Incremental cross-sections used to model and back-analyze the liquefaction-induced upstream slide of the Lower San Fernando Dam (showing the final four cross-sections).

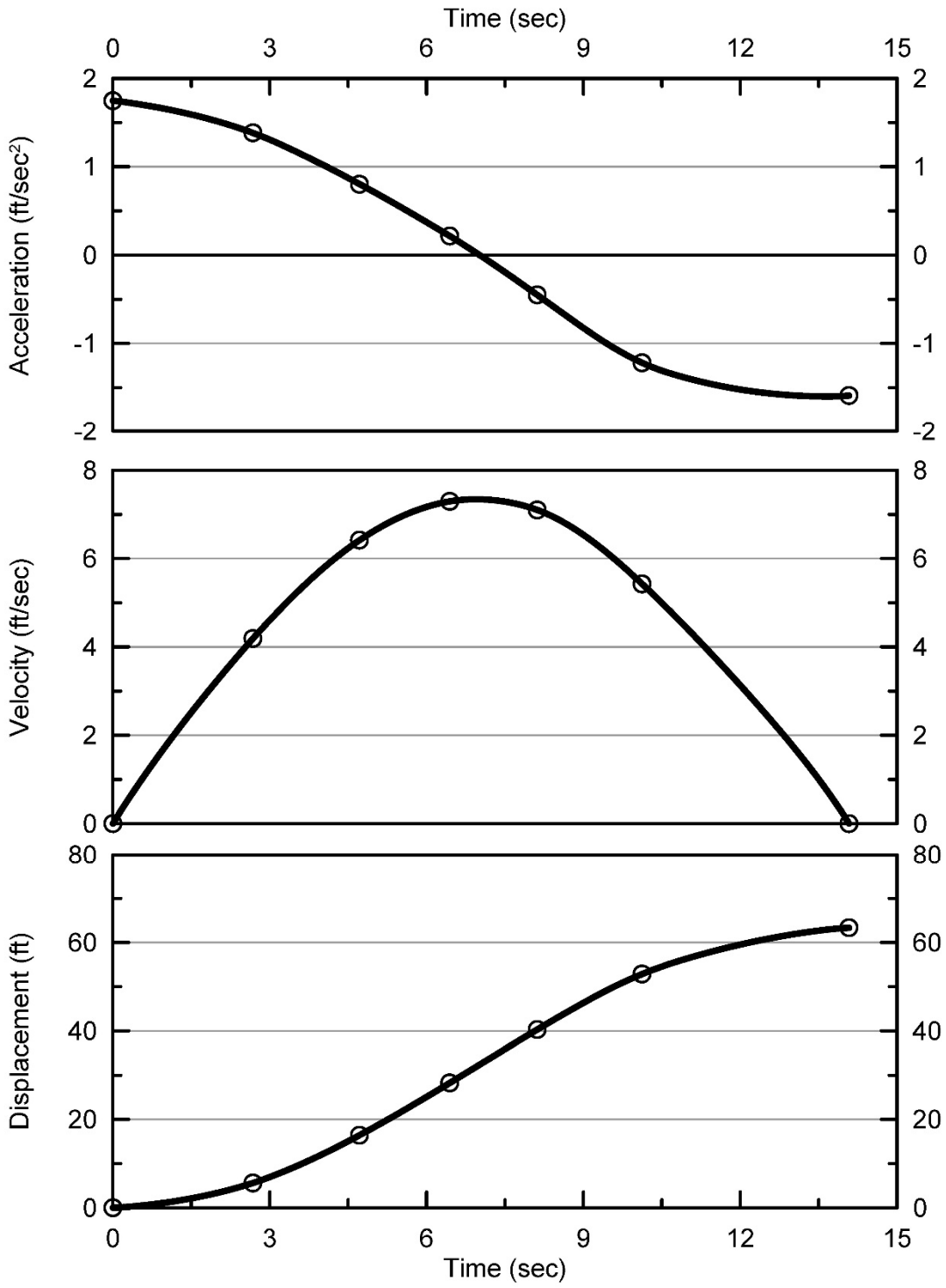

Figure 4.3: Calculated evolution of (1) acceleration vs. time, (2) velocity vs. time, and (3) dis-placement vs. time of the center of gravity of the overall failure mass of the Lower San Fernando dam based on the progression scenario illustrated in Figure 4.2.

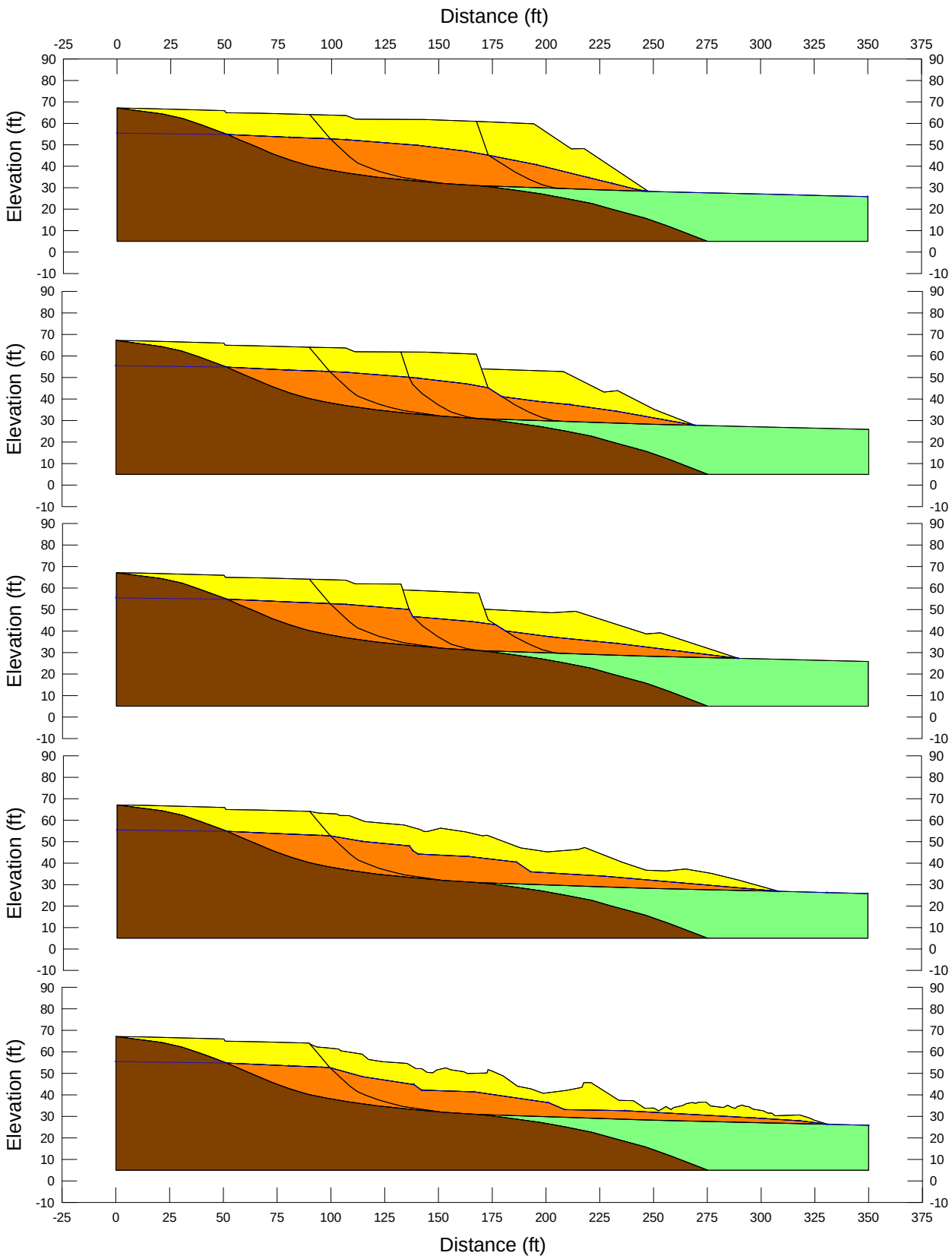

Figure 4.4: Incremental cross-sections used to model and back-analyze the liquefaction-induced failure of the Shibecha-Cho embankment.

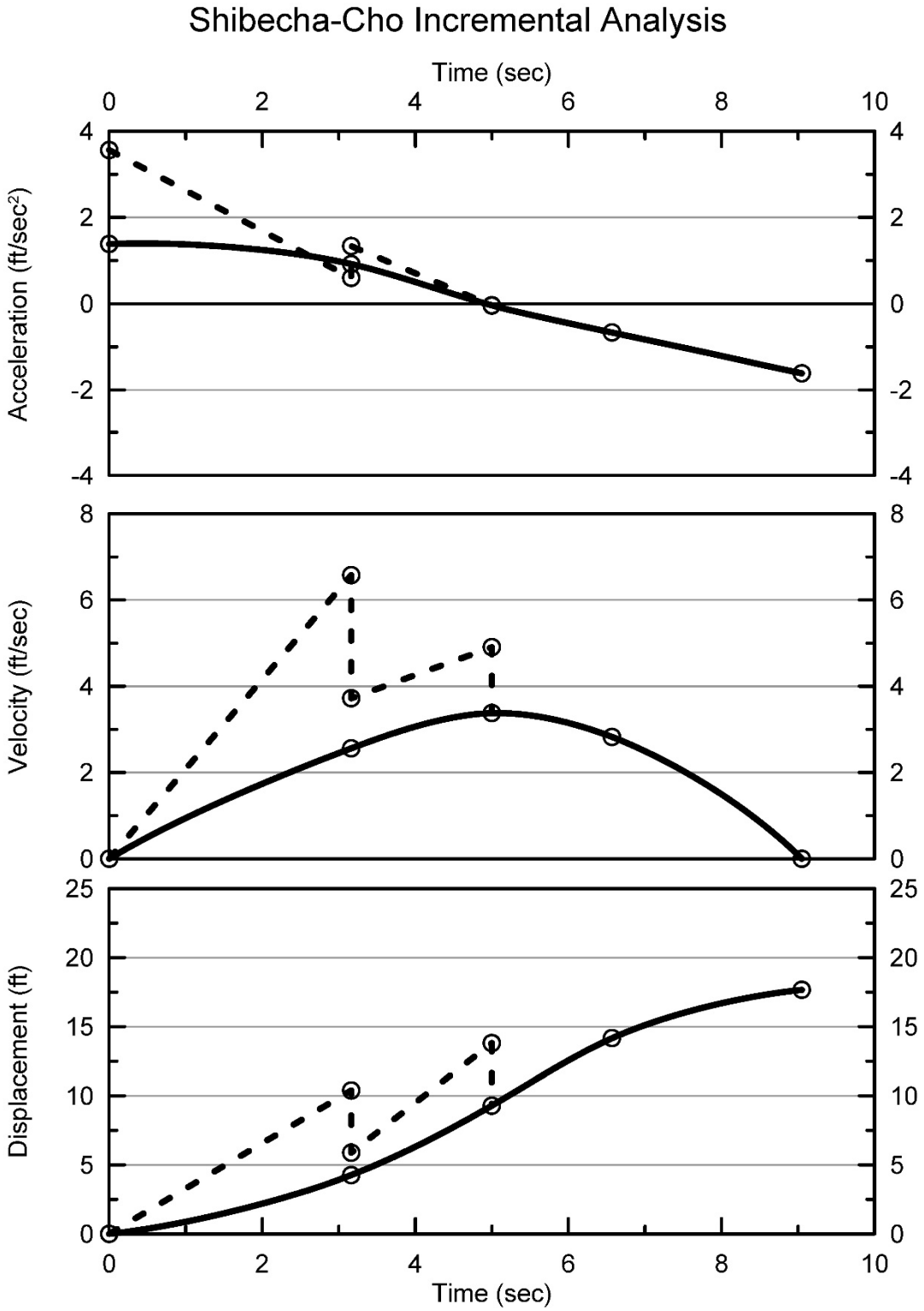

Figure 4.5: Calculated evolution of (1) acceleration vs. time, (2) velocity vs. time, and (3) displacement vs. time of the center of gravity of the overall failure mass of the Shibecha-Cho embankment fill (solid line), and of incremental partial failure masses (dashed lines).

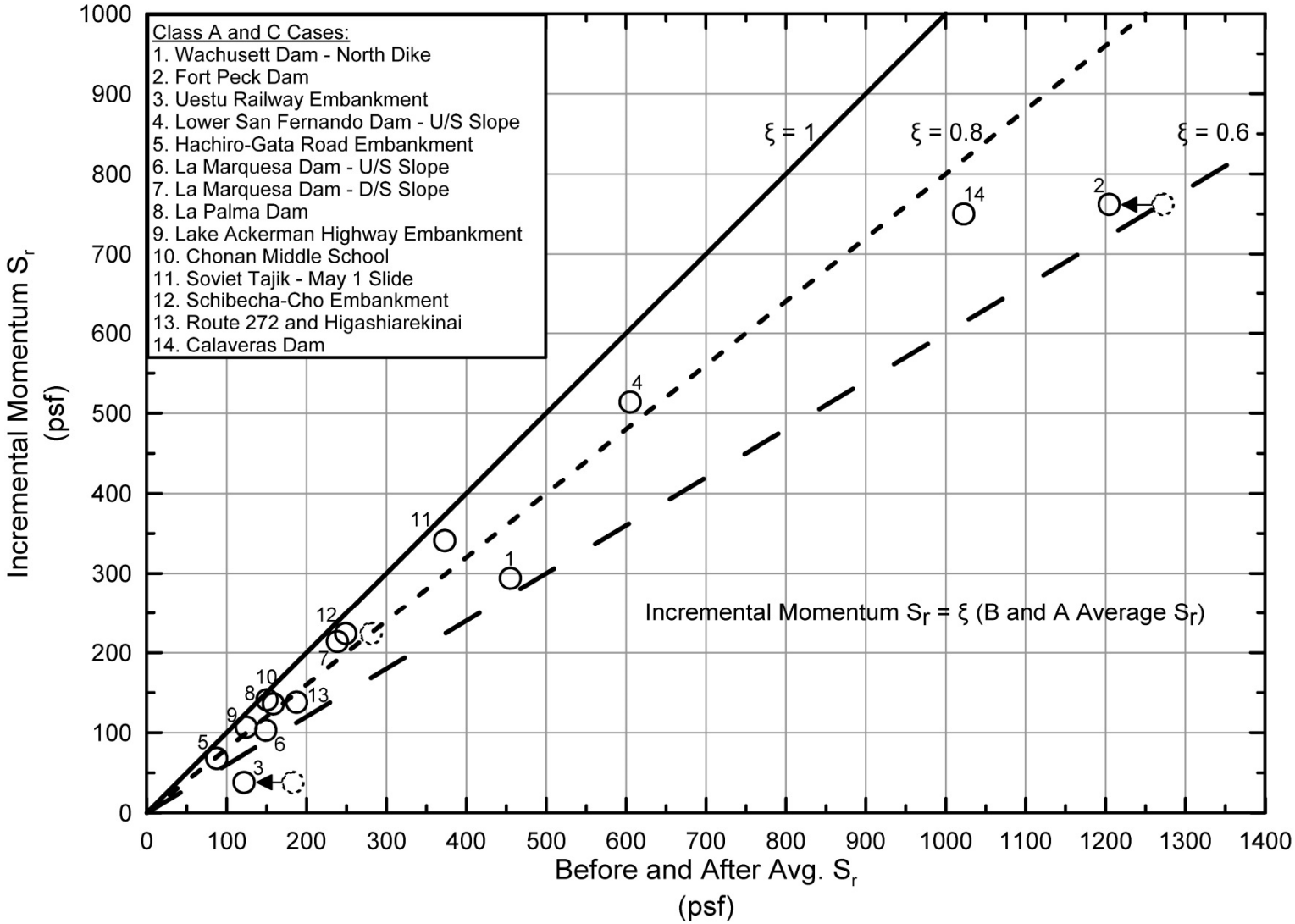

Figure 4.6: Plot of the results of back-analyses of the 14 Class A and C case histories, showing (1) the value of post-liquefaction strength S_r back-calculated by the incremental inertial method vs. (2) "before and after average S_r" which is the average of $S_{r,yield}$ and $S_{r,resid/geom}$ [taken as $(S_{r,yield} + S_{r,resid/geom})/2$].

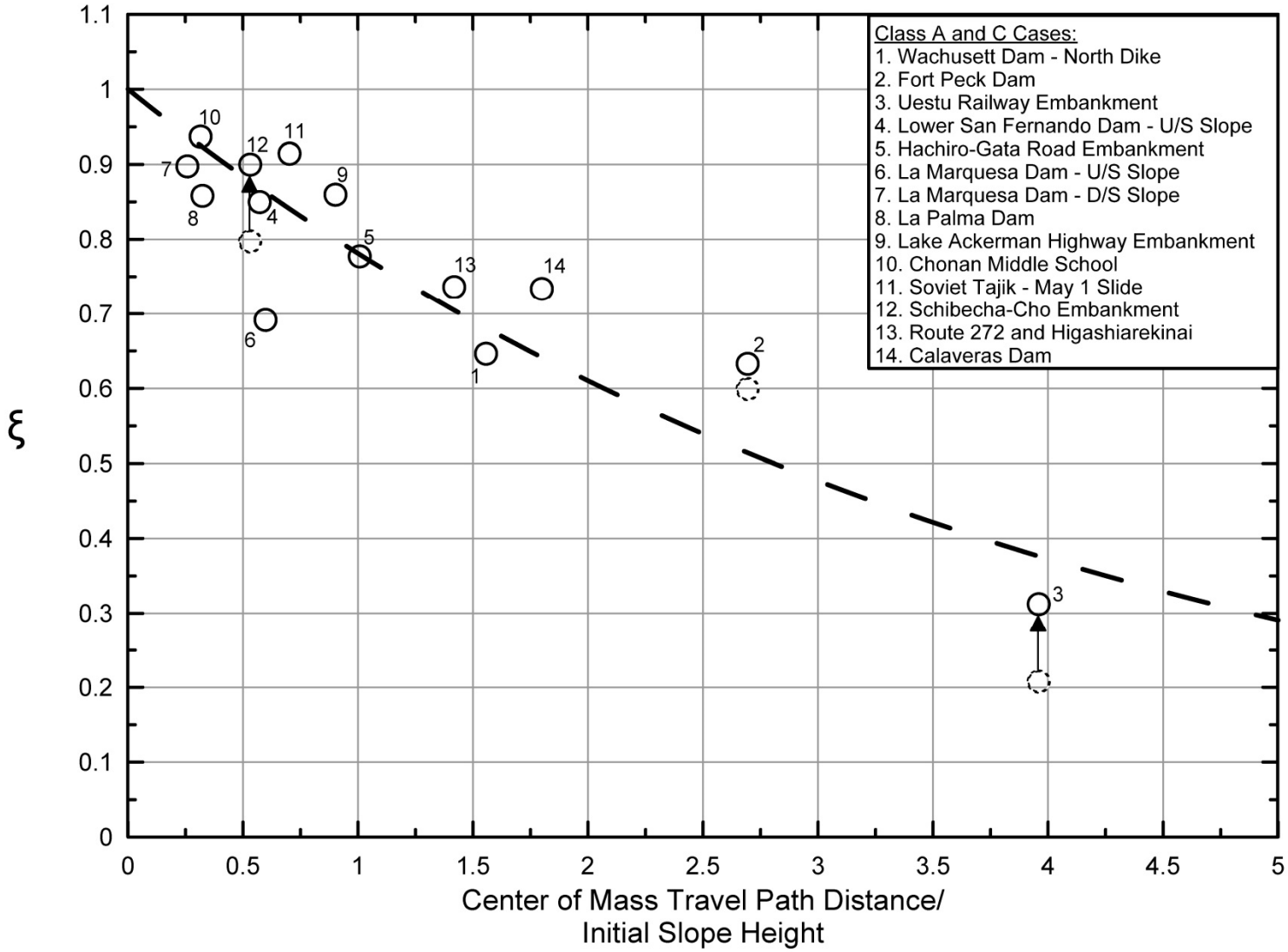

Figure 4.7: The empirical scaling parameter ξ for Equation 4-2, as a function of scaled runout distance.

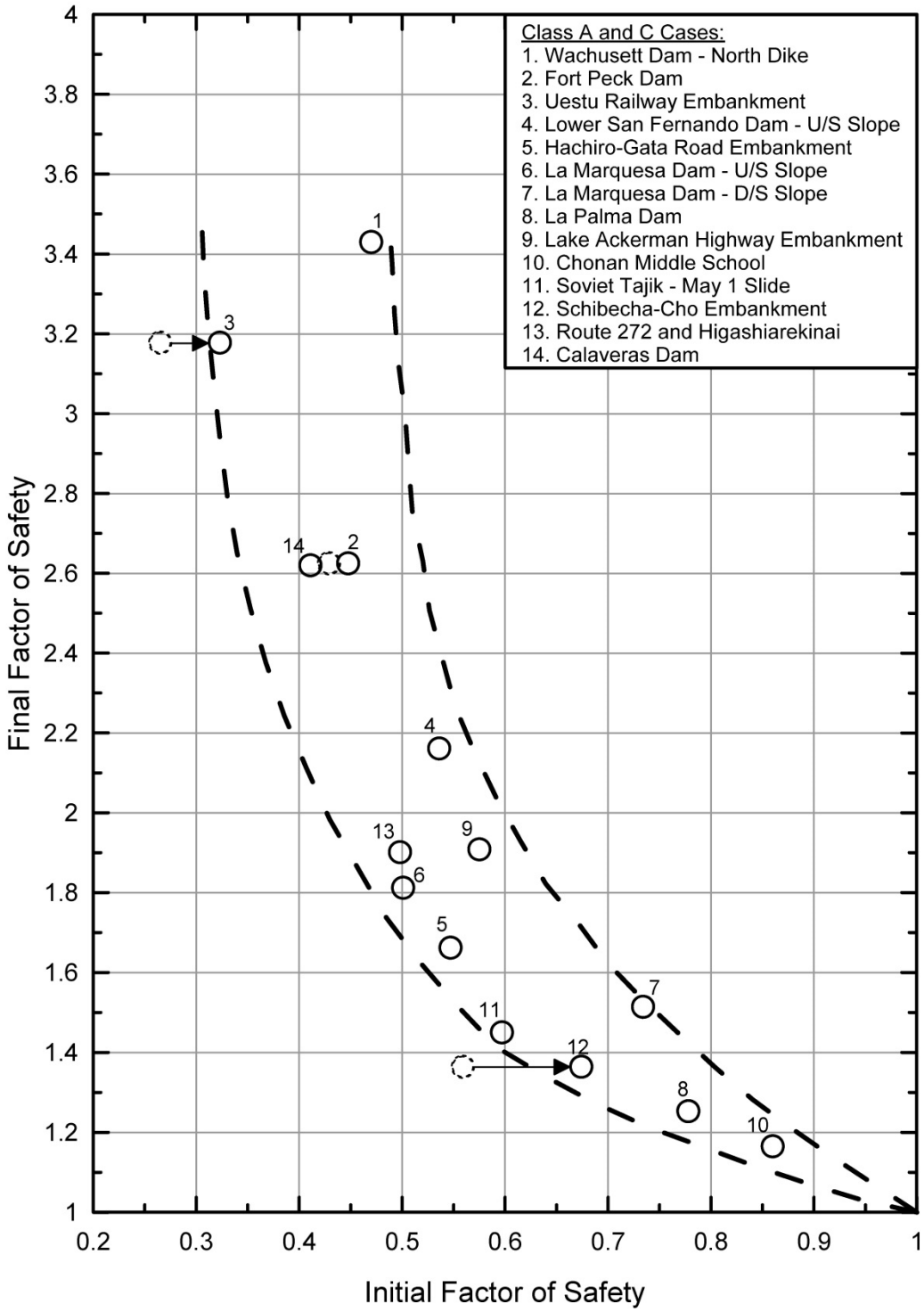

Figure 4.8: Plot of values of pre-failure FS_{liq} vs. post-failure FS_{liq} for the 14 back-analyzed liquefaction failure case histories of Classes A and C.

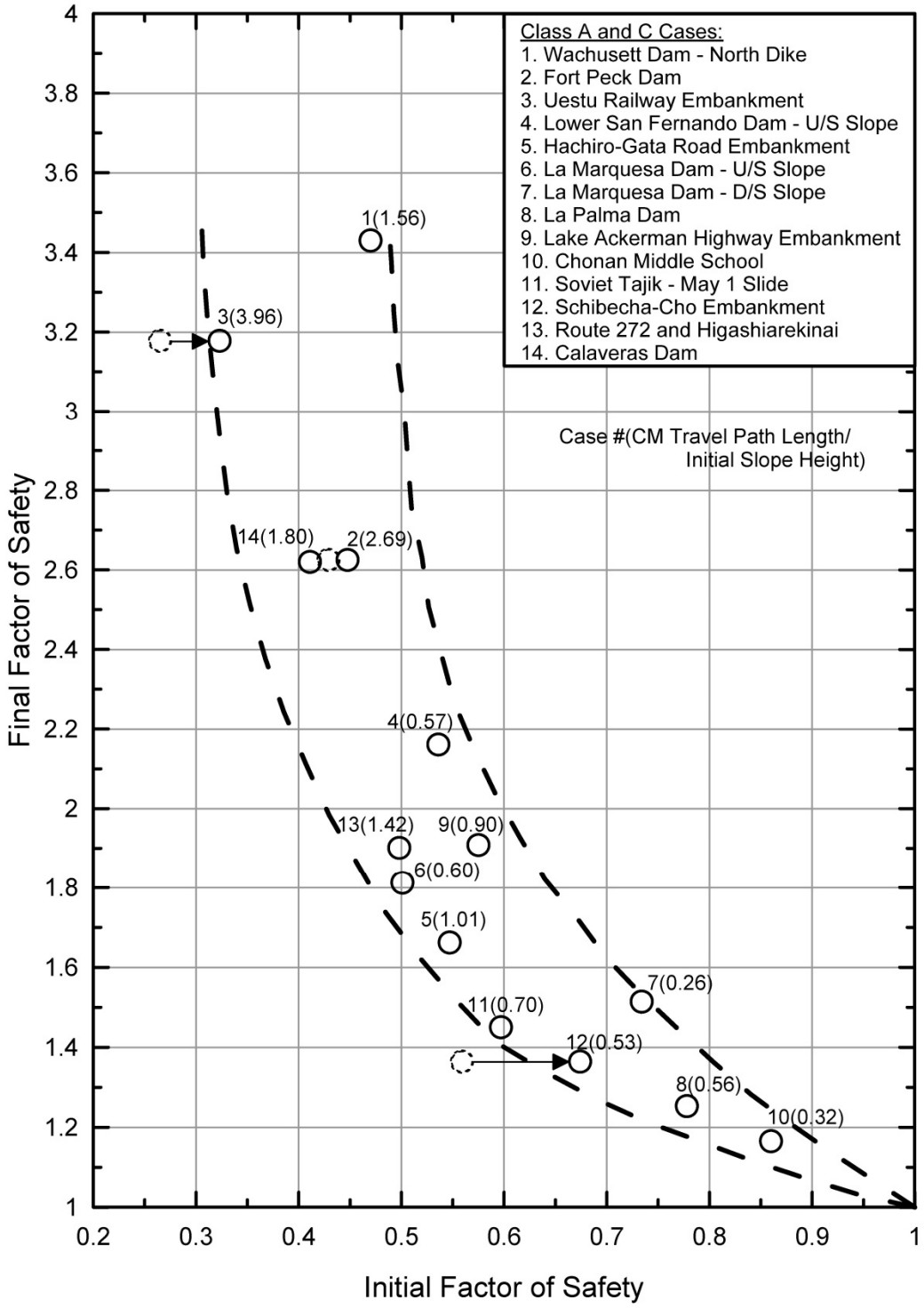

Figure 4.9: Figure 4.8 repeated, this time with the back-analyzed failure case histories annotated (in parentheses) with scaled runout distance ratio (travel distance of the center of gravity of the overall failure mass divided by the initial slope height as measured from the toe to the back heel of the failure).

Table 4.2: Back-analysis results for the well-defined liquefaction case histories of Classes A and C, and cross-comparisons with (1) Seed and Harder (1990), (2) Olsen and Stark (2002) and (3) Wang and Kramer (2003, 2008).

Group	Case	Seed and Harder (1990)		Olson and Stark (2002)				Wang (2003) + Kramer (2008)				This Study			
		S_r (psf)	$N_{1,60,CS}$	S_u(Liq) (psf)	S_u(Liq)/σ'_{vo}	σ'_{vo} (psf)	$N_{1,60}$ (1)	$\bar{S}_r$ (psf) (2)	$\bar{S}_r/\bar{\sigma}'_{vo}$	$\bar{\sigma}'$vo (psf) (3)	$\bar{N}_{1,60,CS}$	$\bar{S}_r$ (psf)	$\bar{S}_r/\bar{\sigma}'_{vo}$	$\bar{\sigma}'_{vo}$ (psf)	$\bar{N}_{1,60,CS}$
A	Wachusett Dam - North Dike			334	0.106	3158	7	348	0.136	2559	7.3(4)	294	0.094	3142	7.5
	Fort Peck Dam	350	10	570	0.078	7341	8.5	671.5	0.091	7379	15.8	762	0.105	7258	12.5
	Uetsu Railway Embankment	40	3	36	0.027	1280	3	43.5	0.048	906	2.9	38	0.026	1448	3
	Lower San Fernando Dam - U/S Slope	400	13.5	390	0.120	3482	11.5	484.7	0.133	3644	14.5	514	0.12	4287	13.5
	Hachiro-Gata Road Embankment			42	0.062	670	4.4	65	0.164	396	5.7	68	0.101	673	7
	La Marquesa Dam - U/S Slope	200	6	65	0.070	911	4.5	(185.2)	0.110	1684	6.5(4)	103	0.105	981	6.5
	La Marquesa Dam - D/S Slope	400	11	111	0.110	1000	9	(343.5)	0.186	1847	9.9(4)	214	0.176	1215	10.5
	La Palma Dam	200	4	100	0.120	789	3.5	(193.3)	0.123	1572	4.2	136	0.177	767	5
	Lake Ackerman Highway Embankment			82	0.076	1076	3	98	0.114	860	4.8	107	0.118	909	3.5
	Chonan Middle School			100	0.091	1119	5.2	(178.7)	0.091	1964	6.4(4)	141	0.137	1032	6.5
	Soviet Tajik - May 1 Slide			175	0.082	2170	7.6	(334)	0.082	4073	8.9(4)	341	0.179	1907	10.5
	Shibecha-Cho Embankement			117	0.086	1351	5.6	208.9	0.200	1045	5.6	224	0.158	1416	7.5
	Route 272 at Higashiarekinai			100	0.097	1030	6.3	130.5	0.125	1044	8.5	138	0.107	1285	8
B	Zeeland - Vlietepolder			115	0.048	2396	7.5	(226.1)	0.048	4710	8.5(4)				
	Sheffield Dam	75	6	75	0.053	1429	5	(99.8)	0.043	2321	8.2(4)				
	Helsinki Harbor			32	0.060	522	6	(52.4)	0.067	782	5.9(4)				
	Solfatara Canal Dike	50	4	50	0.080	624	4	(77.1)	0.063	1224	4.9(4)				
	Lake Merced Bank	100	6	144	0.108	1372	7.5	(139.5)	0.106	1316	5.9(4)				
	El Cobre Tailings Dam			40	0.020	1946	0	(195.2)	0.020	9760	6.8				
	Metoki Road Embankment			38	0.043	875	2.6	(116.8)	0.044	2655	2.0				
	Hokkaido Tailings Dam			100	0.073	1376	1.1	(250.6)	0.074	3386	5.1				
	Upper San Fernando Dam - D/S Slope	600	15												
	Tar Island Dyke			251	0.058	4300	7	(364.2)	0.058	6279	8.9(4)				
	Mochi-Koshi Tailings Dam, Dikes 1 and 2	250	5	75	0.060	1251	2.7	(158.9)	0.091	1746	8.9				
				113	0.104	1090	2.7	(233.6)	0.081	2884	10.0				
	Nerlerk Embankment, Slides 1 ,2 and 3			52	0.086	616	8.7	(178.5)	0.124	1440	11.4(4)				
				36	0.060	650	7.2								
				31	0.034	925	7.2								
	Asele Road Embankment			132	0.104	1251	7	(163.7)	0.104	1574	11.0(4)				
	Nalband Railway Embankment			119	0.109	1101	9.2	(139.9)	0.109	1283	6.3(4)				
	Sullivan Tailings														
	Jamuna Bridge														
C	Calaveras Dam	650	12	721	0.112	6422	8	632.7	0.099	6391	10.5(4)	750	0.106	7100	18

Notes : (1) No fines content correction utilized in Olson and Stark (2002).
(2) Where noted in parentheses, $S_{u,r}$ values in are for secondary cases in Wang (2003) and were not fully reanalyzed

Table 4.3: Back-analysis results for the well-defined liquefaction case histories of Classes A and C, and cross-comparisons with (1) Seed and Harder (1990), (2) Olsen and Stark (2002) [modified], and (3) Wang and Kramer (2003, 2008).

Group	Case	Seed and Harder (1990)		Olson and Stark (2002)				Wang (2003) + Kramer (2008)				This Study			
		S_r (psf)	$N_{1,60,CS}$	$S_u(Liq)$ (psf) [1]	$S_u(Liq)/\sigma'_{vo}$	σ'_{vo} (psf)	$N_{1,60}$ [2]	$\bar{S}_r$ (psf) [3]	$\bar{S}_r/\bar{\sigma}'_{vo}$	$\bar{\sigma}'_{vo}$ (psf) [4]	$\bar{N}_{1,60,CS}$	$\bar{S}_r$ (psf)	$\bar{S}_r/\bar{\sigma}'_{vo}$	$\bar{\sigma}'_{vo}$ (psf)	$\bar{N}_{1,60,CS}$
A	Wachusett Dam - North Dike			334	0.106	3158	7	348	0.136	2559	7.3[5]	294	0.094	3142	7.5
	Fort Peck Dam	350	10	570	0.078	7341	8.5	671.5	0.091	7379	15.8	762	0.105	7258	12.5
	Uetsu Railway Embankment	40	3	36	0.027	1280	3	43.5	0.048	906	2.9	38	0.026	1448	3
	Lower San Fernando Dam - U/S Slope	400	13.5	390	0.120	3482	11.5	484.7	0.133	3644	14.5	514	0.12	4287	13.5
	Hachiro-Gata Road Embankment			42	0.062	670	4.4	65	0.164	396	5.7	68	0.101	673	7
	La Marquesa Dam - U/S Slope	200	6	[104]	0.114	911	4.5	(185.2)	0.110	1684	6.5[5]	103	0.105	981	6.5
	La Marquesa Dam - D/S Slope	400	11	[152]	0.152	1000	9	(343.5)	0.186	1847	9.9[5]	214	0.176	1215	10.5
	La Palma Dam	200	4	[125]	0.158	789	3.5	(193.3)	0.123	1572	4.2	136	0.177	767	5
	Lake Ackerman Highway Embankment			82	0.076	1076	3	98	0.114	860	4.8	107	0.118	909	3.5
	Chonan Middle School			[142]	0.127	1119	5.2	(178.7)	0.091	1964	6.4[5]	141	0.137	1032	6.5
	Soviet Tajik - May 1 Slide			[334]	0.154	2170	7.6	(334)	0.082	4073	8.9[5]	341	0.179	1907	10.5
	Shibecha-Cho Embankement			117	0.086	1351	5.6	208.9	0.200	1045	5.6	224	0.158	1416	7.5
	Route 272 at Higashiarekinai			100	0.097	1030	6.3	130.5	0.125	1044	8.5	138	0.107	1285	8
B	Zeeland - Vlietepolder			[180]	0.075	2396	7.5	(226.1)	0.048	4710	8.5[5]				
	Sheffield Dam	75	6	[159]	0.111	1429	5	(99.8)	0.043	2321	8.2[5]				
	Helsinki Harbor			[44]	0.084	522	6	(52.4)	0.067	782	5.9[5]				
	Solfatara Canal Dike	50	4	[71]	0.114	624	4	(77.1)	0.063	1224	4.9[5]				
	Lake Merced Bank	100	6	[205]	0.149	1372	7.5	(139.5)	0.106	1316	5.9[5]				
	El Cobre Tailings Dam			<40>	0.020	1946	0	(195.2)	0.020	9760	6.8				
	Metoki Road Embankment			[90]	0.103	875	2.6	(116.8)	0.044	2655	2.0				
	Hokkaido Tailings Dam			[138]	0.100	1376	1.1	(250.6)	0.074	3386	5.1				
	Upper San Fernando Dam - D/S Slope	600	15												
	Tar Island Dyke			[401]	0.093	4300	7	(364.2)	0.058	6279	8.9[5]				
	Mochi-Koshi Tailings Dam, Dikes 1 and 2	250	5	[207]	0.165	1251	2.7	(158.9)	0.091	1746	8.9				
				[180]	0.165	1090	2.7	(233.6)	0.081	2884	10.0				
	Nerlerk Embankment, Slides 1 ,2 and 3			[44]	0.071	616	8.7	(178.5)	0.124	1440	11.4[5]				
				[50]	0.077	650	7.2								
				[52]	0.056	925	7.2								
	Asele Road Embankment			[192]	0.153	1251	7	(163.7)	0.104	1574	11.0[5]				
	Nalband Railway Embankment			[121]	0.110	1101	9.2	(139.9)	0.109	1283	6.3[5]				
	Sullivan Tailings														
	Jamuna Bridge														
C	Calaveras Dam	650	12	721	0.112	6422	8	632.7	0.099	6391	10.5[5]	750	0.106	7100	18

Notes : (1) Where noted in brackets, $S_u(Liq)$ and $S_u(Liq)/\sigma'_{vo}$ for Olson (2001) reinterpreted using reported values of Su Yield and S_u Residual in Olson (2001) and the equation $S_u(Liq) = 0.8$ (Su Yield + S_u Residual)/2. Reinterpretation of Su(Liq) performed for cases not calculated using the Kinetic procedure in Olson (2001). Where noted in triangular brackets, no S_u Yield value reported in Olson (2001).

(2) No fines content correction utilized in Olson and Stark (2002).
(3) Where noted in parentheses, $S_{u,r}$ values in are for secondary cases in Wang (2003) and were not fully reanalyzed.
(4) σ'_{vo} not explicitly reported in Wang (2003) or Kramer (2008). Values shown were back calculated from reported Sr and Sr/ σ'vo.
(5) $N_{1,60,CS}$ values were changed in Kramer (2008) from the values reported in Wang (2003). The updated values are shown.

Table 4.4: Back-analysis results for the less well-defined liquefaction case histories of Class B, and cross-comparisons with (1) Seed and Harder (1990), (2) Olsen and Stark (2002) and (3) Wang and Kramer (2003, 2008).

Group	Case	Seed and Harder (1990)		Olson and Stark (2002)				Wang (2003) + Kramer (2008)				This Study			
		S_r (psf)	$N_{1,60,CS}$	S_u(Liq) (psf)	S_u(Liq)/σ'_{vo}	σ'_{vo} (psf)	$N_{1,60}$ (1)	$\bar{S}_r$ (psf) (2)	$\bar{S}_r/\bar{\sigma}'_{vo}$	$\bar{\sigma}'$vo (psf) (3)	$\bar{N}_{1,60,CS}$	$\bar{S}_r$ (psf)	$\bar{S}_r/\bar{\sigma}'_{vo}$	$\bar{\sigma}'_{vo}$ (psf)	$\bar{N}_{1,60,CS}$
A	Wachusett Dam - North Dike			334	0.106	3158	7	348	0.136	2559	7.3(4)				
	Fort Peck Dam	350	10	570	0.078	7341	8.5	671.5	0.091	7379	15.8				
	Uetsu Railway Embankment	40	3	36	0.027	1280	3	43.5	0.048	906	2.9				
	Lower San Fernando Dam - U/S Slope	400	13.5	390	0.120	3482	11.5	484.7	0.133	3644	14.5				
	Hachiro-Gata Road Embankment			42	0.062	670	4.4	65	0.164	396	5.7				
	La Marquesa Dam - U/S Slope	200	6	65	0.07	911	4.5	(185.2)	0.110	1684	6.5(4)				
	La Marquesa Dam - D/S Slope	400	11	111	0.11	1000	9	(343.5)	0.186	1847	9.9(4)				
	La Palma Dam	200	4	100	0.12	789	3.5	(193.3)	0.123	1572	4.2				
	Lake Ackerman Highway Embankment			82	0.076	1076	3	98	0.114	860	4.8				
	Chonan Middle School			100	0.09	1119	5.2	(178.7)	0.091	1964	6.4(4)				
	Soviet Tajik - May 1 Slide			175	0.08	2170	7.6	(334)	0.082	4073	8.9(4)				
	Shibecha-Cho Embankement			117	0.086	1351	5.6	208.9	0.200	1045	5.6				
	Route 272 at Higashiarekinai			100	0.097	1030	6.3	130.5	0.125	1044	8.5				
B	Zeeland - Vlietepolder			115	0.05	2396	7.5	(226.1)	0.048	4710	8.5(4)	156	0.063	2488	8
	Sheffield Dam	75	6	75	0.05	1429	5	(99.8)	0.043	2321	8.2(4)	138	0.106	1308	7
	Helsinki Harbor			32	0.06	522	6	(52.4)	0.067	782	5.9(4)	48	0.057	846	6
	Solfatara Canal Dike	50	4	50	0.08	624	4	(77.1)	0.063	1224	4.9(4)	64	0.096	669	5
	Lake Merced Bank	100	6	144	0.11	1372	7.5	(139.5)	0.106	1316	5.9(4)	136	0.163	834	9
	El Cobre Tailings Dam			40	0.020	1946	0	(195.2)	0.020	9760	6.8	141	0.054	2595	3
	Metoki Road Embankment			38	0.04	875	2.6	(116.8)	0.044	2655	2.0	92	0.106	871	3
	Hokkaido Tailings Dam			100	0.07	1376	1.1	(250.6)	0.074	3386	5.1	131	0.109	1203	4
	Upper San Fernando Dam - D/S Slope	600	15									726	0.224	3238	15
	Tar Island Dyke			251	0.06	4300	7	(364.2)	0.058	6279	8.9(4)	516	0.123	4197	11
	Mochi-Koshi Tailings Dam, Dikes 1 and 2	250	5	75	0.06	1251	2.7	(158.9)	0.091	1746	8.9	211	0.138	1532	6
				113	0.10	1090	2.7	(233.6)	0.081	2884	10.0				
	Nerlerk Embankment, Slides 1 ,2 and 3			52	0.09	616	8.7	(178.5)	0.124	1440	11.4(4)	93	0.079	1171	7.5
				36	0.06	650	7.2								
				31	0.03	925	7.2								
	Asele Road Embankment			132	0.10	1251	7	(163.7)	0.104	1574	11.0(4)	137	0.132	1037	9.5
	Nalband Railway Embankment			119	0.11	1101	9.2	(139.9)	0.109	1283	6.3(4)	167	0.138	1209	7.5
	Sullivan Tailings											277	0.114	2422	9.5
	Jamuna Bridge											175	0.125	1404	10.5
C	Calaveras Dam	650	12	721	0.112	6422	8	632.7	0.099	6391	10.5(4)				

Notes : (1) No fines content correction utilized in Olson and Stark (2002).
(2) Where noted in parentheses, $S_{u,r}$ values in are for secondary cases in Wang (2003) and were not fully reanalyzed
(3) σ'_{vo} not explicitly reported in Wang (2003) or Kramer (2008). Values shown were back calculated from reported Sr and Sr/ σ'vo.
(4) $N_{1,60,CS}$ values were changed in Kramer (2008) from the values reported in Wang (2003). The updated values are shown

Table 4.5: Back-analysis results for the less well-defined liquefaction case histories of Class B, and cross-comparisons with (1) Seed and Harder (1990), (2) Olsen and Stark (2002) [modified], and (3) Wang and Kramer (2003, 2008).

Group	Case	Seed and Harder (1990)		Olson and Stark (2002)				Wang (2003) + Kramer (2008)				This Study			
		S_r (psf)	$N_{1,60,CS}$	S_u(Liq) (psf) [1]	S_u(Liq)/σ'_{vo}	σ'_{vo} (psf)	$N_{1,60}$ [2]	$\bar{S}_r$ (psf) [3]	$\bar{S}_r$/ $\bar{\sigma}'_{vo}$	$\bar{\sigma}'_{vo}$ (psf) [4]	$\bar{N}_{1,60,CS}$	$\bar{S}_r$ (psf)	$\bar{S}_r$/ $\bar{\sigma}'_{vo}$	$\bar{\sigma}'_{vo}$ (psf)	$\bar{N}_{1,60,CS}$
A	Wachusett Dam - North Dike			334	0.106	3158	7	348	0.136	2559	7.3[5]				
	Fort Peck Dam	350	10	570	0.078	7341	8.5	671.5	0.091	7379	15.8				
	Uetsu Railway Embankment	40	3	36	0.027	1280	3	43.5	0.048	906	2.9				
	Lower San Fernando Dam - U/S Slope	400	13.5	390	0.120	3482	11.5	484.7	0.133	3644	14.5				
	Hachiro-Gata Road Embankment			42	0.062	670	4.4	65	0.164	396	5.7				
	La Marquesa Dam - U/S Slope	200	6	[104]	0.114	911	4.5	(185.2)	0.110	1684	6.5[5]				
	La Marquesa Dam - D/S Slope	400	11	[152]	0.152	1000	9	(343.5)	0.186	1847	9.9[5]				
	La Palma Dam	200	4	[125]	0.158	789	3.5	(193.3)	0.123	1572	4.2				
	Lake Ackerman Highway Embankment			82	0.076	1076	3	98	0.114	860	4.8				
	Chonan Middle School			[142]	0.127	1119	5.2	(178.7)	0.091	1964	6.4[5]				
	Soviet Tajik - May 1 Slide			[334]	0.154	2170	7.6	(334)	0.082	4073	8.9[5]				
	Shibecha-Cho Embankement			117	0.086	1351	5.6	208.9	0.200	1045	5.6				
	Route 272 at Higashiarekinai			100	0.097	1030	6.3	130.5	0.125	1044	8.5				
B	Zeeland - Vlietepolder			[180]	0.075	2396	7.5	(226.1)	0.048	4710	8.5[5]	156	0.063	2488	8
	Sheffield Dam	75	6	[159]	0.111	1429	5	(99.8)	0.043	2321	8.2[5]	138	0.106	1308	7
	Helsinki Harbor			[44]	0.084	522	6	(52.4)	0.067	782	5.9[5]	48	0.057	846	6
	Solfatara Canal Dike	50	4	[71]	0.114	624	4	(77.1)	0.063	1224	4.9[5]	64	0.096	669	5
	Lake Merced Bank	100	6	[205]	0.149	1372	7.5	(139.5)	0.106	1316	5.9[5]	136	0.163	834	9
	El Cobre Tailings Dam			<40>	0.020	1946	0	(195.2)	0.020	9760	6.8	141	0.054	2595	3
	Metoki Road Embankment			[90]	0.103	875	2.6	(116.8)	0.044	2655	2.0	92	0.106	871	3
	Hokkaido Tailings Dam			[138]	0.100	1376	1.1	(250.6)	0.074	3386	5.1	131	0.109	1203	4
	Upper San Fernando Dam - D/S Slope	600	15									726	0.224	3238	15
	Tar Island Dyke			[401]	0.093	4300	7	(364.2)	0.058	6279	8.9[5]	516	0.123	4197	11
	Mochi-Koshi Tailings Dam, Dikes 1 and 2	250	5	[207]	0.165	1251	2.7	(158.9)	0.091	1746	8.9	211	0.138	1532	6
				[180]	0.165	1090	2.7	(233.6)	0.081	2884	10.0				
	Nerlerk Embankment, Slides 1 ,2 and 3			[44]	0.071	616	8.7	(178.5)	0.124	1440	11.4[5]	93	0.079	1171	7.5
				[50]	0.077	650	7.2								
				[52]	0.056	925	7.2								
	Asele Road Embankment			[192]	0.153	1251	7	(163.7)	0.104	1574	11.0[5]	137	0.132	1037	9.5
	Nalband Railway Embankment			[121]	0.110	1101	9.2	(139.9)	0.109	1283	6.3[5]	167	0.138	1209	7.5
	Sullivan Tailings											277	0.114	2422	9.5
	Jamuna Bridge											175	0.125	1404	10.5
C	Calaveras Dam	650	12	721	0.112	6422	8	632.7	0.099	6391	10.5[5]				

Notes : (1) Where noted in brackets, S_u(Liq) and S_u(Liq)/σ'_{vo} for Olson (2001) reinterpreted calculated using average of S_u Residual and S_u Yield in Olson (2001) shown for cases not calculated using the Kinetic procedure in Olson (2001). Where noted in triangular brackets, no S_u Yield value reported in Olson (2001).

(2) No fines content correction utilized in Olson and Stark (2002).
(3) Where noted in parentheses, $S_{u,r}$ values in are for secondary cases in Wang (2003) and were not fully reanalyzed.
(4) σ'_{vo} not explicitly reported in Wang (2003) or Kramer (2008). Values shown were back calculated from reported Sr and Sr/ σ'vo.
(5) $N_{1,60,CS}$ values were changed in Kramer (2008) from the values reported in Wang (2003). The updated values are shown.

Table 4.6: Comparison between the back-calculated values of this study with those developed by Wang and Kramer (2003, 2008) for (1) post-liquefaction strength, (2) representative initial vertical effective stress, and (3) penetration resistance, with inclusion of uncertainties.

Group	Case	Wang (2003) + Kramer (2008)							This Study						
		$\bar{S}_r$ (psf) [1]	$\sigma_{\bar{S}}$	$\bar{\sigma}'_{vo}$ (psf) [2]	$\sigma_{\bar{\sigma}}$	$\bar{N}_{1,60,CS}$	$\sigma_{\bar{N}}$	WF	$\bar{S}_r$ (psf)	$\sigma_{\bar{S}}$	$\bar{\sigma}'_{vo}$ (psf)	$\sigma_{\bar{\sigma}}$	$\bar{N}_{1,60,CS}$	$\sigma_{\bar{N}}$	WF
A	Wachusett Dam - North Dike	348	74.8	2559	(-)	7.3[3]	1.9	1.00	294	31	3142	132	7.5	1.6	1.00
	Fort Peck Dam	671.5	130.2	7379	(-)	15.8	0.9	0.85	762	118	7258	687	12.5	2.7	1.00
	Uetsu Railway Embankment	43.5	24.8	906	(-)	2.9	4.2	0.55	38	8	1448	116	3	0.8	1.00
	Lower San Fernando Dam - U/S Slope	484.7	111.0	3644	(-)	14.5	1.1	1.00	514	47	4287	281	13.5	1.8	1.00
	Hachiro-Gata Road Embankment	65	24.7	396	(-)	5.7	2.8	0.55	68	12	673	41	7	1.2	1.00
	La Marquesa Dam - U/S Slope	(185.2)	82.1	1684	(-)	6.5[3]	2.8	0.76	103	33	981	134	6.5	1.8	1.00
	La Marquesa Dam - D/S Slope	(343.5)	113.8	1847	(-)	9.9[3]	3.0	0.72	214	57	1215	103	10.5	2.2	1.00
	La Palma Dam	(193.3)	86.3	1572	(-)	4.2	1.8	0.80	136	23	767	42	5	1.2	1.00
	Lake Ackerman Highway Embankment	98	20.4	860	(-)	4.8	1.2	1.00	107	19	909	61	3.5	0.7	1.00
	Chonan Middle School	(178.7)	32.0	1964	(-)	6.4[3]	6.9	0.74	141	35	1032	82	6.5	2.1	1.00
	Soviet Tajik - May 1 Slide	(334)	110.9	4073	(-)	8.9[3]	5.7	0.22	341	57	1907	177	10.5	2.7	1.00
	Shibecha-Cho Embankement	208.9	38.6	1045	(-)	5.6	2.2	0.70	224	37	1416	95	7.5	1.7	1.00
	Route 272 at Higashiarekinai	130.5	33.5	1044	(-)	8.5	2.6	0.70	138	17	1285	104	8	1.6	1.00
B	Zeeland - Vlietepolder	(226.1)	75.0	4710	(-)	8.5[3]	5.5	0.39	156	37	2488	431	8	2.1	1.00
	Sheffield Dam	(99.8)	29.8	2321	(-)	8.2[3]	6.8	0.37	138	23	1308	71	7	2.3	1.00
	Helsinki Harbor	(52.4)	19.0	782	(-)	5.9[3]	8.0	0.39	48	14	846	105	6	2.0	1.00
	Solfatara Canal Dike	(77.1)	25.6	1224	(-)	4.9[3]	6.9	0.42	64	22	669	59	4.5	1.5	1.00
	Lake Merced Bank	(139.5)	41.4	1316	(-)	5.9[3]	8.0	0.39	136	21	834	102	8.5	2.2	1.00
	El Cobre Tailings Dam	(195.2)	64.8	9760	(-)	6.8	0.9	0.60	141	31	2595	183	3	1.0	1.00
	Metoki Road Embankment	(116.8)	53.7	2655	(-)	2.0	1.5	0.39	92	20	871	85	2.5	0.9	1.00
	Hokkaido Tailings Dam	(250.6)	71.9	3386	(-)	5.1	1.4	0.31	131	45	1203	191	4	1.1	1.00
	Upper San Fernando Dam - D/S Slope								726	138	3238	278	14.5	1.8	1.00
	Tar Island Dyke	(364.2)	115.6	6279	(-)	8.9[5]	9.7	0.32	516	119	4197	484	11	2.3	1.00
	Mochi-Koshi Tailings Dam, Dikes 1 and 2	(158.9)	47.7	1746	(-)	8.9	0.6	0.34	211	38	1532	165	6	1.7	1.00
		(233.6)	78.0	2884	(-)	10.0	1.3	0.67							
	Nerlerk Embankment, Slides 1 ,2 and 3	(178.5)	32.1	1440	(-)	11.4[5]	7.7	0.41	93	19	1171	129	7.5	1.8	1.00
	Asele Road Embankment	(163.7)	54.6	1574	(-)	11.0[5]	10.7		137	27	1037	77	9.5	2.0	1.00
	Nalband Railway Embankment	(139.9)	40.2	1283	(-)	6.3[5]	5.6	0.51	167	15	1209	94	7.5	2.5	1.00
	Sullivan Tailings								277	24	2422	142	9.5	2.4	1.00
	Jamuna Bridge								175	22	1404	210	10.5	2.5	1.00
C	Calaveras Dam	633	223.1	6391	(-)	10.5[5]	9.7	0.55	750		7100		18		0.00

Notes : (1) Where noted in parentheses, $S_{u,r}$ values in are for secondary cases in Wang (2003) and were not fully reanalyzed.
(2) σ'_{vo} not explicitly reported in Wang (2003) or Kramer (2008). Values shown were back calculated from reported Sr and Sr/ σ'_{vo}.
(3) $N_{1,60,CS}$ values were changed in Kramer (2008) from the values reported in Wang (2003). The updated values are shown.

Chapter Five

Development of Relationships for Evaluation of Post-Liquefaction Strength

5.1 Introduction

Chapter 4 presented back-analyses of field liquefaction case histories to develop indices for subsequent use here in the development of empirically-based correlations for engineering assessment of in situ post-liquefaction strengths (S_r) as a function of both (1) penetration resistance and (2) initial effective vertical stress. The indices from the individual case histories were internally cross-checked based on a series of calibrated empirical relationships and guidelines that were dependent upon failure mechanics and runout characteristics, etc. They were also checked against available values from other investigators who employed back-analysis methods that incorporated the effects of momentum and inertia. And they were also cross-checked against additional back-analyses performed by other investigators who employed methods that did not incorporate momentum effects, but for which the apparent resulting biases can now be at least approximately estimated.

The result is an unprecedented data set of reasonably well-constrained values of (1) back-calculated representative post liquefaction strengths (S_r), (2) representative characteristic penetration resistances, and (3) representative initial effective vertical stresses on portions of the failure planes judged to have liquefied. Estimates of variance, or uncertainty, in each of these three indices were also developed for each of the 29 case histories analyzed by these current studies and then subsequently used to develop improved empirical relationships for evaluation of in situ post-liquefaction resistance.

In Chapter 5, this hard-earned data set will now be used to develop improved predictive relationships for assessment of in situ post-liquefaction strength (S_r).

5.2 Non-Probabilistic Regressions

The first step was to perform non-probabilistic (or deterministic) regressions by the least squares method to investigate functional equational forms, and associated shapes of model fitting surfaces, to determine a promising basic equational form for subsequent fully probabilistic regressions to be performed by the Maximum Likelihood Method. These subsequent regressions will incorporate all key sources of uncertainty, and will also permit modeling of heteroskedacity (variance of uncertainty across the domain of interest).

For this first step, the representative median values of $\overline{S_r}$, $\overline{N_{1,60,CS}}$ and $\overline{\sigma'_{vo}}$ for all 29 cases were assembled, as shown in Table 5.1. These mean values are assumed to also represent median values as all three indices are approximated as having normal distributions.

For these deterministic least squares regressions, the median values of Table 5.1 were taken as deterministic "best estimates", with no associated probabilistic likelihood. No weighting factors

were assigned to the different cases, as the purpose of the exercise was only to determine promising potential (or candidate) equational forms for subsequent use in fully probabilistic regressions. This permitted the performance of large numbers of nonlinear least squares regressions, using a large number of candidate equational forms.

Several hundred candidate equational forms were regressed, and the most promising candidate form of equation was judged to be

$$Sr = exp\left(\theta_1 \cdot N1{,}60cs + \theta_2 \cdot \sigma_v'^{\theta_3}\right) \qquad \text{[Eq. 5-1]}$$

The result of the regression with this equational form was found to be the equation

$$Sr = exp\left(0.1296 \cdot N1{,}60cs + 4.372 \cdot \sigma_v'^{0.12}\right) \qquad \text{[Eq. 5-2]}$$

with $R^2 = 0.924$

In this equation:

S_r = Post-liquefaction strength [lbs/ft^2]

$N_{1,60,CS}$ = Overburden and equipment and procedurally corrected SPT penetration resistance with fines adjustment [blows/ft]

σ_v' = Initial vertical effective stress [atmospheres].

Figure 5.1(a) shows the shape of the resulting predictive fitting surface for this relationship, as a multi-colored surface in three-dimensional space with $\overline{S_r}$ plotted on the vertical axis, and $\overline{N_{1,60,CS}}$ and $\overline{\sigma'_{vo}}$ plotted on the two horizontal axes. Residuals for each field case history are plotted, but in the upper figure's oblique view only the residuals above the multi-colored surface can be seen. Figure 5.1(b) shows the residuals for all 29 field case histories, plotted relative to a "flattened" best-fit surface.

The curved surface shown in Figure 5.1(a) simultaneously reflects the influences of both penetration resistance and initial effective vertical stress on post-liquefaction strength (S_r). The calculated R^2 value of $R^2 = 0.924$ indicates an excellent level of "fit" for the data set.

Figure 5.2(a) shows the best-fit Equation 5-2 plotted as $\overline{S_r}$ vs. $\overline{N_{1,60,CS}}$, with the different curves labeled with the initial effective vertical stress $\overline{\sigma'_{vo}}$ (in units of atmospheres). Also plotted in this figure are the values back-calculated for each of the 29 liquefaction failure case histories (from Table 5.1), with case history data points "binned" by ranges of effective vertical stress as indicated in the key in the upper left-hand corner of the figure, and with solid symbols indicating cases of cyclic initiation of liquefaction and open symbols indicating static initiation of liquefaction, and with larger symbols indicating case histories with larger initial effective vertical stresses.

Figure 5.2(b) also shows the best-fit Equation 5-2, but this time plotted in terms of post-liquefaction strength ratio ($\overline{S_r}/\overline{\sigma'_{vo}}$) vs. $\overline{N_{1,60,CS}}$, with the different curves again labeled with the initial effective vertical stress $\overline{\sigma'_{vo}}$ (in units of atmospheres), and the values back-calculated for the 29 liquefaction case histories again binned and labeled as in Figure 5.2(a).

The relationship of Equation 5-2 (and Figures 5.1 and 5.2) provides an R^2 value of $R^2 = 0.924$, indicating a better level of "fit" for this data set and this relationship than has been achieved in previous studies by any regression employing 20 or more field case histories. This does not mean that this is the recommended final relationship, however, as this regression does not yet incorporate the best available information regarding the estimated uncertainties associated with the indices of $\overline{S_r}$, $\overline{N_{1,60,CS}}$ and $\overline{\sigma'_{vo}}$ for each of the 29 liquefaction field case histories. Instead, this is simply the opening step, and it serves mainly to show the promise of the data set and of the equational form selected at this stage.

5.3 Probabilistic Regressions by the Maximum Likelihood Method

Having thus ascertained and established an initially promising functional form for regression, the next step was to incorporate the full available information regarding variance and uncertainties, and to develop fully probabilistically based relationships between post-liquefaction strength and both (1) penetration resistance and (2) effective vertical stress.

The approach here was to employ the Maximum Likelihood Method, which can (1) model all key sources of variance or uncertainty, and (2) model heteroskedastic variation of model error or variance over the problem domain of interest.

Table 5.2 shows the input variables for each of the 29 liquefaction field case histories as evaluated in Chapters 3 and 4, and Appendices A and B. Normal distributions were assumed for mean post-liquefaction strength $\overline{S_r}$, for mean fines-corrected penetration resistance $\overline{N_{1,60,CS}}$, and for mean initial effective vertical stress $\overline{\sigma'_{vo}}$ for portions of the field failure surfaces along which liquefaction was judged to have occurred. Variances in these means were also evaluated, and these also shown in Table 5.2. These variances, expressed as standard deviations of the respective means, were directly incorporated in these probabilistic regressions. It is important to note that the standard deviations listed are not standard deviations of the values of each of the respective indices for each case; instead they are standard deviations of the <u>means</u> of these indices for each individual case.

Because the values listed in Table 5.2 include the engineering team's assessments of all sources of uncertainty or variance, no further (judgmental) weighting factors were applied to each case history to further account for apparent data quality, or level of documentation, etc. The relative "weighting" of the information/data for each case history was thus a natural function of the variances in the three principal indices for each case, with cases that have higher variances or higher standard deviations having a somewhat lesser controlling impact on the regressed relationships developed than cases with lower variances or standard deviations.

A functional form similar to the one already shown to be effective in the deterministic regressions of Section 5.2 was then implemented in a Bayesian regression by the maximum likelihood method. Details are presented in Appendix D.

The resulting best-fit relationship was then determined to be

$$Su,r = exp\left(0.1292 \cdot N1{,}60cs + 4.322 \cdot {\sigma_v'}^{0.12}\right) + \Phi(err) \qquad \text{[Eq. 5-3]}$$

where

$$err = N1{,}60cs^{1.75} + 0.2 * N1{,}60cs \cdot {\sigma_v'}^{2.88} + 33.11 \qquad \text{[Eq. 5-3(a)]}$$

and these can be combined into spreadsheet format as

$$Su,r = exp\left(0.1292 \cdot N1{,}60cs + 4.322 \cdot {\sigma_v'}^{0.12}\right) + \text{NORMINV}(\text{P}, 0, \text{err})$$

Figure 5.3(a) illustrates the resulting median (50th percentile) predictive fitting surface for this relationship, as a multi-colored surface in three-dimensional space with $\overline{S_r}$ plotted on the vertical axis, and $\overline{N_{1,60,CS}}$ and $\overline{\sigma'_{vo}}$ plotted on the two horizontal axes. Residuals for each field case history are plotted, but in his upper figure's oblique view only the residuals above the multi-colored surface can be seen. Figure 5.3(b) shows the median residuals for all 29 field case histories, plotted relative to a "flattened" best-fit surface.

The variance of Equation 5-3(b) is heteroskedastic, meaning that the variance in estimated values of S_r varies over the domain of interest as a function of both $\overline{N_{1,60,CS}}$ and $\overline{\sigma'_{vo}}$. This variance increases with increases in both $\overline{N_{1,60,CS}}$ and $\overline{\sigma'_{vo}}$ as (1) outcomes vary, and (2) data become sparse in these ranges.

Figure 5.4(a) shows the median (50th percentile) predictive relationship of Equation 5-3, this time plotted as curves of post-liquefaction strength S_r vs. $\overline{\sigma'_{vo}}$, with the different curves again labeled with the initial effective vertical stress $\overline{\sigma'_{vo}}$ (in units of atmospheres), and the values back-calculated for the 29 liquefaction case histories again binned and labeled as in Figure 5.2(a).

Figure 5.4(b) shows the median (50th percentile) predictive relationship of Equation 5-3, this time plotted as curves of post-liquefaction strength ratio $S_r/\sigma_{v.i}'$ vs. $\overline{\sigma'_{vo}}$, with the different curves again labeled with the initial effective vertical stress $\overline{\sigma'_{vo}}$ (in units of atmospheres), and the values back-calculated for the 29 liquefaction case histories again binned and labeled as in Figure 5.2(a).

One of the differences between the relationships developed or proposed by Olsen and Stark (2002) and Wang and Kramer (2003, 2008) vs. those of Seed and Harder (1990) and these current studies, was the inclusion of the "non-failure" liquefaction case history for the Upper San Fernando Dam in the 1990 studies and in the current studies. It was the advice of the informal expert advisory panel that this was a suitable case to include, but the sensitivity of the resulting relationship to this decision warrants examination. Figure 5.5 shows a comparison between the median (50th percentile) values of S_r from the probabilistic regression of Figure 5.4(a) (and Equation 5-3) as shown with the black lines vs. the 50th percentile probabilistic regressions results (also by the maximum likelihood method) performed with the Upper San Fernando Dam case history deleted, as shown by the red lines. As shown in this figure, deletion of this case did not make a very significant difference. This was due in large part to the high level of uncertainty, or variance (standard deviation), assigned to the Upper San Fernando Dam case history, so that it did not exert strong control over local regressed shapes in its neighborhood. It is the judgment of this engineering team that the data and information from the Upper San Fernando Dam case history is both valid and useful, and that the probabilistically regressed relationship with this case included (as expressed in Equation 5-3) is to be preferred.

The relationship of Equation 5-3 is fully probabilistic, and values for any percentile of non-exceedance can be generated. It is the recommendation of this engineering team that 35th percentile values (35% of values would be expected to be lower) represent a suitable level of conservatism for typical design applications. This represents a nearly mean-minus-one-half-sigma level, and there is strong tradition of this level of enveloping (or similar) in geotechnical practice. For larger projects, or projects of special importance, a fully probabilistic (or risk-based) analysis can be performed using the full range of values of S_r and their associated probabilities as can be developed using the full form of Equation 5-3.

The recommended simplified "deterministic" values of S_r for routine design are then the 35th percentile values, and these can be calculated by a simplified version of Equation 5-3 as

$$Su,r = exp\left(0.1292 \cdot N1{,}60cs + 4.322 \cdot {\sigma_v'}^{0.12}\right) - 0.38532\left(N1{,}60cs^{1.75} + 0.2 * N1{,}60cs \cdot {\sigma_v'}^{2.88} + 33.11\right) \qquad \text{[Eq. 5-4]}$$

Figure 5.6 repeats Figure 5.4(a), showing the median (50th percentile) predictive relationship of Equation 5-3 plotted as curves of post-liquefaction strength S_r vs. $\overline{\sigma'_{vo}}$, with the different curves again labeled with the initial effective vertical stress $\overline{\sigma'_{vo}}$ (in units of atmospheres), and the values back-calculated for the 29 liquefaction case histories again binned and labeled as in Figure 5.2(a). The red lines added to Figure 5.6 then show the 35th percentile values calculated by Equation 5-4. This serves to illustrate the differences between the 50th percentile and the 35th percentile values of S_r, and it also shows the relative juxtaposition of the recommended "simplified, deterministic" (35th percentile) values relative to the best-estimate values of the 29 back-analyzed individual field case histories.

Figures 5.7 and 5.8 then present the recommended deterministic (also the 35th percentile probabilistic) relationship of Equation 5-4 in two formats (S_r and $S_r/\sigma_{v.i}'$) as functions of penetration resistance and initial effective vertical stress.

5.4 Comparisons with Selected Previous Relationships for Evaluation of Post-Liquefaction Strength (S_r)

5.4.1 Wang (2003) and Kramer (2008)

Kramer (2008) extended the work of Wang (2003), modifying some of the values developed by Wang's back-analyses, and he then performed regressions to develop both probabilistic and recommended simplified deterministic predictive relationships for in situ post-liquefaction strength (S_r). As discussed previously in Section 2.3.7, Kramer and Wang made very different choices with regard to selection of approaches at nearly every step of the way than those choices made by this current investigation team. They also made a number of very different judgments in implementing their selected approaches.

Their table of values employed in the probabilistic regressions of Kramer (2008), as shown previously in Tables 4.3 and 4.5, differs significantly from the values employed in these current studies for a number of the case histories. Differences are especially pronounced for a number of the less well-defined case histories of Class B.

Wang and Kramer employed the Calaveras Dam failure case history, as they were not yet aware of the new investigations (Chen et al, 2002) that showed the hydraulic fill materials to be more variably clayey and cohesive than had previously been suspected. The current engineering team judged that it would not be possible to cross-correlate modern SPT and BPT performed many decades after the slope failure of 1918, given nearly a century of ongoing consolidation and ageing effects in these complicated and challenging soils. So the current studies did not employ the Calaveras Dam case history in our regressions.

The current studies include the back-analyzed non-failure case of the Upper San Fernando Dam, and the regressions of Kramer (2008) do not. This does not have a very significant influence on the relationships developed in these current studies, however, as shown in Figure 5.5.

Very different approaches were taken with regard to evaluation of uncertainties in all parameters, and in the incorporation of these uncertainties in the probabilistic regressions performed by the two investigation teams. Kramer and Wang preferred to assign judgmental weighting factors to the different case histories to account for uncertainties associated with lack of data, or with poor documentation of data. In these current studies, estimated variances in all back-analyzed parameters included these sources of uncertainty, so no additional weighting factors were then applied.

These were all arguably valid approaches, and reasonable judgments given the state of knowledge and information available, and so it is interesting now to cross-compare the overall results of these two studies.

Kramer (2008) selects the 40^{th} percentile values of post-liquefaction strength (Sr) as the recommended "deterministic" values for routine projects. Figure 5.9 presents these 40^{th} percentile values, based on the probabilistically regressed predictive relationship that he developed based on the first-order second moment (FOSM) method.

In these current studies, the 35th percentile values are recommended for routine design, and Figure 5.10 compares Kramer's recommended 40th percentile values (red lines) vs. the 35th percentile values (black lines) recommended in these current studies. The level of approximate agreement between these two sets of recommended values can only be described as surprisingly good. Especially given the very different steps, procedures, assumptions, and judgments that went into the development of each set of values shown.

There are some moderate differences at very low penetration resistances, and it might be noted that the current studies did not need to impose a judgmental constraint on values of S_r at very low confining stresses, as with Kramer (2008). It can also be noted that the two sets of curves would extrapolate a bit differently at higher $N_{1,60,CS}$ values ($N_{1,60,CS}$ > 18 blows/ft).

Overall, however, these two sets of results would appear to represent what passes for "consensus" for these types of challenging geotechnical issues.

5.4.2 Olsen and Stark (2002)

Figure 5.11 shows the recommended relationship between S_r/P and $N_{1,60}$ proposed by Olsen and Stark (2002). Figure 5.12 then shows this relationship super-imposed (red lines) on the 35th percentile relationship developed in these current studies. The relationship of Olsen and Stark modeled the post-liquefaction strength (S_r/P) as being independent of initial effective overburden stress, and so it was to be expected that their recommended relationship would be conservative for very low initial effective overburden stresses, and unconservative for very high initial effective overburden stresses. In addition, because 23 of their 33 liquefaction case histories were back-analyzed in a manner that produced values of $S_{r,resid/geom}$, instead of values of S_r that incorporated momentum effects, 23 of their case histories significantly underestimated S_r. The other 10 cases were back-analyzed by their kinetics method, which did specifically incorporate momentum effects, and this appears to have produced generally good bac-calculated values of S_r for these cases. Overall, however, it would be expected that their relationship would be significantly conservatively biased by the 23 cases for which S_r was systematically underestimated.

This is what Figure 5.12 shows. Their recommended range of S_r/P values appear to be generally suitable at initial effective vertical stresses of approximately 1 to 4 atmospheres, and for $N_{1,60}$ values of less than about 12 blows per foot. At higher values of penetration resistance, their relationship would provide increasingly over-conservative values. And this over-conservatism would also be greater at lower effective overburden stresses.

5.4.3 Idriss and Boulanger (2008)

Figure 5.13 shows the recommended relationship of Idriss and Boulanger (2008) for evaluation of post-liquefaction strength ratio (S_r/P) as a function of penetration resistance. Figure 5.14 shows this relationship of Idriss and Boulanger (red lines) superimposed on the 35th percentile relationship developed in these current studies. It is the lower of the two diverging lines in Figure 5.13 and 5.14 that represents Idriss and Boulanger's recommended relationship for field situations

(in which void redistribution effects can occur). As shown in this figure, the relationship of Idriss and Boulanger (2008) appears to be suitable for initial effective vertical stresses of approximately 1 to 2 atmospheres for $N_{1,60,CS}$ values of less than about 12 blows per foot, but then falls away and becomes increasingly conservative at higher $N_{1,60,CS}$ values.

Figure 5.15 shows the recommended relationship of Idriss and Boulanger (2008) for Sr as a function of penetration resistance. Figure 5.16 shows this relationship of Idriss and Boulanger (red lines) superimposed on the 35th percentile relationship developed in these current studies. Here, too, the relationship appears to be suitable for initial effective overburden stresses of approximately 1 to 2 atmospheres, and the upward curvature out to blowcounts as high as 18 blows per foot appear to continue to be appropriate for this overburden stress range. Their relationship would generally be unconservative for effective overburden stresses significantly greater that 2 atmospheres, and it would be over-conservative for effective overburden stresses significantly lower than 1 atmosphere.

5.4.4 Seed and Harder (1990)

Figure 5.17 shows the relationship recommended by Seed and Harder (1990). Figure 5.18 shows this relationship (red lines) superimposed on the 35th percentile relationship developed in these current studies. The relationship proposed by Seed and Harder (1990) appears to provide reasonable values of S_r for effective overburden stresses of approximately 0.5 to 4 atmospheres, and for $N_{1,60,CS}$ values up to 17 blows per foot and greater. It would be over-conservative for higher initial effective vertical stresses.

Table 5.1: Values of (1) representative post-liquefaction strength, (2) representative penetration resistance, and (3) initial effective vertical effective stress for each of the 29 back-analyzed liquefaction case histories as employed in the deterministic least squares regressions.

Group	Case	This Study		
		$\bar{S}_r$ (psf)	$\bar{\sigma}'_{vo}$ (psf)	$\bar{N}_{1,60,CS}$
A	Wachusett Dam - North Dike	294	3142	7.5
	Fort Peck Dam	762	7258	12.5
	Uetsu Railway Embankment	38	1448	3
	Lower San Fernando Dam - U/S Slope	514	4287	13.5
	Hachiro-Gata Road Embankment	68	673	7
	La Marquesa Dam - U/S Slope	103	981	6.5
	La Marquesa Dam - D/S Slope	214	1215	10.5
	La Palma Dam	136	767	5
	Lake Ackerman Highway Embankment	107	909	3.5
	Chonan Middle School	141	1032	6.5
	Soviet Tajik - May 1 Slide	341	1907	10.5
	Shibecha-Cho Embankement	224	1416	7.5
	Route 272 at Higashiarekinai	138	1285	8
B	Zeeland - Vlietepolder	156	2488	8
	Sheffield Dam	138	1308	7
	Helsinki Harbor	48	846	6
	Solfatara Canal Dike	64	669	4.5
	Lake Merced Bank	136	834	8.5
	El Cobre Tailings Dam	141	2595	3
	Metoki Road Embankment	92	871	2.5
	Hokkaido Tailings Dam	131	1203	4
	Upper San Fernando Dam - D/S Slope	726	3238	14.5
	Tar Island Dyke	516	4197	11
	Mochi-Koshi Tailings Dam, Dikes 1 and 2	211	1532	6
	Nerlerk Embankment, Slides 1 ,2 and 3	93	1171	7.5
	Asele Road Embankment	137	1037	9.5
	Nalband Railway Embankment	167	1209	7.5
	Sullivan Tailings	277	2422	9.5
	Jamuna Bridge	175	1404	10.5

Table 5.2: Values of (1) median post-liquefaction strength, (2) median penetration resistance, and (3) median effective vertical effective stress for each of the 29 back-analyzed liquefaction case histories, and standard deviations for each of these, as employed in the fully probabilistic maximum likelihood regressions.

Group	Case	This Study					
		$\bar{S}_r$ (psf)	$\sigma_{\bar{S}}$	$\bar{\sigma}'_{vo}$ (psf)	$\sigma_{\bar{\sigma}}$	$\bar{N}_{1,60,CS}$	$\sigma_{\bar{N}}$
A	Wachusett Dam - North Dike	294	31	3142	132	7.5	1.6
	Fort Peck Dam	762	118	7258	687	12.5	2.7
	Uetsu Railway Embankment	38	8	1448	116	3	0.8
	Lower San Fernando Dam - U/S Slope	514	47	4287	281	13.5	1.8
	Hachiro-Gata Road Embankment	68	12	673	41	7	1.2
	La Marquesa Dam - U/S Slope	103	33	981	134	6.5	1.8
	La Marquesa Dam - D/S Slope	214	57	1215	103	10.5	2.2
	La Palma Dam	136	23	767	42	5	1.2
	Lake Ackerman Highway Embankment	107	19	909	61	3.5	0.7
	Chonan Middle School	141	35	1032	82	6.5	2.1
	Soviet Tajik - May 1 Slide	341	57	1907	177	10.5	2.7
	Shibecha-Cho Embankement	224	37	1416	95	7.5	1.7
	Route 272 at Higashiarekinai	138	17	1285	104	8	1.6
B	Zeeland - Vlietepolder	156	37	2488	431	8	2.1
	Sheffield Dam	138	23	1308	71	7	2.3
	Helsinki Harbor	48	14	846	105	6	2.0
	Solfatara Canal Dike	64	22	669	59	4.5	1.5
	Lake Merced Bank	136	21	834	102	8.5	2.2
	El Cobre Tailings Dam	141	31	2595	183	3	1.0
	Metoki Road Embankment	92	20	871	85	2.5	0.9
	Hokkaido Tailings Dam	131	45	1203	191	4	1.1
	Upper San Fernando Dam - D/S Slope	726	138	3238	278	14.5	1.8
	Tar Island Dyke	516	119	4197	484	11	2.3
	Mochi-Koshi Tailings Dam, Dikes 1 and 2	211	38	1532	165	6	1.7
	Nerlerk Embankment, Slides 1 ,2 and 3	93	19	1171	129	7.5	1.8
	Asele Road Embankment	137	27	1037	77	9.5	2.0
	Nalband Railway Embankment	167	15	1209	94	7.5	2.5
	Sullivan Tailings	277	24	2422	142	9.5	2.4
	Jamuna Bridge	175	22	1404	210	10.5	2.5

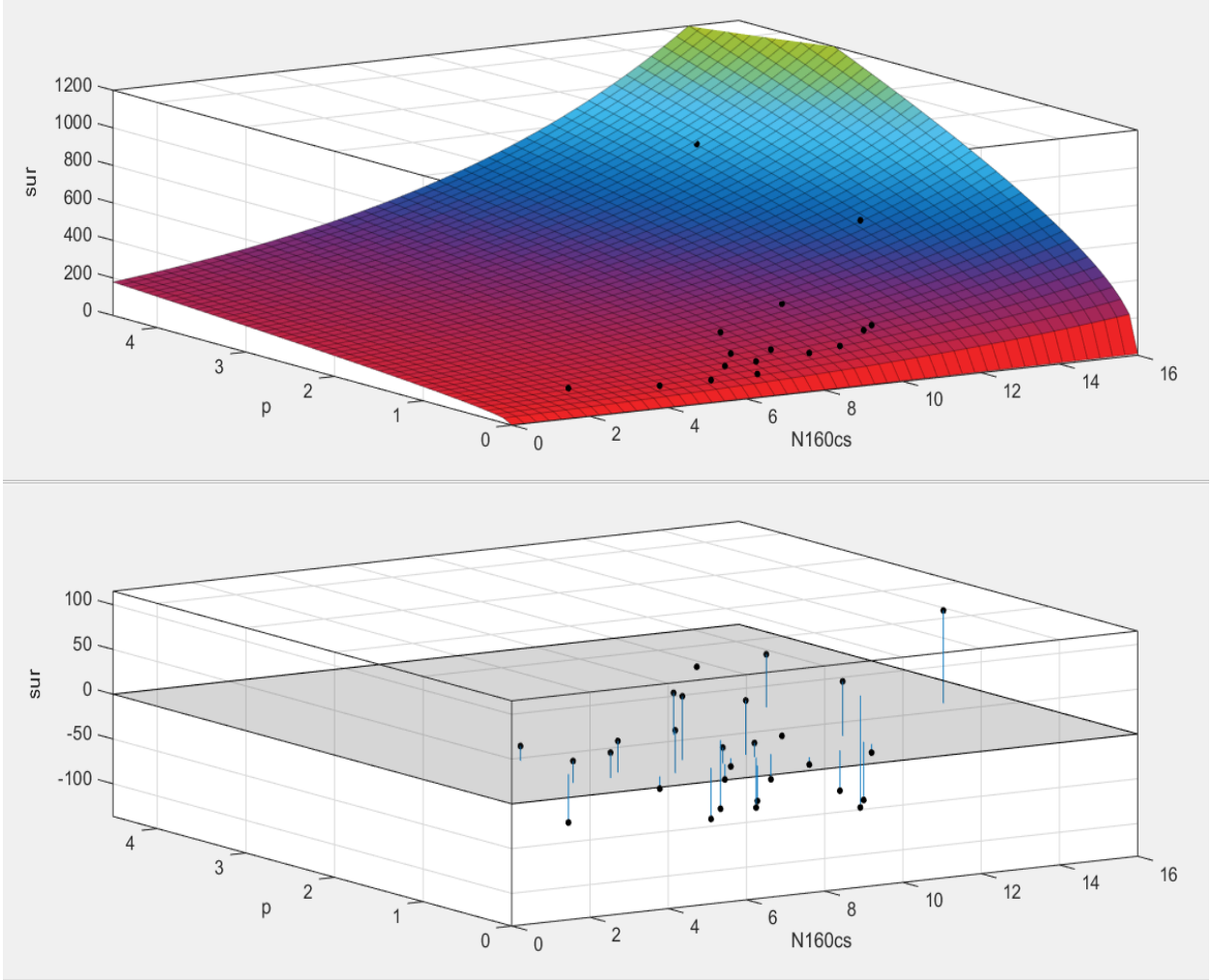

Figure 5.1: Results of deterministic least squares regression showing (a) the relationship for post-liquefaction strength ($\overline{S_r}$) as a function of both $\overline{N_{1,60,CS}}$ and $\overline{\sigma'_{vo}}$, and (b) residuals from the deterministic least squares regression in terms of predicted vs. observed $\overline{S_r}$ for each of the 29 liquefaction field case histories. [Note: Residuals in the lower figure are vertically exaggerated by a factor of 5 for clarity.]

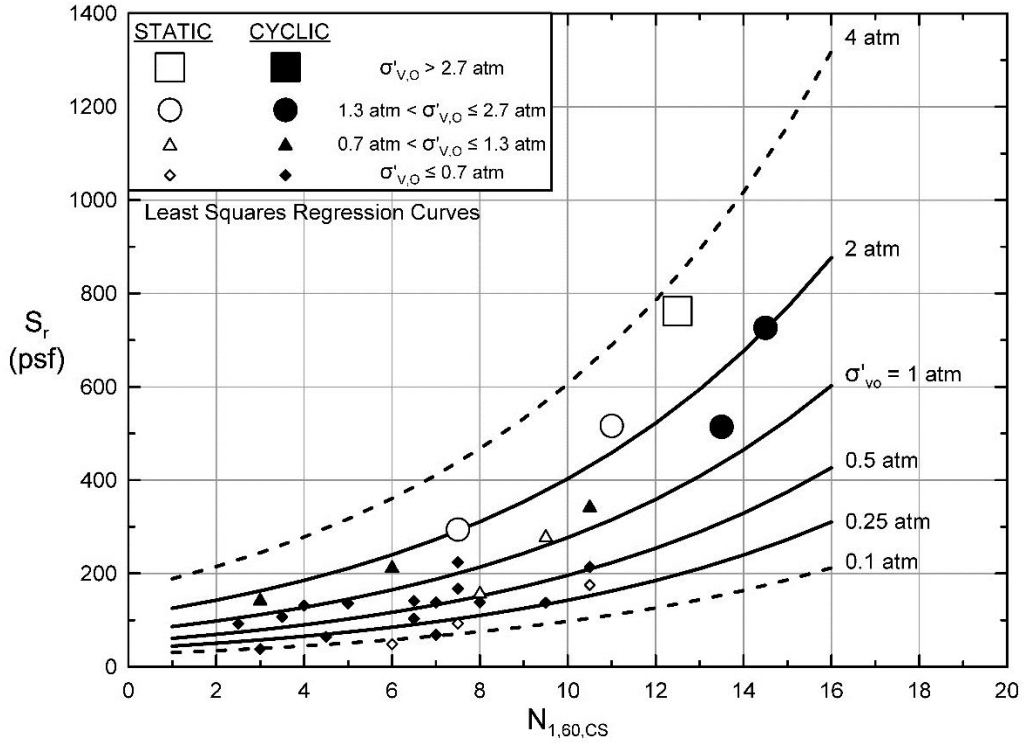

Figure 5.2(a): Results of deterministic regression showing post-liquefaction strength (S_r) as a function of both penetration resistance and initial effective vertical stress.

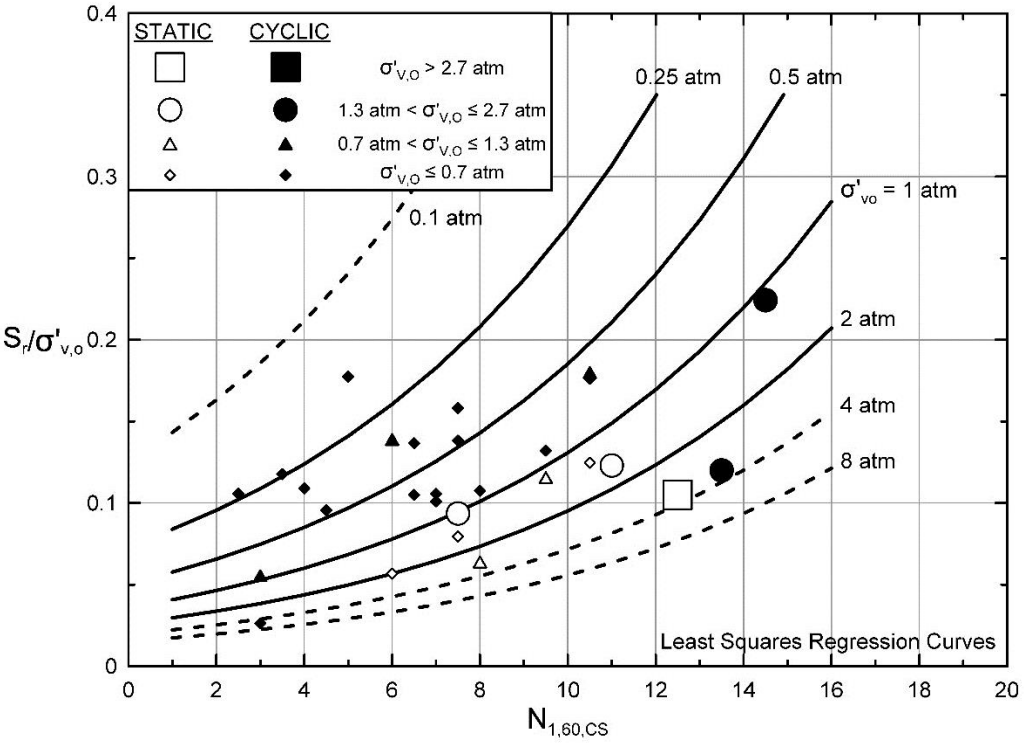

Figure 5.2(b): Results of deterministic regression showing post-liquefaction strength ratio (S_r/P) as a function of both penetration resistance and initial effective vertical stress.

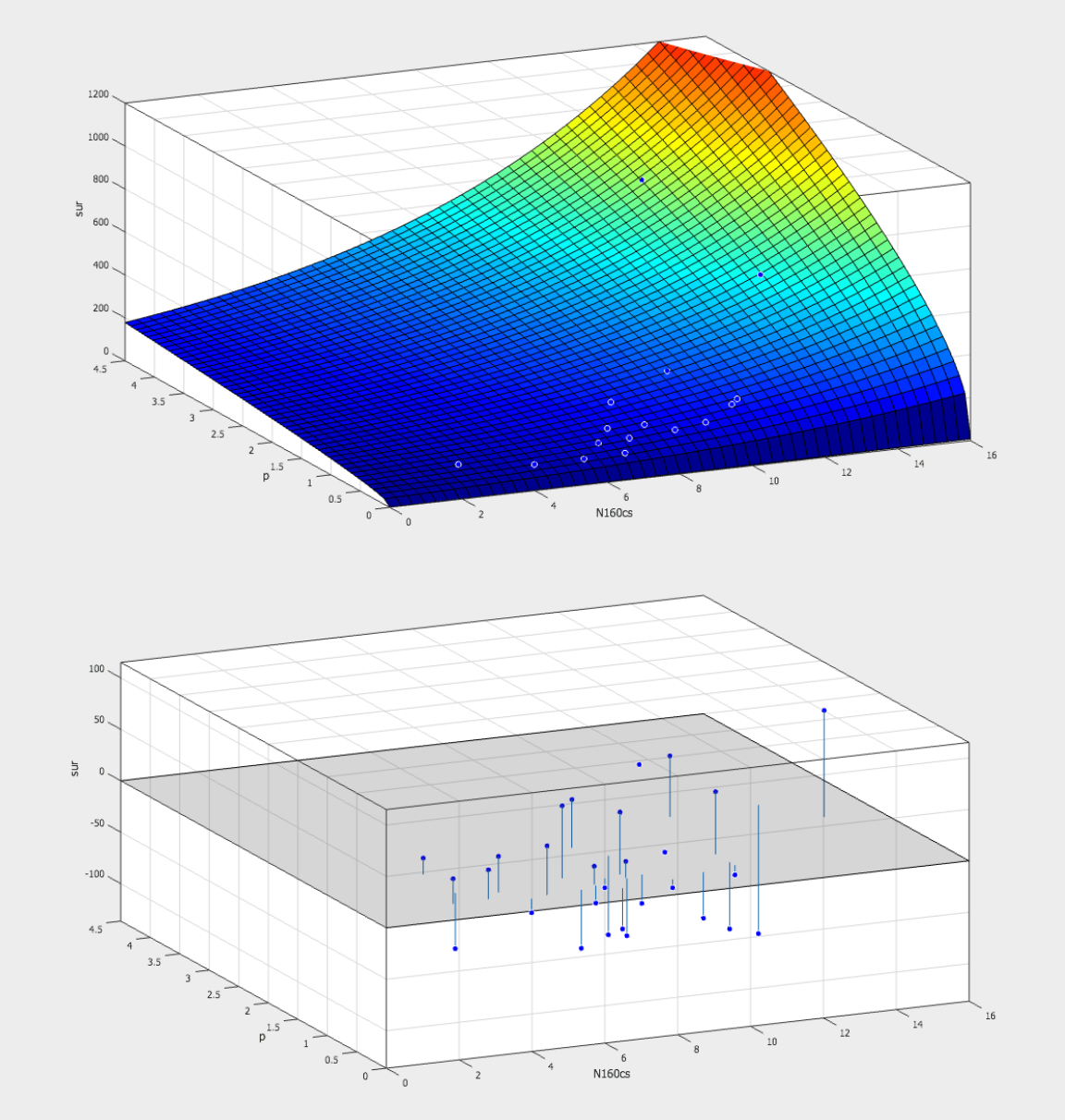

Figure 5.3: Results of probabilistic maximum likelihood regression showing (a) the relationship for post-liquefaction strength ($\overline{S_r}$) as a function of both $\overline{N_{1,60,CS}}$ and $\overline{\sigma'_{vo}}$, and (b) residuals from the deterministic least squares regression in terms of predicted vs. observed $\overline{S_r}$ for each of the 29 liquefaction field case histories. [Note: Residuals in the lower figure are vertically exaggerated by a factor of 5 for clarity.]

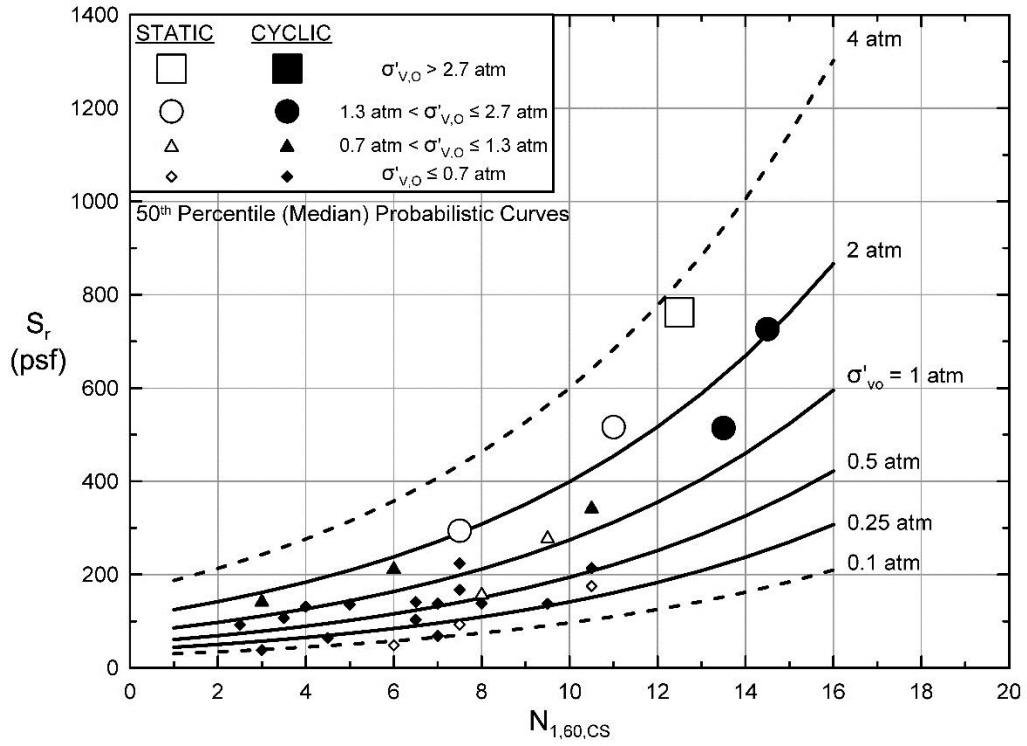

Figure 5.4(a): Results of probabilistic regression showing median values of S_r as a function of both penetration resistance and initial effective vertical stress.

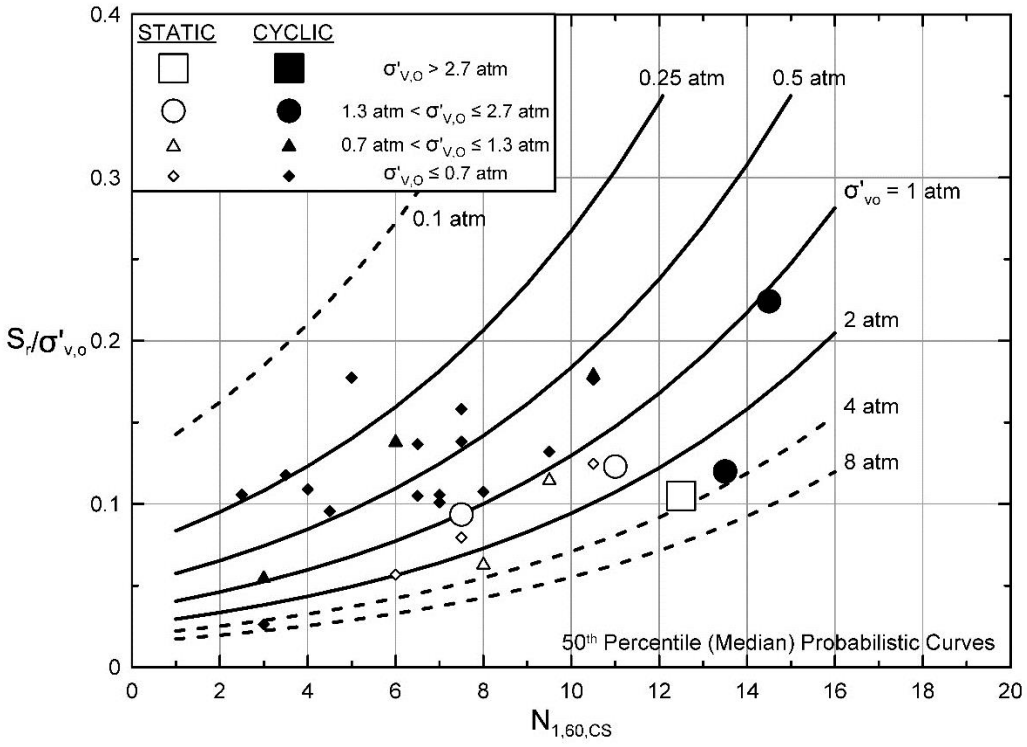

Figure 5.4(b): Results of probabilistic regression showing median values of S_r/P as a function of both penetration resistance and initial effective vertical stress.

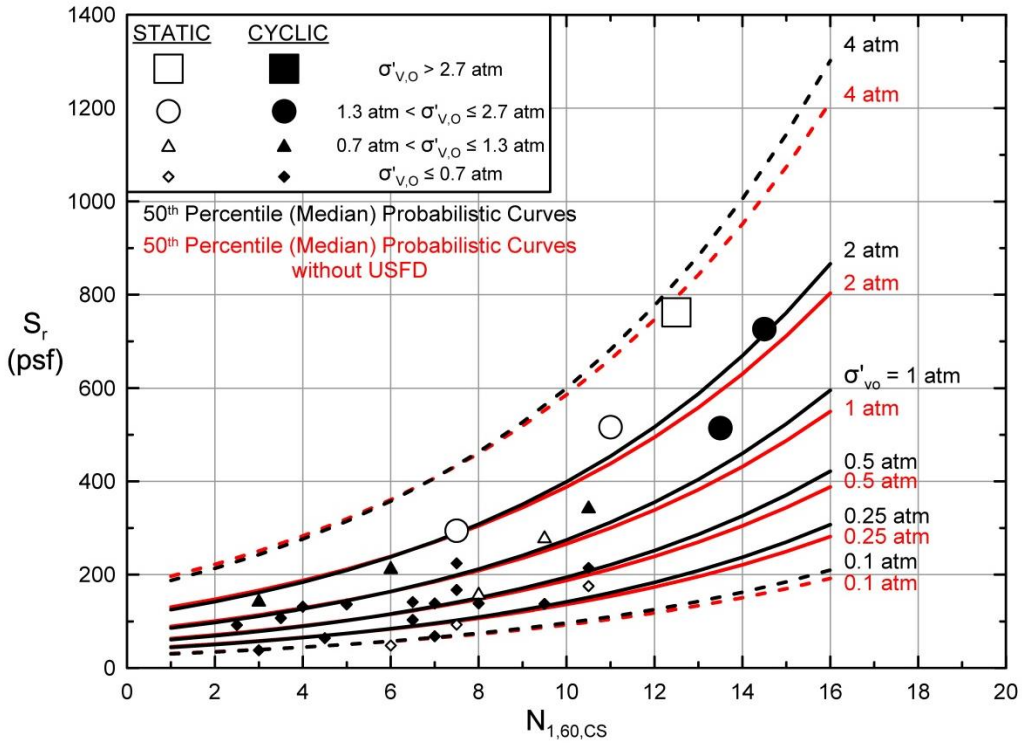

Figure 5.5: Figure 5.4(a) repeated (black lines) showing the results of probabilistic regression performed with the data point from the Upper San Fernando Dam case history deleted (red dashed lines).

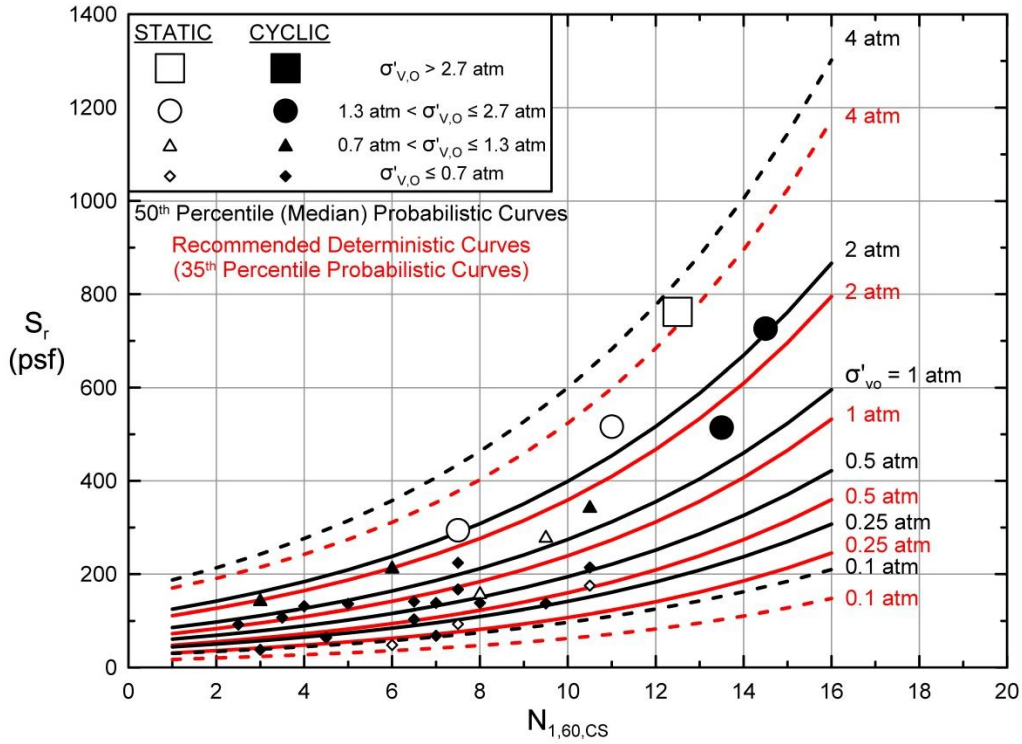

Figure 5.6: Comparison between 35th percentile values of S_r (red lines) and 50th percentile values of S_r (black lines) from the probabilistic relationship of Equation 5-3.

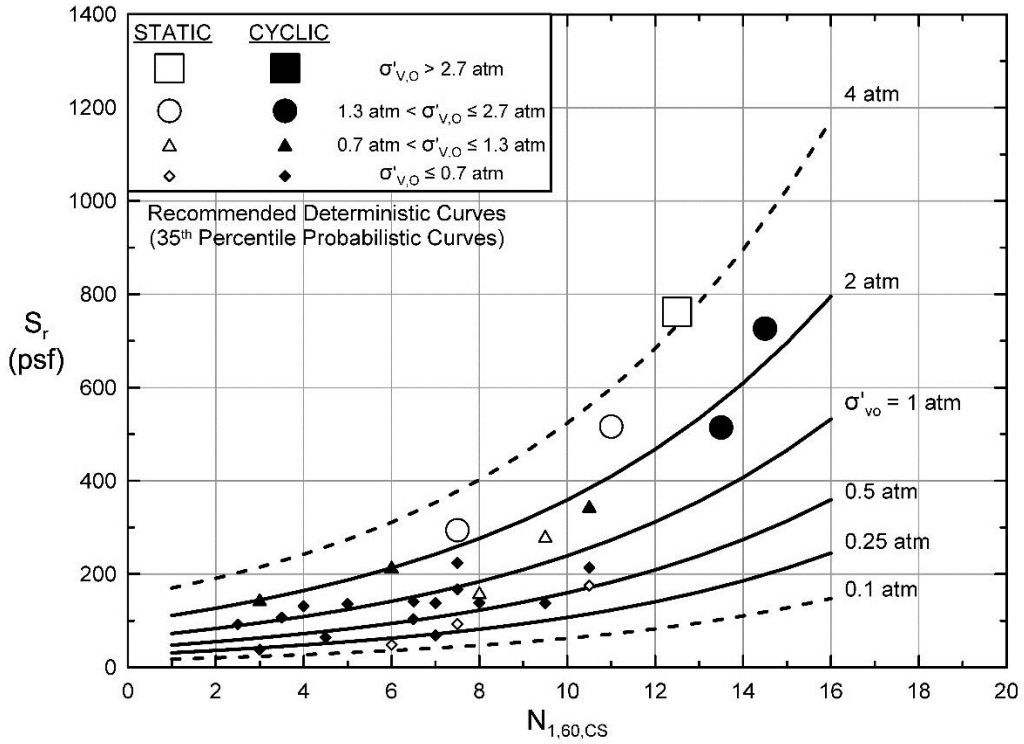

Figure 5.7: Recommended deterministic relationship; 35th percentile values of S_r from the probabilistic relationship of Figures 5.3 and 5.4.

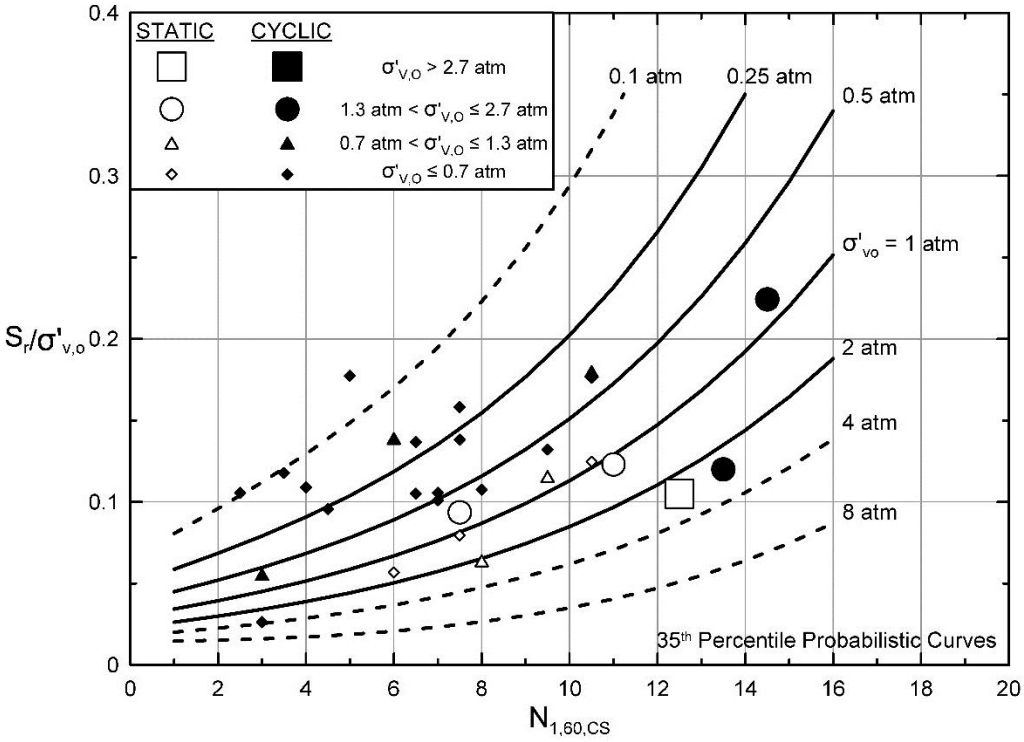

Figure 5.8: Recommended deterministic relationship; 35th percentile values of S_r/P from the probabilistic relationship of Figures 5.3 and 5.4.

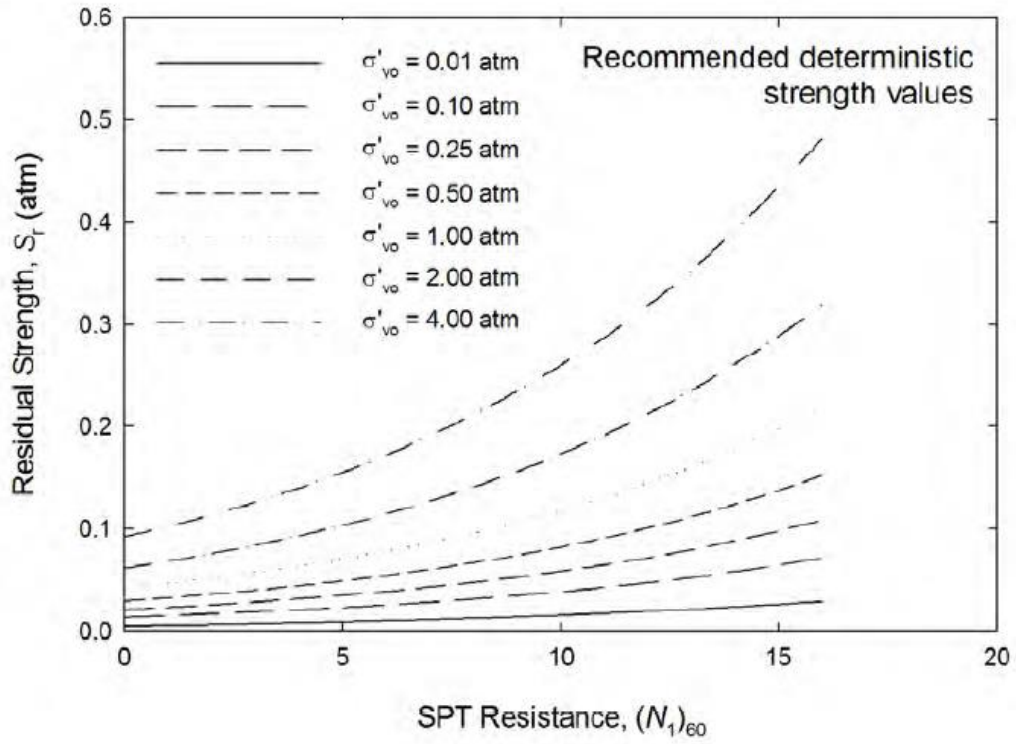

Figure 5.9: Recommended deterministic relationship of Kramer (2008) showing 40th percentile values of S_r as a function of (a) $N_{1,60,CS}$ and (b) effective vertical stress.

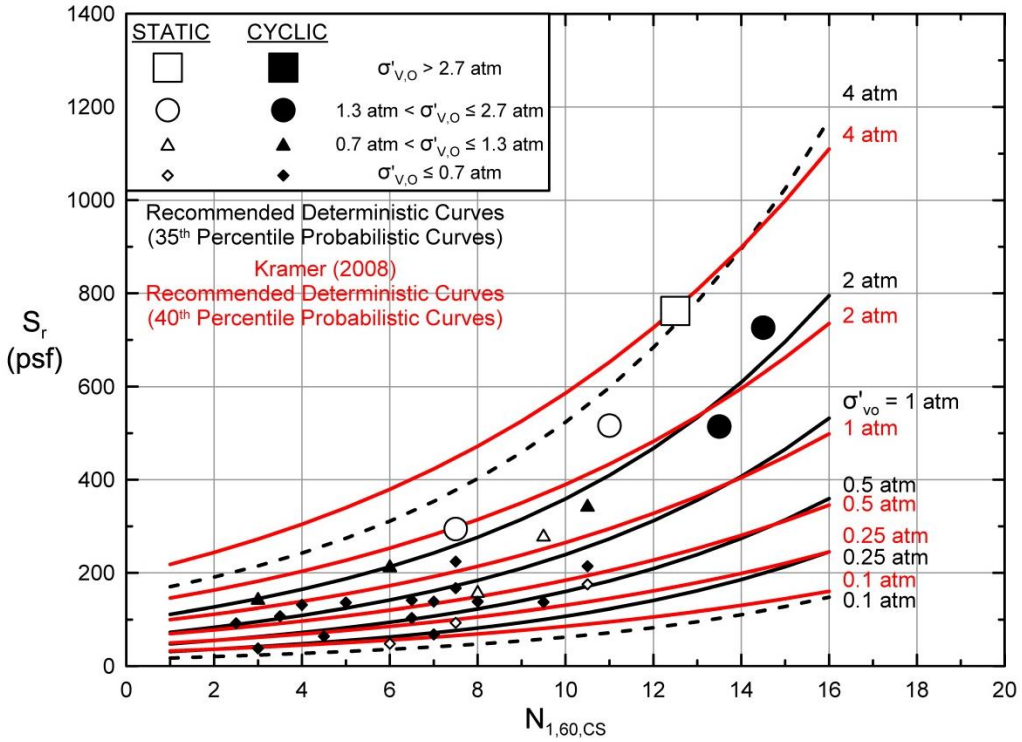

Figure 5.10: Comparison between (recommended deterministic) 40th percentile values of S_r from Kramer (2008) and 35th percentile values from these current studies.

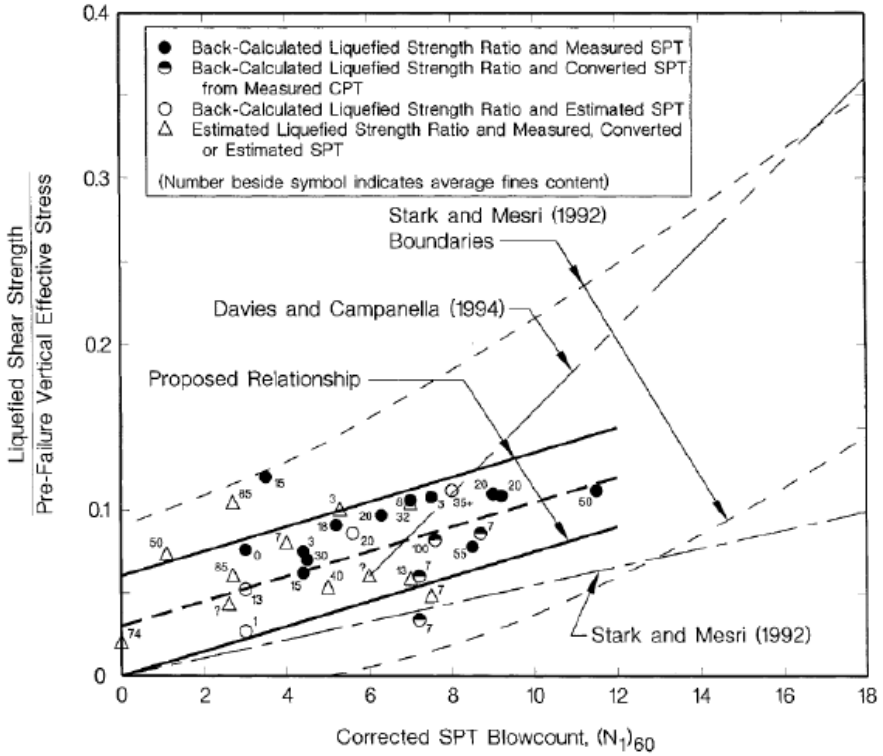

Figure 5.11: Recommended relationship between post-liquefaction strength ratio (S_r/P) and penetration resistance of Olsen and Stark (2002).

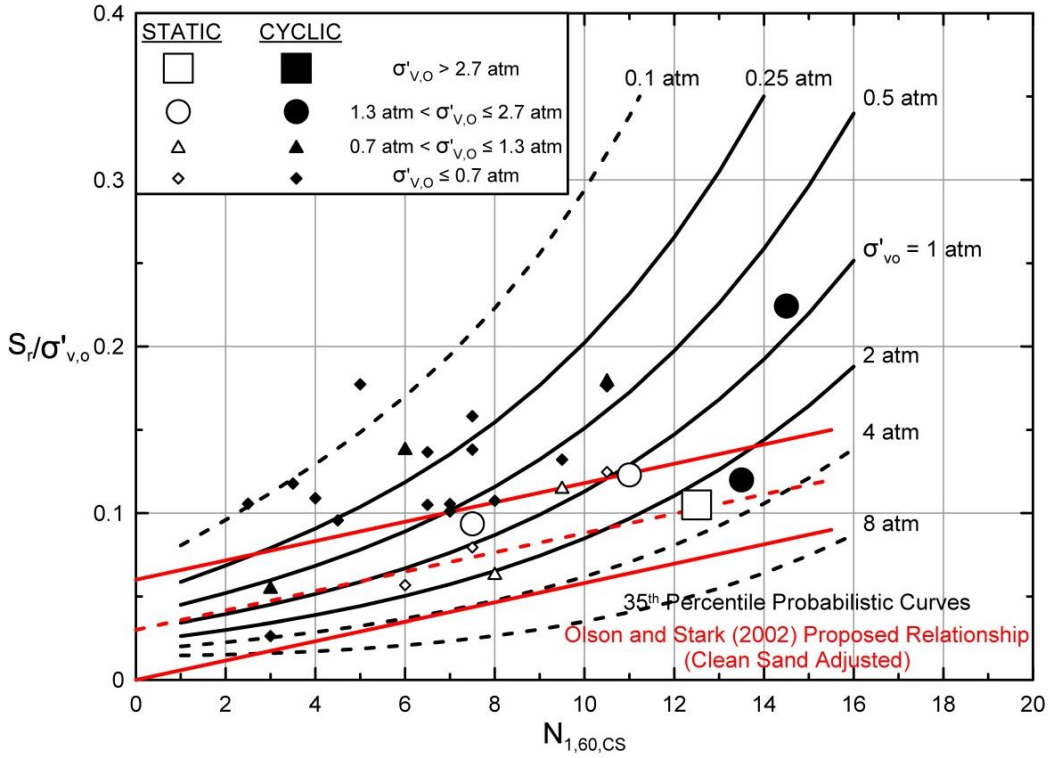

Figure 5.12: Comparison between the relationship of Olsen and Stark (2002), and the recommended deterministic (35th percentile) values of S_r based on these current studies.

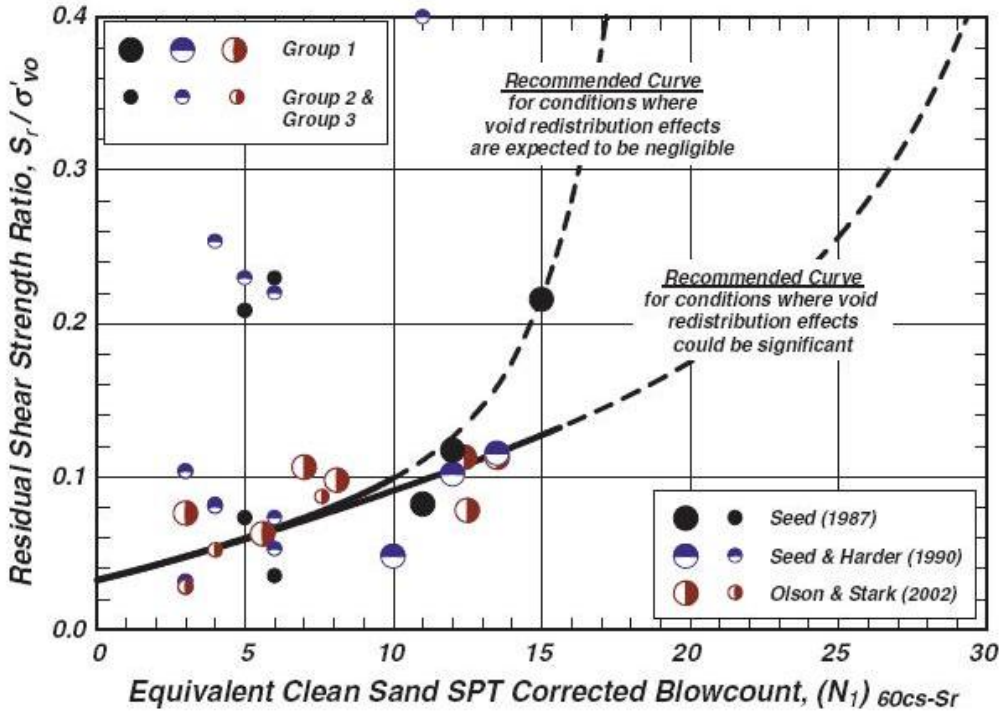

Figure 5.13: Recommended relationships between S_r/P and penetration resistance by Idriss and Boulanger (2008)

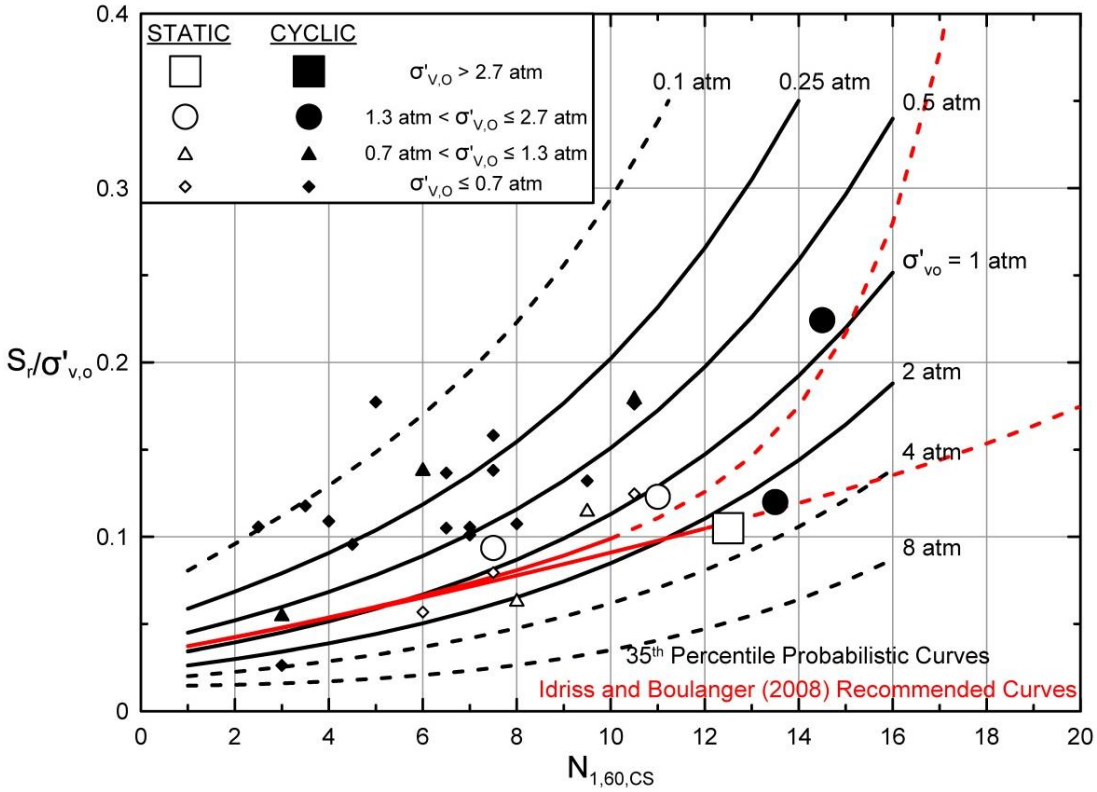

Figure 5.14: Comparison between the recommended relationships of Idriss and Boulanger (2008) from Figure 5.13 (red lines) with the recommended 35th percentile relationship recommended in these current studies (black lines).

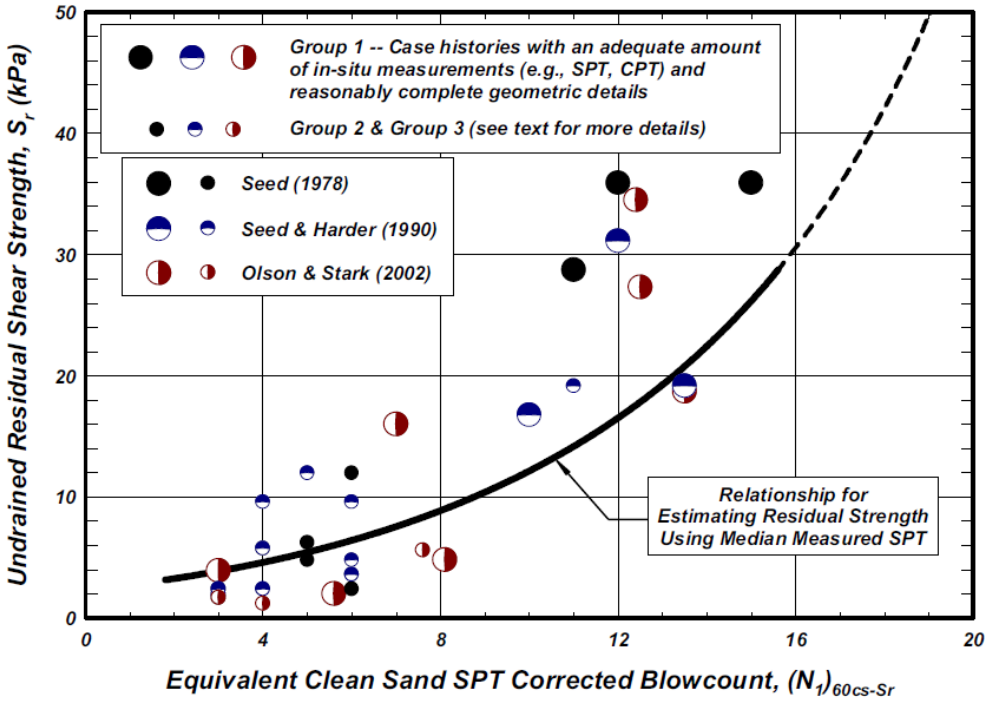

Figure 5.15: Recommended relationships between S_r and penetration resistance by Idriss and Boulanger (2008)

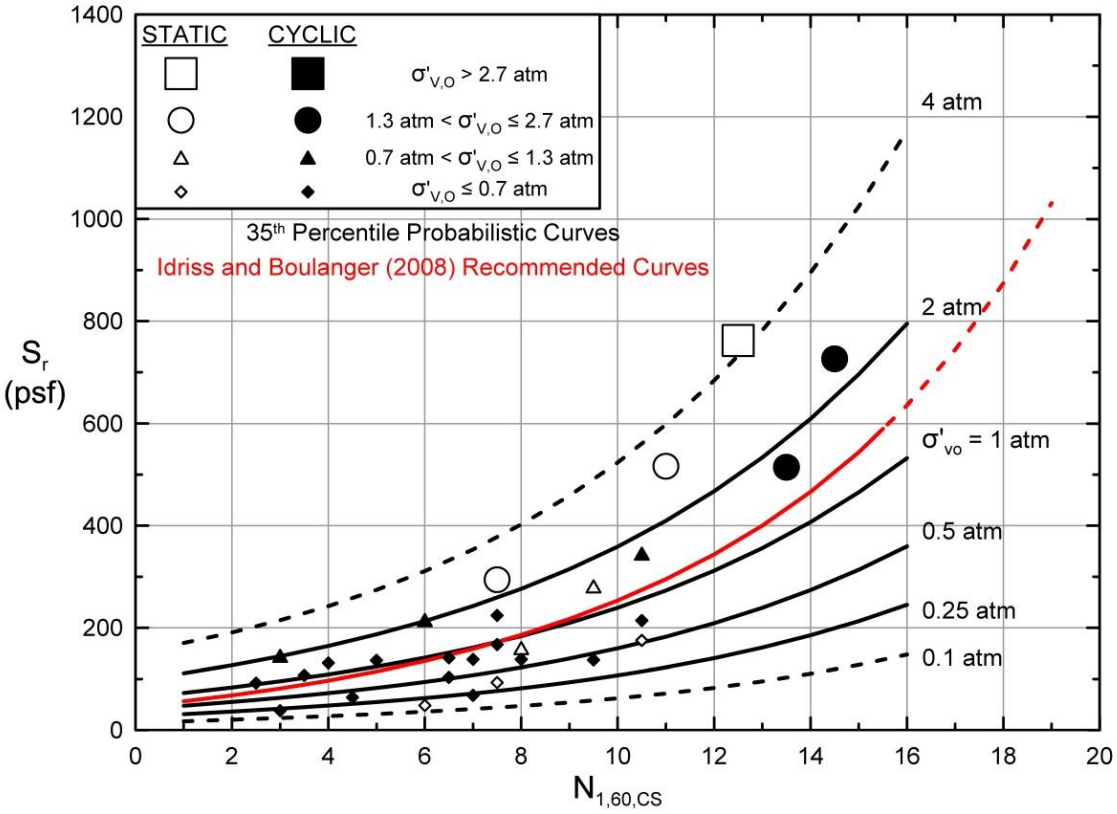

Figure 5.16: Comparison between the recommended relationship of Idriss and Boulanger (2008) from Figure 5.15 (red lines) with the recommended 35th percentile relationship recommended in these current studies (black lines).

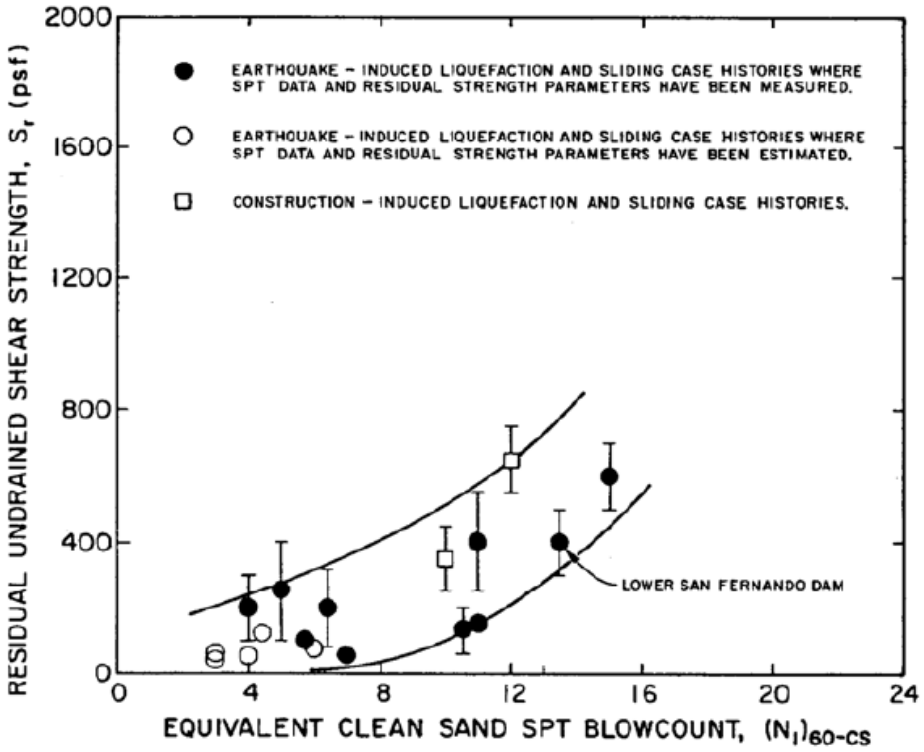

Figure 5.17: Recommended relationship between Sr and penetration resistance of Seed and Harder (1990).

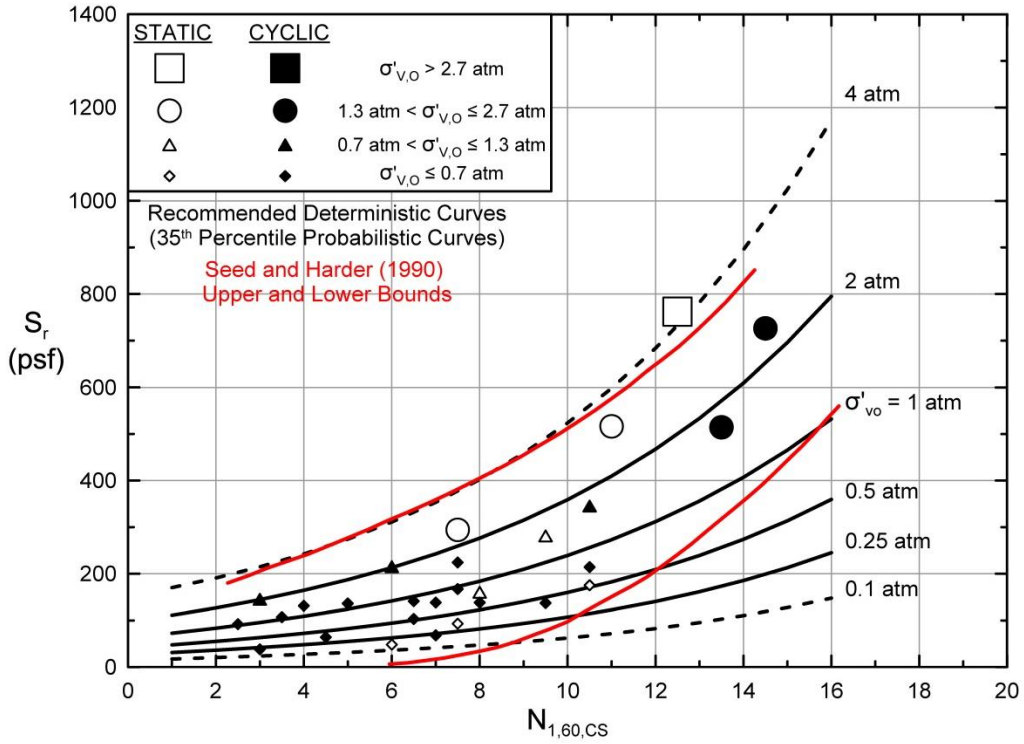

Figure 5.18: Comparison between the recommended relationship of Seed and Harder (1990) from Figure 5.17 (red lines) with the recommended 35th percentile relationship recommended in these current studies (black lines).

Chapter Six

Summary and Conclusions

6.1 Summary and Findings

The issue of evaluation of in situ post-liquefaction strengths has grown rapidly in importance over the past three decades, as engineers have increasingly been called upon to provide more refined evaluations of projected seismic performance both for risk evaluation studies and for project design.

The topic of assessment of post-liquefaction strengths has been fraught with debate, and a number of different recommendations have been developed by different teams of experts and researchers.

These current studies began with a technical review of previous efforts. That proved to be a valuable exercise. Evaluation of previous work, and recommendations, with emphasis on strengths and drawbacks of prior efforts, led to some important insights. It turns out that a number of previous efforts had developed important lessons, and in some cases important pieces of the overall puzzle. They also served to provide ideas and to inspire elements of these current studies. And they provided lessons with regard to mistakes to avoid.

These current studies focused on the development of empirical methods for evaluation of in situ post-liquefaction strengths, largely because of issues and challenges involved in application of laboratory-based testing approaches to evaluation of post-liquefaction strengths for full-scale field conditions.

A suite of full-scale liquefaction failure case histories were reviewed, vetted and selected for back-analyses. New methods were developed for performing these back-analyses, including methods that more accurately and reliably deal with momentum effects in liquefaction failures that experience large displacements. A suite of additional empirical relationships were developed specifically for cross-comparison of the results of back-analyses of large deformation liquefaction failures. In the end, a suite of back-analysis results of unprecedented reliability were developed, based on (1) improved back-analysis procedures, (2) internal cross-checking within the framework of the empirical relationships developed, and (3) external cross-checking against the results obtained by previous investigations, with an informed understanding of the strengths and drawbacks of the back-analysis methods and assumptions employed in those previous studies.

The resulting hard-earned back-analysis database was then used, in the context of probabilistic regressions that incorporated the best available evaluations of uncertainties, to perform probabilistic regressions by the maximum likelihood method, in order to develop new predictive relationships for engineering evaluation of post-liquefaction strength as a function of both (1) corrected SPT penetration resistance, and (2) initial in situ effective vertical stress.

These new relationships were then compared with previous relationships and recommendations. Here, again, with understanding of the strengths and drawbacks of the procedures by which the previous relationships were developed, and of the back-analyses that often provided the parameters for the earlier efforts, a coherent overall pattern emerged and the juxtaposition of values of post-liquefaction strengths provided by different relationships can now be better understood.

The new predictive relationships developed in these current studies agree well with the recent recommendations of Wang (2003) and Kramer (2008) who executed a similar overall effort, but with significant approaches, and judgments, at essentially every step of the way. Their work was poorly documented, and is thus difficult to check and verify. But the agreement of their findings with the result of these current studies is very good.

Similarly, the agreement of the current studies with the recommendations of (1) Seed and Harder (1990), Olsen and Stark (2002) and Idriss and Boulanger (2008) is also found to be good, but only over specific ranges of (1) initial in situ effective vertical stress, and (2) corrected SPT penetration resistance. In other ranges, these previous relationships can now be shown to be either conservative, or unconservative.

The new predictive relationships for engineering evaluation of post-liquefaction strength are presented in a fully probabilistic form, and can be used for fully probabilistic risk studies and design of high-level projects. These are then simplified down to develop deterministic recommendations likely to be more applicable to more routine projects.

In addition to the development of improved relationships for engineering evaluation of post-liquefactions strengths, the suite of new empirical relationships developed for use in cross-checking of back-analyses of liquefaction failure case histories will likely also have applications with regard to checking of engineering analyses of expected performance of actual engineering projects, including high-level analyses involving fully nonlinear finite element or finite difference analyses for critical and/or high risk projects.

REFERENCES

Alarcon-Guzman, A., Leonards, G.A., and Chameau, J.L. (1988). “Undrained monotonic and cyclic strength of sands.” Journal of Geotechnical Engineering, ASCE, 114(10), 1089-1109.

Andresen, A. and Bjerrum, L. (1968). “Slides in subaqueous slopes in loose sand and silt.” Norwegian Geotechnical Institute Publication No. 81, 1-9.

Andrus, R.D. and Youd, T.L. (1987). “Subsurface investigation of a liquefaction-induced lateral spread, Thousand Springs Valley, Idaho.” Geotechnical Laboratory Miscellaneous Paper GL-87-8, U.S. Army Corps of Engineers, 131 p.

Andrus, R.D. and Youd, T.L. (1989). “Penetration tests in liquefiable gravels.” Proc., 12th International Conference on Soil Mechanics and Foundation Engineering, Rio de Janero, Brazil, 679-682.

Arulanandan, K., Yogachandran, C., Meegoda, N.J., Ying, L., and Zhauji, S. (1986). “Comparison of the SPT, CPT, SV and electrical methods of evaluating earthquake induced liquefaction susceptibility in Ying Kou City during the Haicheng Earthquake." Use of In Situ Tests in Geotechnical Engineering, ASCE Geotechnical Special Publication No. 6, 389-415.

Arulanandan, K., Seed, H.B., Yogachandran, C., Muraleetharan, K.K., Seed, R.B., and Kabilamany, K. (1993). “Centrifuge study on volume changes and dynamic stability of earth dams.” Journal of Geotechnical Engineering, ASCE, 119(11), 1717-1731.

Baziar, M.H. and Dobry, R. (1995). “Residual strength and large-deformation potential of loose silty sands.” Journal of Geotechnical Engineering, ASCE, 121(12), 896-906.

Been, K. and Jefferies, M.G. (1985). “A state parameter for sands.” Geotechnique, 35(2), 99-112.

Been, K., Jefferies, M.G., and Hachey, J. (1991). “The critical state of sands.” Geotechnique, Volume 41, Number 3, pp. 365-381.

Been, K., Conlin, B.H., Crooks, J.H.A., Fitzpatrick, S.W., Jefferies, M.G., Rogers, B.T., and Shinde, S. (1987a). “Back analysis of the Nerlerk berm liquefaction slides: Discussion.” Canadian Geotechnical Journal, 24, 170-179.

Been, K., Jefferies, M.G., Crooks, J.H.A., and Rothenburg, L. (1987b). “The cone penetration test in sands: part II, general inference of state.” Geotechnique, 37(3), 285-299.

Been, K., Jefferies, M.G., and Hachey, J. (1991). “The critical state of sands.” Geotechnique, 41(3), 365-381.

Bennett, M.J. (1989). “Liquefaction analysis of the 1971 ground failure at the San Fernando Valley Juvenile Hall, California.” Bulletin of Association of Engineering Geologists, 26(2), 209-

226.

Bennett, M.J. (1990). “Ground deformation and liquefaction of soil in the Marina District.” Effects of the Loma Prieta Earthquake on the Marina District, San Francisco, California, Dept. of the Interior, U.S. Geological Survey, Open File Report 90-253, 44-79.

Bieganousky, W. A., and Marcuson, W. F. (1976). “Liquefaction Potential of Dams and Foundations, Report No. 1, Laboratory Standard Penetration Tests on Reid Bedford Model and Ottawa Sand”, Research Report S-76-2, U.S. Army Engineer Waterways Experiment Station, CE, Vicksburg, Mississippi, October 1976.

Bieganousky, W. A., and Marcuson, W. F. (1977). “Liquefaction Potential of Dams and Foundations, Report No. 2, Laboratory Standard Penetration Tests on Platte River Sand and Standard Concrete Sand”, Research Report S-76-2, U.S. Army Engineer Waterways Experiment Station, CE, Vicksburg, Mississippi, February 1977.

Bjerrum, L. (1971). “Subaqueous slope failures in Norwegian fjords.” Publication 88, Norwegian Geotechnical Institute, Oslo.

Boulanger, R. W., and Truman, S. P. (1996). "Void redistribution in sand under post-earthquake loading." Canadian Geotechnical Journal, 33, 829-834

Boulanger, R.W., Mejia, L.H., and Idriss, I.M. (1997). “Liquefaction at Moss Landing during Loma Prieta earthquake.” Journal of Geotechnical Engineering, ASCE, 123(5), 453-467.

Boulanger, R. W. (2002). “Evaluating Liquefaction Resistance at High Overburden Stresses”, 3rd U.S.-Japan Workshop on Advanced Research on Earthquake Engineering for Dams, San Diego, California, June 22-23, 2002.

Boulanger, R. W. (2003). “High Overburden Stress Effects in Liquefaction Analyses”, Journal of the Geotechnical Engin. Div., ASCE, Vol.129 (GT12), pp. 1071-1082.

Bryant, S.M., Duncan, J.M., and Seed, H.B. (1983). “Application of tailings dam flow analyses to field conditions.” Report No. UCB/GT/83-03, Dept. of Civil Engineering, Univ. of California, Berkeley, CA.

Butler, J.J. (1997). “Analysis of Energy Measurement Methods of SPT Driving Systems”, M.S. Thesis in Civil Engineering, Utah State University, Logan, UT.

Byrne, P.M. (1991). “A model for predicting liquefaction induced displacements.” Proc., Second International Conf. on Recent Advances in Geotechnical Earthquake Engineering and Soil Dynamics, St. Louis, Vol. 2, 1027-1035.

Byrne, P.M. and Janzen, W. (1981). “SOILSTRESS: A computer program for nonlinear analysis of stresses and deformations in soil.” Soil Mechanics Series #52, Dept. of Civil Engineering, Univ. of British Columbia, updated Jan. 1989.

Byrne, P.M., Salgado, F., and Jitno, H. (1992). “Earthquake induced displacement of soil structure systems.” Proc., Tenth World Conf. on Earthquake Engineering, Madrid, Spain, Vol. 3, 1407-1412.

California Dept. of Water Resources [CDWR] - (1975) “Final Geologic Report on Perris Dam and Lake Part I Foundation Conditions, Grouting, and Instrumentation” Project Geology Report C-94, October 1975

California Dept. of Water Resources [CDWR] - (1998) Perris Dam Foundation Study, Results of Phase I Geologic Investigations, Project Geology Section Report No. 58-11-15, May 1998

Canou, J., Bahda, F., Saitta, A., and Dupla, J.C. (1994). “Initiation of sand liquefaction under monotonic and cyclic loading.” Proc., 13th International Conf. on Soil Mechanics and Foundation Engineering, January 5-10, New Delhi, India, Vol. 3, 1297-1300.

Casagrande, A. (1940). “Characteristics of cohesionless soils affecting the stability of slopes and earth fills.” Contributions to Soil Mechanics, 1925-1940, Boston Society of Civil Engineers, October, (Originally published in the Journal of the Boston Society of Civil Engineers, January, 1936), 257-276.

Casagrande, A. (1965). “Second Terzaghi Lecture: the role of "calculated risk" in earthwork and foundation engineering.” Journal of the Soil Mechanics and Foundations Division, ASCE, 91(SM4), 1-40.

Casagrande, A. (1976). “Liquefaction and cyclic deformation of sands: a critical review.” Harvard Soil Mechanics Series No. 88, Harvard University Cambridge, MA.

Castro, G. (1969). “Liquefaction of sands.” Ph.D. Thesis, Harvard University, Cambridge, Massachusetts.

Castro, G., Seed, R. B., Keller, T. O., & Seed, H. B. (1992). Steady-state strength analysis of Lower San Fernando Dam slide. Journal of geotechnical engineering, 118(3), 406-427.

Castro, G. (1995). “Empirical methods in liquefaction evaluation.” Proc., First Annual Leonardo Zeevaert International Conference, Vol. 1, 1-41.

Castro, G. and Poulos, S.J. (1977). “Factors affecting liquefaction and cyclic mobility.” Journal of Geotechnical Engineering Division, ASCE, 103(GT6), 501-516.

Castro, G., Poulos, S.J., and Leathers, F.D. (1985). “Re-examination of slide of Lower San Fernando Dam.” Journal of Geotechnical Engineering, ASCE, 111(9), 1093-1106.

Castro, G., Keller, T.O., and Boynton, S.S. (1989). “Re-evaluation of the Lower San Fernando Dam: Report 1, an investigation of the February 9, 1971 slide.” U.S. Army Corps of Engineers Contract Report GL-89-2, Vols. 1 and 2, U.S. Army Corps of Engineers Waterways Experiment

Station, Vicksburg, Mississippi.

Castro, G., Seed, R.B., Keller, T.O., and Seed, H.B. (1992). “Steady-state strength analysis of Lower San Fernando Dam slide.” Journal of Geotechnical Engineering, ASCE, 118(3), 406-427.

Cetin, K. O. (2000). "Reliability-Based Assessment of Seismic Soil Liquefaction Initiation Hazard." Dissertation in partial fulfillment for the degree of doctor of philosophy, University of California, Berkeley.

Charlie, W.A., Doehring, D.O., Brislawn, J.P., Scott, C.E., and Butler, L.W. (1994). “Liquefaction evaluation with the CSU piezovane.” Proc., 13th International Conference on Soil Mechanics and Foundation Engineering, New Delhi, India.

Chillarige, A.V., Robertson, P.K., Morgenstern, N.R., Christian, H.A. (1997a). “Evaluation of the in situ state of Fraser River sand.” Canadian Geotechnical Journal, 34, 510-519.

Chillarige, A.V., Morgenstern, N.R., Robertson, P.K., and Christian, H.A. (1997b). “Seabed instability due to flow liquefaction in the Fraser River delta.” Canadian Geotechnical Journal, 34, 520-533.

Christian, H.A., Woeller, D.J., Robertson, P.K., and Courtney, R.C. (1997a). “Site investigation to evaluate flow liquefaction slides at Sand Heads, Fraser River delta.” Canadian Geotechnical Journal, 34, 384-397.

Christian, H.A., Mosher, D.C., Mulder, T., Barrie, J.V., and Courtney, R.C. (1997b). “Geomorphology and potential slope instability on the Fraser River delta foreslope, Vancouver, British Columbia.” Canadian Geotechnical Journal, 34, 432-446.

Chu, J. (1995). “An experimental examination of the critical state and other similar concepts for granular soils.” Canadian Geotechnical Journal, 32, 1065-1075.

Cleary, A.J. (1914). “The Calaveras dam, California, the highest earth dam.” Engineering News, 72(14), 692-695.

Coulter, M. and Migliaccio, L. (1966). “Effects of the earthquake of March 27, 1964 at Valdez, Alaska.” Professional Paper 542-C, U.S. Geological Survey, U.S. Dept. of the Interior, Washington, D.C.

Cunning, J.C., Robertson, P.K., and Sego, D.C. (1995). “Shear wave velocity to evaluate in situ state of cohesionless soils.” Canadian Geotechnical Journal, 32, 848-858.

Davies, M.P. and Campanella, R.G. (1994). “Selecting design values of undrained strength for cohesionless soils.” Proc., 47th Canadian Geotechnical Conference, Halifax, Nova Scotia, Vol. 1, 176-186.

Davis, A.P. Jr., Poulos, S.J., and Castro, G. (1988). “Strengths backfigured from liquefaction

case histories." Proc., 2nd Int. Conf. on Case Histories in Geotechnical Engineering, June 1- 5, St. Louis, MO, 1693-1701.

de Alba, P., Seed, H.B., Retamal, E., and Seed, R.B. (1987). "Residual strength of sand from dam failures in the Chilean earthquake of March 3, 1985." Earthquake Engineering Research Center Report No. UCB/EERC-87-11, University of California, Berkeley, CA.

de Alba, P.A., Seed, H.B., Retamal, E., and Seed, R.B. (1988). "Analyses of dam failures in 1985 Chilean earthquake." Journal of Geotechnical Engineering, ASCE, 114(12), 1414-1434.

Deger, T. T. (2014). Overburden stress normalization and rod length corrections for the standard penetration test (SPT). (Doctoral Dissertations, University of California).

DeGregorio, V.B. (1990). "Loading systems, sample preparation, and liquefaction," Journal of Geotechnical Engineering, ASCE, 116(5), 805-821

Dennis, N.D. (1988). "Influence of specimen preparation techniques and testing procedures on undrained steady state shear strength." Advanced Triaxial Testing of Soil and Rock, ASTM STP 977, R.T. Donaghe, R.C. Chaney, and M.L. Silver, eds., American Society for Testing and Materials, Philadelphia, 642-654.

Dierichs, D. and Forster, W. (1985). "Results of liquefaction tests under static conditions." Proc., 11th International Conf. on Soil Mechanics and Foundation Engineering, August 12- 16, San Francisco, CA, Vol. 2, 437-441.

Dobry, R. and Alvarez, L. (1967). "Seismic failures of Chilean tailings dams." Journal of the Soil Mechanics and Foundations Division, ASCE, 93(SM6), 237-260.

Dyvik, R. and Høeg, K. (1999). "Comparison of tests on undisturbed and reconstituted silt and silty sand." Intl. Workshop on the Physics and Mechanics of Soil Liquefaction, P. Lade and J. Yamamuro, eds., Johns Hopkins University, Baltimore, Maryland.

Eckersley, D. (1990). "Instrumented laboratory flow slides." Geotechnique, 40, 489-502.

Ekstrom, A. and Olofsson, T. (1985). "Water and frost – stability risks for embankments of fine-grained soils." Proc., Symposium on Failures in Earthworks, Institution of Civil Engineers, London, March 6-7, Vol. 1, 155-166.

Engineering News-Record. (1925). "What happened to municipal utilities at Santa Barbara." Engineering News-Record, 95(4), 146-149.

Faris, A. T. (2004). Probabilistic models for engineering assessment of liquefaction-induced lateral spreading displacements (Doctoral dissertation, University of California, Berkeley).

Fear, C.E. and Robertson, P.K. (1995). "Estimating the undrained strength of sand: a theoretical framework." Canadian Geotechnical Journal, 32(4), 859-870.

Fiegel, G.F. and Kutter, B.L. (1994). “Liquefaction induced lateral spreading of mildly sloping ground.” Journal of Geotechnical Engineering, ASCE, 120(12), 2236-2243.

Finn, W.D.L. (1990). “Analysis of post-liquefaction deformations in soil structures.” Proc. H.Bolton Seed Memorial Symposium, Bi-Tech Publishing Ltd., Vol. 2, 291-311.

Finn, W.D.L. (1998). “Seismic safety of embankment dams: developments in research and practice 1988-1998.” Proc., Geotechnical Earthquake Engineering and Soil Dynamics III, ASCE Geotechnical Special Publication No. 75, Vol. 2, 812-853.

Gilboy, G. (1942). Discussion of “Fort Peck slide.” by T.A. Middlebrooks, Transactions of the American Society of Civil Engineers, 107, 723-764.

Gilstrap, S.D. (1998) “CPT based liquefaction resistance analysis evaluated using case histories” M.S. Thesis, Brigham Young University, Provo, Utah, 304 p.

Gu, W.H., Morgenstern, N.R., and Robertson, P.K. (1993). “Progressive failure of Lower San Fernando Dam.” Journal of Geotechnical Engineering, ASCE, 119(2), 333-349.

Gutierrez, M. (1998). “Liquefaction and post-liquefaction behavior of granular soils.” Proc., Shear Strength of Liquefied Soils, editors: T.D. Stark, S.M. Olson, S.L. Kramer, and T.L. Youd, University of Illinois-Urbana-Champaign, Illinois, 88-89. (Available only on the World Wide Web at http://mae.ce.uiuc.edu)

GZA GeoEnvironmental, Inc. (1991). “Wachusett Dam – Clinton, Massachusetts – North Dike Stability.” Stage I Report, Volume II, Report to the Commonwealth of Massachusetts, Metropolitan District Commission, Boston, Massachusetts.

Haley & Aldrich, Inc. (1984a). “Report on Phase II Investigation, Wachusett Reservoir Dam, Clinton, Massachusetts.” Prepared for the Commonwealth of Massachusetts, Metropolitan District Commission, Boston, Massachusetts, February.

Haley & Aldrich, Inc. (1984b). “Report on Phase II Investigation, Wachusett Reservoir, North Dike, South Dike, Clinton, Massachusetts.” Prepared for the Commonwealth of Massachusetts, Metropolitan District Commission, Boston, Massachusetts, February.

Hamada, M., H. Sato, T. Kawakami, 1994, “A consideration for the mechanism for liquefaction related large ground displacement," Proceedings of the 5th U.S. Japan Workshop on Earthquake Resistant Design of Lifeline Facilities and Countermeasures for Soil Liquefaction, NCEER Report 94-0026, T. D. O Rourke and M. Hamada, Eds., pp. 217-

Hanzawa, H. (1980). “Undrained strength and stability analysis for a quick sand.” Soils and Foundations, 20(2), 17-29.

Hanzawa, H., Itoh, Y., and Suzuki, K. (1979). “Shear characteristics of a quick sand in the

Arabian Gulf.” Soils and Foundations, 19(4), 1-15.

Harder, L. F. Jr. (1988). "Use of Penetration Tests to Determine the Cyclic Loading Resistance of Gravelly Soils During Earthquake Shaking." Ph.D. Thesis, University of California, Berkeley.

Harder, L.F. Jr. and Boulanger, R. (1997). “Application of Ks and Ka correction factors.” Proc., NCEER Workshop on Evaluation of Liquefaction Resistance of Soils, T.L. Youd and I.M. Idriss, eds., NCEER-97-0022, 167-190.

Hazen, A. (1918). “A study of the slip in the Calaveras Dam.” Engineering News-Record, 81(26), 1158-1164.

Hazen, A. (1920). “Hydraulic-fill dams.” Transactions of the American Society of Civil Engineers, Paper No. 1458, 1713-1821 (including discussions).

Hazen, A. and Metcalf, L. (1918). “Middle section of upstream side of Calaveras dam slips into reservoir.” Engineering News-Record, 80(14), 679-681.

Hedien, J.E., Anderson, R.J., and Niznik, J.A. (1998). “Evaluation of liquefaction potential and seismic safety for Tennessee Valley Authority embankment dams.” Proc., Conference on Current Earthquake Engineering Research in the Central United States (CEERICUS ’98), D.F. Laefer and J.P. Arnett, eds., University of Illinois-Urbana-Champaign, April, II-1 – II-8.

Hicks, M.A. and Boughrarou, R. (1998). “Finite element analysis of the Nerlerk underwater berm failures.” Geotechnique, 48(2), 169-185.

Highter, W.H. and Tobin, R.F. (1980). “Flow slides and the undrained brittleness index of some mine tailings.” Engineering Geology, 16, 71-82.

Highter, W.H. and Vallee, R.P. (1980). “The liquefaction of different mine tailings under stress-controlled conditions.” Engineering Geology, 16, 147-150.

Hoeg, K., Dyvik, R., and Sandbaekken, G. (2000). “Strength of undisturbed versus reconstituted silt and silty sand specimens.” Journal of Geotechnical and Geoenvironmental Engineering, ASCE, 126(7), 606-617.

Holtz, W.G. and Gibbs, H.J. (1979). Discussion of “SPT and relative density in coarse sand.” Journal of the Geotechnical Engineering Division, ASCE, 105(GT3), 439-441.

Hryciw, R.D., Vitton, S., and Thomann, T.G. (1990). “Liquefaction and flow failure during seismic exploration.” Journal of Geotechnical Engineering, ASCE, 116(12), 1881-1899.

Huang, A.-B., Hsu, H.-H., Chang, J.-W. (1999). “The behavior of a compressible silty fine sand.” Canadian Geotechnical Journal, 36(1), 88-101.

Inada (1982). “Methods of in situ soil investigations.” Japanese Society of Soil Mechanics and

Foundation Engineering, 217 p.

Ishihara, K. (1974). “Liquefaction of subsurface soil during earthquakes.” Technocrat Volume 7, Fuji Marketing Research Co., Ltd., No. 5, 1-32.

Ishihara, K. (1984). “Post-earthquake failure of a tailings dam due to liquefaction of the pond deposit.” Proc., Inter. Conf. on Case Histories in Geotechnical Engineering, Rolla, Missouri, May 6-11, Vol. 3, 1129-1143.

Ishihara, K. (1985). “Stability of natural deposits during earthquakes.” Proc., 11th International Conference on Soil Mechanics and Foundation Engineering, San Francisco, CA, Vol. 1, 321-376.

Ishihara, K. (1993). “Liquefaction and flow failure during earthquakes.” Geotechnique, 43(3), 351-415.

Ishihara, K., Silver, M.L., and Kitagawa, H. (1978). “Cyclic strengths of undisturbed sands obtained by large diameter sampling.” Soils and Foundations, 18(4), 61-76.

Ishihara, K. and Koga, Y. (1981). “Case studies of liquefaction in the 1964 Niigata earthquake.” Soils and Foundations, 21(3), 35-52.

Ishihara, K., Yasuda, S., and Yoshida, Y. (1990a). “Liquefaction-induced flow failure of embankments and residual strength of silty sands.” Soils and Foundations, 30(3), 69-80.

Ishihara, K., Okusa, S., Oyagi, N., and Ischuk, A. (1990b). “Liquefaction-induced flow slide in the collapsible loess deposit in Soviet Tajik.” Soils and Foundations, 30(4), 73-89.

Ishihara, K., Acacio, A.A., and Towhata, I. (1993). “Liquefaction-induced ground damage in Dagupan in the July 16, 1990 Luzon earthquake.” Soils and Foundations, 33(1), 133-154.

Iverson, R.M. and LaHusen, R.G. (1993). “Friction in debris flows: inferences from largescale flume experiments.” Proc., Hydraulic Engineering ’93, 1993 Conf. of the Hydraulics Division of the American Society of Civil Engineers, Vol. 2, 1604-1609.

Iverson, R.M., Reid, M.E., and LaHusen, R.G. (1997). “Debris-flow mobilization from landslides.” Annual Review of Earth Planetary Science, 25, 85-138.

Jamiolkowski, M., Ladd, CC., Germaine, J.T., and Lancellotta, R. (1985). “New developments in field and laboratory testing of soils.” Proc., 11th International Conf. on Soil Mechanics and Foundation Engineering, San Francisco, CA, Vol. 1, 57-153.

Jefferies, M.G., Been, K., and Hachey, J.E. (1990). “Influence of scale on the constitutive behavior of sand.” Proc. Canadian Geotechnical Engineering Conference, Laval University, Quebec, Canada, Vol. 1, 263-273.

Jitno, H. (1995). “Liquefaction induced deformation of earth structures.” Ph.D. Thesis, Civil Engineering Dept., Univ. of British Columbia, Vancouver, B.C.

Jitno, H. and Byrne, P.M. (1995). “Predicted and observed liquefaction response of Mochikoshi tailings dam.” Proc., 1st International Conf. on Earthquake Geotechnical Engineering, Nov. 14-16, Tokyo, Japan, Vol. 2, 1085-1090.

Kaneko, M., Sasaki, Y., Nishikawa, J., Nagase, M., and Mamiya, K. (1995). “River dike failure in Japan by earthquakes in 1993.” Proc., 3rd International Conf. on Recent Advanes in Geotechnical Earthquake Engineering and Soil Dynamics, April 2-7, St. Louis, MO, Vol. 1, 495-498.

Kayen, R.E., Mitchell, J.K., Seed, R.B., Lodge, A., Nishio, S., and Coutinho, R. (1992). “Evaluation of SPT-, CPT-, and shear wave-based methods for liquefaction potential assessments using Loma Prieta data.” Proc., 4th Japan-U.S. Workshop on Earthquake Resistant Design of Lifeline Facilities and Countermeasures for Soil Liquefaction, Honolulu, Hawaii, Vol. 1, 177-192.

Koester, J.P. (1998). “Discussion group: theoretical/conceptual issues: soil mechanics perspective.” Proc., Shear Strength of Liquefied Soils, editors: T.D. Stark, S.M. Olson, S.L. Kramer, and T.L. Youd, University of Illinois-Urbana-Champaign, Illinois. (Available only on the World Wide Web at http://mae.ce.uiuc.edu)

Kolbuszewski, J.J. (1948). “An experimental study of the maximum and minimum properties of sand.” Proc., 2nd International Conf. on Soil Mechanics and Foundation Engineering, Rotterdam, 158-165.

Konrad, J.M. (1990a). “Minimum undrained strength of two sands.” Journal of Geotechnical Engineering, ASCE, 116(6), 932-947.

Konrad, J.M. (1990b). “Minimum undrained strength versus steady-state strength of sands.” Journal of Geotechnical Engineering, ASCE, 116(6), 948-963.

Konrad, J.M. (1991). “The Nerlerk berm case history: some consideration for the design of hydraulic sand fills.” Canadian Geotechnical Journal, 28, 601-612.

Konrad, J.M. (1993). “Undrained response of loosely compacted sands during monotonic and cyclic compression tests.” Geotechnique, 43(1), 69-89.

Konrad, J.M. (1998). “Sand state from cone penetration tests: a framework considering grain crushing stress.” Geotechnique, 48(2), 201-215.

Konrad, J.M. and Watts, B.D. (1995). “Undrained shear strength for liquefaction flow failure analysis.” Canadian Geotechnical Journal, 32, 783-794.

Konrad, J.M. and Pouliot, N. (1997). “Ultimate state of reconstituted and intact samples of

deltaic sand." Canadian Geotechnical Journal, 34, 737-748.

Koppejan, A.W., van Wamelen, B.M., and Weinberg, L.J.H. (1948). "Coastal flow slides in the Dutch province of Zeeland." Proc., 2nd International Conf. Of Soil Mechanics and Foundation Engineering, Rotterdam, Netherlands, June 21-30, 89-96.

Kramer, S.L. (1989). "Uncertainty in steady-state liquefaction evaluation procedures." Journal of Geotechnical Engineering, ASCE, 115(10), 1402-1419.

Kramer, S.L. (1996). Geotechnical Earthquake Engineering. Prentice Hall, New Jersey, 653 p.

Kramer, S.L. and Seed, H.B. (1988). "Initiation of soil liquefaction under static loading condition." Journal of Geotechnical Engineering, ASCE, 114(4), 412-430.

Kramer, S. L. (2008). Evaluation of liquefaction hazards in Washington State (No. WA-RD 668.1). Washington State Department of Transportation, Office of Research and Library Services.

Kuerbis, R.H., Negussey, D., and Vaid, Y.P. (1988). "Effect of gradation and fines content on the undrained response of sand," Proceedings of Specialty Conference on Hydraulic Fill Structures, GSP No. 21, 330-345

Kulasingam, R., Malvick, E. J., Boulanger, R. W., and Kutter, B. L. (2004). "Strength loss and localization at silt interlayers in slopes of liquefied sand." Journal of Geotechnical and Geoenvironmental Engineering, ASCE, 130(11), 1192-1202.

Kulhawy, F.H. and Mayne, P.W. (1990). "Manual on estimating soil properties for foundation design." Electric Power Research Institute EL-6800, Project 1493-6, August, 400 pp.

Kulhawy, F.H. and Mayne, P.W. (1991). "Relative density, SPT, and CPT interrelationships." 1st International Symposium on Calibration Chamber Testing, June 28-29, Potsdam, New York, 197-211.

Kutter, B.L. and Voss, T. (1995). "Analysis of data on plow resistance in dense, saturated, cohesionless soil," Contract Report CR95.004, Naval Facilities Engineering Service Center, Port Hueneme, California.

Lade, P.V. (1993). "Initiation of static instability in the submarine Nerlerk berm." Canadian Geotechnical Journal, 30, 895-904.

Lade, P.V. and Yamamuro, J.A. (1997). "Effects of nonplastic fines on static liquefaction of sands." Canadian Geotechnical Journal, 34, 918-928.

Lee, K.L., Seed, H.B., Idriss, I.M., and Makdisi, F.I. (1975). "Properties of soil in the San Fernando hydraulic fill dams." Journal of the Geotechnical Engineering Division, ASCE, 101(GT8), 801-821.

Liao, S.C., and Whitman, R.V. (1986). “Overburden correction factors for SPT in sand.” Journal of Geotechnical Engineering, ASCE, 112(3), 373-377.

Ligtenberg-Mak, C.E., Krajicek, P.V.F.S., and Kuiter, C. (1990). “Geological study of flow slide sensitive sediments.” Proc., 6th International Congress, International Association of Engineering Geology, Amsterdam, Vol. 1, 691-695.

Lucia, P.C. (1981). “Review of experiences with flow failures of tailings dams and waste impoundments.” Ph.D. Thesis, University of California, Berkeley, Calif.

Luternauer, J.L. and Finn, W.D.L. (1983). “Stability of the Fraser River delta front.” Canadian Geotechnical Journal, 20, 603-616.

Marcuson, W.F., III. (1979). “Visit to Japan to observe damage which occurred during the Near Izu Oshima earthquakes January 14 and 15, 1978.” Miscellaneous Paper GL-79-20, U.S. Army Corps of Engineers Waterways Experiment Station, Vicksburg, MS.

Marcuson, W.F., III, and Krinitzsky, E.L. (1976). “Dynamic analysis of Fort Peck dam.” Technical Report S-76-1, U.S. Army Engineer Waterways Experiment Station, Vicksburg, MS, March.

Marcuson, W.F., III, Ballard, R.F., Jr., and Cooper, S.S., (1978). “Comparison of penetration resistance values to in situ shear wave velocities.” Proc., 2nd International Conf. on Microzonation for Safer Construction – Research and Application, San Francisco, CA, Nov. 26 – Dec. 1, Vol. 2, 1013-1023.

Marcuson, W.F., III, Ballard, R.F., Jr., and Ledbetter, R.H. (1979). “Liquefaction failure of tailings dams resulting from the Near Izu Oshima earthquake, 14 and 15 January, 1978.” Proc. 6th Pan-American Conf. on Soil Mechanics and Foundation Engineering, Lima Peru, Vol. 2, 69-80.

Marcuson, W.F., III, Hynes, M.E., and Franklin, A.G. (1990). “Evaluation and use of residual strength in seismic safety analysis of embankments.” Earthquake Spectra, 6(3), 529-572.

McKenna, G.T., Luternauer, J.L., and Kostaschuk, R.A. (1992). “Large-scale mass-wasting events on the Fraser River delta front near Sand Heads, British Columbia.” Canadian Geotechnical Journal, 29, 151-156.

McRoberts, E.C. and Sladen, J.A. (1992). “Observations on static and cyclic sandliquefaction methodologies.” Canadian Geotechnical Journal, 29, 650-665.

Mesri, G., Feng, T.W., and Benak, J.M. (1990). “Postdensification penetration resistance of clean sands.” Journal of Geotechnical Engineering, ASCE, 116(7), 1095-1115.

Meyerhof, G.G. (1957). “Discussion on sand density by spoon penetration.” Proc., 4th Intl. Conf.

on Soil Mechanics and Foundation Engineering, Vol. 3, 110.

Meyerhof, G.G. (1971). “The mechanism of flow slides in cohesive soils.” Geotechnique, 1, 41-49.

Middlebrooks, T.A. (1942). “Fort Peck slide.” Transactions of the American Society of Civil Engineers, 107, 723-764.

Mishima, S. and Kimura, H. (1970). “Characteristics of landslides and embankment failures during the Tokachioki earthquake.” Soils and Foundations, 10(2), 39-51.

Mitchell, D.E. (1984). “Liquefaction slides in hydraulically placed sands.” Proc., 4th International Symposium on Landslides, Toronto, Ontario, Vol. 1, 141-146.

Mitchell, J.K. and Tseng, D.J. (1990). “Assessment of liquefaction potential by cone penetration resistance.” Proc., H.B. Seed Memorial Symposium, BiTech Publishing, Vol. 2, 335-350.

Mitchell, J.K., Lodge, Angela, L., Coutinho, R.Q., Kayen, R.E., Seed, R.B., Nishio, Shinya, and Stokoe, K.H., III. (1994). “Insitu test results from four Loma Prieta earthquake liquefaction sites: SPT, CPT, DMT, and shear wave velocity.” Report No. UCB/EERC- 94/04, Earthquake Engineering Research Center, Univ. of California, Berkeley, CA, April.

Mittal, H.K. and Hardy, R.M. (1977). “Geotechnical aspects of a tar sand tailings dyke.” Proc., Conference on Geotechnical Practice for Disposal of Solid Waste Materials, ASCE Specialty Conference of the Geotechnical Engineering Division, Vol. 1, 327-347.

Miura, K., Yoshida, N., and Wakamatsu, K. (1995). “Damage to fill embankment during the 1993 Kushiro-oki earthquake.” Proc., 1st International Conf. on Earthquake Geotechnical Engineering, Nov. 14-16, Tokyo, Japan, Vol. 2, 1057-1062.

Miura, K., Yoshida, N., Nishimura, M., and Wakamatsu, K. (1998). “Stability analysis of the fill embankment damaged by recent two major earthquakes in Hokkaido, Japan.” Proc., 1998 Geotechnical Earthquake Engineering and Soil Dynamics Specialty Conference, ASCE Geo-Institute Geotechnical Special Publication No. 75, Vol. 2, August 3-6, Seattle, Washington, 926-937.

Miuri, S. and Toki, S. (1982). “A sample preparation method and its effect on static and cyclic deformation-strength properties of sand,” Soils and Foundations, 22(1), 61-77.

Mohamad, R. and Dobry, R. (1986). “Undrained monotonic and cyclic triaxial strength of sand.” Journal of Geotechnical Engineering, ASCE, 112(10), 941-958.

Mori, S. (1993). “Reconnaissance report on the liquefaction aspects of the Kushiro-oki earthquake, January 15, 1993.” Proc., 28th Japan National Conf. on Soil Mechanics and Foundation Engineering, 1091-1094.

Moss, R. E. S. (2009). “Reduced Uncertainty of Ground Motion Prediction Equations through Bayesian Variance Analysis.” PEER Report No. 2009/105, November.

Moss, R. E. S. (2011). "Reduced Sigma of Ground Motion Prediction Equations through Uncertainty Propagation.” Bulletin of Seismological Society of America, 101(1).

Meyerhof, G.G. (1957). Discussion of “Research on determining the density of sands by spoon penetration testing.” by H.J. Gibbs and W.G. Holtz, Proc., International Conf. on Soil Mechanics and Foundation Engineering, Vol. 3, 110.

NAVFAC (Naval Facilities Engineering Command). (1986). Design Manual 7.01 Soil Mechanics, United States Navy, Alexandria, Virginia.

Newmark, N. (1965). “Effects of earthquakes on dams and embankments.” Geotechnique, 15(2), 139-160.

Norris, G., Siddharthan, R., Zafir, Z., and Madhu, R. (1997). “Liquefaction and residual strength of sands from drained triaxial tests.” Journal of Geotechnical and Geoenvironmental Engineering, ASCE, 123(3), 220-228.

Nunn, H. (1925). “Municipal problems of Santa Barbara.” Bulletin, Seismological Society of America, 15(4), 308-319.

Obermeier, S.F. (1996). “Use of liquefaction-induced features for paleoseismic analysis – an overview of how seismic liquefaction features can be distinguished from other features and how their regional distribution and properties of source sediment can be used to infer the location and strength of Holocene paleoearthquakes.” Engineering Geology, 44, 1-76.

Obermeier, S.F., Pond, E.C., and Olson, S.M., with contributions by Green, R. Stark, T.D. and Mitchell, J. (2000). “Paleoliquefaction studies in continental settings – geologic and geotechnical factors in interpretation and back-analysis.” Open File Report 01-29, U.S. Geological Survey (also Invited paper, Geological Society of America).

Ohsaki, Y. (1966). “Niigata earthquake, 1964 building damage and soil condition.” Soils and Foundations, 6(2), 14-37.

Ohya, S., Iwasaki, T., and Wakamatsu, M. (1985). “Comparative study of various penetration tests in ground that underwent liquefaction during the 1983 Nihon-Kai-Chubu and 1964 Niigata earthquakes.” Proc., Workshop on In-Situ Testing Methods for Evaluation of Soil Liquefaction Susceptibility, San Francisco, California, Vol. 1, 56-88.

Okusa, S. and Anma, S. (1980). “Slope failures and tailings dam damage in the 1978 Izu-Ohshima-Kinkai earthquake.” Engineering Geology, 16, 195-224.

Okusa, S., Anma, S., and Maikuma, H. (1980). “Liquefaction of mine tailings in the 1978 Izu-Ohshima-Kinkai earthquake, central Japan.” Proc., 7th World Conf. on Earthquake Engineering,

Sept. 8-13, Istanbul, Turkey, Vol. 3, 89-96.

Okusa, S., Anma, S., and Maikuma, M. (1984). “The propagation of liquefaction pressure and delayed failure of a tailings dam dike in the 1978 Izu-Oshima-Kinkai earthquake.” Proc., 8th World Conf. on Earthquake Engineering, July 21-28, San Francisco, CA, Vol. 1, 389-396.

Olsen, R.S. and Farr, J.V. (1986). “Site characterization using the cone penetrometer test.” Proc., INSITU '86, ASCE Specialty Conference on Use of In Situ Testing in Geotechnical Engineering, ASCE Geotechnical Special Publication No. 6, Virginia Tech, Blacksburg, VA, 854-868.

Olsen, R.S. (1997). “Cyclic liquefaction based on the cone penetrometer test.” Proc., NCEER Workshop on Evaluation of Liquefaction Resistance of Soils, T.L. Youd and I.M. Idriss, eds., NCEER-97-0022, 225-276.

Olson, S.M. (1998). “Post-liquefaction shear strength from laboratory and field tests: field tests.” Proc., Shear Strength of Liquefied Soils, editors: T.D. Stark, S.M. Olson, S.L. Kramer, and T.L. Youd, University of Illinois-Urbana-Champaign, Illinois, 130-152. (Available only on the World Wide Web at http://mae.ce.uiuc.edu)

Olson, S.M. and Stark, T.D. (1998). “CPT based liquefaction resistance of sandy soils.” Proc., 1998 Geotechnical Earthquake Engineering and Soil Dynamics Specialty Conference, ASCE Geo-Institute Geotechnical Special Publication No. 75, Vol. 1, August 3-6, Seattle, Washington, 325-336.

Olson, S.M., Stark, T.D., Walton, W.H., and Castro, G. (2000). “Static liquefaction flow failure of the North Dike of Wachusett Dam.” Journal of Geotechnical and Geoenvironmental Engineering, ASCE, 126(12), 1184-1193.

Olson, S.M. and Stark, T.D. (2001). “Liquefaction analysis of Lower San Fernando Dam using strength ratios." Paper No. 4.05, Proc., 4th International Conf. on Recent Advances in Geotechnical Earthquake Engineering and Soil Dynamics, March 26-31, San Diego, CA.

Olson, S.M. and Stark, T.D. (2002). “Liquefied strength ratio from liquefaction flow failure case histories,” Canadian Geotechnical Journal, 39(5), 629-647.

Palmer, A.C. (1999). “Speed effects in cutting and ploughing,” Geotechnique, 49(3), 285-294.

Peck, R.B. (1979). “Liquefaction potential: science versus practice.” Journal of Geotechnical Engineering, ASCE, 105(3), 393-398.

Peterson, R.W. (1991). “Penetration resistance of fine cohesionless materials.” Proc., 1st International Symposium on Calibration Chamber Testing, June 28-29, Potsdam, New York, 315-328.

Pillai, V.S. and Salgado, F.M. (1994). “Post-liquefaction stability and deformation analysis of Duncan Dam.” Candian Geotechnical Journal, 31, 967-978.

Pillai, V.S. and Stewart, R.A. (1994). “Evaluation of liquefaction potential of foundation soils at Duncan Dam.” Canadian Geotechnical Journal, 31, 951-966.

Plewes, H.D., O'Neil, G.D., McRoberts, E.C., and Chan, W.K. (1989). “Liquefaction considerations for Suncor tailings pond.” Proc., Dam Safety Seminar, Edmonton, Alberta, Sept., Vol. 1, 61-89.

Poulos, S.J. (1981). “The steady state of deformation.” Journal of Geotechnical Engineering Division, ASCE, 17(GT5), 553-562.

Poulos, S.J. (1988). “Liquefaction and related phenomena.” in Advanced Dam Engineering for Design, Construction, and Rehabilitation, R.B. Jansen, ed., Van Nostrand Reinhold, New York, 292-320.

Poulos, S.J. (1998). “Comments on laboratory determination of undrained steady state shear strength.” Proc., Shear Strength of Liquefied Soils, editors: T.D. Stark, S.M. Olson, S.L. Kramer, and T.L. Youd, University of Illinois-Urbana-Champaign, Illinois, 152-232. (Available only on the World Wide Web at http://mae.ce.uiuc.edu)

Poulos, S.J., Castro, G. and France, W. (1985a). “Liquefaction evaluation procedure.” Journal of Geotechnical Engineering, ASCE, 111(6), 772-792.

Poulos, S.J., Robinsky, E.I., and Keller, T.O. (1985b). “Liquefaction resistance of thickened tailings.” Journal of Geotechnical Engineering, ASCE, 111(12), 1380-1394.

Poulos, S.J. Castro, G., and France, W. (1988). Closure to discussion of “Liquefaction evaluation procedure.” Journal of Geotechnical Engineering, ASCE, 114(2), 251-259.

Prandtl, L. (1921). “On the penetrating strengths (hardness) of plastic construction materials and the strength of cutting edges.” Zeit. angew. Math. Mech., 1(1), 15-20.

Richter, C.F. (1958). Elementary Seismology. W.H. Freeman and Company, San Francisco, CA.

Riemer, M.F., Seed, R.B., Nicholson, P.G., and Jong, H.L. (1990). “Steady state testing of loose sands: limiting minimum density.” Journal of Geotechnical Engineering, ASCE, 116(2), 332-337.

Riemer, M.F. and Seed, R.B. (1992). “Observed effects of testing conditions on the residual strength of loose, saturated sands at large strains.” Proc., 4th Japan-U.S. Workshop on Earthquake Resistant Design of Lifeline Facilities and Countermeasures for Soil Liquefaction, Tech. Rpt. No. NCEER-92-0019, M. Hamada and T.D. O’Rourke, eds., Vol. 1, 223-237.

Riemer, M.F. and Seed, R.B. (1997). “Factors affecting apparent position of steady-state line. Journal of Geotechnical and Geoenvironmental Engineering, ASCE, 123(3), 281-288.

Robertson, P.K. (1994). “Suggested terminology for liquefaction.” Proc., 47th Canadian Geotechnical Conf., Halifax, Nova Scotia, 277-286.

Robertson, P.K. and Campanella, R.G. (1983). “Interpretation of cone penetration tests. Part I: sand.” Canadian Geotechnical Journal, 20(4), 718-733.

Robertson, P.K. and Campanella, R.G. (1985). “Liquefaction potential of sands using the CPT.” Journal of Geotechnical Engineering Division, ASCE, 111(3), 384-403.

Robertson, P.K., Sasitharan, S., Cunning, J.C., and Sego, D.C. (1995). “Shear-wave velocity to evaluate in-situ state of Ottawa sand.” Journal of Geotechnical Engineering, ASCE, 121(3), 262-273.

Robertson, P.K., and Wride (Fear), C.E. (1998). “Evaluating cyclic liquefaction potential using the cone penetrometer test.” Canadian Geotechnical Journal, 35(3), 442-459.

Rogers, B.T., Been, K., Hardy, M.D., Johnson, G.J., and Hachey, J.E. (1990). “Re-analysis of Nerlerk B-67 berm failures.” Proc., 43rd Canadian Geotechnical Conf. - Prediction of Performance in Geotechnique, Quebec, Canada, Vol. 1, 227-237.

Ross, G.A. (1968). “Case studies of soil stability problems resulting from earthquakes.” Ph.D. Thesis, University of California, Berkeley, Calif. Saito, K. and Ine, N. (1993). Private communication to K. Miura, reported in Miura et al. (1998).

Sasaki, Y., Oshiki, H., and Nishikawa, J. (1994). “Embankment failure caused by the Kushiro-Oki earthquake of January 15, 1993.” Proc., 13th International Conf. on Soil Mechanics and Foundation Engineering, New Delhi, India, Vol. 1, 61-68.

Sasaki, Y., Tamura, K., Yamamoto, M., and Ohbayashi, J. (1995). “Soil improvement work for river embankment damaged by the 1993 Kushiro-Oki earthquake.” Proc., Earthquake Geotechnical Engineering, Nov. 14-16, Tokyo, Japan, Vol. 1, 43-48.

Sasaki, T., Finn, W.D.L., Shibano, A., and Nobumoto, M. (1996). “Settlement of embankment above a liquefied ground which is covered by non-liquefiable surface layer.” Proc., 6th Japan-U.S. Workshop on Earthquake Resistant Design of Lifeline Facilities and Countermeasures Against Soil Liquefaction, Technical Report NCEER-96-0012, M. Hamada and T. O’Rourke, editors, 361-390.

Sasitharan, S., Robertson, P.K., Sego, D.C., and Morgenstern, N.R. (1993). “Collapse behavior of sand.” Canadian Geotechnical Journal, 30, 569-577.

Sasitharan, S., Robertson, P.K., Sego, D.C., and Morgenstern, N.R. (1994). “Stateboundary for very loose sand and its practical implications.” Canadian Geotechnical Journal, 31, 321-334.

Schmertmann, J.H. (1987). Discussion of “Time-dependent strength in freshly deposited or densified sand.” by J.K. Mitchell and Z.V. Solymar, Journal of Geotechnical Engineering,

ASCE, 113(2), 173-175.

Schofield, A.N. and Wroth, C.P. (1968). Critical State Soil Mechanics. McGraw-Hill, London.

Seed, H.B. and Lee, K.L. (1966). “Liquefaction of saturated sands during cyclic loading,” Journal of the Soil Mechanics and Foundations Division, ASCE, SM6(11), 105-134.

Seed, H.B. (1968). “Landslides during earthquakes due to soil liquefaction.” Journal of the Soil Mechanics and Foundation Division, ASCE, 94(SM5), 1055-1122.

Seed, H.B. (1979). “Considerations in the earthquake-resistant design of earth and rockfill dams.” Geotechnique, 29(3), 215-263.

Seed, H.B. (1987). “Design problems in soil liquefaction.” Journal of Geotechnical Engineering Division, ASCE, 113(8), 827-845.

Seed, H.B. and Idriss, I.M. (1971). “Simplified procedure for evaluating soil liquefaction potential.” Journal of the Soil Mechanics and Foundation Division, ASCE, 97(SM9), 1249-1273.

Seed, H.B., Lee, K.L., and Idriss, I.M. (1969). “Analysis of Sheffield Dam failure.” Journal of the Soil Mechanics and Foundations Division, ASCE, 95(SM6), 1453-1490.

Seed, H.B., Lee, K.L., Idriss, I.M., and Makdisi, F. (1973). “Analysis of the slides in the San Fernando Dams during the earthquake of Feb. 9, 1971.” Earthquake Engineering Research Center 73-2, University of California, Berkeley, Calif.

Seed, H.B., Lee, K.L., Idriss, I.M., and Makdisi, F. (1975). “Dynamic analysis of the slide in the Lower San Fernando Dam during the earthquake of February 9, 1971.” Journal of the Geotechnical Engineering Division, ASCE, 101(GT9), 889-911.

Seed, H.B. and Idriss, I.M. (1982). Ground Motions and Soil Liquefaction During Earthquakes. Monograph No. 5, Monograph Series, Earthquake Engineering Research Institute, 82 pp.

Seed, H.B., Idriss, I.M. and Arango, I. (1983). “Evaluation of liquefaction potential using field performance data.” Journal of Geotechnical Engineering Division, ASCE, 109(3), 458-482.

Seed, H.B., Tokimatsu, K., Harder, L.F., and Chung, R. (1984). “The influence of SPT procedures on soil liquefaction resistance evaluations.” Report No. UCB/EERC-84/15, Earthquake Engineering Research Center, Univ. of California, Berkeley, CA, October.

Seed, H.B., Tokimatsu, K., Harder, L.F., and Chung, R. (1985). “Influence of SPT procedures in soil liquefaction resistance evaluations.” Journal of Geotechnical Engineering Division, ASCE, 111(12), 861-878.

Seed, H.B. and de Alba, P. (1986). “Use of SPT and CPT tests for evaluating the liquefaction resistance of sands.” Proc., INSITU '86, ASCE Specialty Conference on Use of In Situ Testing in

Geotechnical Engineering, Virginia Tech, Blacksburg, VA, Geotechnical Special Publication No. 6, 281-302.

Seed, H.B., Seed, R.B., Harder, L.F., and Jong, H.-L. (1989). “Re-evaluation of the Lower San Fernando Dam: Report 2, examination of the post-earthquake slide of February 9, 1971.” U.S. Army Corps of Engineers Contract Report GL-89-2, U.S. Army Corps of Engineers Waterways Experiment Station, Vicksburg, Mississippi.

Seed, R.B. and Harder, L.F. Jr. (1990). “SPT-based analysis of cyclic pore pressure generation and undrained residual strength.” Proc. H.Bolton Seed Memorial Symposium, Bi- Tech Publishing Ltd., Vol. 2, 351-376.

Shibata, T. and Teparaksa, W. (1988). “Evaluation of liquefaction potentials of soils using cone penetration tests.” Soils and Foundations, 28(2), 49-60.

Silvis, F. and de Groot, M.B. (1995). “Flow slides in the Netherlands: experience and engineering practice.” Canadian Geotechnical Journal, 32, 1086-1092.

Skempton, A.W. (1951). “The bearing capacity of clays.” Proc., British Building Research Congress, Vol. 1, 180-189.

Skempton, A.W. (1986). “Standard penetration test procedures and the effects in sand of overburden pressure, relative density, particle size, ageing, and overconsolidation.” Geotechnique, 36, 425-447.

Sladen, J.A. (1989). “Problems with interpretation of sand state from cone penetration test.” Geotechnique, 39(2), 323-332.

Sladen, J.A., D'Hollander, R.D., and Krahn, J. (1985a). “The liquefaction of sands, a collapse surface approach.” Canadian Geotechnical Journal, 22, 564-578.

Sladen, J.A., D'Hollander, R.D., Krahn, J., and Mitchell, D.E. (1985b). “Back analysis of the Nerlerk berm liquefaction slides.” Canadian Geotechnical Journal, 22, 579-588.

Sladen, J.A. and Handford, G. (1987). “A potential systematic error in laboratory testing of very loose sands.” Canadian Geotechnical Journal, 24, 462-466.

Sladen, J.A., D'Hollander, R.D., Krahn, J., and Mitchell, D.E. (1987). “Back analysis of the Nerlerk berm liquefaction slides: Reply.” Canadian Geotechnical Journal, 24, 179-185.

Sladen, J.A. and Hewitt, K.J. (1989). “Influence of placement method on the in situ density of hydraulic sand fills.” Canadian Geotechnical Journal, 26, 453-466.

Sladen, J.A. and Oswell, J.M. (1989). “The behaviour of very loose sand in the triaxial compression test.” Canadian Geotechnical Journal, 26, 103-113.

Spencer, E. (1967). “A method of analysis of the stability of embankments assuming parallel inter-slice forces.” Geotechnique, 17(1), 11-26.

Stark, T.D. and Mesri, G. (1992). “Undrained shear strength of liquefied sands for stability analysis.” Journal of Geotechnical Engineering, ASCE, 118(11), 1727-1747.

Stark, T.D. and Olson, S.M. (1995). “Liquefaction resistance using CPT and field case histories.” Journal of Geotechnical Engineering, ASCE, 121(12), 856-869.

Stark, T.D., Olson, S.M., Kramer, S.L., and Youd, T.L. (1998). “Shear strength of liquefied soils.” Proc., Workshop on Post-Liquefaction Shear Strength of Granular Soils, April 17-18, 1997, University of Illinois at Urbana-Champaign, Urbana, Illinois, 288 p. (Available only on the World Wide Web at http://mae.ce.uiuc.edu)

Stokoe, K.H., II, Andrus, R.D., Rix, G.J., Sanchez-Salinero, I., Sheu, J.C., and Mok, Y.J. (1988). “Field investigations of gravelly soils which did and did not liquefy during the 1983 Borah Peak, Idaho, earthquake.” Geotechnical Engineering Report. GR87-1, Civil Eng. Dept., University of Texas, Austin, 206 p.

Sully, J.P., Fernandez, A., and Zalzman, S. (1995). “Backanalysis of deformations for case histories involving flow-type failures.” Proc., 3rd International Conf. on Recent Advances in Geotechnical Earthquake Engineering and Soil Dynamics, April 2-7, St. Louis, MO, Vol. 1, 499-502.

Suzuki, Y., Tokimatsu, K., Koyamada, K., Taya, Y., and Kubota, Y. (1995). “Field correlation of soil liquefaction based on CPT data.” Proc., International Symposium on Cone Penetration Testing (CPT ’95), Vol. 2, Linköping, Sweden, October, 1995, 583-588.

Takeshita, S., Takeishi, M., and Tamada, K. (1995). “Static liquefaction of sands and its liquefaction index.” Proc., 1st International Conf. on Earthquake Geotechnical Engineering, Nov. 14-16, Tokyo, Japan, Vol. 1, 177-182.

Tatsuoka, F., Zhou, S., Sato, T., and Shibuya, S. (1990). Evaluation method of liquefaction potential and its application. Report on Seismic Hazards on the Ground in Urban Areas, Ministry of Education of Japan, Tokyo, 75-109 (in Japanese).

Terzaghi, K., Peck, R.B., and Mesri, G. (1996). Soil Mechanics in Engineering Practice, Third Edition. John Wiley & Sons, Inc., New York, 549 p.

Thevanayagam, S. (1998). “Effect of fines and confining stress on undrained shear strength of silty sands.” Journal of Geotechnical and Geoenvironmental Engineering, ASCE, 124(6), 479-491.

Thevanayagam, S., Ravishankar, K., and Mohan, S. (1996a). “Steady state strength, relative density and fines content relationship for sands.” Proc. Transportation Research Board Annual Meeting, January, Washington, D.C.

Thevanayagam, S., Wang, C.C., and Ravishankar, K. (1996b). “Determination of postliquefaction strength: steady state vs. residual strength.” Proc., Uncertainty in the Geologic Environment: From Theory to Practice, ASCE Geotechnical Special Publication No. 58, July 31-August 3, Madison, Wisconsin, Vol. 2, 1210-1224.

Tocher, D. (1959). “Seismographic results from the 1957 San Francisco earthquakes.” In Special Report 57, State of California Division of Mines, San Francisco, CA.

Tokimatsu, K. and Seed, H.B. (1987). “Evaluation of settlements in sands due to earthquake shaking.” Journal of Geotechnical Engineering, ASCE, 113(8), 861-878.

Tokimatsu, K., Kojima, H., Kuwayama, S., Alie, A., and Midorikawa, S. (1994). “Liquefaction induced damage to buildings in 1990 Luzon earthquake.” Journal of Geotechnical Engineering Division, ASCE, 120(2), 290-307.

Tsuchida, H. (1970). “Prediction and countermeasure against the liquefaction of sand deposits.” Abstract of the Seminar in the Port and Harbor Research Institute, 3.1-3.33.

Tuttle, M., Law, K.T., Seeber, L., and Jacob, K. (1990). “Liquefaction and ground failure induced by the 1988 Saguenay, Quebec, earthquake.” Canadian Geotechnical Journal, 27, 580-589.

U.S. Army Corps of Engineers. (1939). “Report on the slide of a portion of the upstream face of the Fort Peck Dam, Fort Peck, Montana.” United States Government Printing Office, Washington, D.C.

U.S. Army Corps of Engineers. (1949). “Report on investigation of failure of Sheffield Dam, Santa Barbara, California.” Office of the District Engineer, Los Angeles, California, June.

Uzuoka, R., Sento, N., and Kazama, M. (2005). “Numerical analysis of rate-dependent reaction of pile in saturated or liquefied soil,” Seismic Performance and Simulation of Pile Foundations in Liquefied and Laterally Spreading Ground, R.W. Boulanger and K. Tokimatsu, eds., Geotechnical Special Publication No. 145, ASCE, 204-217.

Vaid, Y.P. and Chern, J.C. (1983). “Effect of static shear on resistance to liquefaction.” Soils and Foundations, 23(1), 47-60.

Vaid, Y.P. and Chern, J.C. (1985). “Cyclic and monotonic undrained response of saturated sands.” in Advances in the Art of Testing Soils under Cyclic Conditions, V.Khosla, ed., ASCE, New York, 120-147.

Vaid, Y.P., Chung, E.F.K., and Kuerbis, R.H. (1990). “Stress path and steady state,” Canadian Geotechnical Journal, 27(1), 1-7.

Vaid, Y.P. and Thomas, J. (1995). “Liquefaction and post-liquefaction behavior of sand.”

Journal of Geotechnical Engineering, ASCE, 121(2), 163-173.

Vaid, Y.P. and Sivathayalan, S. (1996). “Static and cyclic liquefaction potential of Fraser Delta sand in simple shear and triaxial tests.” Canadian Geotechnical Journal, 33(2), 281- 289.

Vaid, Y.P., Sivathayalan, S., and Stedman, D. (1998). ‘Influence of specimen reconstituting method on the undrained response of sand.” submitted to ASTM Geotechnical Testing Journal.

Vaid, Y.P., Sivathayalam, S., and Stedman, D. (1999). “Influence of specimen reconstituting method on the undrained response of sand,” Geotechnical Testing Journal, ASTM, 22(3), 187-195.

Vasquez-Herrera, A. and Dobry, R. (1989). “Re-evaluation of the Lower San Fernando Dam: Report 3, the behavior of undrained contractive sand and its effect on seismic liquefaction flow failures of earth structures.” U.S. Army Corps of Engineers Contract Report GL-89-2, U.S. Army Corps of Engineers Waterways Experiment Station, Vicksburg, Mississippi.

Verdugo, R. (1992). “Characterization of sandy soil behavior under large deformation.” Ph.D. Thesis, Dept. of Civil Engineering, University of Tokyo, Japan.

Verdugo, R., Castillo, P., and Briceño, L. (1995). “Initial soil structure and steady state strength.” Proc., 1st International Conf. on Earthquake Geotechnical Engineering, Nov. 14- 16, Tokyo, Japan, Vol. 1, 209-214.

Verdugo, R. and Ishihara, K. (1996): "The steady state of sandy soils," Soils and Foundations, Vol. 36, No. 2, pp. 81-92.

Wang, C. (2003). Prediction of the residual strength of liquefied soils. (Doctoral Dissertation, University of Washington).

Wang, W. (1984). “Earthquake damages to earth dams and levees in relation to soil liquefaction.” Proc., International Conference on Case Histories in Geotechnical Engineering, St. Louis, MO.

Willis, B. (1925). “A study of the Santa Barbara earthquake of June 29, 1925.” Bulletin, Seismological Society of America, 15(4), 255-278.

Wride (Fear), C.E. (1996). “In situ testing for liquefaction evaluation of sandy soils.” Ph.D. Thesis, University of Alberta, Edmonton, Alberta.

Wride (Fear), C.E., McRoberts, E.C., and Robertson, P.K. (1999). “Reconsideration of case histories for estimating undrained shear strength in sandy soils.” Canadian Geotechnical Journal, 36, 907-933.

Wride, C.E. (Fear), Hofmann, B.A., Sego, D.C., Plewes, H.D., Konrad, J.-M., Biggar, K.W., Robertson, P.K., and Monahan, P.A. (2000). “Ground sampling program at the CANLEX test

sites," Canadian Geotechnical Journal, 37(3), pp. 530-542.

Wright, S.G. (1992). UTEXAS3: A computer program for slope stability calculations. Geotechnical Engineering Software GS86-1, Dept. of Civil Engineering, University of Texas, Austin.

Wu, J. (2003). "Liquefaction Triggering and Post Liquefaction Deformations of Monterey 0/30 Sand Under Uni-Directional Cyclic Simple Shear Loading." Dissertation in partial fulfillment for the degree of doctor of philosophy, University of California, Berkeley.

Yamada, G. (1966). "Damage to earth structures and foundations by the Niigata earthquake June 16, 1964, in JNR." Soils and Foundations, 6(1), 1-13.

Yamamuro, J.A. and Lade, P.V. (1997). "Static liquefaction of very loose sands." Canadian Geotechnical Journal, 34, 905-917.

Yamamuro, J.A. and Lade, P.V. (1998). "Steady-state concepts and static liquefaction of silty sands." Journal of Geotechnical and Geoenvironmental Engineering, ASCE, 124(9), 868-877.

Yashima, A., Oka, F., Konrad, J.M., Uzuoka, R., and Taguchi, Y. (1997). "Analysis of a progressive flow failure in an embankment of compacted till." Proc., Deformation and Progressive Failure in Geomechanics, Vol. 1, 599-604.

Yasuda, S. et al. (1993). "Mechanical properties of soil where ground failure occurred during the Kushiro-oki earthquake." Proc., 22nd JSCE Earthquake Engineering Symposium, 395-398.

Yegian, M.K., Ghahraman, V.G., and Harutinunyan, R.N. (1994). "Liquefaction and embankment failure case histories, 1988 Armenia earthquake." Journal of Geotechnical Engineering, ASCE, 120(3), 581-596.

Yoshimi, Y., Hatanaka, M., and Oh-Oka, H. (1978). "Undisturbed Sampling of Saturated Sands by Freezing," Soils and Foundations, Japanese Society of Soil Mechanics and Foundation Engineering, Tokyo, Japan,18(3), pp 59-73.

Yoshimine, M. and Ishihara, K. (1998). "Flow potential of sand during liquefaction." Soils and Foundations, 38(3), 189-198.

Yoshimine, M., Robertson, P.K., and Wride (Fear), C.E. (1999). "Undrained shear strength of clean sands to trigger flow liquefaction." Canadian Geotechnical Journal, 36(5), 891-906.

Yoshimine, M. (2003). "Liquefied soil-pile interaction and its rate effects," First Japan-U.S. Workshop on Testing, Modeling, and Simulation in Geomechanics, Boston

Youd, T.L. and Bennett, M.J. (1983). "Liquefaction sites, Imperial Valley, California." Journal of Geotechnical Engineering Division, ASCE, 109(3), 440-457.

Youd, T. L., Harp, E. L., Keefer, D. K., & Wilson, R. C. (1985). The Borah peak, Idaho earthquake of October 28, 1983-liquefaction. Earthquake spectra, 2(1), 71-89.

Youd, T.L. (1995). “Liquefaction-induced lateral ground displacement.” Proc., 3rd International Conf. on Recent Advances in Geotechnical Earthquake Engineering and Soil Dynamics, April 2-7, St. Louis, MO, Vol. 2, 911-925.

Youd, T.L. and I.M. Idriss (1997). “Summary report.” Proc., NCEER Workshop on Evaluation of Liquefaction Resistance of Soils, NCEER-97-0022, 1-40.

Youd, T.L., I. M. Idriss, Ronald D. Andrus, Ignacio Arango, Gonzalo Castro, John T. Christian, Richardo Dobry, W. D. Liam Finn, Leslie F. Harder Jr., Mary Ellen Hynes, Kenji Ishihara, Joseph P. Koester, Sam S. C. Liao, William F. Marcuson III, Geoffrey R. Martin, James K. Mitchell, Yoshiharu Moriwaki, Maurice S. Power, Peter K. Robertson, Raymond B. Seed, and Kenneth H. Stokoe II. (2001). “Liquefaction Resistance of Soils: Summary Report from the 1996 NCEER and 1998 NCEER/NSF Workshops on Evaluation of Liquefaction Resistance of Soils.” Journal of Geotechnical and Geoenvironmental Engineering, 124(10).

Youd, T. L., Hansen, C. M., and Bartlett, S. F. (2002). “Revised Multilinear Regression Equations for Prediction of Lateral Spread Displacement”, Journal of Geotechnical and Geoenvironmental Engineering, Vol. 128, No. 12, pp. 1007-1017.

Zlatovic, S. and Ishihara, K. (1995). “On the influence of nonplastic fines on residual strength.” Proc., 1st International Conf. on Earthquake Geotechnical Engineering, Nov. 14- 16, Tokyo, Japan, Vol. 1, 239-244.

Zhang, H. and Garga, V.K. (1997). “Quasi-steady state: a real behavior?” Canadian Geotechnical Journal, 34, 749-761.

Appendix A

Back-Analyses of Class A and Class C Liquefaction Failure Case Histories

Class A Case Histories:

A.1: Wachusset Dam
A.2: Fort Peck Dam
A.13: Route 292 Embankment

A.1 North Dike of Wachusett Dam (Massachusetts, USA)

A.1.1 Brief Summary of Case History Characteristics

Name of Structure	Wachusett Dam
Location of Structure	Massachusetts, USA
Type of Structure	Poorly compacted earthen dam
Date of Failure	April 11, 1907
Nature of Failure	Non-seismic, during initial reservoir filling
Approx. Maximum Slope Height	88 ft.

A.1.2 Introduction and Description of Failure

The best description and summary of field data regarding the failure of the North Dike of Wachusett Dam is presented by Olsen et al. (2000), and the description here is based largely on Olsen et al. (2000) and Olsen (2001). GZA GeoEnvironmental (1991) performed geotechnical studies of the dam to investigate seismic stability of the North Dike, and Haley & Aldrich (1984a,b) also performed geotechnical studies of the North Dike.

Construction of the dike began in 1898 with the excavation of cut-off trenches in the foundation. Backfilling of these cut-of trenches occurred in 1902 and 1902. These cut-off trenches were not involved in the failure. Construction of the main dike embankment began in 1902, and fill placement for the North Dike was completed in 1904, approximately three years prior to the slope failure.

A slope failure occurred on the upstream side of the North Dike embankment on April 11, 1907, during initial filling of the reservoir. Figures A.1.1 and A.1.2 show pre-failure and post-failure cross-sections through the failure zone (Olsen et al, 2000). The failure was centered over the former river channel, at the location of the maximum height embankment section where the dam reached a height of approximately 24.4 m (80 ft). The reservoir had risen to an elevation approximately 40 feet below the crest of the embankment when the failure occurred. The zone of likely "jetting" shown in Figure A.1.2 refers to "jetting" that was performed during the post-failure slope repair to try to inter-mix (and knit) the repair fill and the slope scarp. This "jetting" occurred after the failure, and is not pertinent to the back-analyses of the failure.

Olsen et al. postulate that the cause of the failure was reduction in effective stress along the base of the failure mass due to increasing buoyancy as the reservoir filled, while there was a commensurate (but lesser) reduction in driving shear stresses along this failure surface as much of the embankment fill remained above the reservoir level. It is suggested here that a more likely cause would have been wetting-induced "collapse" of the very loose, cohesionless soils comprising the upstream shell. As discussed a bit later, saturation (wetting) was employed to "compact" the similar downstream shell fill materials, and this was observed to produce volumetric reductions of approximately 6% to 12% as each lift was saturated. No similar "saturation" was applied during placement of lifts of the upstream shell, and so there

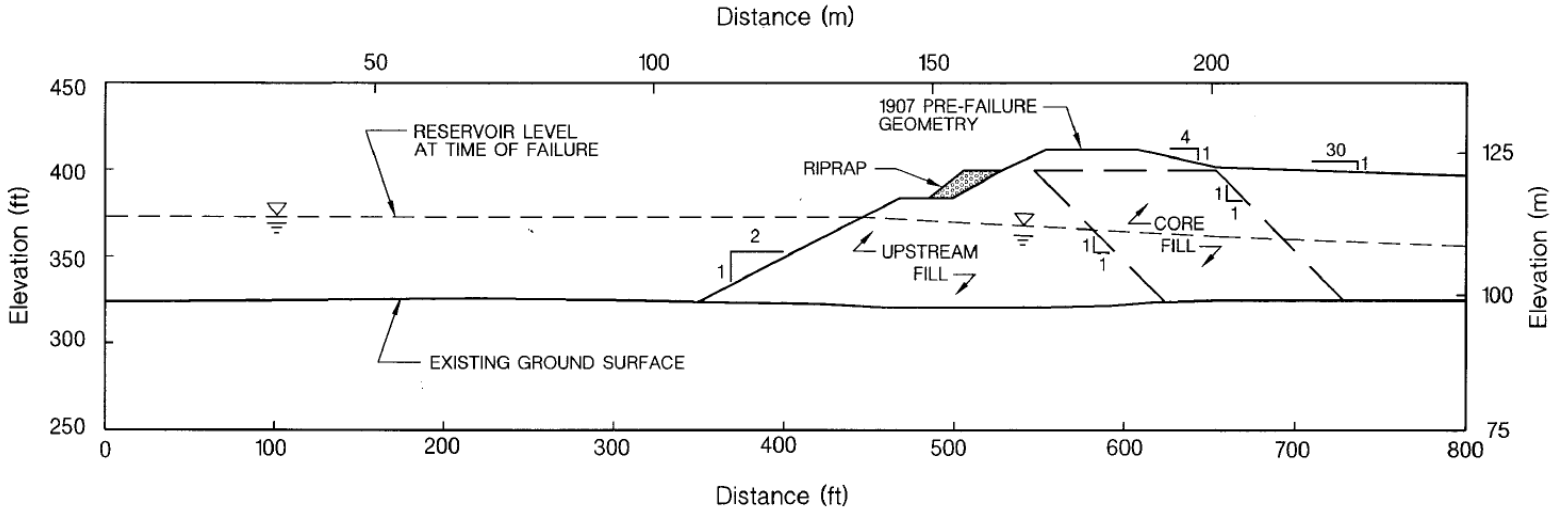

Figure A.1.1: Pre-failure cross-section of the North Dike of Wachusett Dam at Station 23+20 (from Olsen et. al, 2000)

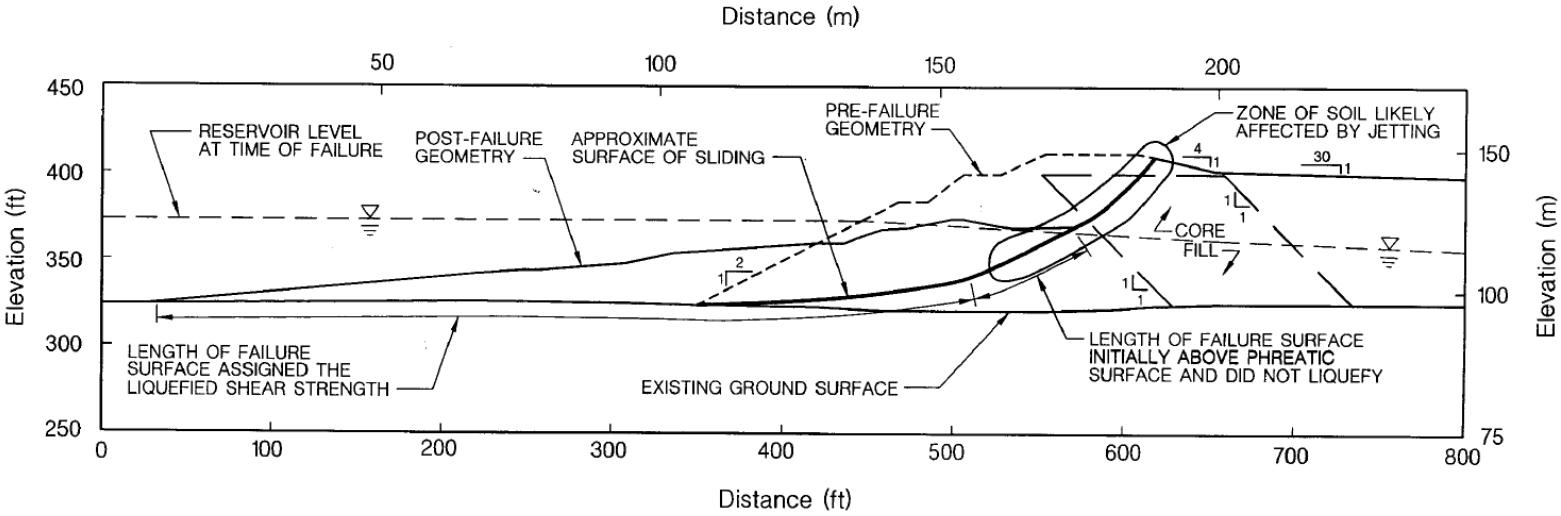

Figure A.1.2: Post-failure cross-section of the North Dike of Wachusett Dam at Station 23+20, showing the approximate location of the apparent sliding surface (from Olsen et. al, 2000)

is a high likelihood that significant wetting-collapse would have occurred as the reservoir was filled for the first time. Regardless of the actual details of the triggering of the failure, the ensuing flow-type failure can be safely judged to have been initiated "statically", with no cyclic or dynamic triggering forces. As shown in Figures A.1.1 and A.1.2, movements of the failure mass into the reservoir were large.

The failed zone of the Dike was rebuilt in 1907, and the reservoir was re-filled without incident.

Foundation soils beneath the dike are comprised mainly of dense to very dense sands, gravels and non-plastic silts. A large portion of the fill soils for the embankment's shell zones consisted of fine sands, which were spoils from the excavation of the cut-off trenches into these foundation soils. Materials for the core were also stripped from the reservoir, and consisted of sandy silt to silty sand.

As shown in Figure A.1.1, the core was approximately 100 feet in width, with slopes of 1:1 towards the upstream direction on both the upstream and downstream sides of the core zone. The core soils were placed in lifts of approximately 6 inches, and were rolled by horse drawn carts. No direct measurements of the resulting unit weights of the core materials were made during construction, but more recent investigations indicate that current unit weights are on the order of 120 to 130 lbs/ft^3.

The downstream shell consists of sand to silty sand, with some gravel. As shown in Figure A.1.1, the downstream face has a slope of 4:1 near the crest, but the rest of the downstream face is sloped at 30:1 towards Coachlace Pond. The downstream shell soils were reportedly placed in lifts of approximately 7 to 8 foot lifts, and were "compacted" by flooding with water. Approximately 6 to 12 inches of settlement was observed following saturation of each lift. Further details of the downstream shell zone are not pertinent to these current analyses, as the downstream shell zone was not involved in the failure.

The upstream shell also consists of sand to silty sand with some gravel. Fines contents were low, typically on the order of approximately 5% to 10%, though some soils had somewhat higher fractions of largely non-plastic fines. Unlike the downstream shell, the upstream shell received neither compaction nor flooding with water during construction. As a result, the upstream shell was in a very loose condition, and likely prone to some degree of volumetric "collapse" upon initial wetting during the first filling of the reservoir. The slope of the upstream face was relatively steep at 4:1, with a bench near the crest, and with riprap on the upstream face above this bench.

A.1.3 Initial Yield Stress Analyses

Figure A.1.3(a) shows the cross-section used for back-analyses of the post-liquefaction initial yield strength $S_{r,yield}$ that would be required within the liquefied upstream shell materials to produce a calculated Factor of Safety equal to 1.0. This is not the actual post-liquefaction strength, but it proves to be useful in developing a number of charts and relationships for these overall studies.

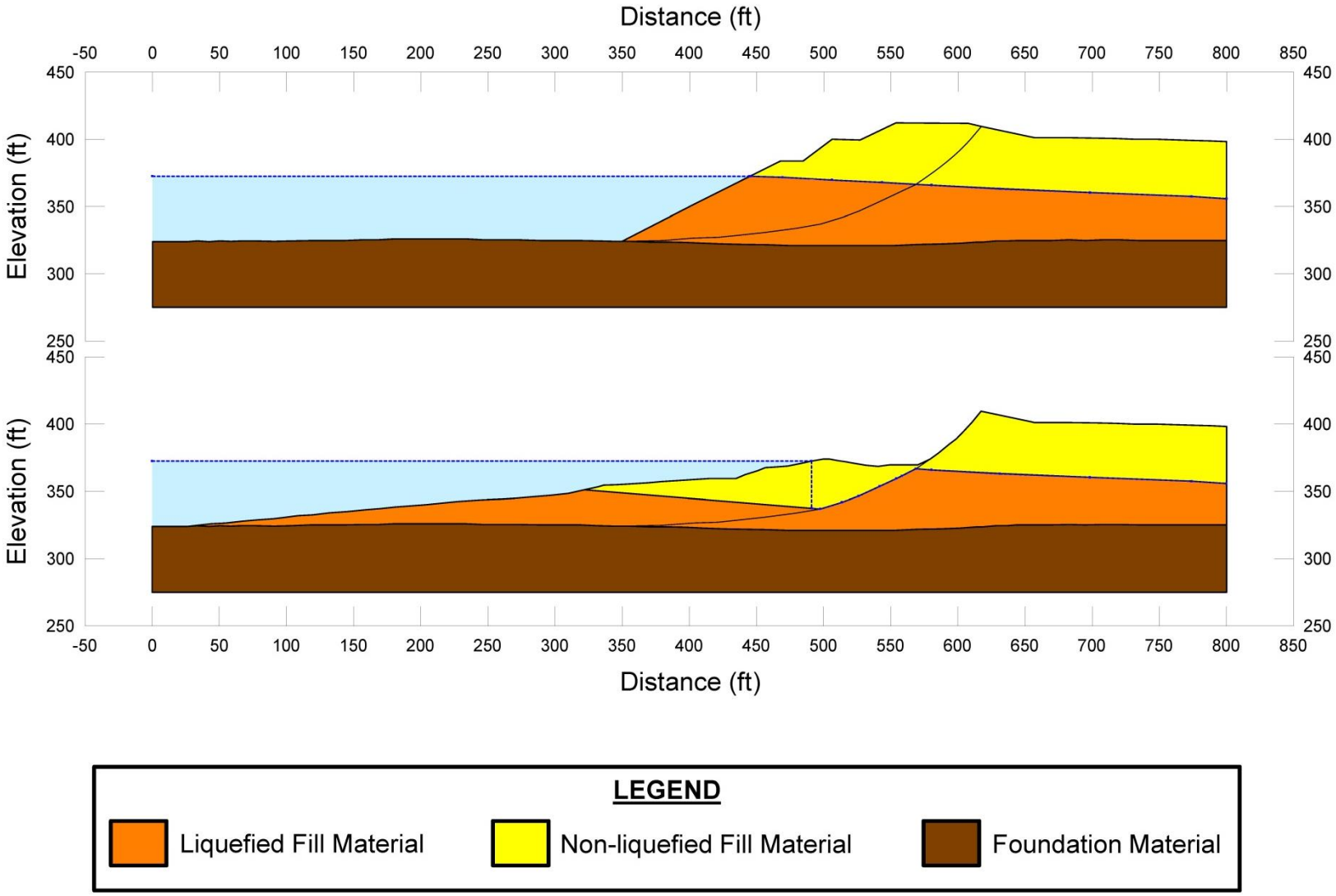

Figure A.1.3: Wachusett Dam at Station 23+20: (a) Pre-failure geometry and best-estimate failure surface for initial yield stress analyses, and (b) post-failure geometry and best-estimate failure surface for post-failure residual geometry analyses.

Figure A.1.3(a) also shows the best estimate failure surface. The failure surface is relatively well constrained at the back heel by the observable failure scarp. The precise location of the failure surface at the base of the failure is uncertain, but the most critical failure surfaces in terms of lowest Factor of Safety for a giver value of strength within the liquefied shell fill materials are those that go right to the bottom of the fill. The potential depths are then constrained by the very dense foundation soils. Additional analyses were performed, varying this failure surface; the shape at the lower back heel was varied, and the failure surface was allowed to occur at various elevations slightly above the base of the shell fill. These variations were performed to evaluate sensitivity of the resulting calculated values of $S_{r,yield}$.

Shear strength of the non-saturated, loose sand to silty shell and crest fill materials was modeled as frictional, with Ø´ = 30°. Unit weights of non-saturated shell and crest fills were taken as 111 lbs/ft^3. Shear strength of the moderately compacted, non-saturated sandy silt to silty sand of the upper "core" zone through which part of the failure surface passes was modeled with Ø´ = 30°. A unit weight of 111 lbs/ft^3 was modelled for these non-saturated "core" materials.

The saturated portions of the upstream shell were considered to be potentially liquefiable, and shear strengths of portions of potential failure surfaces were modeled with post-liquefaction yield strength $S_{r,yield}$. $S_{r,yield}$ was modeled as uniform along any potential failure surface, and the calculation of the value of $S_{r,yield}$ was the primary objective of these analyses.

Permeabilities of the upstream shell zone were relatively high, and permeabilities of the siltier core zone are lower than those of the upstream shell. Accordingly, it is assumed that the phreatic surface on the upstream side of the core equilibrate relatively rapidly with reservoir elevation increase during the first filling in 1907. The phreatic surface within the core zone, and further downstream during this first reservoir filling cannot be estimated with similar confidence, but this is not important because the failure occurred to the upstream side of the potentially saturated portions of the core.

For the best estimate geometry, conditions, and failure surface described above and shown in Figure A.1.3, the resulting value of post-liquefaction yield strength was found to be $S_{r,yield}$ = 829 lbs/ft^2. Sensitivity analyses were then performed, varying the details and location (at depth) of the failure surface, unit weights, and friction angles for the non-liquefied upper crest and non-liquefied upper core zones. These analyses suggested that there was little likelihood that this failure would have proceeded in an incrementally progressive manner, and so this failure was modeled only as a monolithic event, with the full eventual sliding mass beginning to move largely coherently at the inception of failure. The resulting range of values of $S_{r,yield}$ for combinations of modeling assumptions and details considered to be reasonable was found to be $S_{r,yield} \approx$ 752 to 909 lbs/ft^3.

Olsen (2001) also performed back-analyses to determine $S_{r,yield}$. Failure surfaces analyzed were similar. Olsen reported values of $S_{r,yield} \approx$ 37.6 to 41.9 kPa (784 to 875 lbs/ft^3).

A.1.4 Residual Strength Analyses Based on Residual Geometry

The calculation of the "apparent" post-liquefaction strength ($S_{r,resid/geom}$) required to produce a calculated Factor of Safety equal to 1.0 based on residual geometry is illustrated in Figure A.1.4. This figure shows the phreatic surface, and the failure surface, used to calculate the best-estimate value of $S_{r,resid/geom}$, based on the best estimate modeling parameters as described in the previous section. An additional detail here is the shear strength modeled at the base of the portion of the upstream toe of the embankment that traveled out into the reservoir. This was the first filling of the reservoir, so there were no loose reservoir sediments accumulated yet at the upstream toe. There may have been some hydroplaning, however, as the embankment materials moved rapidly into the reservoir. The incremental inertial analyses presented in Section A.1.4 that follows indicate that the maximum velocity was on the order of approximately 14.3 ft/sec, and the velocity during most of the run-in was lower. As discussed, it is not possible to fully accurately determine the degree of hydroplaning that would have occurred. The best estimate analysis of $S_{r,resid/geom}$ was performed assuming that shear strength at the base of the embankment materials that entered into the reservoir was 100% of $S_{r,resid/geom}$. The resulting best estimate calculated value of "apparent" post-liquefaction strength based on post-failure residual geometry was $S_{r,resid/geom} \approx 81$ lb/ft^2.

Variations were then made in parameters, and in location of the pre-failure phreatic surface, as was described in the preceding section in order to evaluate uncertainty or variability. Varying degrees of potential hydroplaning were also modeled, with the average shear strength at the base of the portion of the failure mass that entered the reservoir being modeled as varying from a low of 20% of $S_{r,resid/geom}$ to a high of 100% of $S_{r,resid/geom}$. Considering ranges of variations in modeling details and parameters considered to be reasonable, the resulting likely range of post-liquefaction strength required to provide a calculated Factor of Safety equal to 1.0 based on residual geometry was considered to be $S_{r,resid/geom} \approx 71$ to 87 lb/ft^3.

Olsen (2001) also calculated post-liquefaction strength required to produce a calculated Factor of Safety equal to 1.0 based on residual geometry, and reported a best estimate value of $S_{r,resid/geom} \approx 3.8$ kPA (79 lb/ft^3). No range was reported.

A.1.5 Incremental Momentum Back-Analyses and Overall Estimates of S_r

Incremental inertial back-analyses were performed using the same sets of properties and geometries (including failure surfaces and phreatic surfaces) as described in the previous sections.

Figure A.1.5 shows the best-estimate progressive incremental inertial analysis, showing the five stages of geometry evolution modeled as the failure proceeds. Figure A.1.6 shows the associated calculations of (1) acceleration vs. time, (2) velocity vs. time, and (3) displacement of the overall center of gravity vs. time. The resulting best estimate value of post-liquefaction strength was $S_r = 294$ lb/ft^3.

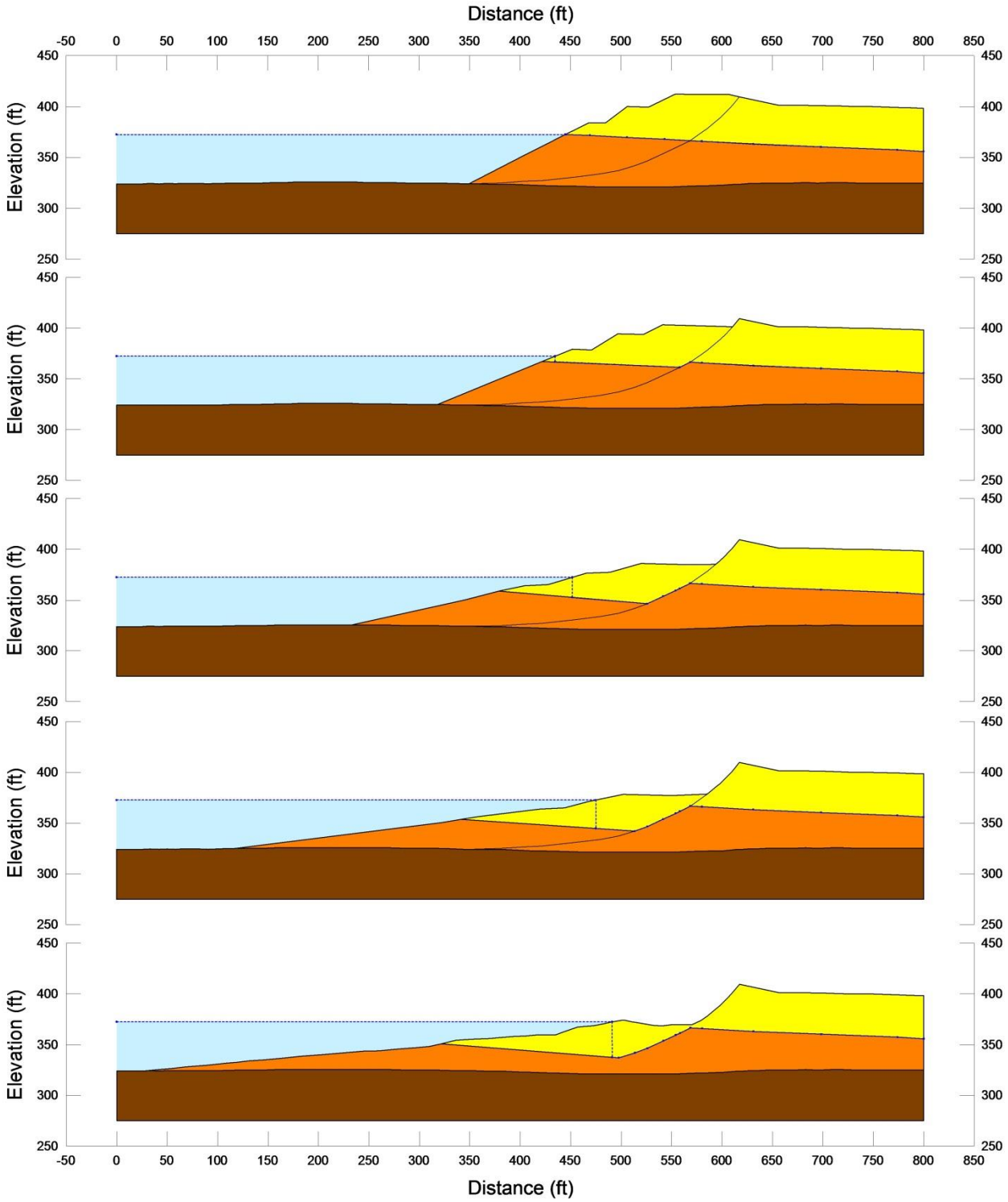

Figure A.1.5: Incremental inertial analysis of the failure of the North Dike of the Wachusetts Dam, showing progressive evolution of cross-section geometry modeled

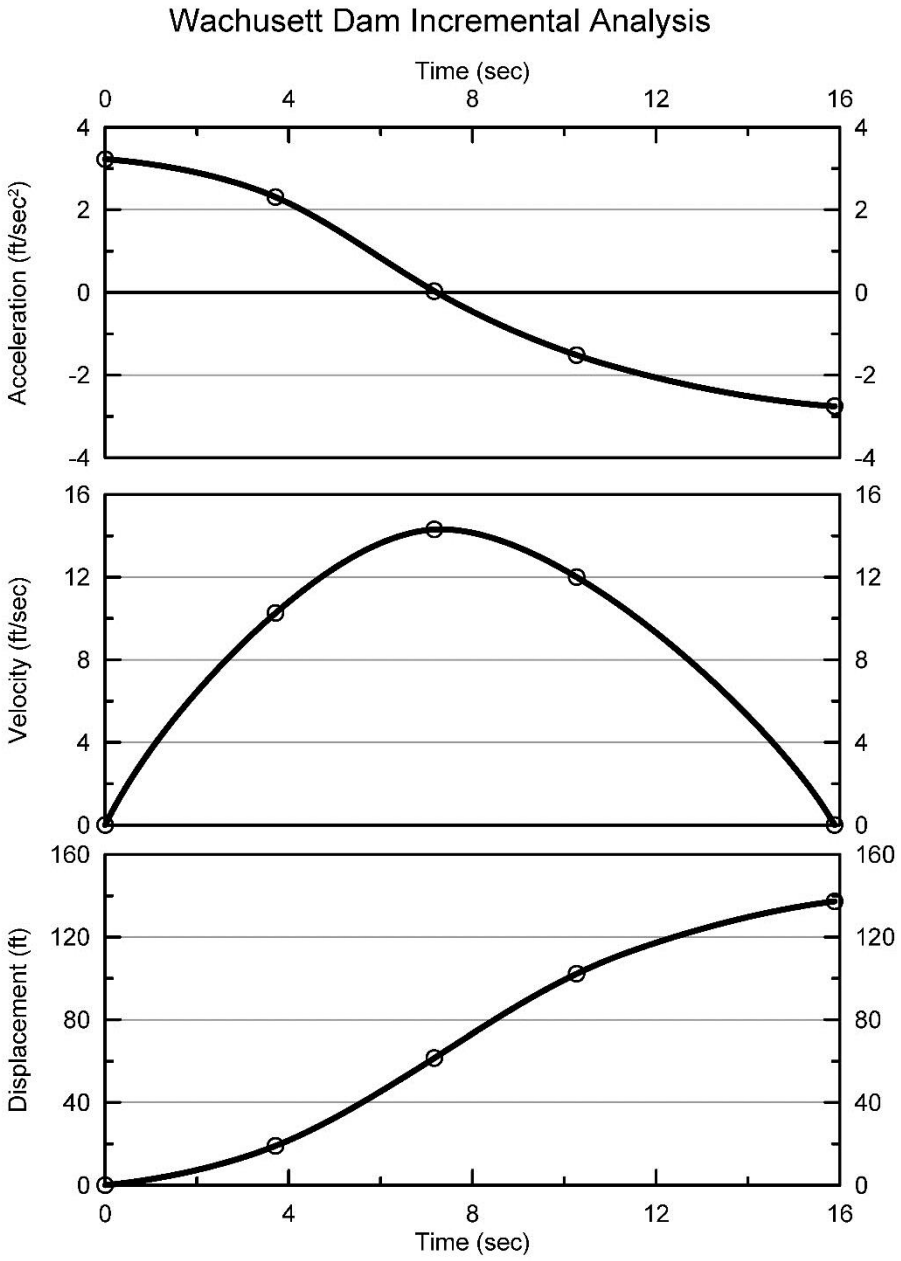

Figure A.1.6: Incremental inertial analysis of the failure of the North Dike of the Wachusetts Dam, showing progressive evolution of: (1) acceleration vs. time, (2) velocity vs. time, and (3) displacement vs. time of the overall center of gravity of the failure mass

The main sources of uncertainty, or variability, in back-calculated values of S_r were (1) frictional strengths of the non-liquefied embankment fill materials, (2) degree of potential hydroplaning as the failure mass entered into the reservoir, (3) the precise location and shape of the failure plane at depth, and (4) unit weights.

Based on all analyses performed, and the considerations discussed, the overall best estimate value of post-liquefaction strength for the failure of the North Dike of Wachusett Dam was judged to be $S_r \approx 294$ lbs/ft^3, with a likely range of $S_r \approx 236$ to 360 lbs/ft^3. Based on the factors contributing to uncertainty or variance for this case history, it was the judgment of the investigation team that this range represented approximately ± 2 standard deviations. This range of variance is not symmetrical about the best estimate value, so minor further adjustments were made to produce a representative estimate of S_r suitable for regression analyses.

Overall, based on an assumed normal distribution, it was judged that the (mean and median) best estimate of post-liquefaction strength for this case history is

$$\overline{S_r} = 294 \text{ lbs/ft}^3$$

and that the best estimate of standard deviation of mean overall post-liquefaction strength is

$$\sigma_{\overline{S}} = 31 \text{ lbs/ft}^3$$

Wachusetts Dam was more recently developed as a case history than most of the other cases considered in these studies, and it has not been back-analyzed by many investigators. Olsen (2001) and Olsen and Stark (2002) present one set of results, and Wang (2003) and Kramer (2008) present a second set of results. Interestingly, both the Olsen/Stark and Wang/Kramer efforts specifically account analytically for inertial effects. Olsen (2001) and Olsen and Stark (2002), reported a best estimate value of $S_r = 16.0$ kPa (335 lbs/ft^2), based on their inertial displacement analyses that considered kinetics, and a range of $S_r = 10.4$ to 19.1 kPa (217 to 400 lbs/ft^3). Wang (2003) and Wang and Kramer (2008) employed their zero inertial force (ZIF) method to incorporate inertial effects in their back-analyses of this failure, and they developed estimates of both mean $\overline{S_r} = 348.0$ lbs/ft^2 as well as the associated standard deviation $\sigma_{\overline{S}} = 74.8$ lbs/ft^2. The details of their analyses, and the cross-sections and failure mass assumptions employed, are not presented and so cannot be checked.

This is an unusually well-defined case history, and the three sets of back-analyses that analytically incorporate inertial effects are all in good agreement.

A.1.6 Evaluation of Initial Effective Vertical Stress

Average initial (pre-failure) effective vertical stress was assessed for the liquefied zones of each of the failure surface shown in Figure A.1.3. Additional sensitivity analyses were then performed for reasonable ranges of variations in (1) the location of the phreatic surface, (2) unit weights, and (3) the precise location of the overall failure surface in order to evaluate uncertainty or variance.

The resulting best estimate of average pre-failure effective stress within the liquefied materials controlling the failure was then $\sigma_{vo}' \approx 3{,}142$ lb/ft^3, with a reasonable range of $\sigma_{vo}' \approx$ 2,886 to 3,414 lbs/ft^3. This range is slightly non-symmetric about the median value, and this range was judged by the engineering team to represent approximately ± 2 standard deviations. Overall, the best characterization of initial (pre-failure) average effective vertical stress was then taken to be represented by a mean value of

$$\overline{\sigma'_{vo}} \approx 3{,}142 \text{ lbs/ft}^3$$

and with a standard deviation of

$$\sigma_{\overline{\sigma}} \approx 132 \text{ lbs/ft}^3$$

Estimates of σ_{vo}' were also reported by Olsen and Stark and by Wang and Kramer, and these are shown in Table A.1.1(c). Average initial vertical effective stresses were not directly reported by Olsen (2001) and Olsen and Stark (2002), but they can be inferred from their reported values of S_r and S_r/P to have been on the order of approximately $\sigma_{vo}' \approx 3{,}158$ lb/ft^3. Similarly, Wang (2003) and Kramer (2008) also do not directly report calculated values of average initial vertical effective stresses, but they can be inferred from their reported values of S_r and S_r/P to have been on the order of approximately $\sigma_{vo}' \approx 2{,}559$ lb/ft^3. Wang (2003) presents no detailed cross-section for his analyses, so it is not possible to know why his estimated value of σ_{vo}' is slightly lower than the values calculated by Olsen and Stark and in these current studies.

A.1.7 Evaluation of $N_{1,60,CS}$

The field investigations reported by GZI Environmental (1991) and by Haley & Aldrich (1984a,b) included six SPT borings at the reconstructed failure section at Station 23+20. These are shown in Figure A.1.7. All of the borings were advanced by rotary wash boring, and a donut hammer with rope and cathead was used to drive the SPT samplers. It is assumed that the SPT hammer energy ration was approximately 45%. Thirty of the SPT's were performed in the upstream shell materials involved in the 1907 flow failure. Thirteen of these were performed near to the apparent shear failure surface, and these are shown with open circles in Figure A.1.7. A source of uncertainty, therefore, is how to weight the SPT blowcounts apparently "near" the failure surface vs. the rest of the SPT blowcounts in the upstream shell material. In these current studies, equal weighting was given to the thirteen blowcounts near the failure zone vs. the full ensemble of blowcounts in the upstream shell materials (assuming that variation is random, and that blowcounts might be distributed differently at nearby locations).

Corrections for effective overburden stress (C_N) were made using the relationships proposed by Deger (2014), as presented and discussed in Section C.1.1. Corrections for fines content were made using the relationship proposed by Cetin et al. (2004), and a representative fines content of approximately 5% to 10%; resulting in a null to minor fines adjustment. The resulting median $N_{1,60,CS}$ value for the thirteen SPT tests near to the failure surface was found to

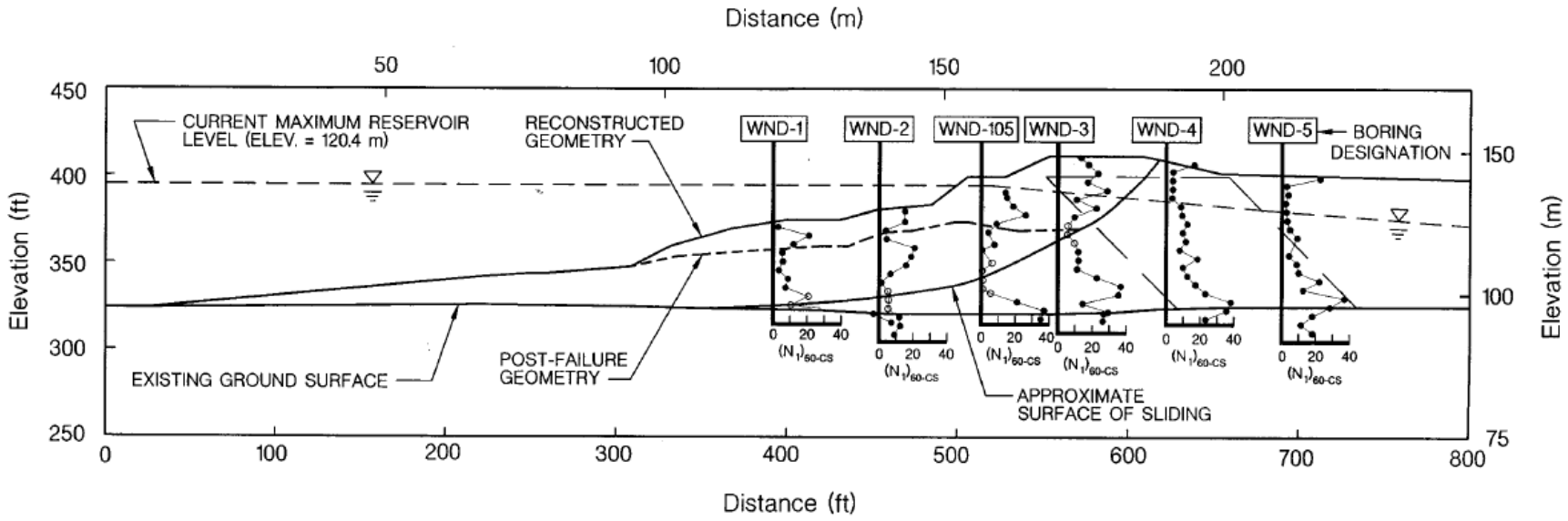

Figure A.1.7: Reconstructed cross-section of the North Dike of Wachusetts Dam showing the locations and results of recent standard penetration tests (from Olsen et al., 2000)

be approximately 8 blows/ft, and the median value for the full ensemble of SPT blowcounts (including the thirteen near the failure surface) was found to be approximately 7.5 blows/ft. The resulting best estimate median $\overline{N_{1,60,CS}}$ value for these current studies is then taken as $\overline{N_{1,60,CS}} \approx$ 7.5 blows/ft. Variance of $\overline{N_{1,60,CS}}$ was estimated primarily on the basis of the perceived uncertainties associated with the (1) the use of blowcounts from within the failure zone, (2) likely increases in blowcounts over time since the failure (the fill had been only recently placed at the time of the failure)the perceived high level of variability among the SPT data available. It appears unlikely that jetting of the interface between the failure scarp and the repair fill would have adversely affected these SPT data. Considering all of these, the representation of uncertainty in the representative median value of $\overline{N_{1,60,CS}}$ was taken as $\sigma_{\overline{N}} \approx 1.7$ blows/ft.

Table A.1.1(b) shows values of representative $N_{1,60}$ or $N_{1,60,CS}$ values developed by two other teams of investigators, and variance or standard deviations in these representative values if available. Olsen and Stark (2001, 2002) developed an estimated representative value of $N_{1,60} = 7$ blows/ft, but for this case history they proposed no range. Wang (2003) and Kramer (2008) jointly developed a representative value of $\overline{N_{1,60,CS}} = 7.3$ blows/ft, and their estimated standard deviation of that overall mean value for this case history was $\sigma_{\overline{N}} = 1.8$ blows/ft. Details of the development of this interpretation by Wang and Kramer are not presented. Overall agreement between the three independent assessments of representative $\overline{N_{1,60,CS}}$ values is excellent, and variance or uncertainty in $\overline{N_{1,60,CS}}$ appears to be relatively low.

A.1.8 Additional Indices from the Back-Analyses

A number of additional results, and indices, can be extracted from the analyses performed. Some of these are useful in developing some of the over-arching relationships and figures presented in the main text of this report. These values are presented in Table A.1.2.

Table A.1.1: Representative values for the North Dike of Wachusetts Dam case history of: (a) post-liquefaction strength (S_r), (b) initial vertical effective stress (σ_{vo}'), and (c) $N_{1,60,CS}$ developed by various investigation teams, and estimates of variance in each of these indices when available.

(a) Post-Liquefaction Strength:	
Olsen (2001) and Olsen and Stark (2002)	S_r = 335 psf, and range = 217 to 399 psf
Wang (2003) and Kramer (2008)	$\overline{S_r}$ = 348.0 psf, and $\sigma_{\overline{S}}$ = 74.8 psf
This Study	$\overline{S_r}$ = 294 psf and $\sigma_{\overline{S}}$ = 31 psf
(b) Representative $N_{1,60}$ or $N_{1,60,CS}$ Value:	
Olsen (2001) and Olsen and Stark (2002)	$N_{1,60}$ = 7 bpf
Wang (2003) and Kramer (2008)	$\overline{N_{1,60,CS}}$ = 7.3 bpf, and $\sigma_{\overline{N}}$ = 1.9 bpf
This Study	$\overline{N_{1,60,CS}}$ = 7.5 bpf, and $\sigma_{\overline{N}}$ = 1.6 bpf
(c) Representative Initial Vertical Effective Stress:	
Olsen (2001) and Olsen and Stark (2002)	Not reported, but can be inferred from reported S_r/P ratio to be $\sigma_{vo}' \approx$ 1,030 psf. Likely range is not provided.
Wang (2003) and Kramer (2008)	Not reported, but can be inferred from reported S_r/P ratio to be $\sigma_{vo}' \approx$ 1,044 psf. Variance or standard deviation is not provided.
This Study	$\overline{\sigma'_{vo}}$ = 3,142 psf, and $\sigma_{\overline{\sigma}}$ = 132 psf

Table A.1.2: Additional results and indices from the analyses of the North Dike of Wachusetts Dam failure case history.

Maximum distance traveled by the center of gravity of the overall failure mass	137.3 ft.
Initial post-liquefaction Factor of Safety prior to displacement initiation, and based on best estimate value of S_r	FS = 0.47
Final post-liquefaction Factor of Safety at final (residual) post-failure geometry, and based on best estimate value of S_r	FS = 3.43

A.2 Fort Peck Dam (Montana, USA)

A.2.1 Brief Summary of Case History Characteristics

Name of Structure	Fort Peck Dam
Location of Structure	Montana, USA; Missouri River
Type of Structure	Hydraulic Fill Dam
Date of Failure	September 22, 1938
Nature of Failure	Static, During Construction
Approx. Maximum Slope Height	196 ft.

A.2.2 Introduction

The Fort Peck Dam embankment failed during construction on September 22, 1938. This failure was well-investigated, and details of the initial failure, investigations of that failure, and the repair (reconstruction) operations are well documented by the U.S Army Corps of Engineers (1939, 1976), Middlebrooks (1942), Casagrande (1965, 1976), Marcuson and Krinitsky (1976), and Marcuson et al. (1978). This case has also been studied by numerous teams investigating post-liquefaction strengths, as will be discussed in the Sections that follow.

The dam is located on the Missouri River, in northeastern Montana. The dam is a hydraulic fill structure, with a maximum height of 250 ft. (76.3 m) above the original river bed, and a crest length of approximately 10,580 ft. There is an additional dike, extending west of the main dam, with a crest length of approximately 10,450 ft. The main dam was constructed by traditional hydraulic fill methods; with starter dikes, and with dredged materials being deposited from both the upstream and downstream sides to develop relatively cohesionless "shells" and a central "puddle core" of finer materials near the center.

Dredging operations began on October 13, 1934. Nearly four years later, on the morning of September 22, 1938, hydraulic fill placement of the dam embankment section was nearing full design crest height. The reservoir was also partially filled, and at the time of failure was on the lower third of the upstream face of the dam. On the morning of September 22, settlements of as much as 1.5 feet were noted at the top of the upstream face near the right abutment (east abutment). At about 1:15 in the afternoon, a major slide occurred in the upstream slope at the right abutment, as shown in Figures A.2.1 through A.2.4.

Casagrande (1965) summarized observations of the failure as it occurred: "The movement began by a bulging out of the western portion of the affected upstream slope with simultaneous subsidence of the core pool. Then a transverse crack developed at the western end which widened rapidly into a deep gap while the moving portion of the slope started to swing in a rotational movement as if hinged at the abutment. Through this gap the core pool drained with enormous speed. The western portion which was moving out faster and further, broke into several large blocks and came to rest in the fan-shaped pattern seen in the aerial photographs."

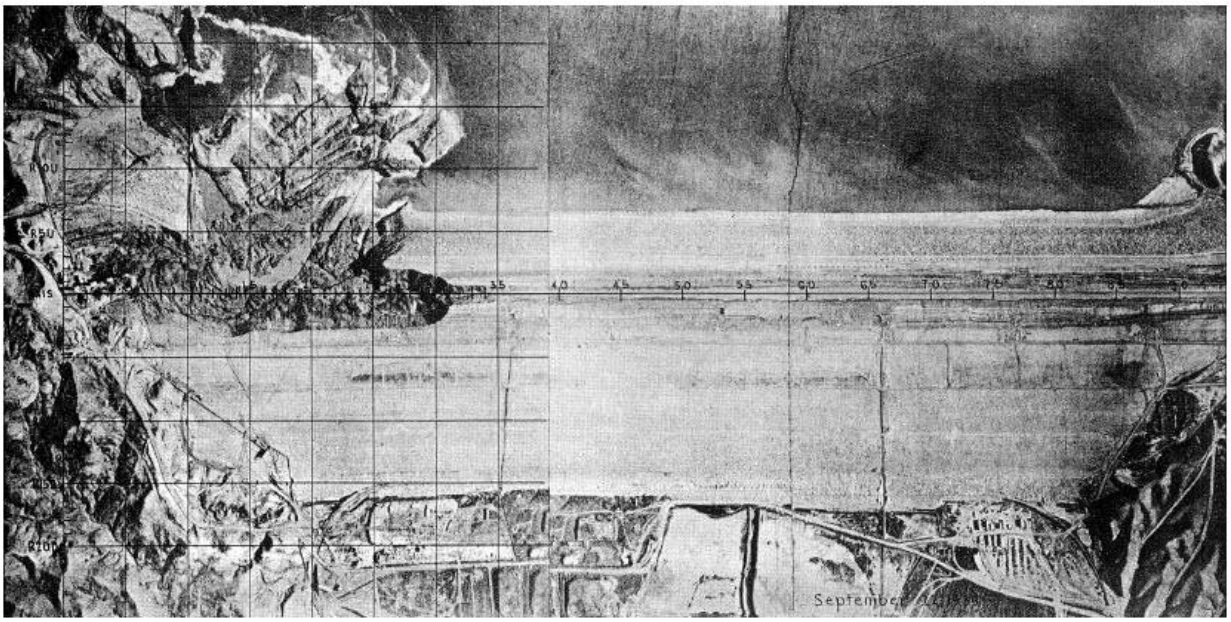

Figure A.2.1: Aerial view of post failure geometry. (U.S. Army Corps of Engineers, 1939)

Figure A.2.2: Enlarged aerial photo from Figure A.2.1 showing failure at the east end of the dam. (from http://www.midrivers.com/~rafter/lake/)

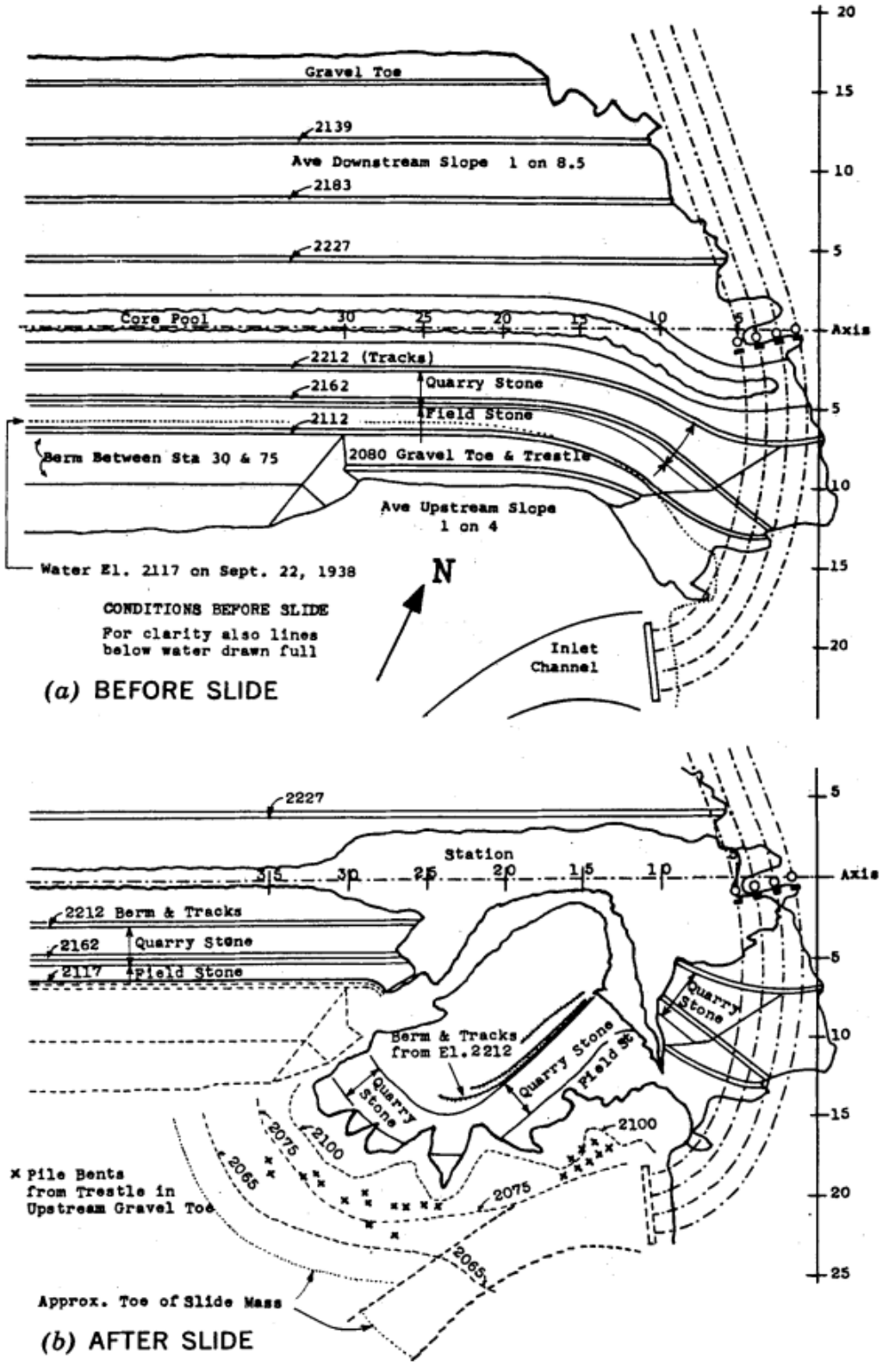

Figure A.2.3: (a) Pre-failure and (b) post-failure plan views of the east end of Fort Peck Dam, showing locations of identifiable elements and structures that can be tracked from inception of failure to final resting position. (Casagrande, 1965)

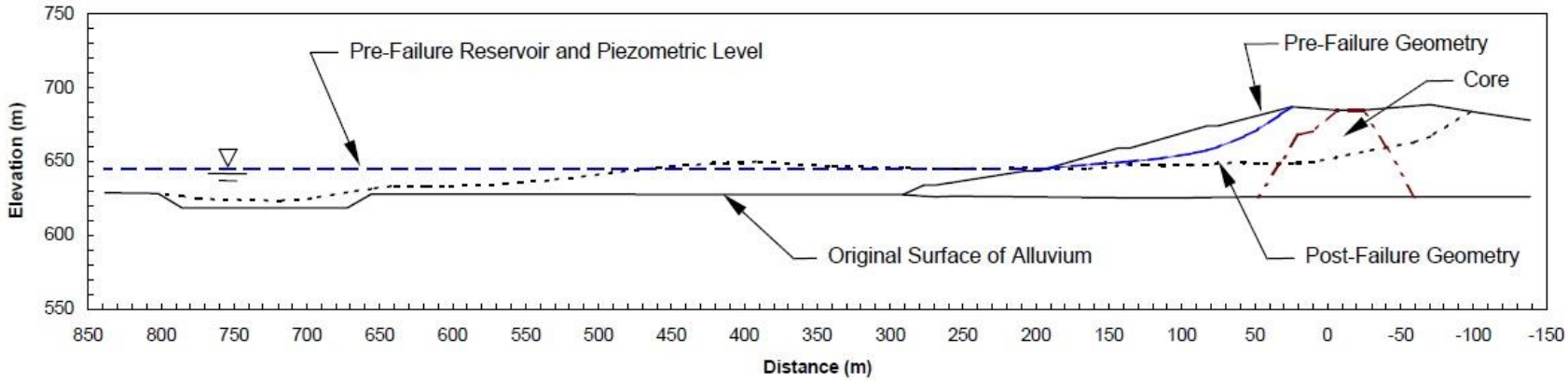

Figure A.2.4: Pre-failure and post-failure cross-section geometry of Fort Peck Dam. (from Olsen, 2001; after Middlebrooks, 1942 and Casagrande, 1965)

Casagrande also summarized his initial observations upon visiting the site; noting that large, intact blocks of the embankment travelled "like floating islands in a mass of thoroughly disturbed materials". He also noted that the materials between the intact blocks was "dangerously quick", and that numerous sand boils were still actively discharging both sand and water ten days after the failure.

Following the initial investigations, a debate arose as to the actual cause of the failure. This debate can largely be tracked in Middlebrooks (1942) and in the associated follow-on Discussions in the ASCE Journal. A Board of Consultants was formed to determine the cause of this failure, and their majority conclusion was that the failure had been triggered by sliding along weak, nearly horizontal beds of Bearpaw Shale within the upper foundation. A few Board members had dissenting opinions, and felt that the initial movement may have been initiated by slippage along the shale beds, but that this, in turn, had triggered liquefaction of the overlying loose, saturated embankment shell and core materials (Gilboy, 1942; Casagrande, 1965). Gilboy summarized the expert panel minority view nicely as "liquefaction was triggered by shear failure in the shale, and the great magnitude of the failure was principally due to liquefaction."

Soil liquefaction was not very well understood at the time of the failure, and this debate was in part a product of the era; and so the majority opinion of the original Board of Consultants was that the shale beds were the principal culprits. Casagrande (1965) went on to better justify the alternate view that this was a liquefaction-induced flow failure, and his arguments and data were eventually compelling. As a result, this failure has been one of the most studied case histories for purposes of engineering evaluation of post-liquefaction strengths.

A.2.3 Geology and Site Conditions

Fort Peck Dam was constructed by hydraulic fill placement of local river sands and other alluvial soils (Casagrande, 1965). Most of the surficial clay deposits were removed prior to placement of base cutoff sheet piles and embankment fill. The remaining foundation alluvial deposits consist of alternating and interbedded layers of gravels, sands and clays, as can be seen in Figure A.2.5, which has an exaggerated vertical scale. Also shown in Figure A.2.5 is the contact between the site's alluvium and the underlying Bearpaw clay-shale deposit, which consists of layers of shale interbedded with thin layers of bentonite (Casagrande, 1965; Marcuson and Krinitzsky, 1976).

An extensive site investigation was performed at the Fort Peck Dam site as part of the static and seismic stability studies reported in Marcuson and Krinitzsky (1976). Figure A.2.6 shows a cross-section of the repaired and completed dam, and the locations of a number of the SPT borings performed as part of these studies. A number of rotary wash borings with SPT measurements were performed, and these will be discussed in more detail in the Sections that follow. Figure A.2.6 also shows the zonation developed by the USACE at station 42+00, based on these borings as well as previous cross-sections from the original failure investigations. This mid-1970's site investigation also included a limited number of Dutch cone soundings, but only one of the soundings penetrated into the sandy hydraulic fill materials of the dam shells.

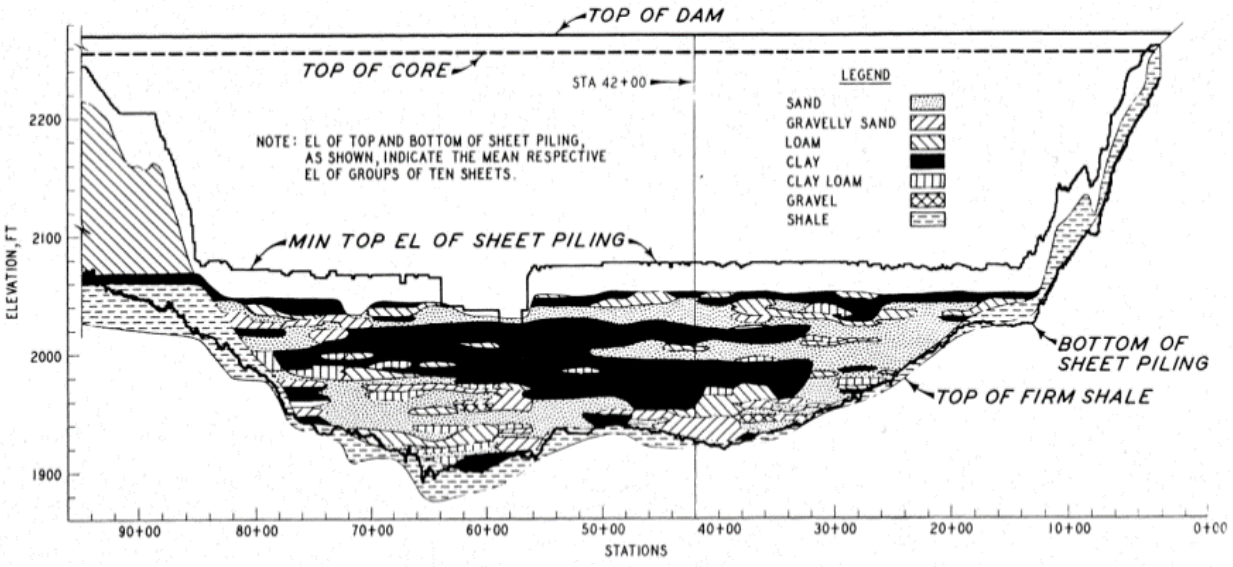

Figure A.2.5: Foundation site conditions at Fort Peck Dam. (Marcuson and Krinitzsky, 1976).

A.2.4 Evaluation of Representative Post-Liquefaction Residual Strength

A.2.4(a) Initial Yield Stress Analyses

The pre-failure and post-failure cross-sections utilized for back analyses were based in large part on the cross-sections presented in Casagrande (1965), as presented in Figure A.2.7. Figure A.2.8(a) shows the pre-failure cross-section geometry modelled as the best estimate case. This figure also shows the best estimate failure surface for these initial yield stress analyses. Initial yield stress ($S_{r,yield}$) is defined as the theoretical post-liquefaction strength within liquefiable materials on the eventual failure surface that would be necessary to develop a calculated Factor of Safety equal to 1.0 for the pre-failure geometry.

The unit weights of the hydraulic fill materials at the time of failure above and below the phreatic surface were estimated considering the recent time since placement, the nature of the hydraulic fill materials that comprised the dam, the values used by other investigators, and data developed by available field studies. Conventional Mohr-Coulomb type shear strength parameters were estimated for non-liquefied soils on a similar basis. Table A.2.1 summarizes the best estimate material properties employed for these analyses. Additional analyses were performed, varying these properties, to investigate sensitivity of resulting calculated post-liquefaction residual strengths.

The principal stratigraphy shown in Figure A.2.8(a) is separated into three main layers: (1) the foundation strata, (2) the liquefied hydraulic fill zones, and (3) non-liquefied hydraulic fill. The location of the interface between the foundation strata and liquefied embankment soils is primarily based on the results of SPT tests and the geologic cross section presented in Marcuson and Krinitzsky (1976) at station 42+00. The interface between the liquefied and non-liquefied

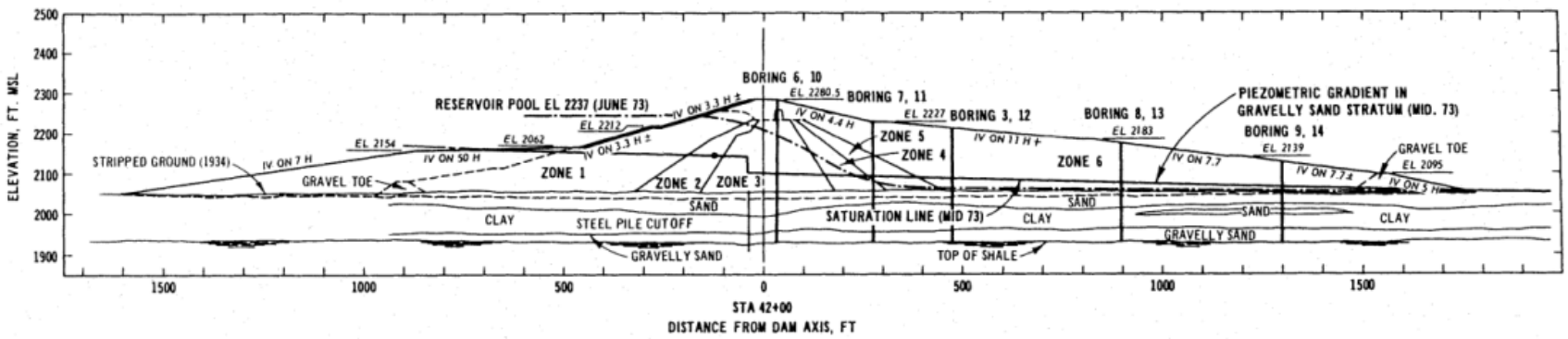

Zone	Elevation (ft)	Average D_{10} (mm)	Average Clay Content (%)
1 and 6	Below 2100	> 0.1	< 3
1 and 6	2100 – 2180	> 0.1	< 5
1 and 6	Above 2180	> 0.05	< 8
2 and 5	Below 2255	> 0.005	< 10
3	Below 2200	< 0.005	> 10 & < 30
3	Above 2200	< 0.01	< 30
4	Below 2255	Same as Zone 3 or Zone 5	
Sand Plugs	Below 2180	< 0.1	< 20
Above Sand Plugs	2180 - 2255	< 0.01	< 30

Figure A.2.6: Fort Peck Dam cross-section at Station 42+00. (Marcuson and Krinitzsky, 1976).

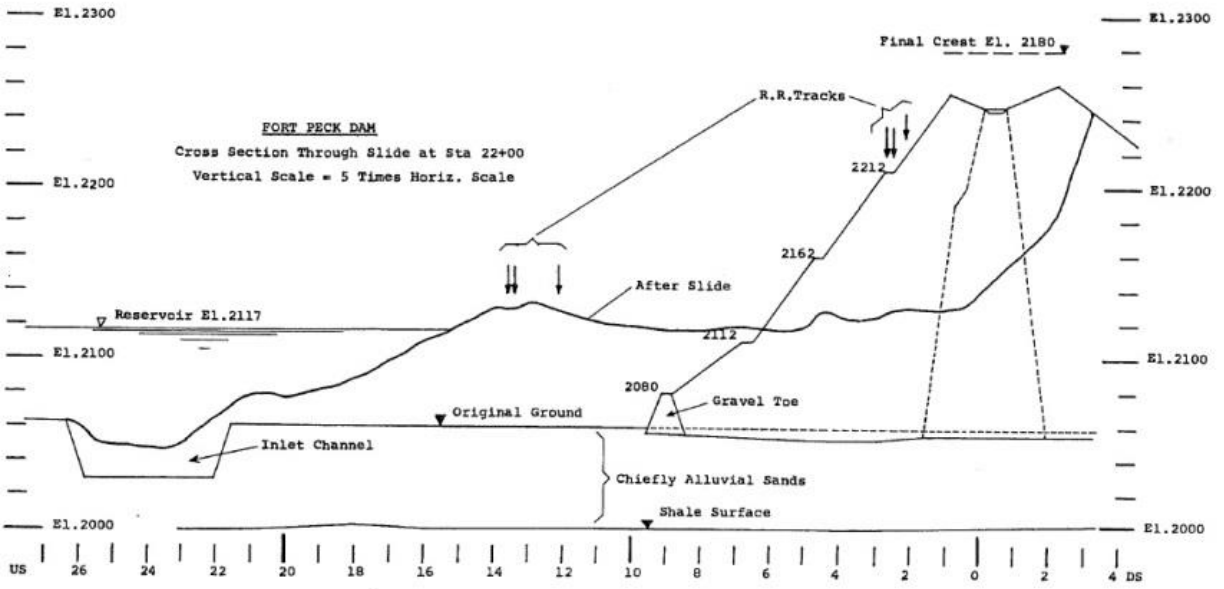

Figure A.2.7: Pre-failure and post-failure geometry of Fort Peck Dam at Station 22+00, with significant vertical scale exaggeration. (Casagrande, 1965).

Table A.2.1: Best estimate material properties for back-analyses of the failure.

Material	Unit Wt.	Mohr-Coulomb Strength Properties	
		Cohesion	Phi
Foundation	125 pcf	c′ = 0	Ø′ = 35°
Liquefied Hydraulic Fill	122 pcf	S_r = Back-Analyzed	Ø′ = 0
Non-Liquefied Hydraulic Fill	115 pcf	c′ = 0	Ø′ = 30

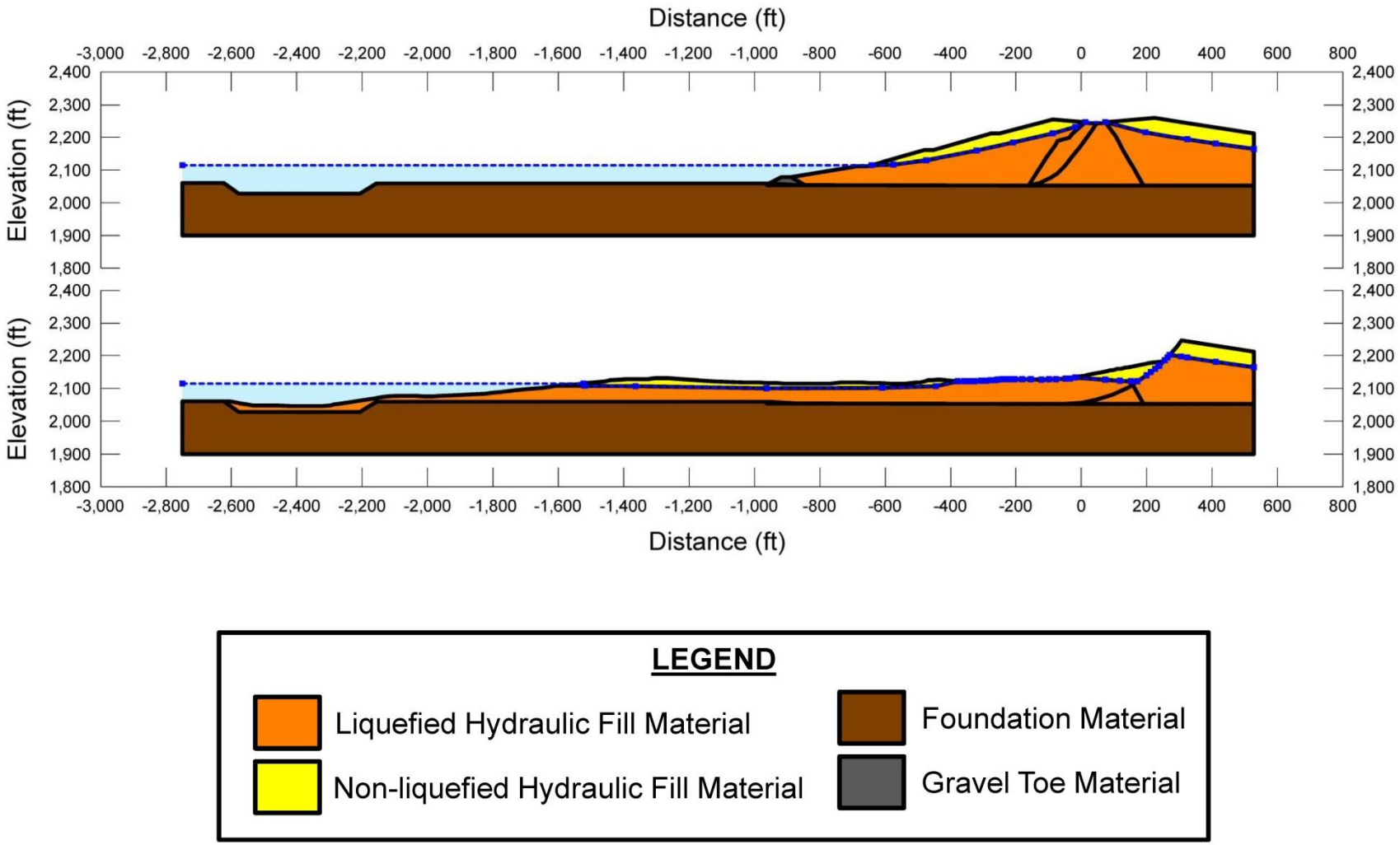

Figure A.2.8: Fort Peck Dam: (a) Pre-failure geometry and best-estimate failure surface for initial yield stress analyses, and (b) post-failure geometry and best-estimate failure surface for post-failure residual geometry analyses.

hydraulic fill material is based on the assumed phreatic surfaces on the upstream and downstream sides of the rising embankment fill. The locations of these phreatic surfaces are based on knowledge of the water level within the reservoir and the approximate elevation of the puddle core pool where material was actively being hydraulically placed at the time of the failure. With the control points at the upstream toe and the crest known, a phreatic surface was assumed in the relatively recently placed hydraulic fill. Resulting calculated post-liquefaction strengths were found not to be very sensitive to the phreatic surface modelled here, as the principal failure occurred at depth.

Conditions within the central "puddle core" and transition zones are complicated, and represent a challenge with regard to back-analyses of the post-liquefaction strength of the hydraulic fill materials of the upstream shell. Hydraulic fill was deposited from rail lines along the upstream and downstream edges of the rising fill, and was contained within starter dykes at the upstream and downstream sides. As a result, coarser materials tended to settle nearer the upstream and downstream faces, while finer soils tended to settle more slowly, and thus to propagate towards the center of the rising dam. The intent was to construct an embankment with a naturally transitioning gradation from coarser, free draining sandy shells towards a more clayey "puddle core".

In actuality, the result was more randomly variable and poorly controlled, with layers and lenses of coarser and finer soils interlayered together in a complex manner. Nine of the SPT borings from the 1976 stability studies provide the best available basis for characterization of the hydraulic fill materials comprising the dam. These 1976 stability studies were focused mainly on the potentially "liquefiable" coarser sands and silty sands of the shell zones, and only two of these nine borings penetrated the central "puddle core" and/or the adjacent "transition" zones. These two borings are presented in Figures A.2.9 and A.2.10. Boring No. 6 (shown in Figure A.2.9) was performed through the center of the "puddle core", as shown in the cross-section of Figure A.2.6. A second boring (Boring No. 10) was co-located at the same central core location, but it was performed for installation of a piezometer and was not carried to full depth and was not performed or logged as an SPT boring. Boring No. 7 (shown in Figure A.2.10) was performed through the downstream edge of the downstream side "transition" zone, as also shown in the cross-section of Figure A.2.6. Close examination of Borings No's. 6 and 7 show that layers and lenses of relatively clean sandy soils, with variable silt and clay content, extend right through the central "puddle core", while clayey and silty layers can also extend away from the central puddle core zone and across the adjacent "transition" zones and likely into the "shells".

As shown in Figures A.2.8(a) and A.2.8(b), the main failure surface passes through the lower portion of the central puddle core region as well as both the upstream and downstream transition regions. The apparent initial (smaller) failure surface nearer to the face of the dam passes through the upper portions of the central puddle core zone as well. Modeling of conditions, and shear strengths, across the central "puddle core" and "transition" embankment region is thus an important issue in back-analyses of the 1938 slope failure. Different approaches have been taken by different investigation teams and analysts. In these current studies, it was considered that some fraction of the sandier materials in the central "puddle core" were likely to perform as potentially liquefiable hydraulic fill soils, and that conditions were even more "mixed" in the even more variable adjacent transition zones. As a best estimate case,

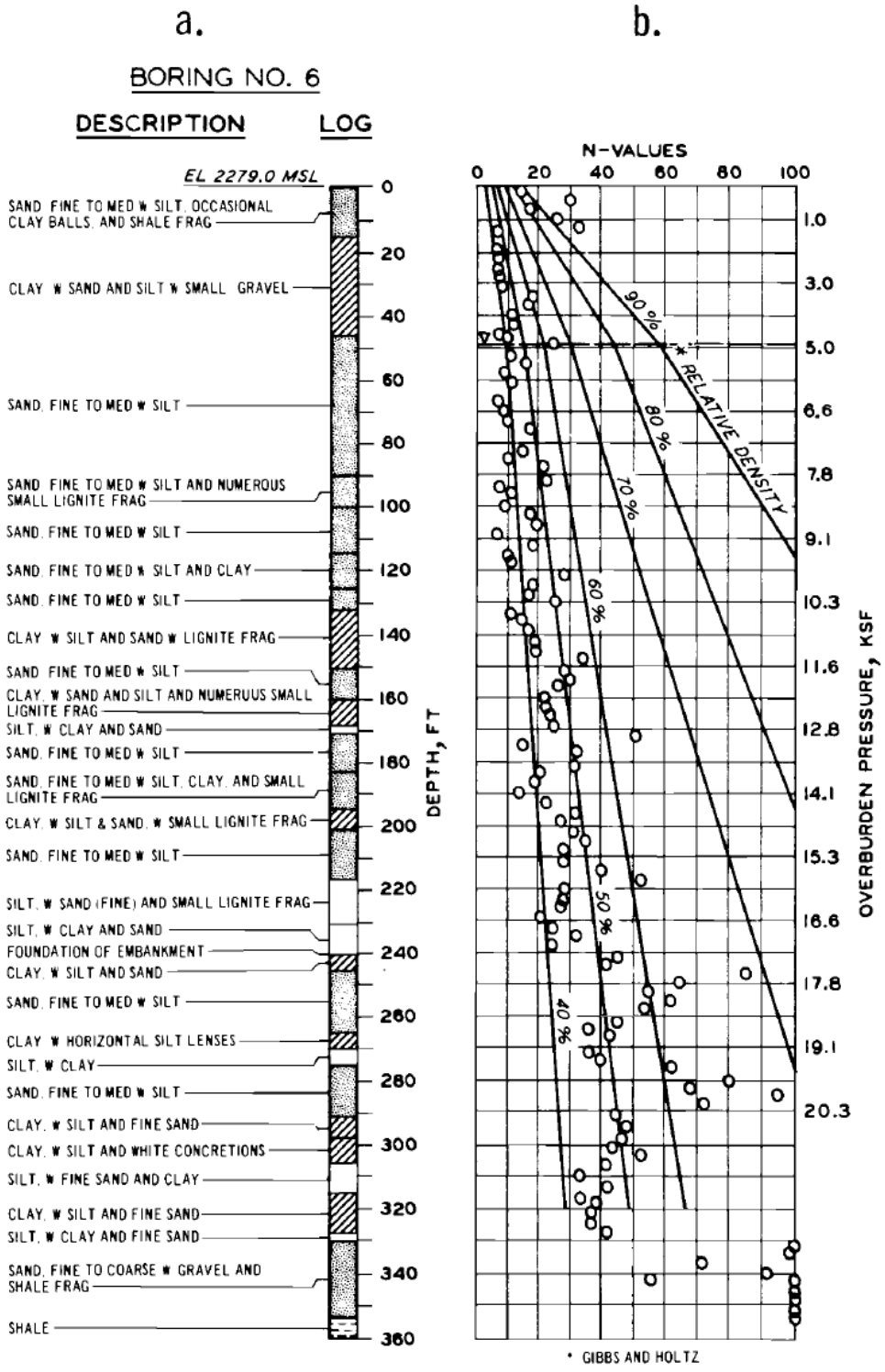

Figure A.2.9: Boring No. 6 through the central puddle core zone of Fort Peck Dam. (Marcuson and Krinitzsky, 1976)

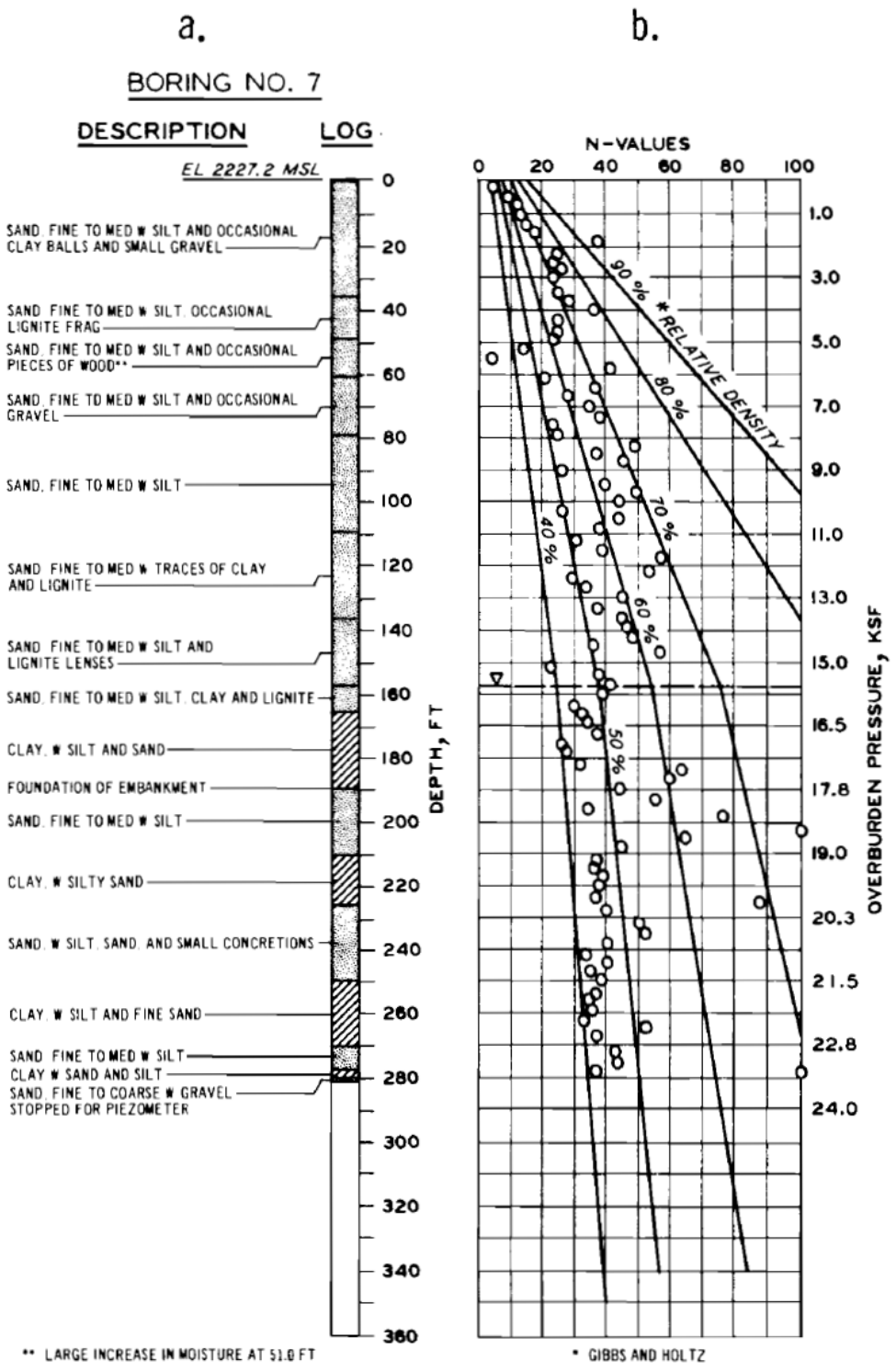

Figure A.2.10: Boring No. 7 through the upstream transition zone of Fort Peck Dam. (Marcuson and Krinitzsky, 1976)

it was considered that a considerable majority of the failure surface passing through the central "puddle core" zone shown in Figures A.2.5 through A.2.7 would pass through soils that would behave as clay-dominated materials with regard to undrained shear strength, and that only a small fraction of any potential failure surface would pass through soils that would behave as classically "liquefiable" sandy and silty soils. Similarly, it was assumed that a majority (but not all) of the transition zones would be best modeled as being comprised of soils likely to behave in a more classically "liquefiable" manner.

In this current study, the central puddle core zone materials were modeled as "clayey" soils with undrained residual strength $S_{u,r}$, and the adjacent transition zones were modeled as being comprised of potentially liquefiable hydraulic fill materials with post-liquefaction strength S_r. It is clear that cohesive, clayey soils occur into the transition zones, and that more cohesionless soils extend into the core zone, and this simplified modeling is intended to accomplish some "averaging" across this complicated region.

The lowest of the central puddle core and transition fill materials had been in place for a bit less than four years when the 1938 slope failure occurred. As a result, it was assumed that these primarily clayey soils in the central region of the embankment were likely underconsolidated to varying degrees. It is also noted, however, that largely horizontal layers and lenses of coarser, more free-draining sandy and silty soils would have helped to promote lateral drainage and would have accelerated consolidation of the more clayey materials to some degree. It is difficult to make a precise estimate of the undrained shear strength, and especially the large-strain undrained residual shear strength, of the clayey soils in this central embankment region. More recent testing data is of little assistance here, as multiple decades had passed and these soils had consolidated and gained strength over that period. As a best estimate scenario, it was assumed that these partially under consolidated soils would have an S_u/P ratio of approximately 0.1 to 0.18, and that they would also have significant sensitivity due to their loose (underconsolidated) condition. Sensitivity ratios of approximately 3 to 5 were assumed for these soils which were not likely flocculated (as they were freshwater deposited), but which were likely strongly contractive when sheared. This leads to a residual strength ratio in the range of $S_{u,r}/P \approx 0.02$ to 0.06 for these clayey soils. A value of $S_{u,r}/P$ of 0.04 was taken as the best estimate case, and additional analyses were performed exploring the likely range (upper and lower bounds) with $S_{u,r}/P = 0.02$ and $S_{u,r}/P = 0.06$ to study the sensitivity of calculated post-liquefaction strengths to these modeled conditions in the central embankment region.

Olsen (2001), and Olsen and Stark (2002) made a slightly different set of modeling assumptions. They also modeled shear strength across the lower portion of the central "puddle core" as being clay-dominated, with an average shear strength of $S_u \approx 4.8$ kPa (~100.3 lbs/ft^2), regardless of depth or effective overburden stress. They do not explain this choice. Most other investigators do not even describe how they modeled shear strengths across this region, so this is often a "black box" within back-analyses for this particular case history.

Based on the best estimate analysis of the failure scenario shown in Figure A.2.8(a), the resulting best estimate value of average initial yield stress (the value of post-liquefaction $S_{r,yield}$ required to produce a calculated Factor of Safety equal to 1.0 for pre-failure geometry) within the liquefiable hydraulic fill was found to be $S_{r,yield} \approx 2{,}370$ lbs/ft^2 for the smaller initial failure surface

shown in Figure A.2.8(a) and $S_{r,yield} \approx 2{,}100$ lbs/ft^2 when the final failure surface shown in Figure A.2.8(b) is imposed on the initial geometry . The representative value was then taken as intermediate between these two at $S_{r,yield} \approx 2{,}235$ lbs/ft^2. Failure surfaces were varied to evaluate sensitivity to modelling assumptions and details. Shear strengths across the central embankment were also varied, as discussed above, to evaluate sensitivity to modelling assumptions and details. Strengths of the non-liquefied embankment soils were also varied. Resulting values of representative $S_{r,yield}$ for variations considered reasonable were on the order of $S_{r,yield} \approx 2{,}023$ to 2,468 lbs/ft^2. Initial yield stress is not intended to represent the operative post-liquefaction strength that controlled the full field failure that occurred, but it is useful in calibrating and checking the more rigorous analyses that will follow, and in development of relationships useful in evaluation of other back-analysis case histories.

Stark and Olsen also calculated initial yield stress ($S_{r,yield}$), and they reported a best estimate value of $S_{r,yield}$ = 82.9 kPa (1,731 lbs/ft^2), with a range of $S_{r,yield}$ = 69.9 to 89.6 kPa (1,441 to 1,871 lbs/ft^2), in generally good agreement with the values calculated in these current studies.

A.2.4(b) Residual Strength Analyses Based on Residual Geometry

Similar "static" stability analyses were performed to evaluate the "apparent" shear strength within the liquefiable hydraulic fill (S_r) that would result in a calculated Factor of Safety equal to 1.0 for the post-failure residual geometry of Figure A.2.8(b). Assumptions and modeling details were largely the same as described in the previous Section A.2.4(a), and sensitivity analyses with varying combinations of modeling and parameter details were performed here as well.

An additional modeling detail that affects these analyses is the possible occurrence of hydroplaning as the toe of the embankment failure mass enters rapidly into the reservoir, or the possibility of the failure mass being borne along upon weak reservoir sediments of even lower strength than the liquefied embankment materials as the toe of the embankment failure mass enters rapidly into the reservoir. As this was the first filling of the reservoir, it is assumed that there were not yet any significant deposits of loose, weak reservoir sediments accumulated. The question of hydroplaning is a more interesting one. The incremental momentum and displacement analyses described in Section A.2.4(c), which follows, show that peak translational velocities were momentarily as high as approximately 30 feet per second and more at the toe; a rate at which some degree of hydroplaning could occur (see Section 4.2.1). Scale model experiments for soil masses entering into water indicate, however, that hydroplaning seldom occurs over a distance beneath the base of materials entering the reservoir of more than about ten times the thickness of the entering soil thickness (see Section 4.2.1). In these studies, it was assumed that hydroplaning had negligible effect on the residual condition, because the shear strengths at the base of the forward tip of the materials that entered farthest into the reservoir were not modeled as contributing to overall stability of the larger failure mass farther upslope. Hydroplaning will be discussed again in the incremental momentum and displacements analyses described in Section A.2.4(c), which follows.

The full length of the potential failure plane at the base of the residual slide mass was not used to calculate $S_{r,resid/geom}$ because if the extended extreme toe section of the displaced slide mass developed significant resistance to translation, then the failure plane would have risen upwards to

daylight through the very thin residual deposits of material at the final toe. Accordingly, the failure surface was assumed to "daylight" as a downstream station of approximately -1,800 feet in Figure A.2.8(b).

Based on the modeling conditions and assumptions described above, the resulting best estimate value of the post-liquefaction shear strength required for FS = 1.0 with residual geometry is $S_{r,resid/geom} \approx 174$ lbs/ft^2. The approximate range, based on reasonable variations in parameters and modeling details, is $S_{r,resid/geom} \approx 150$ to 202 lbs/ft^2.

Olsen (2001) also calculated $S_{r,resid/geom}$ for this case history, and reports a best estimate value of $S_{r,resid/geom} \approx 3.8$ kPa (79 lbs/ft^2), and a range of $S_{r,resid/geom} \approx 0.7$ to 15.1 kPa (15 to 315 lbs/ft^2). These values are in good agreement with the values calculated by the current studies, except that Olsen's lower bound is much lower. Olsen's lower bound value appears to be very low, and insufficient details are presented so this cannot be examined in further detail.

Overall, it was judged that there was good agreement between the two sets of analyses, despite differences in analysis and modeling details and choices made by the two investigation teams.

A.2.4(c) Incremental Momentum and Displacement Analyses and Overall Evaluation of Post-Liquefaction strength

Full incremental momentum and displacement analyses were performed using similar modeling assumptions and details as described in the preceding Sections. Figure A.2.11 shows the best estimate case analysis. It is difficult to see in detail, owing to the scale of the overall problem and the very large lateral displacements that accrue. But it is useful to see the progression of the increments in a single consecutive sequence. This figure is then repeated in six enlarged increment figures in Figure A.2.12 so that more detail can be seen. In these enlarged figures, the progressive locations of the overall center of mass of the active failure mass are also shown.

The modeled stratigraphy, phreatic surface, and failure progression can be seen in Figures A.2.11 and A.2.12. Figure A.2.13 then shows (1) acceleration vs. time, (2) velocity vs. time and (3) displacement vs. time for the center of gravity of the failure mass of Figures A.2.11 and A.2.12.

A total of six cross-sections were used for the progression of the failure mass, due to the very large displacements that accrue, and also due to the potential complexity of this progression. Based on eye witness reports, as well as the post-failure geometry observed, the initial failure surface (first time step) passes through the front edge of the modeled puddle core. By the second step, the failure surface is then modeled to progress to the larger assumed eventual maximum

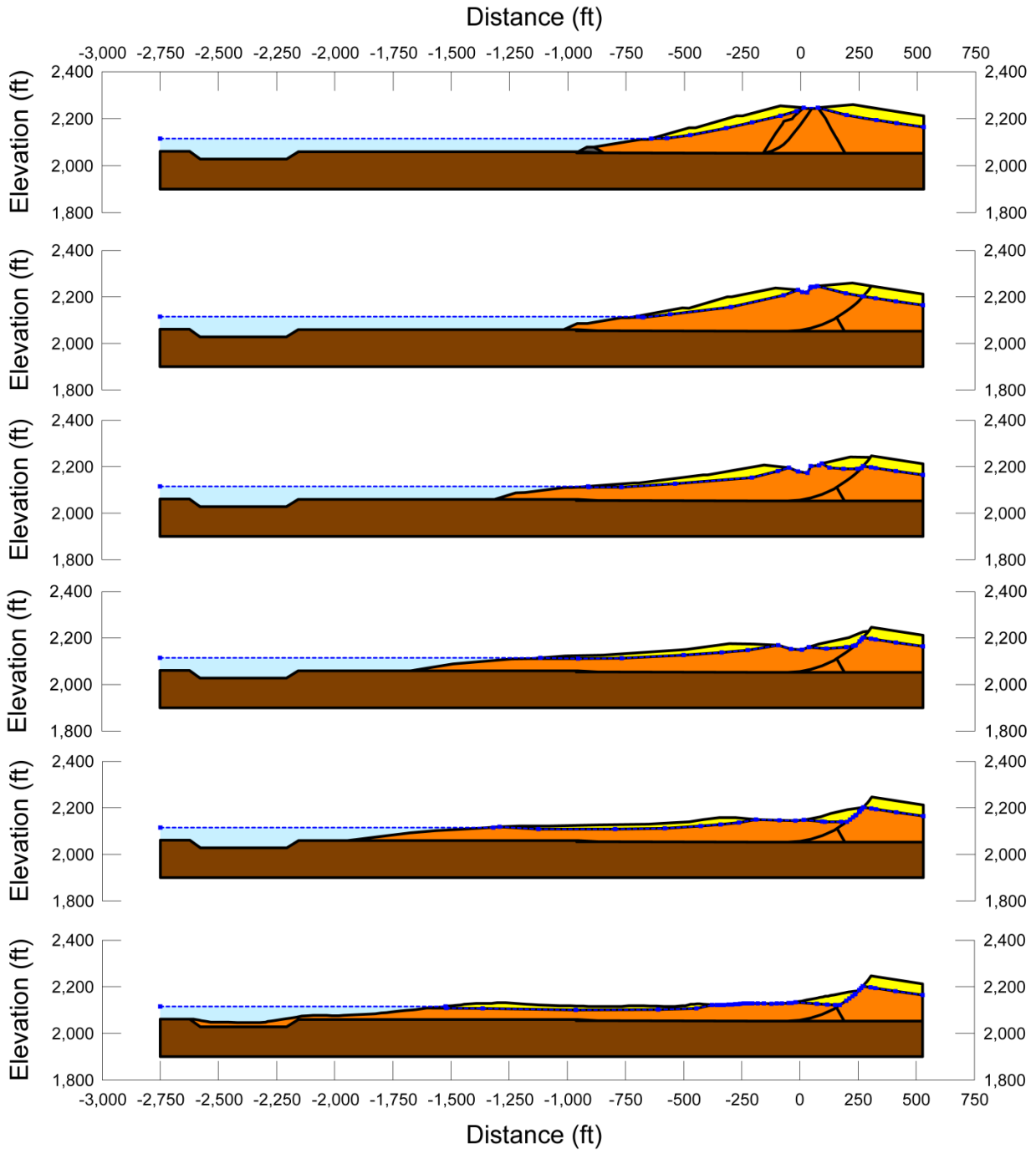

Figure A.2.11: Incremental displacement stages for the incremental momentum and displacement analyses for the best estimate scenario for Fort Peck Dam.

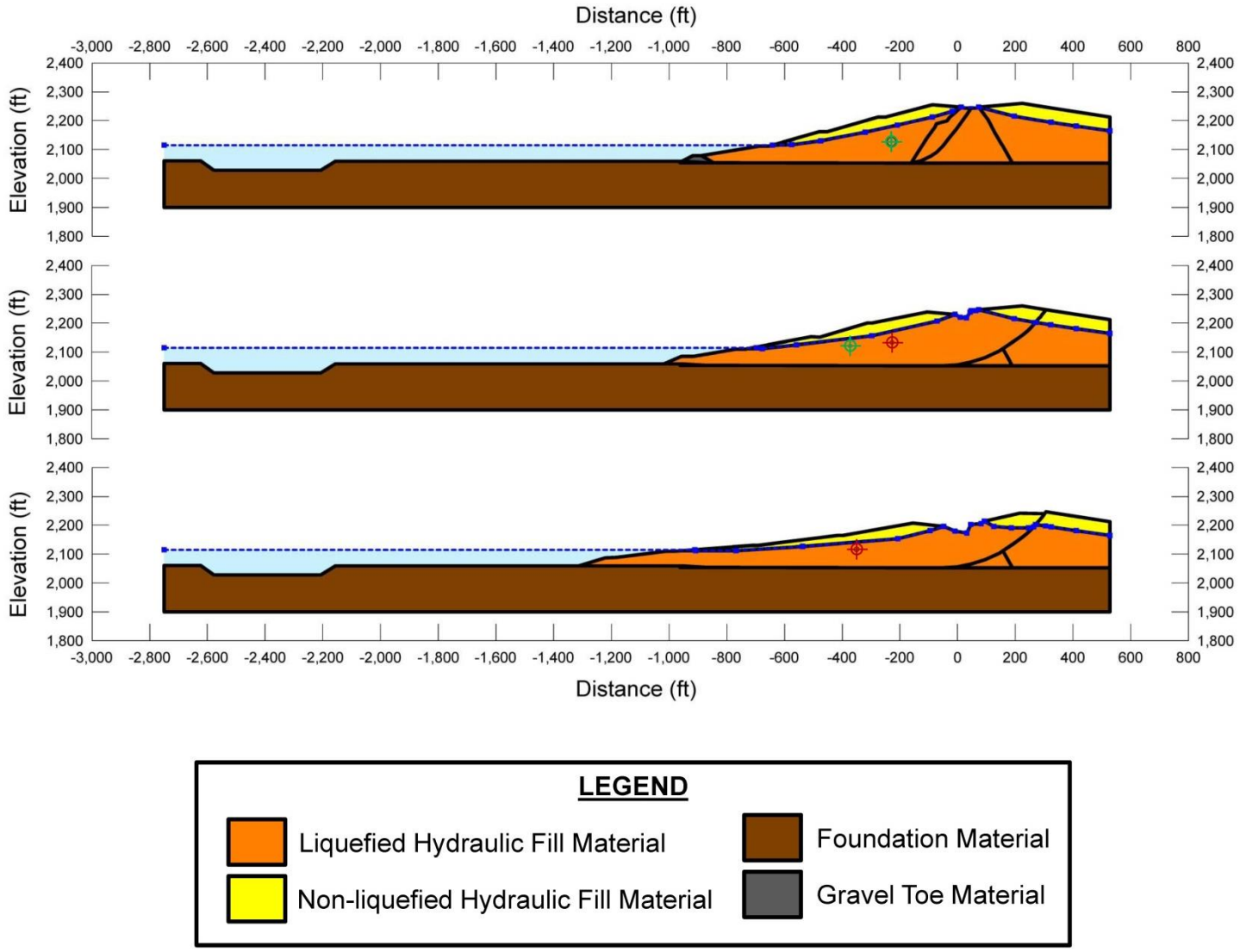

Figure A.2.12: Enlarged view of the incremental displacement stages for the incremental momentum and displacement analyses of Fort Peck Dam from Figure A.2.12 (first three incremental stages).

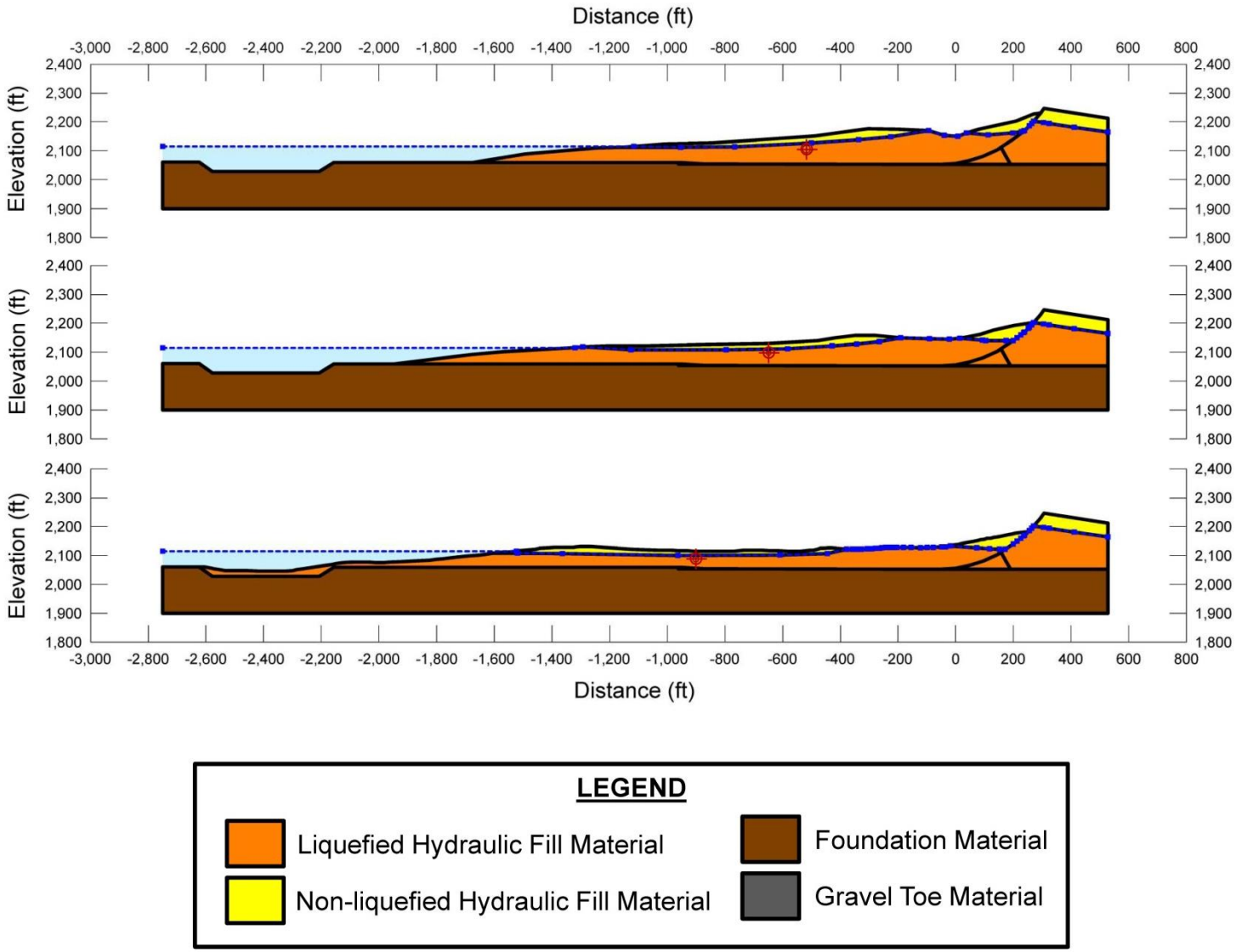

Figure A.2.12 (cont'd): Enlarged view of the incremental displacement stages for the incremental momentum and displacement analyses of Fort Peck Dam from Figure A.2.11 (additional three stages to completion).

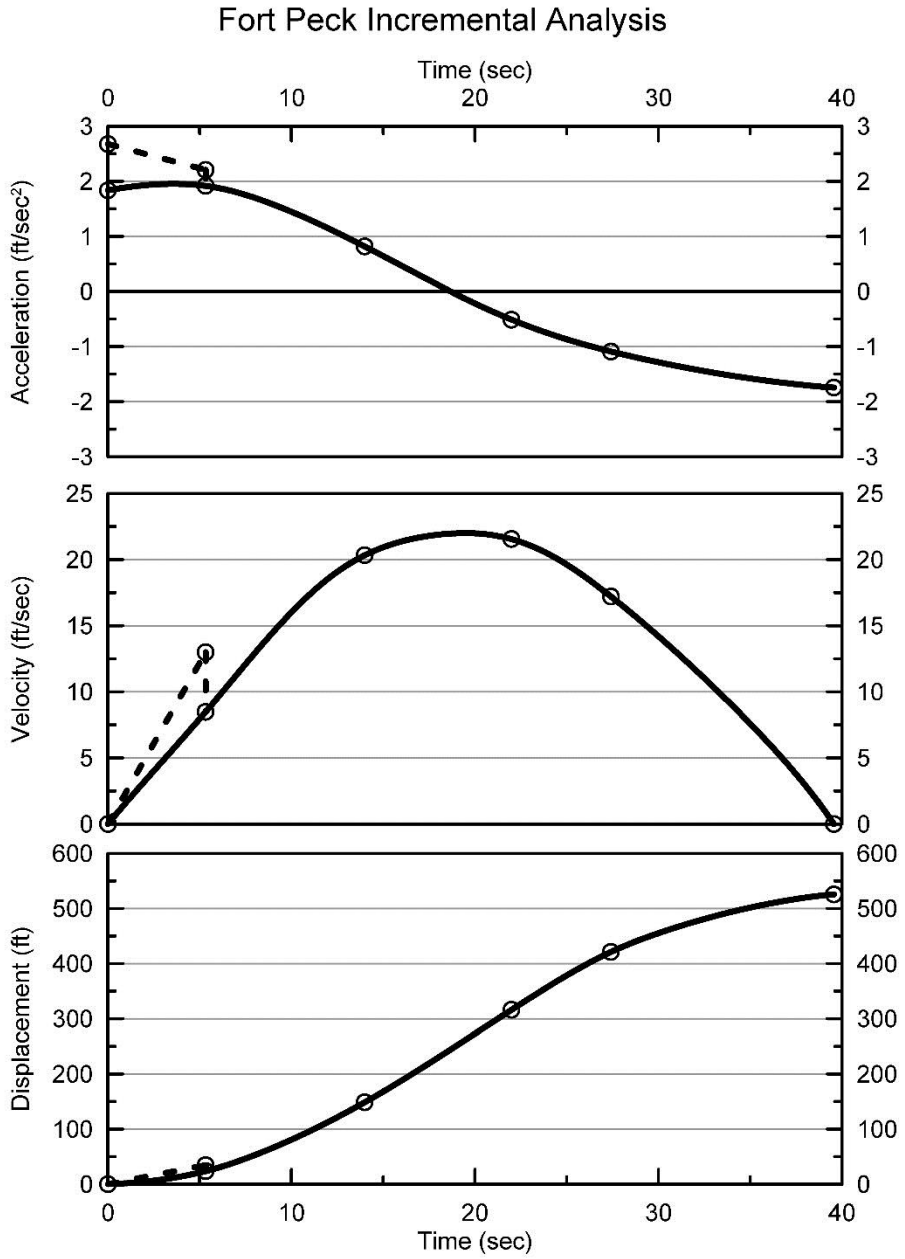

Figure A.2.13: Calculated development of (1) acceleration vs. time, (2) velocity vs. time and (3) displacement vs. time for the incremental momentum and displacement analyses of Figures A.2.11 and A.2.12.

failure surface. This is a slightly progressive development of failure, and it serves to provide for the separation observed at the "crest" section of the residual geometry.

This can be seen most clearly in the enlarged sequence of evolving cross-sections of Figure A.2.12. In this enlarged figure, centers of gravity have been added to the figure. The green cross-hairs of the first cross section are the initial position of the center of gravity delineated by the initial failure surface passing near to the front of the upstream crest. In the second figure, this initial failure mass has progressed, and the center of gravity has moved towards the reservoir. At this second stage, the failure of the eventual overall larger full failure mass along the most downstream back heel scarp begins to move. The red cross-hairs show the location of the new (combined) centers of gravity of the initial failure mass and the incremental additional mass. In the subsequent figures (stages), this center of gravity of the overall failure mass then moves towards the reservoir as the overall failure mass translates and elongates towards the upstream side.

Shear strengths for the "clayey" soils within the central puddle core zone are modeled with $S_{u,r}/P = 0.04$, and the shear strength assigned to the adjacent "transition" zones was the post-liquefaction strength S_r. Post-liquefaction strength (S_r) in the liquefied hydraulic fill soils of the shell and transition zones was iteratively adjusted until a value was found such that the final overall displacement agreed with the observed field displacement.

The failure occurred during first filling of the reservoir, so there were no significant accumulations of soft, weak reservoir sediments. The velocities calculated suggest that some degree of hydroplaning may have occurred as the toe of the embankment entered rapidly into the reservoir (see Section 4.2.1 of the main report). But the assumption that entrapment of fluids beneath the advancing front would occur over a lateral dimension of less than 10 times the thickness of the entering soils, coupled with the relatively flat pre-failure slope of the toe and increasing thinning of the toe failure "tip", suggest that hydroplaning would have likely been localized near to the advancing tip. For the best estimate case illustrated in Figures A.2.11 through A.2.13, it was assumed that hydroplaning would reduce the shear strength (S_r) at the base of the portion of the overall failure mass that entered into the reservoir and eventually moved farther upstream that lateral Station -1,800 feet in Figures A.2.11 and A.2.12 because embankment soils that eventually traveled farther upstream than this continued to thin and spread far beyond the more nearly coherent toe of the remainder of the failure mass. Even if hydroplaining had not occurred beneath these extreme toe materials, it would not have been possible for these extremely thin toe failure materials to provide significant resistance to movements of the failure materials farther to the right (farther upstream), and the failure surface would have "daylighted" upwards to the surface at about downstream Station -1,800 feet. So negligible shear strength was modeled for materials that passed farther downstream than lateral Station -1,800 feet from the crest centerline.

The resulting back-calculated post-liquefaction strength of the liquefied hydraulic fill that was calculated based on this particular combination of "best estimate" conditions is $S_r = 762$ lbs/ft^2.

A number of variations in parameters were analyzed to investigate variability and sensitivity with regard to calculated post-liquefaction strengths. The shear strengths of the cohesive clayey soils in the central puddle core Zone C were modeled with strengths ratios as low as $S_{u,r}/P = 0.02$, and as high as 0.06. Friction angles in the non-liquefied soils above the phreatic

surface were increased and decreased by 3°. The maximum average reduction in average shear strength at the base of the portion of the embankment failure mass that entered into the reservoir due to potential hydroplaning was taken as 90%, and the lateral distance upstream of the advancing toe was increased to nearly twice the best estimate scenario, and reduced to zero. Unit weights were varied up and down by several ponds per cubic foot.

Based on combinations of modeled conditions considered to be reasonable, the range of calculated values of representative S_r was found to be $S_r \approx 575$ to 929 lbs/ft^2. It was the judgment of this engineering team that this represented a range corresponding to approximately +/− 1.5 standard deviations. This range was nearly symmetric about the best estimate value of 762 lbs/ft^2, so no significant further adjustments were necessary. Overall, based on an assumed normal distribution, the best estimate (median) value of post-liquefaction strength from these studies was judged to be

$$\overline{S_r} = 762 \text{ lbs/ft}^2$$

with a standard deviation of

$$\sigma_{\overline{S}} = 118 \text{ lbs/ft}^2$$

The best previous studies for cross-comparisons here are those of Davis et al. (1988), Olsen (2001) and Wang (2003), all of whom specifically performed analyses incorporating dynamic inertial effects. As shown in Table A.2.2, the results calculated here are just slightly higher than the other investigation teams in this group. The details of Wang's analyses are not presented, but it is noted that his results agree well with this current study. The full details of Davis' analyses are also not presented, but his value is in reasonably good agreement as well. The studies of Davis et al. and of Olsen and Stark did not consider hydroplaning and so may be somewhat conservative.

Additional investigators have also analyzed this case, including Lucia (1981), Bryant et al. (1983), Seed (1987), Seed and Harder (1990), and others. The estimated S_R values from these previous studies range from approximately 240 to 599 lbs/ft^2, and serve to demonstrate the considerable variability in previous estimates made. Many of these earlier analyses employed conservative simplified approaches, and it is to be expected that their results would provide generally lower values of S_r.

Table A.2.2: Representative values for the Fort Peck Dam case history of: (a) post-liquefaction strength (S_r), (b) initial vertical effective stress (σ_{vo}'), and (c) $N_{1,60,CS}$ developed by various investigation teams, and estimates of variance in each of these indices when available.

(a) Post-Liquefaction Strength:	
Olsen (2001) and Olsen and Stark (2002)	S_r = 570 psf, and range = 63 to 211 psf
Wang (2003) and Kramer (2008)	$\overline{S_r}$ = 671.5 psf, and $\sigma_{\overline{S}}$ = 130.1 psf
Davis et al. (1988)	S_r = 701 psf
This Study	$\overline{S_r}$ = 762 psf, and $\sigma_{\overline{S}}$ = 118 psf
(b) Representative $N_{1,60,CS}$ or $N_{1,60}$ Value:	
Olsen (2001) and Olsen and Stark (2002)	$N_{1,60}$ = 8.5 bpf, and range = 4 to 14 bpf
Wang (2003) and Kramer (2008)	$\overline{N_{1,60,CS}}$ = 15.8 bpf, and $\sigma_{\overline{S}}$ = 0.9 bpf
Poulos (1988)	$N_{1,60}$ = 5.3 blows/ft
This Study	$\overline{N_{1,60,CS}}$ = 13.5 bpf, and $\sigma_{\overline{N}}$ = 2.7 bpf
(c) Representative Initial Vertical Effective Stress:	
Olsen (2001) and Olsen and Stark (2002)	Not reported, but can be inferred from reported S_r/P ratio to be approximately σ_{vo}' = 7,341 psf. Likely range is not provided.
Wang (2003) and Kramer (2008)	Not reported, but can be inferred from reported S_r/P ratio to be approximately σ_{vo}' = 7,379 psf. Variance or standard deviation is not provided.
This Study	$\overline{\sigma'_{vo}}$ = 7,258 psf, and $\sigma_{\overline{\sigma}}$ = 687 psf

A.2.5 Evaluation of Representative SPT Penetration Resistance

As part of the seismic stability analyses of Fort Peck Dam in the study reported by Marcuson and Krinitzsky (1976), a total of nine investigative SPT borings were drilled in the dam's crown and downstream slope. It is assumed that these SPT borings provide data largely representative of the upstream side failure zone due to the approximate symmetry of hydraulic fill placement operations prior to the 1938 slope failure. But the upstream face was much flatter in slope than the downsteam face, so that the distance from the upstream side hydraulic fill spigots depositing material to the center of the final crest was significantly greater than for the downstream side spigots, so perfect symmetry did not occur.

These investigation borings were performed by the rotary wash method, and SPT were performed at fairly regular intervals. The results of the SPT were filtered to exclude the results from tests performed outside the zone where liquefaction was assumed to have potentially occurred, and also for tests where clay dominated the material tested in an individual test. The remaining tests were corrected to $N_{1,60,CS}$ values based on the corrections and adjustments for equipment, test procedure, rod length, effective overburden stress, and fines content as per Cetin et al. (2004), and with the effective overburden stress correction (C_N) of Deger (2014).

The resulting corrected SPT data were then binned into sets based on lateral station along the dam's axis and relative distance from the dam's centerline. Materials tended to have higher fines contents near the dam's centerline (beneath the crest), and lower fines contents farther out towards the faces. $N_{1,60}$ blowcounts uncorrected for fines, on the other hand, tended to increase a bit with distance from the centerline.

Borings 1 through 5, plus 8 and 9, were judged to be most likely representative of $N_{1,60,CS}$ values for the sandy hydraulic fill materials of the downstream side shell zone. These were examined to eliminate the few SPT performed in potentially clayey samples. A small number of very high $N_{1,60}$ values (2% of the total number of SPT) were also deleted based on the assumption of gravel having potentially biased the results. The remaining SPT $N_{1,60}$ values were then binned jointly for these 7 borings, and both median and mean $N_{1,60}$ values were determined. The mean value was determined to be 13.7 blows/ft., and the median value was determined to be 13.3 blows/ foot. The representative $N_{1,60}$ value was taken to be the median value of $N_{1,60}$ = 13.3 blows/ft. Because the shell materials generally had low fines contents of between 0% to 10%, fines adjustments per Cetin et al. would increase this representative value by a factor of between 1.00 to 1.08. A factor of 1.04 was applied, and the estimated representative value of fines adjusted penetration resistance was then $N_{1,60,CS} \approx 13.8$ blows/foot.

A single boring (B-7) provided SPT N-values for soils within the downstream transition zone. Similar processing was performed for this boring, including elimination of SPT performed in clayey soils, deletion of spuriously high values (there were none of these), determination of the mean and median values of $N_{1,60}$, and application of fines adjustments. $N_{1,60}$ values were somewhat lower in this transition zone, with a mean of 12.6 blows/ft and a median of 12.5 blows/ft. The median value was taken as representative. Fines adjustments were higher in the finer soils encountered in the transition zone, and based on typical reported fines contents of between 10% to 30%, the representative value of fines adjusted penetration resistance was $N_{1,60,CS} \approx 14.8$ blows/ft. This value was considered along with the value of 13.8 blows/foot for the sandier shell zones calculated above. Based on approximate weighted averages based on contribution of the downstream shell and the transition zones to the overall failure surface, the representative penetration resistance was taken to be $N_{1,60,CS}$ = 13.9 blows/ft.

An additional adjustment was then made to account for likely "ageing" effects over the roughly four decades that elapsed between the date of the failure and the performance of SPT tests in the 1970's. It is known that both cyclic resistance to triggering of liquefaction, and also penetration resistances, increase somewhat over time since placement or since deposition. Quantification of this with regard to SPT penetration resistance is difficult however. There is some research available regarding increases in both SPT N-values and in CPT tip resistances over time, due in large part to the relatively common use of CPT to evaluate ground improvement by means of densification using vibro-densification, deep dynamic compaction, blasting, etc. (e.g.: Skempton, 1986; Schmertmann, 1993; Lewis et al., 1999; etc.). Skemption (1986) proposes an equation for estimation of increase in SPT N-values over time, but this should be considered highly approximate. Over a period from 1 year after placement to 40 years after placement, Skempton's relationship predicts an increase in N-values of approximately 37%, but this should be considered very approximate. Kulhawy and Mayne (1990) propose an alternate relationship, logorithmicaly linear over time, and this would predict an increase in N-values of approximately 8% over a period from 1 year after placement to 40 years after placement. It is clear that some adjustment should

be made here; otherwise the "representative" $N_{1,60,CS}$ value based on the 1970's SPT data would overestimate the representative value at the time of the failure. Values of between 5 to 40 % were considered here. For conservatism in developing relationships between $N_{1,60,CS}$ vs S_r, an adjustment nearer to the low side was made here. In the end an adjustment of 10% was adopted. The representative blowcount of 13.9 blows/ft from the 1970's SPT data was then reduced by 1 / 1.10 to a final best estimate of $\overline{N_{1,60,CS}} \approx 12.6$ blows/ft.

Only one other failure case history back-analyzed by these current studies had similar potential ageing effects, and that was the Wachusett Dam embankment failure. That failure occurred in 1907, and modern SPT investigations were finally performed seven decades later. As described in Section A.1.1, the representative $N_{1,60,CS}$ value for that case (without correction for ageing effects) was found to be $\overline{N_{1,60,CS}} \approx 8.2$ blows/ft, and a similar adjustment of approximately 10% was then made for ageing effects to produce a final estimate of $\overline{N_{1,60,CS}} \approx 7.5$ blows/ft for the fine sand shell materials of the Wachsett Dam which had been loosely placed in thick lifts. Only two case histories among the thirty case histories back-analyzed warranted adjustments for "ageing" effects, and the adjustments applied were relatively minor. These had relatively little effect on the overall predictive correlations eventually developed based on the back-analyses of the full 30 case histories.

Uncertainty, or variance in the overall average or representative $N_{1,60,CS}$ value was not so much a function of variance in individual contributing N-values. Instead it was a function of (1) perceived differences in localized $N_{1,60,CS}$ values at different locations that did not appear to be consistently correlated with distance from the core, (2) uncertainty with regard to the use of downstream side SPT data to represent upstream side conditions, especially given the non-symmetric geometry of the wider upstream vs. downstream shells, and (3) passage of time (approximately four decades) from the occurrence of the slope failure to the performance of the field SPT investigations of the 1970's. Overall, it was judged that the penetration resistance of the potentially liquefiable hydraulic fill materials of the downstream shell and the transition zones would be suitably modeled with a normal distribution with mean (and median) $N_{1,60,CS} = 12.5$ blows/ft, and with a standard deviation of $\sigma_{\overline{N}} = 1.7$ blows/ft.

As shown in Table A.2.2(c), Olsen and Stark developed a somewhat lower estimate of $N_{1,60} = 8.5$ of blows/ft, and range = 4 to 14 blows/ft. Kramer and Wang developed slightly higher estimates of $\overline{N_{1,60,CS}} = 15.8$ blows/ft, with a lower standard deviation of $\sigma_{\overline{S}} = 0.9$ blows/ft. They made no adjustment for ageing effects, and their estimate of standard deviation for this case was driven primarily by the variance within the large suite of SPT N-values available, and did not include the factors in the preceding paragraph above and so likely underestimated uncertainty to some degree. Poulos (1988) working with Davis et al. (1988) proposed a best estimate value of 5.3 blows/ft, but this was lower than the values proposed by any other investigators, and it was not intended to represent a mean or median estimate as Poulos took the "representative" value to be a less than median value within the range of blowcounts available based on the observation that failure would tend to pass through the weaker soils within the failure zones. Accordingly, his estimate is not directly comparable with the others and would be expected to be lower. Each of these investigation teams explain the general approach taken, but do not provide much detail with regard to fine points that might have affected their assessments here.

Overall, it is clear that there is significant uncertainty associated with estimation of representative $N_{1,60,CS}$ for this case history. The values of this current study fall within the ranges of values proposed by previous investigators, and appear to be reasonably well supported given the different approaches taken by the previous investigation teams.

A.2.6 Additional Indices from the Back-Analyses

A number of additional results, and indices, can be extracted from the analyses performed. Some of these are useful in developing some of the over-arching relationships and figures presented in the main text of this report. These values are presented in Table A.2.3.

Table A.2.3: Additional results and indices from the analyses of the Fort Peck Dam embankment failure case history.

Maximum distance traveled by the center of gravity of the overall failure mass	528 ft.
Initial post-liquefaction Factor of Safety prior to displacement initiation, and based on best estimate value of S_r	FS = 0.43
Final post-liquefaction Factor of Safety at final (residual) post-failure geometry, and based on best estimate value of S_r	FS = 2.63

A.13 Route 272 Roadway Embankment (Higashiarekinai, Japan)

A.13.1 Brief Summary of Case History Characteristics

Name of Structure	Route 272 Embankment
Location of Structure	Higashiarekinai, Japan
Type of Structure	Side Hill Highway Embankment
Date of Failure	September 22, 1933
Nature of Failure	Seismic, During 1993 Kushiro-Oki Earthquake (M_L = 7.8)
Approx. Maximum Slope Height	26 ft.

A.13.2 Introduction and Description of Failure

The Route 272 roadway embankment failed during Kushiro-Oki Earthquake of January 15, 1993 (M_L = 7.8), and was investigated by Sasaki et al. (1994). Sasaki et al. developed an event-specific acceleration attenuation relationship for the Kushiro-Oki Earthquake, and estimated that the peak ground acceleration at this site was approximately 0.38 g.

Figure A.13.1 shows a cross-section through the failure. The highway embankment was a sidehill fill underlain by pumice bearing volcanic sands and silts, and by partially pumice tuff.

After the failure, two SPT borings were performed and these are shown in Figure A.13.1 (from Sasaki et al., 1994). These two borings reasonably well constrain the key ground conditions at the base of the failure. Construction details are not reported, and it is assumed that the sandy fill was locally sourced, and that it received minimal compaction effort. This embankment is not far from the Shibeca-Cho Embankment discussed previously in Section A.12, and fill material is assumed to have been locally available volcanic sands and silty sands.

Close inspection of the two borings shown in Figure A.13.1 shows that the transition from fill to underlying native soils appears to be relatively clearly demarcated by a transition from very low SPT blowcounts within the fill to slightly higher penetration resistances in the immediately underlying pumice bearing volcanic sand. The back heel of the final failure surface is also well constrained. As a result, the approximate location of the overall bounding failure surface is relatively well constrained for this case by the clear heel scarp, and by the transition to firmer materials at the base of the liquefiable fill. The location of the phreatic surface at the time of the earthquake was not so well constrained, but potential variability with regard to location of the phreatic surface was at least reasonably bounded.

A difficulty encountered in performing back-analyses of this failure is that the post-failure volume of the failed slope materials shown in Figure A.13.1 is approximately 27% larger than the pre-failure volume. This is accommodated in the back-analyses that follow, and it is found that this volume discrepancy has only a moderate effect on uncertainty, or variance, in back-calculated post-liquefaction strengths for this case history.

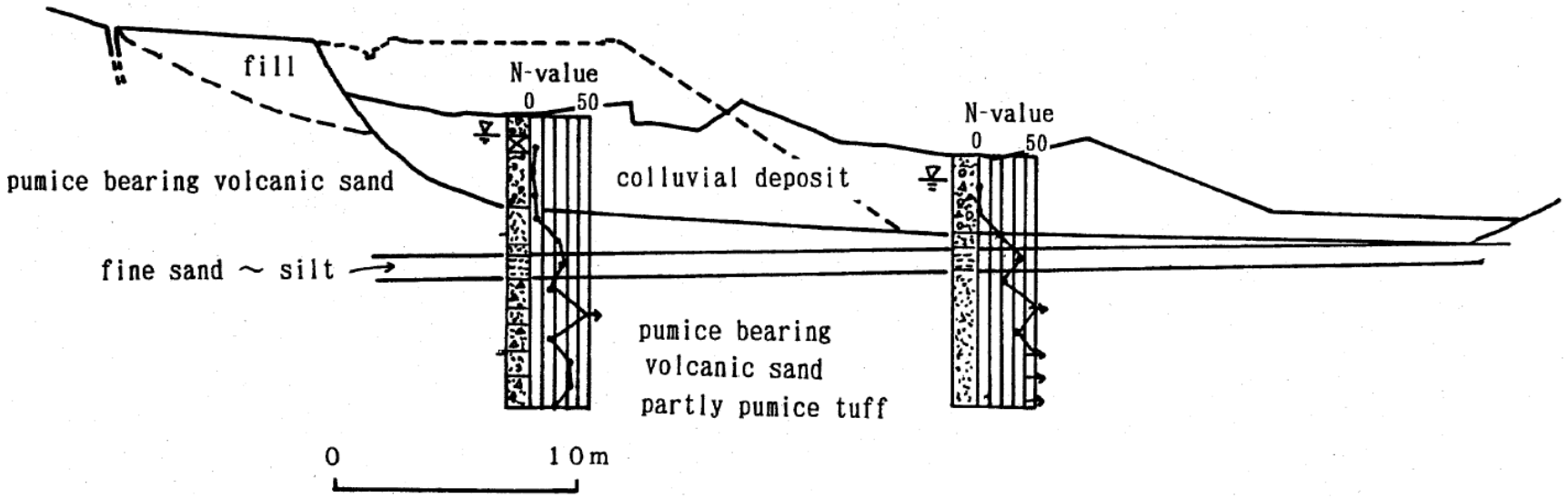

Figure A.13.1: Cross-section through the Route 272 highway embankment showing pre-failure and post-failure geometry and the available SPT boring logs (from Sasaki et al., 1994)

A.13.3 Initial Yield Strength Analysis

It is not known whether this failure initiated as a monolithic failure, or as an incrementally progressive failure that retrogressed towards the back heel in progressive slices. Based on an assumed phreatic surface that passes approximately through the mid-height of the slope, and exits at the toe, a search was made for the most critical static failure surface assuming liquefaction had been "triggered" in all potentially liquefiable materials below the phreatic surface. This exercise showed that the most critical potential failure surfaces for this set of assumptions would have been for a failure initially closer to the slope face than the final rear scarp shown in Figure A.13.1. These analyses neglected seismic inertial forces, however, and they also did not account for likely progressive development of triggering of liquefaction within the slope.

The post-failure geometry shown in Figure A.13.1 is suggestive, on the other hand, of a more monolithic failure, possibly articulating itself into sub-sections as it progressed.

Figure A.13.2(a) shows two potential failure surfaces analyzed. The rear-most surface is the eventual "final" underlying (or bounding) failure surface, which is reasonably well constrained by the data provided by Sasaki et al. (1994). The other failure surface is the surface that was found to be the most critical initial yield surface (requiring the highest value of post-liquefaction yield strength in order to produce a calculated static Factor of Safety = 1.0). Silty sand materials above the phreatic surface were modeled with $Ø' \approx 32°$, and a unit weight of $\gamma_m \approx 103$ lbs/ft^3. Materials below the phreatic surface were considered to liquefy, down to the base of the failure surfaces analyzed, and were assigned an undrained post-liquefaction yield strength of $S_{r,yield}$ that was constant along any given failure surface, and a unit weight of $\gamma_s \approx 108$ lbs/ft^3.

The resulting best-estimated value of $S_{r,yield}$ for the most critical initial (smaller) failure surface was $S_{r,yield} = 374$ lbs/ft^3, and the best-estimated value for the eventual "final" larger failure surface was $S_{r,yield} = 307$ lbs/ft^3.

Parameters and geometry were then varied to examine potentially variability. The location of the phreatic surface was varied, raising it by up to 1.5 m (5 ft.) at the back heel of the final failure surface, and lowering it by up to a similar distance. The phreatic surface was considered to exit at or near the toe of the slope, based on the observed failure (and post-failure geometry). Unit weights were also varied over the ranges considered likely, and the friction angle of non-liquefied material above the phreatic surface was varied from 28° to 36°. The resulting range of values of $S_{r,yield}$ for the most critical initial failure surface was $S_{r,yield} \approx 360$ to 391 lbs/ft^3, and the best-estimated range for the eventual "final" larger failure surface (which would be pertinent if the failure initiated monolithically) was $S_{r,yield} \approx 286$ to 319 lbs/ft^3.

Given the uncertainty as to whether or not this failure was initiated largely monolithically, or was progressively retrogressive towards the back heel, the overall best estimate value of post-liquefaction initial yield strength was developed by considering both sets of possible mechanisms and then taking a middle position with regard to the median value, and then considering the full range of variability for both mechanisms, again averaged for the two

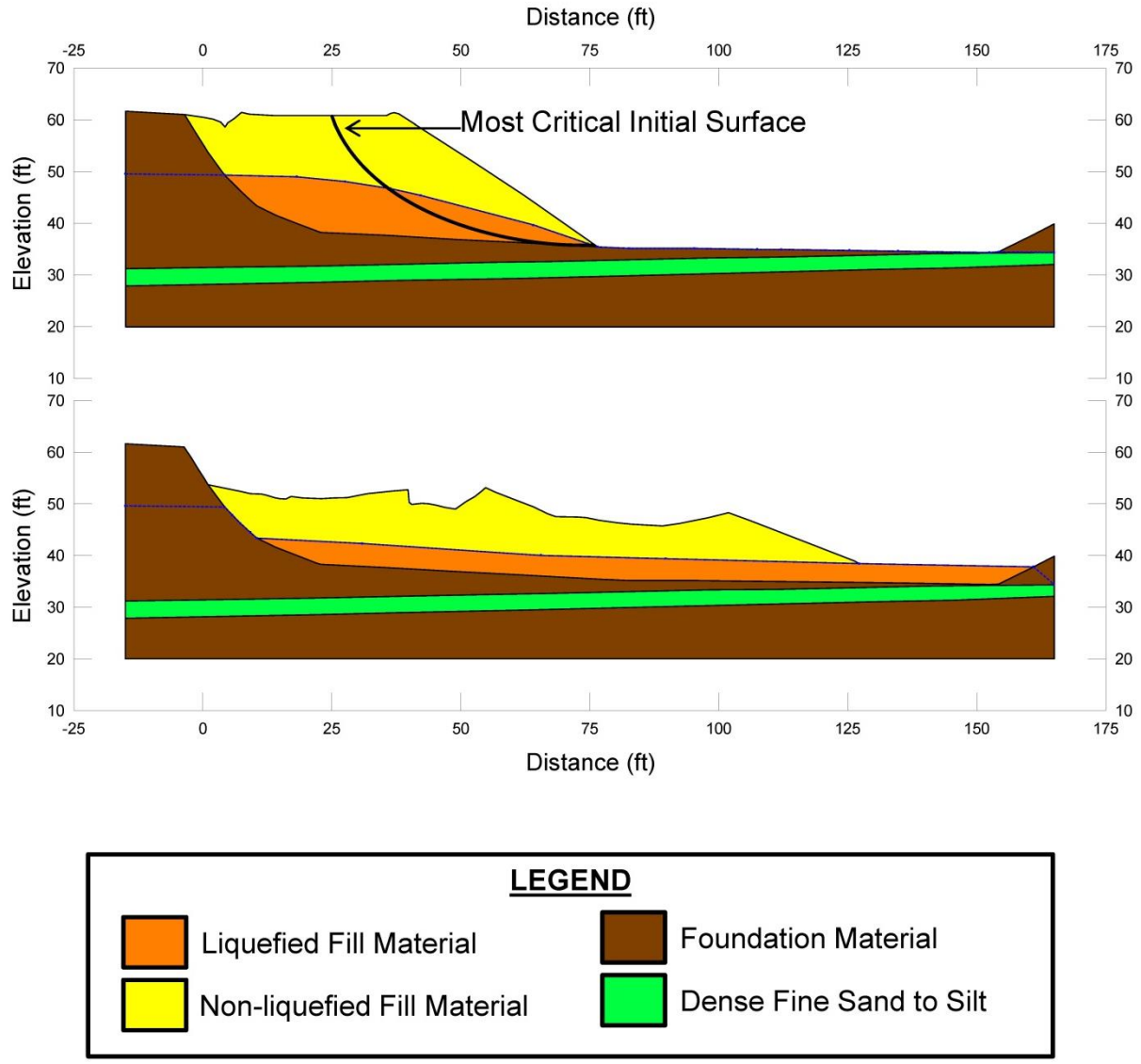

Figure A.13.2: Route 272 embankment cross-sections showing (a) pre-failure geometry of the embankment and the failure surfaces used for calculation of post-liquefaction initial yield strength $S_{r,yield}$, and (b) post-failure residual geometry and the failure surface used to calculate $S_{r,resid/geom}$.

potential failure surfaces. The resulting best estimate (median) value was found to be on the order of $S_{r,yield} \approx 341$, with a likely range of $S_{r,yield} \approx 302$ to 380 lbs/ft^3.

Olsen (2001) also performed back-analyses to determine $S_{r,yield}$. Failure surfaces analyzed were similar, but did not appear to include surfaces extending fully back to the rear heel of the eventual "final" yield surface. Olsen reported values of $S_{r,yield} \approx 13.0$ to 13.4 kPa (272 to 280 lbs/ft^3).

A.13.4 Residual Strength Analysis Based on Residual Geometry

The calculation of the "apparent" post-liquefaction strength ($S_{r,resid/geom}$) required to produce a calculated Factor of Safety equal to 1.0 based on residual geometry is illustrated in Figure A.13.2(b). This figure shows the phreatic surface, and the failure surface, used to calculate the best-estimate value of $S_{r,resid/geom} \approx 69$ lb/ft^3. Variations were then made in parameters, and in location of the pre-failure phreatic surface, as was described in the preceding section in order to evaluate uncertainty or variability. The resulting likely range of post-liquefaction strength required to provide a calculated Factor of Safety equal to 1.0 based on residual geometry was considered to be $S_{r,resid/geom} \approx 65$ to 74 lb/ft^3.

Olsen (2001) also calculated post-liquefaction strength required to produce a calculated Factor of Safety equal to 1.0 based on residual geometry, and reported a range of $S_{r,resid/geom} \approx 2.9$ to 3.0 kPA (61 to 63 lb/ft^3), in good agreement with the values calculated in these current studies.

A.13.5 Incremental Momentum Back-Analyses and Overall Estimates of S_r

Incremental inertial back-analyses were performed using the same sets of properties and geometries (including failure surfaces and phreatic surfaces) as described in the previous sections. Overall volume of the failure mass was subtly increased progressively throughout the increments because, as discussed previously, the post-failure geometry shown in Figure A.13.1 (Sasaki et al., 1994) shows an increase in the volume of the failure mass of approximately 27% from pre-failure to post-failure geometry. This anomalous volume discrepancy was progressively shared relatively equally from inception of failure to cessation of movements in the incremental inertial analyses.

Figure A.13.3 shows the best-estimate progressive incremental inertial analysis, showing the 5 stages of geometry evolution modeled as the failure proceeds. Figure A.13.4 shows the associated calculations of (1) acceleration vs. time, (2) velocity vs. time, and (3) displacement of the overall center of gravity vs. time. For the geometry and phreatic surface shown in Figure A.13.3, and the monolithic initiation of failure modeled in Figures A.13.3 through A.13.5, the best estimate value of post-liquefaction strength was $S_r = 138$ lb/ft^3.

The main sources of uncertainty, or variability, in back-calculated values of S_r were (1) the location of the phreatic surface, (2) whether or not the failure initiated largely monolithically or retrogressed progressively towards the back heel, (3) unit weights, (4) strength within the non-

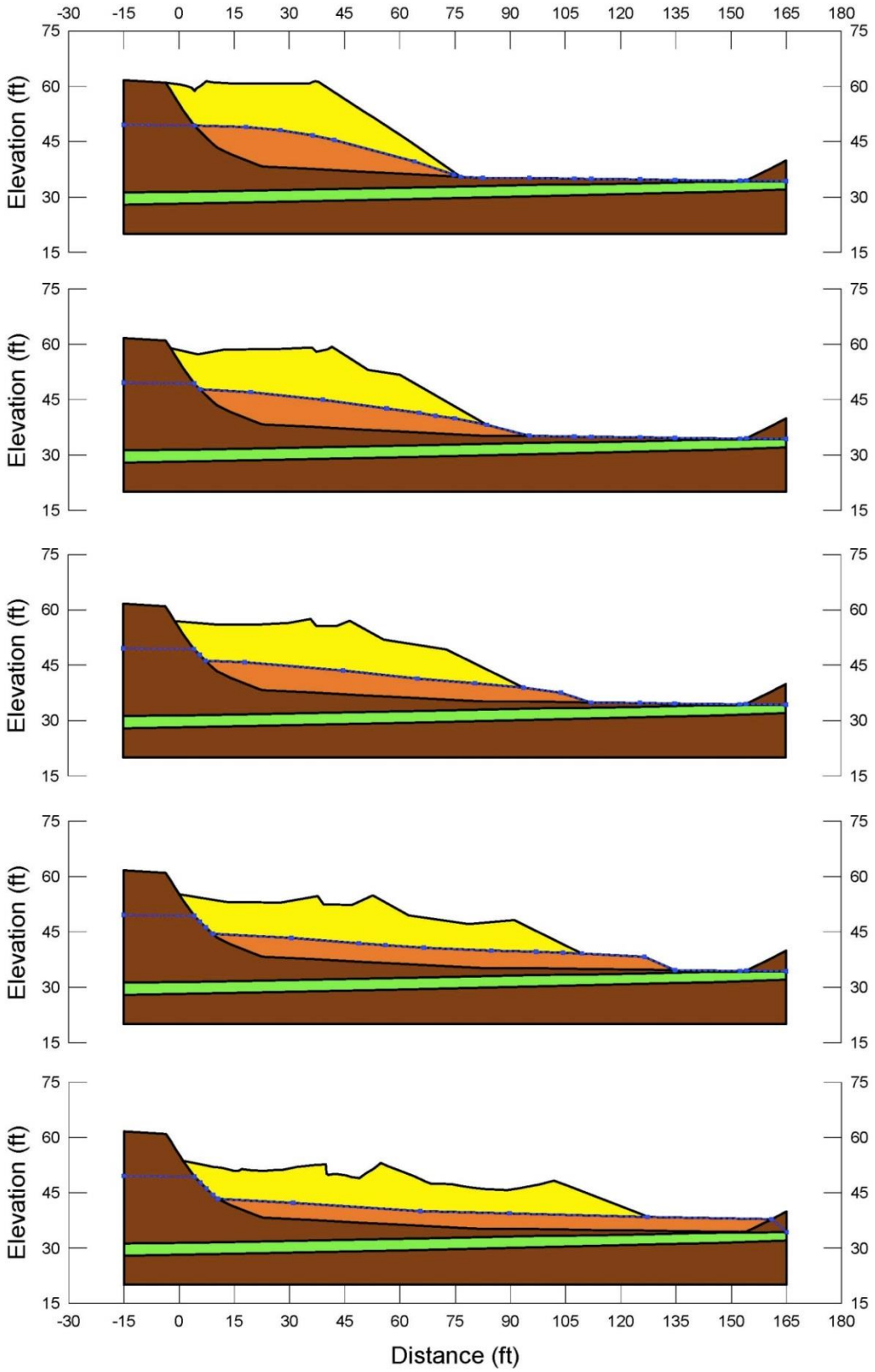

Figure A.13.3: Incremental inertial analysis of the failure of the Route 272 embankment, showing progressive evolution of cross-section geometry modeled

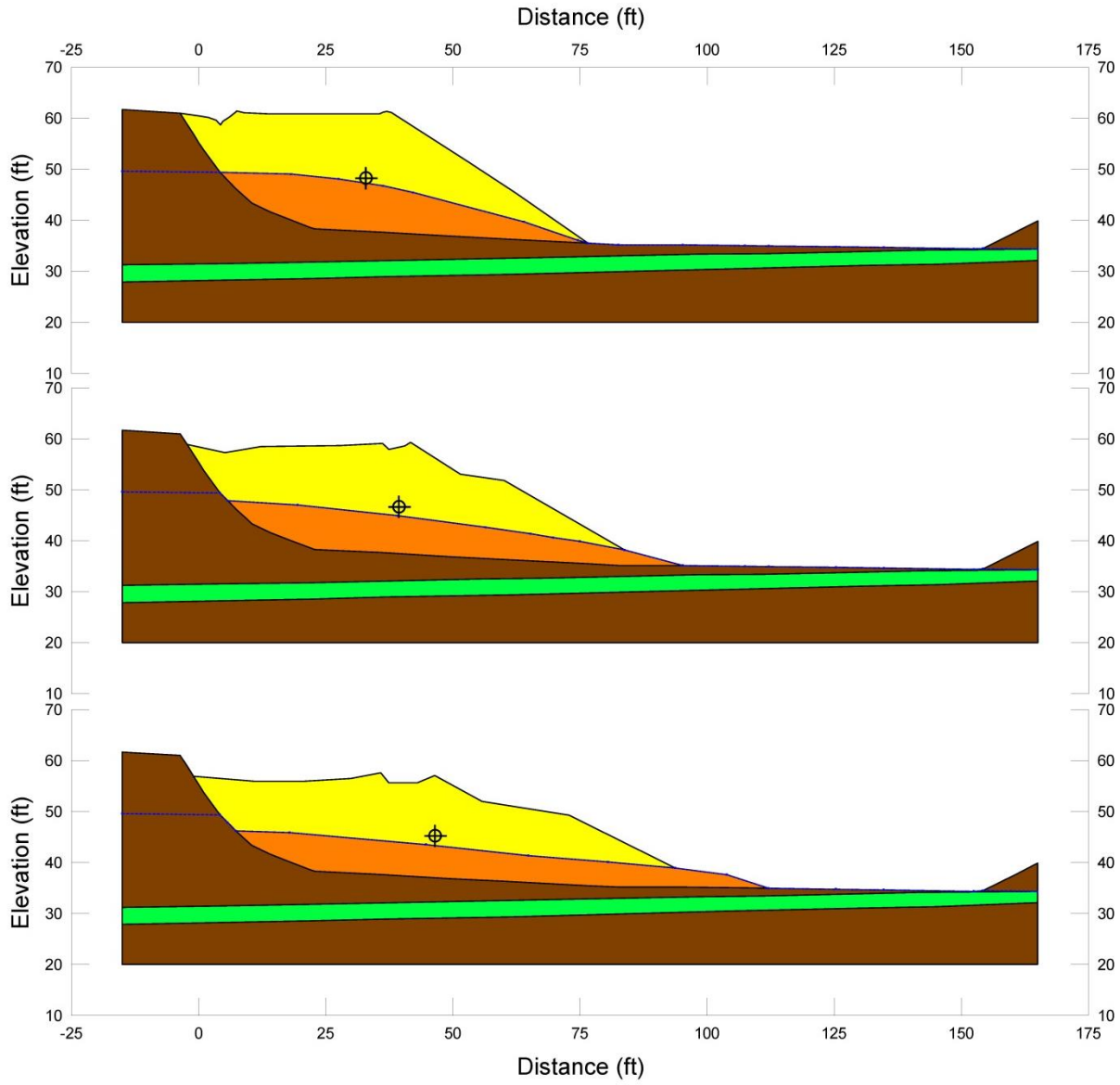

Figure A.13.4: Figure A.13.3 repeated, at larger scale, now also showing the progressive locations of the center of gravity of the overall failure mass.

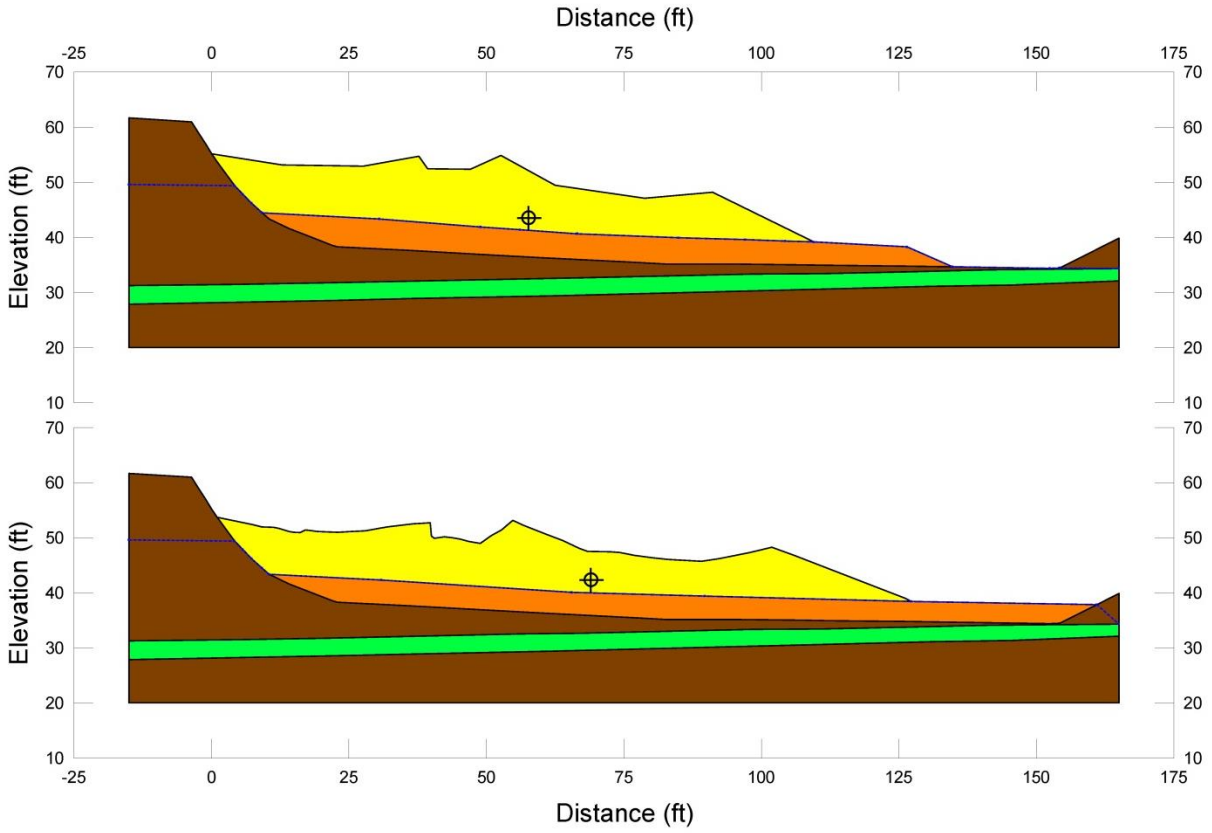

Figure A.13.4 (Cont'd): Figure A.13.3 repeated, at larger scale, now also showing the progressive locations of the center of gravity of the overall failure mass.

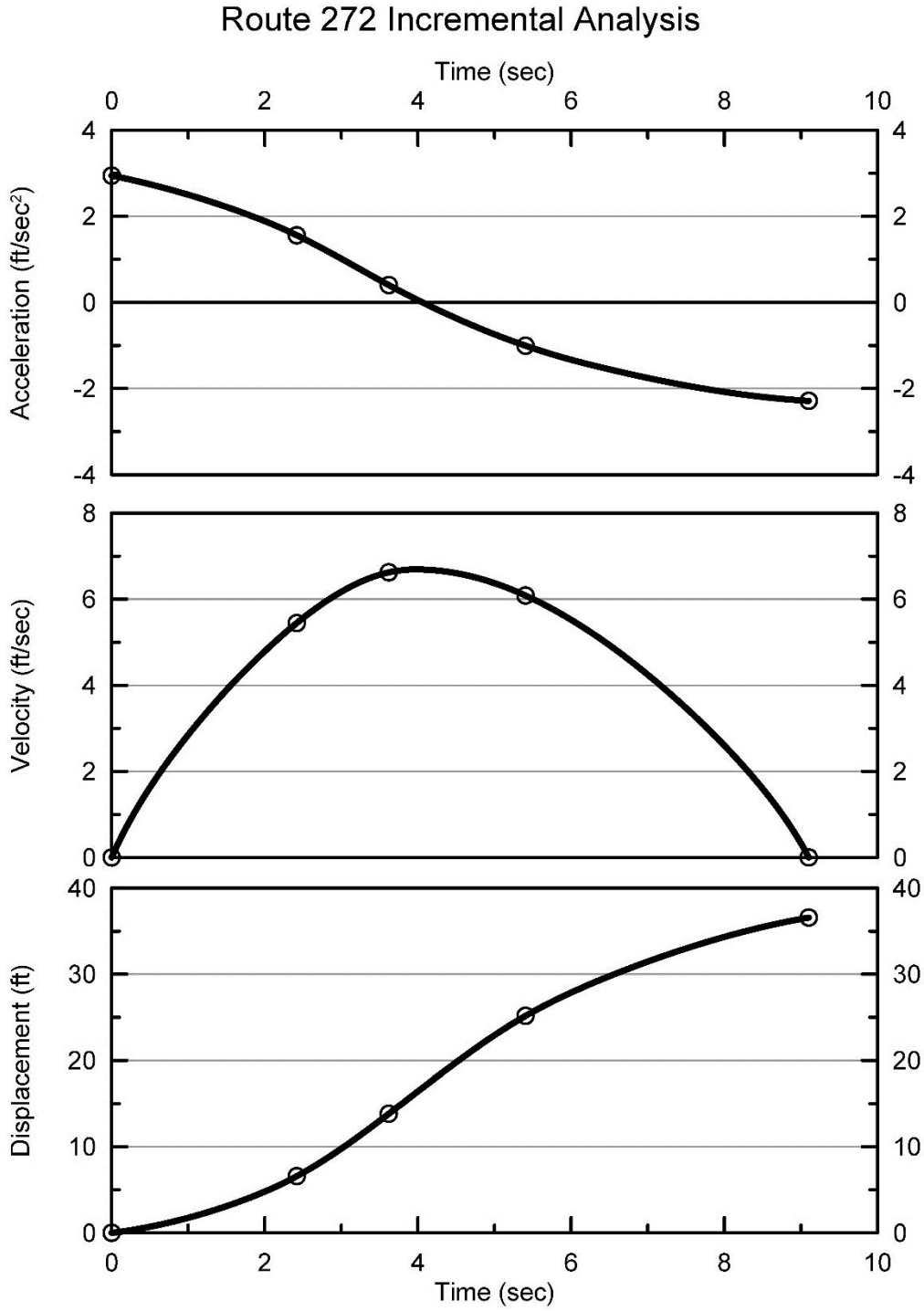

Figure A.13.5: Incremental inertial analysis of the failure of the Route 272 embankment, showing progressive evolution of: (1) acceleration vs. time, (2) velocity vs. time, and (3) displacement of the overall center of gravity vs. time

liquefied materials at the top of the back heel scarp, and (5) the precise location of the overall failure surface.

Because the location of the overall final failure surface was relatively well constrained in this case history, the two main sources of uncertainty, or variability, were (1) the location of the phreatic surface, and (2) the question as to whether the actual failure initiated largely monolithically, or progressed retrogressively towards the back heel.

The analysis shown in Figures A.13.3 through A.13.5 neglects cyclic inertial forces, and so may represent a slightly conservative assessment of actual post-liquefaction strength mobilized. Incremental inertial back-analyses assuming that failure initiates with a failure surface similar to the forward-most initial failure surface shown in Figure A.13.2(a) and then retrogresses back towards the eventual back heel scarp develop somewhat lower overall calculated values of S_r, with the amount of decrease being dependent upon the rate at which subsequent progression of retrogressive failure towards the back heel initiates. It is not feasible to produce the final post-failure geometry actually documented in the field by Sasaki et al. (1994) if an initial yield surface from the forward section of the eventual failure mass is allowed to "run out" too very far before a subsequent second failure extending further rearwards towards the eventual final back heel of the failure initiates. There may have been only a single monolithic inception of failure, or there may have been multiple retrogressive initiations (two or more). But the additional analyses performed suggest that retrogressive progressive failures would have reduced the S_r values from those calculated based on the largely monolithic failure shown in Figures A.13.3 and A.13.4 by on the order of approximately 5 to 12%. It was then judged that the best-estimate value of post-liquefaction strength would have been intermediate between a monolithic initiation of failure and a progressively retrogressive initiation.

Based on all analyses performed, and the considerations discussed herein, the overall best estimate value of post-liquefaction strength for the Route 272 embankment failure was judged to be $S_r \approx 138$ lbs/ft^3, with a likely range of $S_r \approx 107$ to 175 lbs/ft^3. Based on the factors contributing to uncertainty or variance for this case history, it was the judgment of the investigation team that this range represented approximately +/− 2 standard deviations. This range of variance is not quite symmetrical about the best estimate value, so minor further adjustments were made to produce a representative estimate of S_r suitable for regression analyses.

Overall, based on an assumed normal distribution, it was judged that the (mean and median) best estimate of post-liquefaction strength for this case history is

$$S_r = 138 \text{ lbs/ft}^3 \text{ (6.61 kPa)}$$

and that the best estimate of standard deviation of mean overall post-liquefaction strength is

$$\sigma_{\bar{S}} = 17 \text{ lbs/ft}^3 \text{ (0.81 kPa)}$$

Estimates of S_r were also reported by several other investigation teams, and these are shown in Table A.13.1(a). Olsen (2001) and Olsen and Stark (2002), reported a best estimate

Table A.13.1: Representative values for the Route 272 Roadway Embankment case history of: (a) post-liquefaction strength (S_r), (b) initial vertical effective stress (σ_{vo}'), and (c) $N_{1,60,CS}$ developed by various investigation teams, and estimates of variance in each of these indices when available.

(a) Post-Liquefaction Strength:	
Olsen (2001) and Olsen and Stark (2002)	S_r = 100 psf, and range = 63 to 211 psf
Wang (2003) and Kramer (2008)	$\overline{S_r}$ = 130.5 psf, and $\sigma_{\overline{S}}$ = 33.5 psf
This Study	$\overline{S_r}$ = 138 psf, and $\sigma_{\overline{S}}$ = 17 psf
(b) Representative $N_{1,60}$ or $N_{1,60,CS}$ Value:	
Olsen (2001) and Olsen and Stark (2002)	$N_{1,60}$ = 6.3 bpf, and range = 2.4 to 10.0 bpf
Wang (2003) and Kramer (2008)	$\overline{N_{1,60,CS}}$ = 8.5 bpf, and $\sigma_{\overline{N}}$ = 2.6 bpf
This Study	$\overline{N_{1,60,CS}}$ = 8.0 bpf, and $\sigma_{\overline{N}}$ = 1.6 bpf
(c) Representative Initial Vertical Effective Stress:	
Olsen (2001) and Olsen and Stark (2002)	Not reported, but can be inferred from reported S_r/P ratio to be approximately σ_{vo}' = 1,030 psf. Likely range is not provided.
Wang (2003) and Kramer (2008)	Not reported, but can be inferred from reported S_r/P ratio to be approximately σ_{vo}' = 1,044 psf. Variance or standard deviation is not provided.
This Study	$\overline{\sigma'_{vo}}$ = 1,285 psf, and $\sigma_{\overline{\sigma}}$ = 104 psf

value of S_r = 4.8kPa (100 lbs/ft^2), based on their inertial displacement analyses that considered kinetics, and a range of S_r = 3.0 to 5.7 kPa (63 to 119 lbs/ft^3). Wang (2003) and Wang and Kramer (2008) employed their zero inertial force (ZIF) method to incorporate inertial effects in their back-analyses of this failure, and they also developed estimates of both mean $\overline{S_r}$ = 130.5 lbs/ft^2 as well as the associated standard deviation $\sigma_{\overline{S}}$ = 33.5 lbs/ft^2. These other studies each employed different approaches, and different sets of modeling and analysis assumptions. Given this, overall agreement among these investigations is very good.

A.13.6 Evaluation of Initial Effective Vertical Stress

Average initial (pre-failure) effective vertical stress was assessed for the liquefied zones of each of the two failure surfaces shown in Figure A.13.2(a). The best estimate of the overall average initial vertical effective stress was then taken as the average of these two averages. Reasonable variations were then made in (1) the location of the phreatic surface, (2) unit weights, and (3) the precise location of the overall failure surface.

The resulting best estimate of average pre-failure effective stress within the liquefied materials controlling the failure was then $\sigma_{vo}' \approx 1{,}285$ lb/ft^3, with a reasonable range of $\sigma_{vo}' \approx$ 1097 to 1512 lb/ft^3. This range is slightly non-symmetric abut the median value, and this range was judged by the engineering team to represent approximately +/− 2 standard deviations. Overall, the best characterization of initial (pre-failure) average effective vertical stress was then taken to be represented by a mean and median value of

$$\sigma_{VO}' \approx 1{,}285 \text{ lb/ft}^3 \text{ (61.5 kPa)}$$

with a standard deviation of

$$\sigma_{\sigma O}' \approx 104 \text{ lb/ft}^3 \text{ (4.98 kPa)}$$

Estimates of σ_{VO}' were also reported by other investigation teams, and these are shown in Table A.13.1(c). Average initial vertical effective stresses were not directly reported by Olsen (2001) and Olsen and Stark (2002), but they can be inferred from their reported values of S_r/P to have been on the order of approximately $\sigma_{vo}' \approx 1{,}030$ lb/ft^3. Similarly, Wang (2003) and Kramer (2008) also do not directly report calculated values of average initial vertical effective stresses, but they can be inferred from their reported values of S_r/P to have been on the order of approximately $\sigma_{vo}' \approx 1{,}044$ lb/ft^3. Olsen and Stark appear to have developed a slightly lower value of σ_{vo}' due to analysis of a slightly shallower failure surface. Wang (2003) presents no detailed cross-section for his analyses, so it is not possible to know why his estimated value of σ_{vo}' is slightly lower than the value calculated in these current studies. Overall, agreement among these three studies is acceptable here.

A.13.7 Evaluation of $N_{1,60,CS}$

As shown in Figure A.13.1, only 5 SPT were performed within the liquefiable upper stratum. As a result, lack of numbers of SPT data is a significant contributor to uncertainty or variability with respect to the median or mean value representative of this material. Seed et al. (1985) and Ishihara (1993) assumed an energy ratio of approximately 72%, and current study does the same. Corrections for effective overburden stress (C_N) were made using the relationships proposed by Deger (2014), as presented and discussed in Section C.1.1. Corrections for SPT equipment and procedural details, and for fines content, were made based on Cetin et al. The resulting median $\overline{N_{1,60,CS}}$ value was 8.1 blows/ft.

Variance of $N_{1,60,CS}$ within this limited data set was used to calculate the associated variance in the mean (and thus approximately the median) value of $\overline{N_{1,60,CS}}$, but this under-estimated the actual variance or uncertainty. Additional factors significantly affecting variance or uncertainty in the median representative $\overline{N_{1,60,CS}}$ value were (1) lack of numbers of SPT data, and (2) uncertainty as to actual SPT equipment and procedural details. Overall, it was the judgment of the investigation team that SPT penetration resistance could be suitably represented with a representative (median) value of $\overline{N_{1,60,CS}} = 8.1$ blows/ft., and with a standard deviation of the median/representative value of approximately $\sigma_{\overline{N}} = 1.6$ blows/ft.

Table A.13.1(b) shows values of representative $N_{1,60}$ or $N_{1,60,CS}$ values developed by other investigators, and variance or standard deviations in these representative values when available. Olsen and Stark (2001, 2002) developed an estimated representative value of $N_{1,60}$ = 6.3 blows/ft, and an estimated range of representative values of $N_{1,60} \approx$ 2.4 to 10 blows/ft, but did not quantify variance or standard deviation in probabilistic terms. Wang (2003) and Kramer (2008) jointly developed a representative value of $\overline{N_{1,60,CS}}$ = 8.5 blows/ft, and their estimated standard deviation of that overall mean value for this case history was $\sigma_{\overline{N}}$ = 2.6 blows/ft. The representative $N_{1,60}$ value of Olsen and Stark is about 2 to 2.5 blows/ft lower than the other two sets of values in the table, in part because Olsen and Stark did not make a fines correction, which would have served to increase their $N_{1,60}$ values as they became $N_{1,60,CS}$ values in these silty sands.

The investigation teams whose results are presented in Table A.13.1(c) each employed slightly different approaches with regard to corrections for effective overburden stress, fines content, and SPT equipment and procedural details. Given this, the agreement with the value employed in this current study is good. Wride, McRoberts and Robertson (1999) developed a somewhat lower estimate of representative $N_{1,60,CS}$ for this case history, but their approach targeted determination of a more nearly lower bound value, and so is this lower value is to be expected and is not directly comparable with the others shown.

A.13.8 Other Results and Indices

A number of additional results, and indices, can be extracted from the analyses performed. Some of these are useful in developing some of the over-arching relationships and figures presented in the main text of this report. These values are presented in Table A.13.2;

Table A.13.3: Additional results and indices from the analyses of the Route 272 Roadway Embankment failure case history.

Maximum distance traveled by the center of gravity of the overall failure mass	36.6 ft.
Initial post-liquefaction Factor of Safety prior to displacement initiation, and based on best estimate value of S_r	FS = 0.50
Final post-liquefaction Factor of Safety at final (residual) post-failure geometry, and based on best estimate value of S_r	FS = 1.90